Repeat-associated non-AUG (RAN) Translation in GC-rich Repeats of C9ALS/FTD and FXTAS

by

Yi-Ju Tseng

A dissertation submitted in partial fulfillment
of the requirements for the degree of
Doctor of Philosophy
(Cellular and Molecular Biology)
in the University of Michigan
2023

Doctoral Committee:

Professor Peter K. Todd, Chair
Associate Professor Sami J. Barmada
Professor Andrew P. Lieberman
Assistant Professor Stephanie Moon
Associate Professor Stephen C.J. Parker

Yi-Ju Tseng

yjtseng@umich.edu

ORCID: 0000-0002-2242-6200

Dedication

To my best friend and forever support, Tung-Yi Chiu.

Table of Contents

List of Figures

List of Tables

Abstract

Repetitive elements comprise over half of the human genome. Expansion of a subtype within these repetitive elements known as short tandem repeats (STRs) causes over fifty human disorders. C9orf72-associated amyotrophic lateral sclerosis and frontotemporal dementia (C9ALS/FTD) and Fragile X-associated tremor/ataxia syndrome (FXTAS) represent two instances where an STR expansion results in neurodegenerative disease. C9ALS/FTD results from a GGGGCC (G4C2) hexanucleotide repeat expansion within the first intron of C9orf72 while FXTAS is caused by CGG repeat expansion in the 5'UTR of FMR1. These repeat-containing RNAs elicit toxicity at least in part by triggering repeat-associated non-AUG (RAN) translation. RAN translation is a non-canonical process where repetitive regions within mRNAs initiate translation in the absence of a canonical AUG start codon. RAN translation can happen in multiple reading frames and can occur in transcriptional contexts (5'UTRs, introns, 3'UTRs, and antisense RNAs) that do not typically support mRNA translation. The protein products generated by RAN translation with these repeat expansions and are thought to contribute to disease pathogenesis. However, the mechanisms by which RAN translation occurs remain unclear. The goal of this thesis is to better define how RAN translation works and identify selective modifiers of RAN translation. To accomplish this goal, I have taken three approaches.

First, I analyzed DHX36 which directly interacts with repeat mRNA and influences its translational efficiency. G4C2 and CGG repeats form stable RNA secondary structures such as G-quadruplex and/or hairpin structures. DEAH-Box Helicase 36 (DHX36) plays an active role in RNA and DNA G-quadruplex resolution. Therefore, I evaluated whether altering the expression of DHX36 impacts repeat transcription and RAN translation. These studies revealed that DHX36 depletion suppresses RAN translation from reporter constructs in a repeat length-dependent manner.

Second, performing a candidate-based target screen, I identified factors from the mRNA and protein surveillance pathways that affect the efficiency of translation through GC-rich repeat sequences. I identified three key factors - NEMF, LTN1, and ANKZF1 - from the ribosome-associated quality control (RQC) pathway that impact the generation of RAN products. Depletion of these RQC factors increases the accumulation of RAN proteins while overexpression of RQC factors decreases RAN protein accumulation. To assess this further, I used a dual tagging system to detect partially generated products from G4C2 and CGG repeats. These findings suggest that RQC factors play a critical role in both suppressing RAN translation and in maintaining protein and translational homeostasis in the face of toxic repeats.

Third, we completed and analyzed a genome-wide high-throughput small-interfering RNA (siRNA) screen for selective RAN translational modifiers. From gene ontology analysis, we surprisingly found that multiple siRNAs target genes encoding 20S proteasome subunits act as selective suppressors of RAN translation while a separate group of siRNAs targeting genes from the eIF5A hypusination pathway act as selective

enhancers of RAN translation. These two are interesting novel pathways emerging as areas for future studies.

Taken together, these studies provide insight into the factors and pathways required for RAN translation at two GC-rich nucleotide repeat expansions. These results suggest that repeat RNA structure, translational elongation, and protein homeostasis play active roles in regulating RAN translation. By coupling these newly identified pathways to assays of repeat-associated toxicity in mammalian cell-based reporter systems, Drosophila models of disease, and patient-derived human neurons will reveal novel targets for future therapeutic development.

Chapter 1: Introduction

1.1. Abstract

Microsatellite disorders are a class of neurological diseases caused by nucleotide-repeat expansions within the human genome. Expanded repeats support repeat-associated non-AUG (RAN) translation, a non-canonical mode of translational initiation whereby proteins are generated from repetitive RNA motifs in the absence of an AUG start codon. RAN translation generates toxic proteins which contribute to neuronal toxicity. The mechanisms underlying RAN translation are unclear, and no currently effective treatments for RAN translation-related repeat expansion disorders. This introduction will provide a background on microsatellite disorders in general, with additional details on two different repeat expansion diseases where RAN translation is thought to contribute to pathogenicity: CGG repeats in fragile X-associated tremor ataxia syndrome (FXTAS) and GGGGCC (G4C2) repeat in C9orf72-associated amyotrophic lateral sclerosis (ALS) and frontotemporal dementia (FTD). I will then focus on what we currently know about the RAN translation at a mechanistic level and what factors are known to act as modifiers of this process. I will close with a set of questions that provide a basis for my thesis research.

1.2. Introduction

Microsatellite disorders are a heterogeneous group of neurodegenerative diseases

and neuromuscular disorders that impact a large number of patients worldwide (Bañez-Coronel et al. 2012; Gao and Richter 2017; Gusella and MacDonald 1996; He and Todd 2011; James Kent et al. 2002; Lafrenière et al. 1997; Malik, Kelley, et al. 2021; Margolis et al. 1999; Mirkin 2007; Nagafuchi et al. 1994; Nelson, Orr, and Warren 2013; Orr and Zoghbi 2007; Paulson 2018; Rodriguez and Todd 2019; Sato et al. 2009; Stoyas and La Spada 2018; Swinnen, Robberecht, and Van Den Bosch 2020; Todd et al. 2013; Wenninger, Montagnese, and Schoser 2018). Microsatellite disorders are characterized by a sequence of tandemly repeated DNA motifs. These repetitive DNA motifs alter gene expression at all human genome stages, leading to neuronal disorders (Malik, Kelley, et al. 2021; Paulson 2018; Rodriguez and Todd 2019). There are three main mechanisms caused by the repeat that led to toxicity (Bañez-Coronel et al. 2012; Gao and Richter 2017; Gitler and Tsuiji 2016; Ling, Polymenidou, and Cleveland 2013; Nishimura and Arias 2021). Repeat sequences can induce transcriptional silencing of genes harboring repeats, leading to a loss of protein expression from these loci. Transcription of repeats can also trigger DNA-RNA hybrids known as R-loops, which activate the DNA damage response and transcriptional silencing (Boivin et al. 2020; Coffee et al. 2002; Farg et al. 2017; He et al. 2023; Lin et al. 2010; Liu et al. 2014; Russ et al. 2015; Sutcliffe et al. 1992; Usdin and Kumari 2015; Xi et al. 2013, 2015; Xu, Chong, and Wang 2021). Repeats as RNA can bind to RNA-binding proteins and sequester them into phase-separated compartments known as RNA foci. These condensates impede the normal functions of the RNA binding proteins, leading to alterations in splicing and RNA localization (Burguete et al. 2015; Conlon and Manley 2017; Cooper-Knock et al. 2015; Miller et al. 2000; Mizielinska et al. 2013; Kohji Mori et al. 2013; Taneja et al. 1995; Van Treeck and Parker

2018; White et al. 2010; Zhang and Ashizawa 2017). Third, when expanded repeats are translated into proteins, they can accumulate into aggregates that both evade and impair protein quality control pathways. This protein-mediated gain-of-function mechanism was originally thought to only be relevant to trineucleotide repeats that reside in open reading frames. However, in 2011 Laura Ranum's group discovered that a CAG-repeat expansion which causes human spinocerebellar ataxia type 8 (SCA8) can support translation in the absence of an AUG start codon. They termed this non-canonical initiation process repeat-associated non-AUG (RAN) translation (Zu et al. 2011). Subsequently, it has become clear that RAN translation can occur in multiple reading frames from both sense and antisense generated transcripts to produce multiple different peptides- many of which accumulate in patient tissues. Moreover, RAN translation occurs on regions of RNA that typically do not engage with a ribosome, such as 5' UTRs, introns and non-coding RNAs. In total, there are now more than 10 different disorders where RAN translation has been reported to occur with more emerging regularly **(Figure1.1.)** (Ash et al. 2013; Bañez-Coronel et al. 2012, 2015; Cleary and Ranum 2013; Fujino, Mori, and Nagai 2023; Koob et al. 1999; Liquori et al. 2001; K. Mori et al. 2013; Sato et al. 2009; Todd et al. 2013; Zu, Pattamatta, and Ranum 2018). This literature suggests that RAN translation is both prevalent and important to the pathogenesis of a large set of human neurodegenerative disorders for which there are no effective treatments.

1.3. Initiation of Global Translation

Canonical translation initiation in eukaryotes starts with recognition of the 5' methyl-7- guanosine (m^7G) on an mRNA by the eIF4F complex (Sonenberg et al. 1978,

1979), which is composed of eIF4E (the subunit that binds to the mRNA 5' cap directly); eIF4G (the scaffolding subunit); eIF4A (a DEAD-box RNA helicase); and eIF4B and eIF4H (stimulatory helicases that support eIF4A activity) (Jackson, Hellen, and Pestova 2010; Koromilas, Lazaris-Karatzas, and Sonenberg 1992; Pyronnet et al. 1999). Within the eIF4F complex, eIF4G recognizes the polyadenosine-binding protein (PABP) associated with the 3' polyA tail to create a circular mRNA complex that is important in translational efficiency (Borman 2000; Gingras et al. 1999; Kessler and Sachs 1998; Pyronnet et al. 1999). Next, the 43S pre-initiation complex (PIC) joins the eIF4F complex at the m^7G cap to form the 48S scanning competent complex (Çetin and O'Leary 2022; Coots et al. 2017; Izidoro et al. 2022; Pestova, Shatsky, and Hellen 1996). The 43S PIC is comprised of the 40S ribosomal subunit, eIF1, eIF1A, eIF3, eIF5, and the ternary complex (the methionine-conjugated tRNA ($tRNA^{Met}$) bound to the multi-subunit GTPase initiation factor eIF2 in its GTP-bound state (Algire, Maag, and Lorsch 2005; Bogorad, Lin, and Marintchev 2017; Kedersha et al. 2002; Unbehaun 2004). Joining of the 43S PIC is mediated by interactions between eIF4G and eIF3 (Çetin and O'Leary 2022; Gradi et al. 1998; Pestova et al. 1996; Sha et al. 2009; Yang et al. 2003). In the ribosomal scanning model of translation initiation, the assembled 48S complex scans along the 5' UTR from the m^7G cap in a 5' to 3' orientation (Hinnebusch 2014; Kozak 1978), sampling individual codons for an AUG initiation site in an appropriate (Kozak) sequence context. eIF4A acts to resolve RNA-RNA secondary structures during scanning (Jackson 1991; Zhang et al. 2015). Once an AUG codon is recognized, eIF1 is ejected by the base-pairing between the AUG codon and CAU anti-codons from $tRNA^{Met}$ (Pestova 2002; Unbehaun 2004; Yoon and Donahue 1992). This allows eIF2 to hydrolyze its GTP with the assistance of

eIF5, the associated GTPase-activating protein (GAP) and recruit the 60S ribosomal subunit to join with the 40S ribosomal subunit (Algire et al. 2005; Asano 1999; Asano et al. 2000; Das, Ghosh, and Maitra 2001; Kimball 1999; Phan et al. 1998). Most eIFs are ejected at this stage and when eIF5B hydrolyzes its bound GTP, and translation elongation starts with formation of the first peptide bond in conjunction with a second tRNA entering and decoding the second codon in the A-site **(Figure1.2.)** (Dever and Green 2012; Pestova et al. 2000).

1.4. Non-AUG and uORF Mediated RAN Translation Initiation

In some contexts, RAN translational initiation has significant mechanistic overlap with many of the central features observed with global translation initiation. In Rabbit Reticulocyte Lysate (RRL) *in vitro* assays and transfected human cells at both CGG repeats in the context of the *FMR1* 5'UTR and at intronic G4C2 repeats embedded within linear reporters, RAN translation largely requires binding the m7G cap with the 43S PIC and eIF4F complex (Green et al. 2017; Michael G. Kearse et al. 2016; Sellier et al. 2017). However, without access to a canonical AUG start codon, RAN translation initiation occurs predominantly at near-cognate (one base off from AUG) codons located just 5' upstream to the repeat sequences (Schwab et al. 2004; Young, Baird, and Wek 2016). RAN translation at *FMR1* 5' UTR CGG repeats is cap-dependent, utilizing a ribosome scanning model to initiate translation from ACG or GUG (Kearse et al. 2016; Zhang et al. 2022). RAN translation from linearized *C9orf72* ALS/FTD repeats also shows dependence on the m7G cap and eIF4A, with the most robust initiation occurring at a specific near-cognate start codon, CUG, located 5' upstream of the G4C2 repeats

(Figure1.15.3. A) (Cheng et al. 2018; Green et al. 2017; Tabet et al. 2018). More details of this scanning model of RAN translation will be discussed later in this introduction.

1.5. Internal Ribosome Entry Sites and Cap-independent Translational Initiation

While the ribosomal scanning model described above applies to most eukaryotic mRNA transcripts, some alternative initiation mechanisms use specific RNA secondary structures to bypass the requirement of canonical translation. Internal ribosomal entry site (IRES)-mediated translational initiation is quite common in viral mRNA translation (JAN et al. 2001; Lozano and Martínez-Salas 2015; Stoneley and Willis 2004; J. E. Wilson et al. 2000). IRES elements in mRNAs are quite varied in their sequence and structure as well as in their requirements for specific initiation factors, but most are definitionally capable of bypassing the typical requirement of 5' m7G cap interactions with eIF4E, allowing for direct ribosomal recruitment (Fernández et al. 2014; Kieft et al. 2001; Komar and Hatzoglou 2011) within the middle of an mRNA. At their most extreme, IRESes can support initiation with just a 40S ribosomal subunit and an alanine-conjugated tRNA (JAN et al. 2001; Joan E Wilson et al. 2000). IRES elements such as the cricket paralysis virus (CrPV) can also bypass the need for an AUG start codon, instead utilizing CCU as an initiation codon to synthesize protein with an N-terminal alanine (Pestova, Lomakin, and Hellen 2004; J. E. Wilson et al. 2000). IRESes exist primarily in viruses but are also known to occur within some eukaryotic mRNAs including c-Myc, Apaf-1, Bcl-2, XIAP, and DAP5 (Hellen and Sarnow 2001; Komar and Hatzoglou 2005). Viral and cellular IRESes seem to have evolved as a way of evading global translational initiation suppression that can

occur under specific cellular conditions, such as the integrated stress response **(Figure1.3. B)** (Chappell, Edelman, and Mauro 2006; Juszkiewicz et al. 2020; Kozak 1978, 1986; Mechanism et al. 2010; Sendoel et al. 2017; Sonenberg and Hinnebusch 2009). However, their activities have acquired additional roles outside of these pathological contexts in regulating spatial and temporal translational dynamics in complex cells such as muscle and neurons.

1.6. Translational Elongation

Incorporation of amino acids onto the elongating nascent peptide chain occurs through three critical steps: tRNA selection, peptide bond formation, and translocation of the tRNA-mRNA complex (Chu et al. 2014; Dever, Dinman, and Green 2019; Dever and Green 2012). The first step is loading and selection of the proper tRNA into the A site of the ribosome- a process that relies on matching the anti-codon from the aminoacyl-tRNA to the codon from mRNA (Inada 2019; Lyu et al. 2021; Saint-Léger and Ribas De Pouplana 2015; Wu et al. 2019; Yip et al. 2019; Yu et al. 2015). This process is supported by eEF1A (elongation factor Tu in bacteria, EFTu), which is a GTPase ternary complex that assists with delivery of aminoacyl-tRNAs into the A site (Carvalho, Carvalho, and Merrick 1984; Fischer et al. 2015; Negrutskii et al. 2023; Shao et al. 2016). When the anti-codon from the tRNA and the codon from the mRNA are sensed and matched, eEF1A hydrolyzes GTP to fully load the tRNA at the ribosomal A site (Shao et al. 2016; Zaher and Green 2009). After aminoacyl-tRNA loading, the tRNAs from the P and A site form peptide bonds to grow the peptide chain (Behrmann et al. 2015; Budkevich et al. 2011; Djumagulov et al. 2021; Moazed and Noller 1989). Chemical catalysis occurs through a

concerted proton shuttle mechanism at the ester linkage of the peptidyl-transferase center to form the peptide bond (Beringer and Rodnina 2007; Moazed and Noller 1989). The amino group of the incoming amino acid from the A site nucleophilic attacks the ester linkage of the peptidyl-tRNA from the P site to transfer the elongating nascent peptide chain to the tRNA at the A site (Moazed and Noller 1989). After forming the peptide bond, tRNAs rotate in a hybrid state at the E/P and P/A sites (Shoji, Walker, and Fredrick 2009; Spahn et al. 2004; Taylor et al. 2007). In this transition state, eEF2 (elongation factor G in bacteria, EFG), with its GTPase activity, translocates and fully settles the loaded tRNAs into the E and P sites and empties the A site (Spahn et al. 2004; Taylor et al. 2007). This then allows for recruitment of a new aminoacyl-tRNA into the A site and continuation of this cycle. Elongation typically continues in this fashion until the translating ribosome reaches a stop codon, which recruits a special set of tRNAs without a paired amino acid, leading to chain termination (Jackson, Hellen, and Pestova 2012; Shcherbik et al. 2016). Finally, by reaching the end of the ORF, translation termination begins when ribosome senses a stop codon (UAA, UAG or UGA) (Dever and Green 2012). A single release factor, eRF1, promotes the releases to nascent peptide chain and together with a specialized GTPase, eRF3, which dissociate eRF1 following peptide release **(Figure1.4.)** (Alkalaeva et al. 2006; Frolova et al. 1996, 1999; Salas-Marco and Bedwell 2004).

1.7. Slowing and Stalling During Translational Elongation

Multiple circumstances during translation elongation can slow down the process, and temporary pausing or terminal stalling of ribosomes within an open reading frame can lead to ribosomal collisions. Inefficient translational elongation can result from 1)

Specific amino acid sequences, 2) RNA structural elements, 3) The charge of the nascent peptide chain, 4) Defects or modifications in the mRNA or tRNAs 5) Loss of a stop codon, leading to translation into a polyA tail, 6) Cellular or ribosomal stressors, including P-body formation, Ribosomopathies and tRNA synthetase deficiencies **(Figure1.5)** (Pop et al. 2014; Schuller and Green 2018).

During the elongation process of decoding amino acids, there are 400 combinations of forming possible peptide bonds between two peptidyl-tRNAs. Not all 400 peptide bonds are formed with the same efficiency (Dever et al. 2019; Pavlov et al. 2009; Riba et al. 2019; Shoemaker and Green 2011; Wohlgemuth et al. 2008). For example, proline is an amino acid with a more reactive cyclic structure of its N-alkyl group. This cyclic structure of the N-alkyl group from Pro-tRNA^{Pro} forms its peptide bond by reducing the nitrogen nucleophilicity and adding the secondary amine (Doerfel et al. 2015; Huter et al. 2017; Pavlov et al. 2009; Wohlgemuth et al. 2008). The formation of cyclic N-alkyl groups in polypeptides and proteins creates a poor peptidyl acceptor orientation to the A site, which slows down the rate of elongation (Doerfel et al. 2015; Pavlov et al. 2009; Wohlgemuth et al. 2008). This lack of entropy also makes Proline a poor donor at the P site. Therefore, the formation of poly-proline stretches within a protein is a challenge (Dever et al. 2019; Doerfel et al. 2013; Riba et al. 2019; Ude et al. 2013; Wohlgemuth et al. 2008; Woolstenhulme et al. 2013). Gutierrez et al. found that a specific translation factor, eIF5A, plays a crucial role in assisting peptide bond formation of Pro-Pro peptides (Gutierrez et al. 2013). eIF5A is highly abundant and essential in cells. A unique post-translational modification called hypusination functionally activates eIF5A (Park et al. 2022; Schmidt et al. 2015; Wątor et al. 2023). Hypusination is a polyamine biosynthetic

pathway that generates hypusine from spermidine and incorporates it into eIF5A. First, deoxyhypusine synthase (DHPS) cleaves the 4-aminobutyl moiety of spermidine and transfers it to the ε-amino group of a specific lysine residue on the eIF5A precursor protein to form an intermediate, deoxyhypusine [Nε-(4-aminobutyl)lysine]. Deoxyhypusine hydroxylase (DOHH) forms hypusine by hydroxylating thise eIF5A precursor into mature eIF5A (Landau et al. 2010; Miller-Fleming et al. 2015; Puleston et al. 2019; Schnier et al. 1991; Tiburcio et al. 2014). Schmidt et al. used cryo-EM to solve the structure of eIF5A on the ribosome (Schmidt et al. 2015). They found that the hypusine modification integrates into the peptidyl-transferase center of the ribosome, where the hypusine moiety contacts A76 of the CCA-end of the P-site tRNA (Schmidt et al. 2015; Wątor et al. 2023). This helps stabilize the CCA-end of $tRNA^{Pro}$. In this fashion, eIF5A establishes interactions with the CCA-ends of both the A and P site tRNAs. This interaction stimulates peptide bond formation for Pro-Pro and other peptide motifs (Schuller et al. 2017). In cells lacking functional eIF5A, ribosomes redistribute toward the 5' end of transcripts with pausing of ribosomes specifically at P-P amino acids motifs (Schuller et al. 2017).

RNA with GC-rich transcripts can form a stable secondary structure such as hairpins and g-quadruplexes. The efficiency of translation elongation through these structured mRNA regions is impaired and this can affect the expression of proteins generated from structure-harboring transcripts (Bao et al. 2020, 2022; Georgakopoulos-Soares, Parada, and Hemberg 2022; Hanson et al. 2018; Mauger et al. 2019).

Translating charged nascent peptides such as poly-arginine or poly-lysine can also elicit ribosomal stalling (Chandrasekaran et al. 2019; Juszkiewicz and Hegde 2017; Kriachkov et al. 2023; Park et al. 2021; Viera Ortiz et al. 2022; Wilson, Arenz, and

Beckmann 2016). Cryo-EM studies demonstrate that the serial translation of charged amino acids leads to interactions of the nascent peptide chain with negatively charged RNA elements within the ribosomal exit tunnel (Wątor et al. 2023). However, in some circumstances it appears that the amino acid charge effects on stalling are actually secondary to the mRNA sequence rather than exit tunnel interactions in isolation. Chandrasekaran et al. were able to detect both poly-lysine within the exit tunnel and a polyA stretch within the mRNA transcript within the decoding center of a stalled ribosome (Chandrasekaran et al. 2019). When they changed the sequence from which they translated poly-lysine to non-AAA codons, they discovered that the polyA transcript caused most of the ribosomal stalling. The polyA stretch transcript is not only in the coding region, when the transcript is lacking a termination codon, ribosomes may run through the polyA tail in the transcript which also cause ribosome stalling (Borman 2000; Juszkiewicz and Hegde 2017; Kahvejian 2005; Saito, Hosoda, and Hoshino 2013). Together with the occasion of encountering a premature termination codon, these are considered defective transcripts that slow down the translation elongation process causing stalling of the ribosome.

If translational initiation occurs on a transcript where a leading ribosome has paused or stalled during elongation, it can lead to ribosome collisions (Ikeuchi et al. 2019; Joazeiro 2019; Lu 2023; Matsuo et al. 2020). When ribosomes collide, it triggers a series of protein and mRNA surveillance pathways that can lead to degradation of both the nascent peptide and the mRNA on which the collision occurs. This process allows for ribosomal recycling (Joazeiro 2019). These quality control pathways act to ensure protein fidelity in cells and maintain protein homeostasis. Traditionally, ZNF598 and RACK1 act

to first detect ribosome stalls and collisions. Then ABCE1, PELO, and HBS1L occupy the A site of the ribosome to terminate elongation (Garzia et al. 2017; Juszkiewicz et al. 2018; Pisarev et al. 2010; Pisareva et al. 2011; Sundaramoorthy et al. 2017; Wu et al. 2018). These factors then act to split the 80S ribosome into the 60S which contains a still-associated partially made nascent peptide chain and 40S which still contains the mRNA. The RNA is then degraded by XRN1 and the exosome by RNA no-go decay, non-stop decay (lacking stop codon), or nonsense-mediated decay (presence of premature termination codon) (Becker et al. 2011; Chen et al. 2010; Doma and Parker 2006; Harigaya and Parker 2010; He et al. 2003; Inada 2019; Nagarajan et al. 2013; Orban and Izaurralde 2005; Preker et al. 2008; Saito et al. 2013; Shoemaker, Eyler, and Green 2010; Veltri et al. 2022). The 60S with the partially made nascent peptide chain then engages with the ribosome-associated quality control (RQC) pathway to target the partially made peptide for proteasome degradation (Duttler, Pechmann, and Frydman 2013; Kuroha et al. 2018; Matsuo et al. 2017; Matsuo, Uchihashi, and Inada 2023; Petrucelli and Dawson 2004; Shao and Hegde 2014; Shao, Von der Malsburg, and Hegde 2013).

1.8. RAN Translation in Nucleotide Repeat-expansion Disorders

A novel translational initiation process, Repeat-Associated Non-AUG (RAN) translation, was first described in 2011 by Laura Ranum's group (Zu et al. 2011). An expansion of a CAG repeat from the gene Ataxin 8 (*ATXN8os*) causes the neurodegenerative disorder spinocerebellar ataxia type 8 (SCA8) (Koob et al. 1999). CAG repeat transcripts can form hairpin structures (De Mezer et al. 2011). To assess whether these RNA hairpins might contribute to disease, they removed an upstream AUG codon and expressed the repeat.

Surprisingly, in the absence of AUG start codon, the expanded CAG repeats still supported generation of homopolymeric polyG (glutamine), polyA (alanine), and polyS (serine) proteins from the sense reading frames (Bañez-Coronel et al. 2012, 2015; Davies and Rubinsztein 2006; Stoyas and La Spada 2018). The efficiency of RAN translation was dependent on repeat size, as shorter repeats produced either less or no proteins (Bañez-Coronel et al. 2015; Zu et al. 2011). Importantly, the structure of the repeat was important, as a CAA repeat of the same size (which cannot form a hairpin) did not support RAN translation in reporter assays (Zu et al, 2011). They then found that the antisense repeat (CUG repeats) could also support RAN translation of polyL (leucine), polyA (alanine), and polyC (cystine) (Zu et al. 2011). A pathogenic hallmark of neurodegenerative disease is the aggregation of toxic proteins accumulated within neurons. In an SCA8 mouse model and human patient cerebellum, they found that an antibody against SCA8-polyAla recognizes the protein *in vivo* (Zu et al. 2011).

Since this initial discovery, other research groups have demonstrated RAN translation in different repeat-expansion diseases across different model organisms. RAN translation can occur on different repetitive elements: CGG repeats in the 5' UTR of the Fragile X Messenger Ribonuclearprotein 1 (*FMR1*) gene, as occurs in fragile X-associated tremor/ataxia syndrome (FXTAS); intronic G4C2 repeats in *C9orf72*-associated amyotrophic lateral sclerosis (C9 ALS) and frontotemporal dementia (FTD); CAG repeats in the protein-coding sequence of Huntingtin (HTT) in Huntington disease; intronic CCTG repeats in CNBP that cause Myotonic dystrophy type2 (DM2); and intronic CTG repeats in TCF4 that cause Fuchs endothelial corneal dystrophy 3 (Bañez-Coronel et al. 2015;

Soragni et al. 2018; Todd et al. 2013; Zu et al. 2013, 2017). This introduction will focus on some highlights of C9 ALS/FTD and FXTAS in RAN translation.

1.9. RAN Translation at G4C2 Repeats in C9 ALS/FTD

The most common genetic cause of amyotrophic lateral sclerosis (ALS) and frontotemporal dementia (FTD) is a G4C2 repeat expansion in the first intronic region of *C9orf72* (DeJesus-Hernandez et al. 2011; Renton et al. 2011). ALS is also known as Lou Gehrig's disease or motor neuron disease (MND). This disease is a terminal illness that causes progressive death of motor neurons. With the increasing amount of dead motor neurons, the brain loses control of muscle movements. Hence, voluntary muscle action progressively fades in patients until muscles are completely paralyzed, typically leading to death within two to five years after onset (Boxer et al. 2011; Ringholz et al. 2005; Shi et al. 2018; Umoh et al. 2016). FTD is a progressive neurodegenerative disorder with progressive neuronal loss in the frontal and temporal lobes. Two major types of FTD are Behavior variant frontotemporal dementia (bvFTD), which features impairments in behavioral conduct, judgment, empathy, and foresight, and primary progressive aphasia (PPA), which presents with semantic or non-fluent/agrammatic language problems (Boxer et al. 2011; Ling et al. 2013; Neary et al. 1998).

There are three transcript variants of the *C9orf72* gene. For variants 1 and 3, the G4C2 repeat resides in the first intron between two alternatively spliced exons. In Variant 2 the rrpeat resides within the promoter(DeJesus-Hernandez et al. 2011; Renton et al. 2011). The G4C2 repeat sizes in healthy individuals are around 2-25, while C9 ALS/FTD patients typically have more than 20 repeats, with increases to more than a thousand repeats (Boxer et al. 2011). Transcription of the *C9orf72* gene is bidirectional, generating both

G4C2 and C4G2 repeat RNAs (Donnelly et al. 2013; Mizielinska et al. 2013; Xinmei et al. 2014; Zu et al. 2013). Both sense and antisense transcripts can support translation in multiple frames to generate toxic dipeptide repeat (DPR) proteins. These DPR, which are polyGA (glycine-alanine, GA), polyGP (glycine-proline, GP), and polyGR (glycine-arginine, GR) from the sense strand, and polyPA (proline-alanine, PA), polyPR (proline-arginine, PR), and again, polyGP (glycine-proline, GP) from the antisense strand (Ash et al. 2013; Gendron et al. 2013; Zu et al. 2013) - although it is worth noting that translation of PA and PR may utilize AUG codons for initiation. The relative levels of RAN products generated from different reading frames of the same repeat are quite different, suggesting that they may exhibit different rates of initiation and elongation (Cheng et al. 2018; Green et al. 2017). C9 RAN from linear transcripts is largely cap-dependent and relies on eIF4E and the eIF4A helicase (Cheng et al. 2018; Green et al. 2017). A near-cognate CUG codon upstream of the G4C2 repeat initiates the GA frame, while without ribosomes initiate at this CUG codon, ribosome scanning may continue in the GP and GR frame (Green et al. 2017). On the other hand, a bi-cistronic reporter system suggests that RAN translation in from G4C2 repeat can also occur through a cap-independent process by utilizing an IRES-like initiation mechanism in all reading frames (Cheng et al. 2018).

1.10. RAN Translation at CGG Repeats in FXTAS

Fragile X-associated tremor/ataxia syndrome (FXTAS) is an adult-onset neurodegenerative disease caused by an expansion of CGG repeats in the 5' UTR of the *FMR1* gene (Verkerk et al. 1991). FXTAS individuals carrying between 55 to 200 repeats of CGG are "permutation carriers" (Buijsen et al. 2014; Jacquemont et al. 2004; Pembrey

et al. 1985; Tassone et al. 2007). These premutation sized CGG repeat expansions are transcribed as part of *FMR1* RNA, which is toxic in model systems (Ajjugal, Kolimi, and Rathinavelan 2021; Todd et al. 2013). In contrast, in patients with more than 200 CGG repeats, the *FMR1* locus is transcriptionally silenced, leading to the loss of *FMR1* RNA and Fragile X protein (FMRP) (Pembrey et al. 1985). This causes Fragile X Syndrome- which is the most common monogenic cause of autism and intellectual disability. FXTAS patients are clinically characterized by intention tremor, ataxia, cognitive/intellectual decline, and inclusion of ubiquitinated aggregates in the cerebral cortex, brainstem, and cerebellum (Cronisteret al. 1991). Premutation women carriers are at risk of premature ovarian insufficiency (FXPOI) (Cronister et al. 1991). The CGG-expanded *FMR1* 5' UTR was found to support RAN translation initiation (Todd et al. 2013). In the absence of an AUG start codon, translation initiation from the 5' UTR generates FMRpolyG (glycine) and FMRpolyA (Alanine) from GGC (+1) and GCG (+2) reading frames respectively (Michael G. Kearse et al. 2016). FMRpolyG accumulates within ubiquitinated inclusions in neurons within patient tissues and animal models and in cultured human cells, including ovarian stromal cells in the FXTAS mouse model and FXPOI patients (Buijsen et al. 2016). RAN translation at CGG repeats is largely cap-dependent, utilizing both eIF4A and eIF4E in the scanning model but with different initiation codons across multiple reading frames in both in vitro assays and in transfected cells (Kearse et al. 2016).

1.11. RNA Secondary Structure and RNA Binding Proteins in G4C2 and CGG Repeats

CGG and G4C2 repeat RNAs can form both hairpin and G-quadruplex structures.

Whether it is a hairpin, G-quadruplex, or both *in vivo* remains enigmatic. For G4C2 repeats, Fratta et al. utilized biophysical approaches, including NMR and CD, and in silico computational analysis by QGRS mapper to show that G4C2 repeats readily form a G-quadruplex structure in vitro (Fratta et al. 2012). Later, Reddy et al. and Haeusler et al. demonstrated the RNA structure of G4C2 repeats as parallel-stranded G-quadruplexes, with potassium but not lithium further stabilizing the secondary structure (Haeusler et al. 2014; Reddy et al. 2013). These structured RNAs interact with RNA-binding proteins to form RNA foci. The RNA foci are mainly nuclear, but cytoplasmic foci are also observed in G4C2 repeat-expressing neurons. Conlon et al. showed that RNA foci containing hnRNPH colocalize with G-quadruplex RNA structures and found that this interaction is associated with disrupted splicing of the C9 transcript in the patient's brain (Conlon et al. 2016). On the other hand, Wang et al. suggested that RAN translation occurs most avidly on hairpin structures of G4C2 repeats and has the most biological relevance (Wang et al. 2019). Studies from both Reddy et al. and Haeusler et al. showed the antisense transcript CCCCGG (C4G2) forms hairpin structures by folding with K^+ ions, by CD spectroscopy, and EMSA. For CGG repeats, Ajjugal et al. showed that G-quadruplexes can form from the sense transcript CGG repeat and hairpins can from the antisense transcript GCC repeat by CD, EMSA, and molecular dynamics (MD) simulations (Ajjugal et al. 2021; Haeusler et al. 2014; Reddy et al. 2013). Asamitsu et al. showed CGG repeat RNA has a higher potential to form G-quadruplex formation, which later causes dysfunction of neurons (Asamitsu et al. 2021). By knowing the GC-rich repeat form RNA structures, studies have shown RNA secondary structures play a critical role in biological processing. However, the role of RNA secondary structure in RAN translation is still unclear.

1.12. Secondary Structure and RNA Helicases

DEAH-box helicase 36 (DHX36) is a DNA/RNA helicase known to bind and resolve the G-quadruplex structures. DHX36 resolves G-quadruplex structures mainly by its ATP hydrolase activity (Sauer et al. 2019; Tippana et al. 2019; Yangyuoru et al. 2018). Studies have shown the functions of DHX36 in post-transcriptional regulation including mRNA stability and translation. Sauer et al. found that DHX36 is recruited to stress granules to assist with the release of G-quadruplex containing mRNAs which are later targeted for degradation (Sauer et al. 2019). They also showed cells with complete deletion of DHX36 are prone to form stress granules. These suggested that DHX36 plays a role in maintaining cellular homeostasis, predominantly when G-quadruplex RNA induces cellular stress. DHX36 can regulate mRNA translation of both AUG and non-AUG. Murat et al. and Vester et al. utilized transcriptome-wide ribosome profiling to determine what transcripts are regulated by DHX36 (Murat et al. 2018; Vester et al. 2019). Both studies suggested that DHX36 unwinds G-quadruplex structures in 5'UTRs to assist translation with an increased expression level from the downstream ORF. Perhaps not surprisingly there are multiple studies demonstrating a role for DHX36 in cancer-related changes in gene expression (Matsumura et al. 2017; Wang et al. 2023; Zeng et al. 2020). Thus, RNA helicases can influence RNA translation on a genome wide scale.

Translation elongation through RNA secondary structures can cause ribosome stalling and/or ribosome collisions. Besides RNA structure, translating charged peptides, cellular stress, or damage is also known to cause ribosome stalling (Filbeck et al., 2022; Joazeiro 2017, 2019). When translation elongation slows down because of stalled or

collided ribosomes, it triggers splitting of the 80S ribosome into 60S and 40S subunits as sensed by ZNF598 and RACK1 (Garzia et al. 2017; Juszkiewicz et al. 2018; Sundaramoorthy et al. 2017). Subsequently, it induces mRNA and protein surveillance pathways that degrade aberrant mRNA and target partially made protein for proteasome degradation to maintain protein homeostasis in cells (Harigaya and Parker 2010; Matsuo et al. 2017, 2020; Orban and Izaurralde 2005). The ribosome-associate quality control (RQC) pathway is part of this mechanism that degrades the partially made nascent peptide and recycles the 60S subunit (Juszkiewicz and Hegde 2017; Matsuo et al. 2017; Shao and Hegde 2014; Shao et al. 2013). Formation of the RQC complex on the 60S subunit is one of the critical processes of this mechanism. When forming the RQC complex, it first recruits NEMF to the 60S (Mizuno et al. 2021; Shen et al. 2015; Yonashiro et al. 2016). It adds additional C-terminal Alanine and Threonine residues (CAT-tail) to the partially made nascent peptide and exposes it to the ribosome exit tunnel (Defenouillère et al. 2016; Howard and Frost 2021; Kostova et al. 2017; Lytvynenko et al. 2019; Rimal et al. 2021; Sitron and Brandman n.d.; Thrun et al. 2021; Udagawa et al. 2021). Listern (LTN1) is recruited to the RQC complex by NEMF to ubiquitinate the aberrant peptide outside of the ribosome exit tunnel for proteasome degradation (Choe et al. 2016; Chu et al. 2009; Shao et al. 2013). ANKZF1 assists downstream with peptidyl-tRNA hydrolase and/or nucleases activity to release the aberrant peptide for degradation (Huang et al. 2023; Kuroha et al. 2018; Verma et al. 2018).

RQC pathway dysfunction contributes to multiple neurodegenerative diseases (Ahmed et al. 2021; Chu et al. 2009; Martin et al. 2020) and CAT-tailing has been proposed as an important process that causes protein aggregation and neuronal death

(Lu et al. 2023; Udagawa et al. 2021). Previous studies have also shown that RQC plays an important role in regulating GR or PR DPR production due to translation of repetitive charged arginine that cause ribosome stalling (Park et al. 2021; Viera Ortiz et al. 2022). In these assays, depletion of RQC factors increases the production of GR protein generated from the peptide sequence **(Figure1.6.)**.

1.13. Modifiers of RAN Translation at C9orf72 and FMR1 Repeat Expansions

Multiple groups have identified regulators of RAN translations in both G4C2 and CGG repeats. Targeted candidate-based and genome-wide screens are common approaches to discover modifiers of repeats transcripts and RAN product-associated toxicity. Jovičić et al. performed two unbiased genome-wide gain- and loss-of-function screens in yeast of PR toxicity (Jovičić et al. 2015). Results from the screen reveal genes involved in nuclear import and export proteins and ribosomal RNA processing. They demonstrated the critical roles of genes in nucleocytoplasmic transport, mediating C9-related toxicity in yeast when overexpressed (Jovičić et al. 2015). Boeynaems et al. performed an unbiased screen in C9 ALS/FTD flies expressing 50 PR repeats (PR50) with results similar to those of Jovičić et al. (Boeynaems et al. 2016). DPR toxicity in these animals was enhanced upon knockdown of importins and exportins, Ran-GTP cycle regulators, nuclear pore components, and arginine methylases (Boeynaems et al. 2016). Kramer et al. performed a CRISPR-Cas9 screen in human cells and validated hits in primary neurons expressing PR20 and GR20 (Kramer et al. 2018). They discovered the endo-lysosomal trafficking gene, Rab7, and ER-resident transmembrane thioredoxin protein, Tmx2, as two of the top hits from the screen (Kramer et al. 2018). Knockout of

these genes protected against C9 DPR toxicity. Further, the depletion of Tmx2 in C9 patient-derived induced pluripotent stem cell (iPSC) neurons showed increased neuron survival (Kramer et al. 2018). Goodman et al. performed an unbiased large-scale RNA interference (RNAi)-based screen in *Drosophila melanogaster* expressing toxic 49 repeats of G4C2 (Goodman et al. 2019). From the screen, they discovered RNA polymerase II-associated factor 1 complex (PAF1C) as a regulator of RAN translation in G4C2 repeats 47 (Goodman et al. 2019). PAF1C is composed of *Paf1*, *Leo1*, *CDC73*, *Ctr9*, and *Rtf1* (Chen et al. 2022; Krogan et al. 2002; Nene et al. 2018; Ng, Dole, and Struhl 2003; Rodrigues and Lydall 2018; Xu et al. 2017). Downregulation of PAF1C affects the elongation rate of RNAPII (Yang et al. 2016). In *Drosophila*, among the component of *PAF1C*, downregulation of *dPAF1* and *dLeo1* suppresses the toxicity from $(G4C2)_{49}$ encoding-RNA, and is selective for transcription of long but not short G4C2 repeats (Goodman et al. 2019). A similar effect has been shown in *Saccharomyces cerevisiae* where *PAF1C* knockdown disturbs the transcription of G4C2 RNA (Goodman et al. 2019). Furthermore, upregulation of *PAF1C* was detected In fly, mouse, C9 human patient-derived iPSC, and C9 FTD patient tissue carrying expanded *C9orf72* repeats.

Yamada et al. performed a screen in yeast harboring $(G4C2)_{66}$ with a library of yeast mutants, including ribosomal subunit and other translation factors (Yamada et al. 2019). They identified small ribosomal protein subunit 25 (RPS25) playing a role in regulating G4C2 RAN translation. RPS25 is involved in several unconventional translation events, including IRES-mediated pathways by direct recruitment of 40S subunit to the IRES RNA and ribosomal shunting (Hertz et al. 2013; Landry, Hertz, and Thompson 2009). Compared to wild-type yeast, deletion of RPS25 decreases GP by 50% without

affecting GFP or the abundance of $(G4C2)_{66}$ RNA (Yamada et al. 2019). Linsalata *et al.* reported findings of modifiers in *FMR1* RAN translation by a targeted screen in flies (Linsalata et al. 2019). Downregulation of a DEAD-box RNA helicase, *belle/DDX3X* suppresses *FMR1* RAN translation in *Drosophila*, cultured human cells and decreases protein toxicity in *Drosophila* and primary rodent neurons (Linsalata et al. 2019). The effect of DDX3X is repeat length-dependent and extends across different reading frames. Knockdown of eIF4B and eIF4H also rescues the rough-eye phenotype caused by the repeat-induced toxicity. However, eIF4B and eIF4H are more likely to affect not only RAN translation but also global translation. eIF1 and eIF5 are critical for start codon fidelity during translational initiation. Overexpression of eIF1 and eIF5 in cultured human cells modulates RAN translation by enhancing AUG start codon specificity. Overexpression of eIF1 decreases the expression of $(CGG)_{100}$ in the +1 and +2 frames and decreases the expression of CUG-initiated transcripts. Interestingly, while inserting an AUG start codon into the transcript abolish the previous observation. These observations reveal that RNA secondary structure and start codon specificity mediate *FMR1* RAN translation (Linsalata et al. 2019). Our lab has performed a genome-wide siRNA screen on G4C2 and CGG repeats. We utilized a C-terminal nano-luciferase fuse with a 3xFLAG tag with upstream C9 intronic G4C2 70 repeats in the GA reading frame and FMR1 5'UTR CGG 100 repeats in the ployG frame to express RAN products in the HEK293 cells. Malik et al. developed a CGG repeat RNA-tagging system to capture RNA binding proteins of the CGG repeats with mass spectrometry in mammalian cells (Malik, et al. 2021). The results show a group of SR proteins and SR protein kinases (SRPKs) as key regulators of CGG repeats RNA showing SRPK1 as a potential modifier of repeat toxicity and RAN translation in CGG

repeats (Malik, et al. 2021). We also performed a genome-wide siRNA screen which the results from the genome-wide siRNA screen reveal a group of genes as proteasome subunits showing depletion of proteasome subunits decrease the production of RAN product. Surprisingly, a screen performed by Kramer et al. also revealed a group of proteasome subunits, knockdown of which decreases PR and GR toxicity in cells (Kramer et al. 2018). Another interesting hit is DOHH which is involved in the hypusination of eIF5A. Depletion of DOHH increases the production of RAN products. Multiple screens discovered potential therapeutic targets for C9 ALS/FTD and other nucleotide repeat expansion diseases. However, more mechanistic studies are required to understand how these regulators specifically modulate RNA translation thoroughly.

1.14. Conclusions and Open Questions

Nucleotide-repeat expansions underlie multiple neurodegenerative disorders, which currently have no effective treatments. Proposed pathogenic mechanisms in these disorders include loss of downstream protein function, RNA sequestration, and RAN translation. RAN translation produces toxic homopolymeric or dipeptide proteins that accumulate and aggregate across model systems, including *Drosophila*, mice, cultured human cells, patient tissues, and patient-derived iPSC neurons. The production of these toxic RAN proteins differs from the canonical translation of the ribosomal scanning model. It bypasses the recognition of the AUG start codon to initiate translation. However, the detailed mechanisms by which RAN translation occurs is still unclear. Identifying modifiers of RAN translation can inform our understanding of this novel translational initiation process. With the hypothesis that GC-rich repeat regions will cause pausing and

stalling of the ribosome during translation elongation, I looked into factors involved in unwinding the repeat RNA secondary structures and protein and mRNA surveillance pathways. I also conducted and then re-analyzed a genome-wide siRNA screen of potential modifiers of CGG and G4C2 RAN translation in human cells and found novel roles for the proteasome and hypusination of eIF5A in RAN translational processes. In sum, these data suggest that translation elongation through GC-rich regions are not smooth. Instead, it can trigger RQC pathways and generate short and truncated products that could contribute to neurodegeneration. Of note, ribosome collisions also trigger the ribo-toxic stress response and activate the GCN2-mediated integrated stress response pathways. Whether those pathways are also involved in the RAN translation of GC-rich transcripts remained unknown. Kinetics studies of RAN translation elongation within the GC-rich transcript can also help reveal how different frames translate RAN products and how the translation rate is related to ribosome collision. Other than understanding the process of RAN translation elongation, studies of finding critical selective targets that modulate RAN translation without altering global translation could provide potential therapeutic design in clinical trials.

1.15. Figures

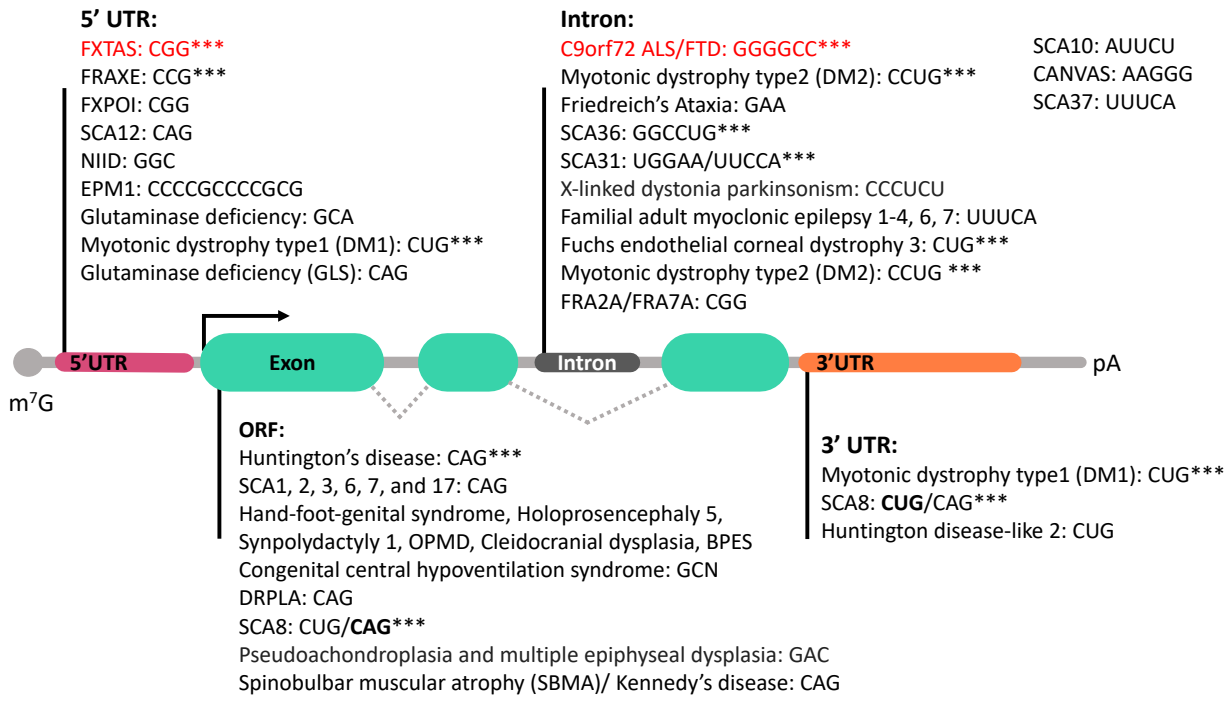

Figure 1-1. Short tandem repeats, RAN translation, and diseases

Short Tandem Repeat (STR) expansions cause more than 50 neurological disorders. Disease causing STRs can reside within gene coding exons, 5' UTRs, 3' UTRs, or introns. At least 10 STR expansions (marked with ***) trigger a non-canonical translational initiation process known as repeat-associated non-AUG (RAN) translation that generates toxic proteins from the STR region without an AUG-start codon and often in genomic contexts that are not normally associated with ribosomal engagement.

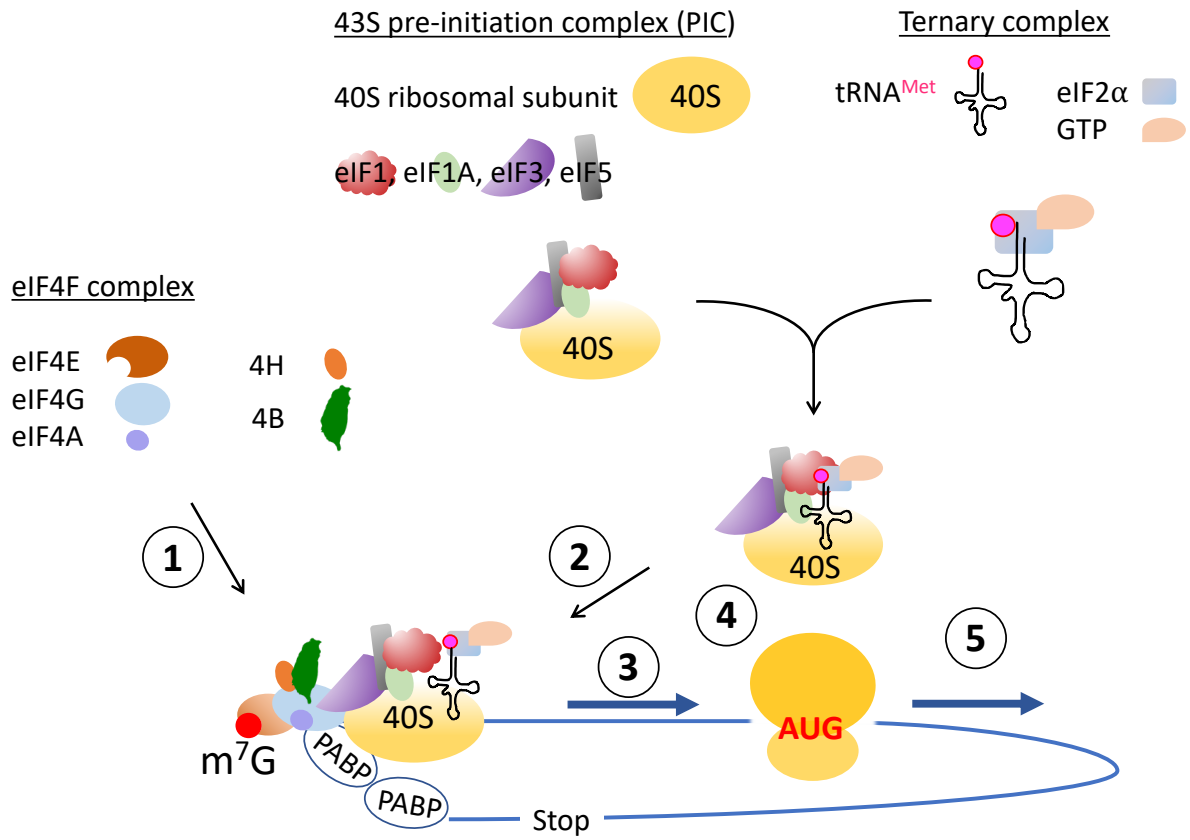

Figure 1-2. Canonical AUG-initiated translation

RNA Translational initiation at AUG start codons classically follows a 5' M7G cap-dependent scanning model that comprises several steps. First, eIF4E, eIF4G, and eIF4A composed the eIF4F complex, which binds to the 5' m7G (7 methyl-guanosine) cap with eIF4B and/or eIF4H. PABP (poly-adenosine binding protein) then associates with eIF4G to circularize the mRNA. Second, the eIF4F complex recruits the 43S PIC (preinitiation complex), which includes the 40S ribosomal subunit, eIF1, eIF1A, eIF3, eIF5, and the ternary complex, consisting of the initiator methionine-tRNA, eIF2, and GTP. Third, the 43S PIC and the eIF4F complex scan through the 5'UTR from 5' to 3' until the complex finds an AUG start codon within an ideal Kozak context. Fourth, by encountering an AUG start codon, eIF1 dissociates from the PIC, and eIF2 hydrolyzes GTP with the assistance

of eIF5, where the 60S is recruited to the 40S by eIF5B-GTP. eIF5B-GTP recruits 60S ribosomal subunit and detaches most eIFs (eukaryotic initiation factor). Finally, eIF5B hydrolyzes its bound GTP and establishes the elongation-competent 80S ribosomal subunit at the AUG start codon.

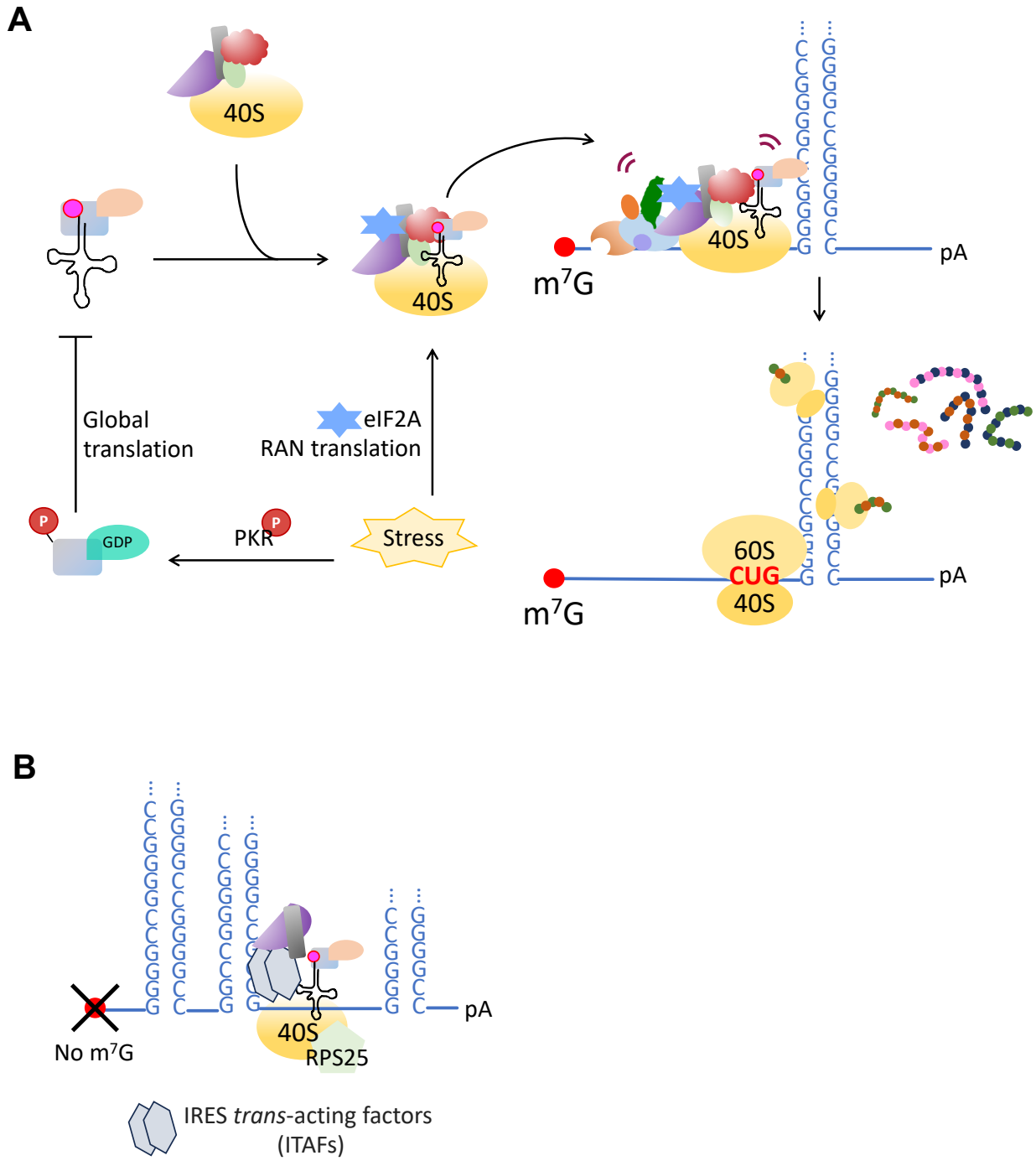

Figure 1-3. Repeat associated non-AUG initiated translation at GC rich repeats

RAN translation can proceed through two potentially distinct mechanisms. **(A)** In uORF-like RAN translation initiation, RAN translation begins in a cap-dependent manner like

canonical translational initiation. It requires the scanning of the 43S PIC and ternary complex along the 5'UTR. However, the repeat sequence triggers stalling of the scanning PIC, allowing for an increased dwell time of the complex at specific near-cognate start codons just upstream of the repeat. For example, a CUG codon just 5' to the G4C2 repeat is important for RAN translation of the GA DPR from this repeat in patients and reporters. This form of RAN translation is paradoxically activated by the integrated stress response (ISR), which triggers phosphorylation of eIF2α and typically inhibits global translation. **(B)** In IRES-like RAN translation, initiation starts with the repeat acting as an internal ribosome entry site (IRES) to initiate in a cap-independent manner. This form of translation is supported by the auxiliary 40S ribosomal subunit 25 (RPS25) and other IRES trans-acting factors (ITAFs) and initiation factors, including eIF3 and eIF5. The efficiency of this event is less than RAN translation from linear reporters. However, there is evidence that spliced lariats with repeats can evade degradation and escape to the cytoplasm. In these cases, an IRES-based mode of RAN translation is requisite as such mRNAs do not have an accessible 5' end.

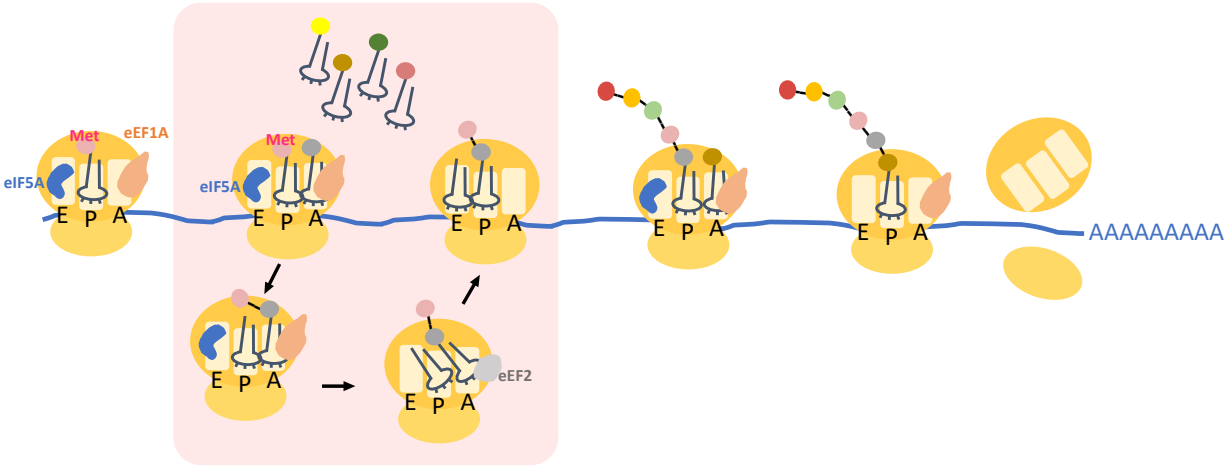

Figure 1-4. Translational elongation

Translation elongation begins after recognizing the AUG start codon and assembling the 80S ribosome at the AUG start codon. The first step of translation elongation is binding the methionyl-tRNA in the ribosomal P site with eIF5A at the E site and eEF1A at the A site. Aminoacyl-tRNA selection begins to find the match of their anticodon to the codon on mRNA. eEF1A assists matched aminoacyl-tRNA to load into the A site. Next, the peptide bond formation transfers the incoming amino acid to the growing peptide chain. This is the step in which that ribosome subunit rotates and tRNA transits into a “hybrid” state that crosses between the P/E and the A/P state. The rotated state of the ribosome recruits eEF2, another GTPase, to translocate the mRNA and tRNA complex back to the “classical” state with tRNAs in the E site and the P site. After releasing the empty tRNA from the E site, the elongation process repeats (pink block) until reaching a stop codon to terminate the process.

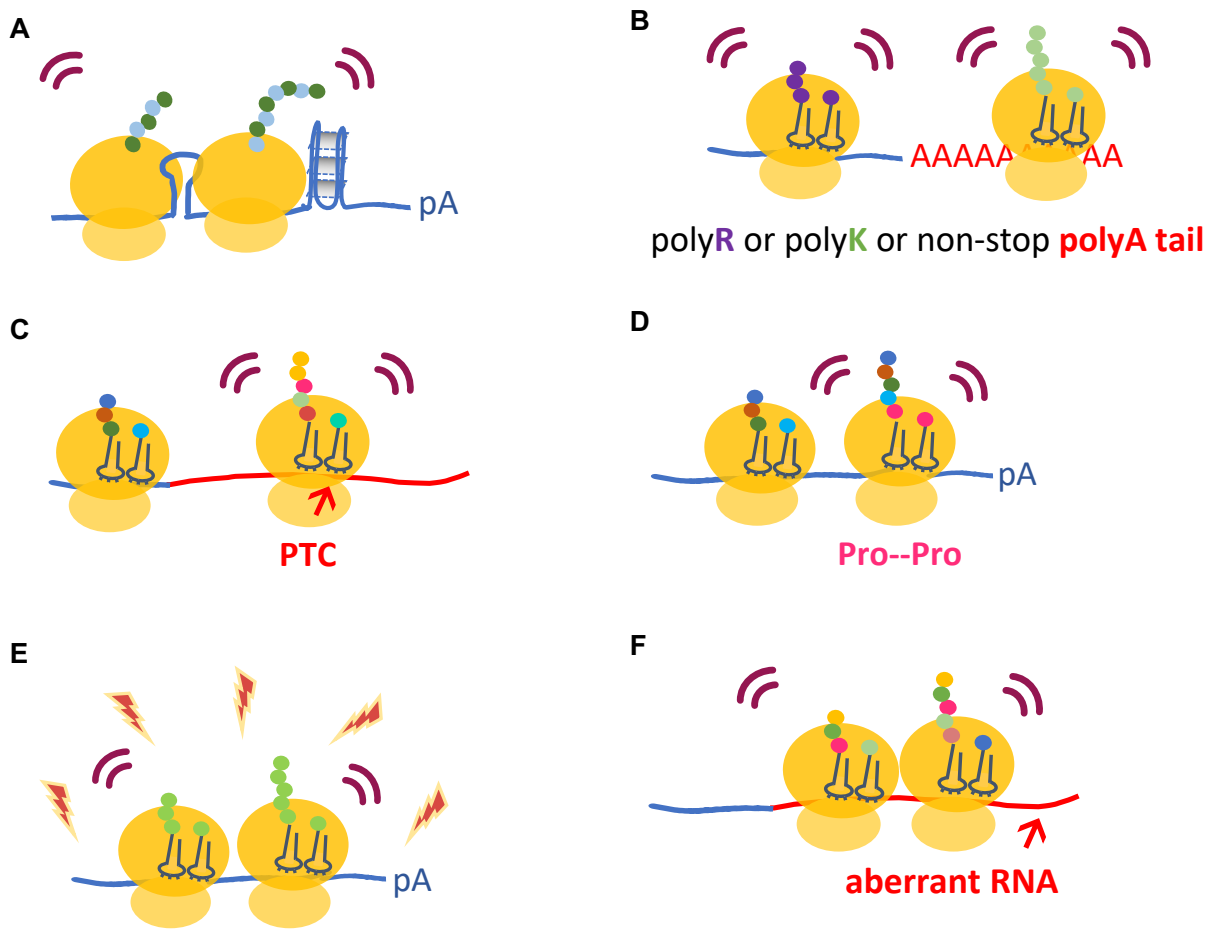

Figure 1-5. Triggers of ribosome stalling during translational elongation

Multiple circumstances can cause a slowdown in translational elongation. Ribosome stalling can be a temporary pause or can trigger irreversible ribosome collisions that activate other downstream mechanisms to resolve the event. Stalling of ribosomes can be caused by **(A)** RNA secondary structures, **(B)** the charge of the nascent peptide chain, or a polyA tail sequence (which also encodes a poly-lysine peptide chain), **(C)** pre-mature stop codons, **(D)** formation of Proline-Proline peptide bond, **(E)** cellular stresses such as osmotic stress and amino-acid depletion/starvation, and **(F)** encountering other aberrant "slippery" RNA sequences.

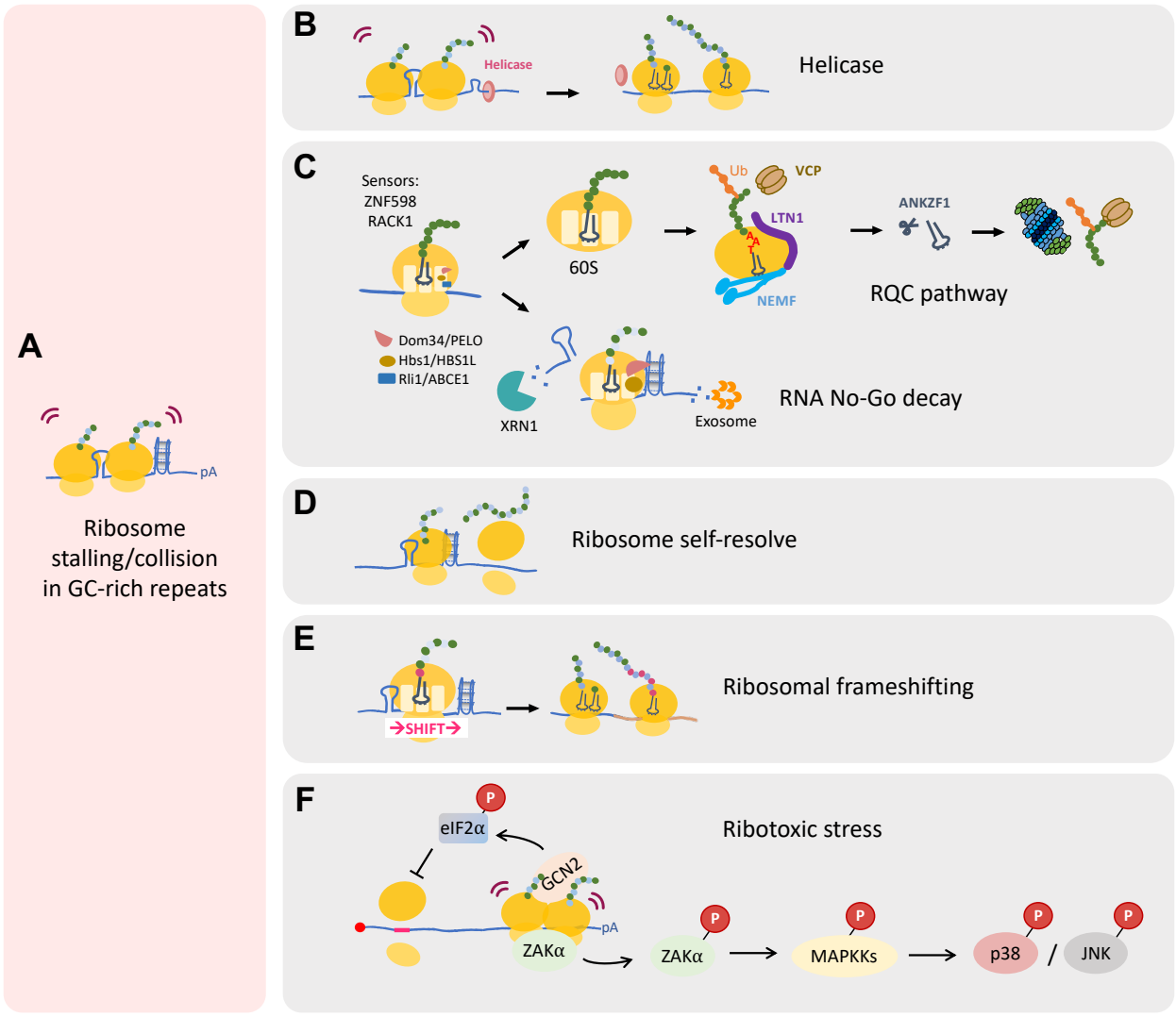

Figure 1-6. Ribosome stalling by GC-rich repeats

(A) GC-rich repeats form stable secondary structures, which cause ribosome stalling during translation elongation. Stalling of ribosomes during elongation can generate partially made products or full-length products by multiple downstream mechanisms. **(B)** Helicases such as DHX36, which binds and unwinds g-quadruplex structures, are proposed to resolve RNA secondary structures and facilitate translation elongation. **(C)** Stalling of ribosomes is sensed by RACK1 and ZNF598, which triggers mRNA and protein

surveillance pathways. These pathways include the ribosomal-associated quality control (RQC) pathway and RNA no-go decay pathway when RNA secondary structure is involved. The RQC pathway maintains protein homeostasis by degrading falsely made nascent chains by proteasome with key factors: NEMF, LTN1, ANKZF1, and VCP. While the no-go decay pathway degrades the aberrant RNA with Xrn1 and exosome. Both RQC and no-go decay pathways help recycle ribosomes to the translation machinery, which are surveillance pathways to rescue the stalling events. **(D)** Temporarily stalled ribosomes have also been proposed to self-resolve at certain conditions. However, the exact mechanism is still unknown. **(E)** When the ribosome stalls, it can cause a slippery moment that can shift the reading frame one or two nucleotides. This causes ribosomal frameshifting and results in generating of different chimeric peptides. **(F)** Stalling of ribosomes could trigger ribotoxic stress responses that activate ZAKα. Phosphorylated ZAKα activates GCN2 to phosphorylate eIF2α, therefore, inhibiting global translation. On the other hand, phosphorylated ZAKα also triggers the signaling pathway of phosphorylating MAPKKs and p38/JNK. However, whether stalling of RNA secondary structure is directly linked to ribotoxic stress response remains unclear.

1.16. References

Ajjugal Y, Kolimi N, Rathinavelan T. 2021. Secondary structural choice of DNA and RNA associated with CGG/CCG trinucleotide repeat expansion rationalizes the RNA misprocessing in FXTAS. Sci Rep 11. doi:10.1038/s41598-021-87097-y

Algire MA, Maag D, Lorsch JR. 2005. Pi release from eIF2, not GTP hydrolysis, is the step controlled by start-site selection during eukaryotic translation initiation. Mol Cell 20. doi:10.1016/j.molcel.2005.09.008

Alkalaeva EZ, Pisarev A V., Frolova LY, Kisselev LL, Pestova T V. 2006. In Vitro Reconstitution of Eukaryotic Translation Reveals Cooperativity between Release Factors eRF1 and eRF3. Cell 125. doi:10.1016/j.cell.2006.04.035

Asamitsu S, Yabuki Y, Ikenoshita S, Kawakubo K, Kawasaki M, Usuki S, Nakayama Y, Adachi K, Kugoh H, Ishii K, Matsuura T, Nanba E, Sugiyama H, Fukunaga K, Shioda N. 2021. CGG repeat RNA G-quadruplexes interact with FMRpolyG to cause neuronal dysfunction in fragile X-related tremor/ataxia syndrome. Sci Adv. doi:10.1126/sciadv.abd9440

Asano K. 1999. Conserved bipartite motifs in yeast eIF5 and eIF2Bepsilon , GTPase-activating and GDP-GTP exchange factors in translation initiation, mediate binding to their common substrate eIF2. EMBO J 18. doi:10.1093/emboj/18.6.1673

Asano K, Clayton J, Shalev A, Hinnebusch AG. 2000. A multifactor complex of eukaryotic initiation factors, eIF1, eIF2, eIF3, eIF5, and initiator tRNA(Met) is an important translation initiation intermediate in vivo. Genes Dev 14. doi:10.1101/gad.831800

Ash PEA, Bieniek KF, Gendron TF, Caulfield T, Lin W-L, DeJesus-Hernandez M, van Blitterswijk MM, Jansen-West K, Paul JW, Rademakers R, Boylan KB, Dickson

DW, Petrucelli L. 2013. Unconventional Translation of C9ORF72 GGGGCC Expansion Generates Insoluble Polypeptides Specific to c9FTD/ALS, Neuron. doi:10.1016/j.neuron.2013.02.004

Bañez-Coronel M, Ayhan F, Tarabochia AD, Zu T, Perez BA, Tusi SK, Pletnikova O, Borchelt DR, Ross CA, Margolis RL, Yachnis AT, Troncoso JC, Ranum LPW. 2015. RAN Translation in Huntington Disease. Neuron 88:667–677. doi:10.1016/j.neuron.2015.10.038

Bañez-Coronel M, Porta S, Kagerbauer B, Mateu-Huertas E, Pantano L, Ferrer I, Guzmán M, Estivill X, Martí E. 2012. A pathogenic mechanism in huntington's disease involves small CAG-repeated RNAs with neurotoxic activity. PLoS Genet 8. doi:10.1371/journal.pgen.1002481

Bao C, Loerch S, Ling C, Korostelev AA, Grigorieff N, Ermolenko DN. 2020. mRNA stem-loops can pause the ribosome by hindering A-site tRNA binding. Elife 9. doi:10.7554/eLife.55799

Bao C, Zhu M, Nykonchuk I, Wakabayashi H, Mathews DH, Ermolenko DN. 2022. Specific length and structure rather than high thermodynamic stability enable regulatory mRNA stem-loops to pause translation. Nat Commun 13. doi:10.1038/s41467-022-28600-5

Becker T, Armache JP, Jarasch A, Anger AM, Villa E, Sieber H, Motaal BA, Mielke T, Berninghausen O, Beckmann R. 2011. Structure of the no-go mRNA decay complex Dom34-Hbs1 bound to a stalled 80S ribosome. Nat Struct Mol Biol 18. doi:10.1038/nsmb.2057

Behrmann E, Loerke J, Budkevich T V., Yamamoto K, Schmidt A, Penczek PA, Vos MR, Bürger J, Mielke T, Scheerer P, Spahn CMT. 2015. Structural snapshots of actively translating human ribosomes. Cell 161. doi:10.1016/j.cell.2015.03.052

Beringer M, Rodnina M V. 2007. The Ribosomal Peptidyl Transferase. Mol Cell. doi:10.1016/j.molcel.2007.03.015

Boeynaems S, Bogaert E, Michiels E, Gijselinck I, Sieben A, Jovičić A, De Baets G, Scheveneels W, Steyaert J, Cuijt I, Verstrepen KJ, Callaerts P, Rousseau F, Schymkowitz J, Cruts M, Van Broeckhoven C, Van Damme P, Gitler AD, Robberecht W, Van Den Bosch L. 2016. Drosophila screen connects nuclear transport genes to DPR pathology in c9ALS/FTD. Sci Rep 6. doi:10.1038/srep20877

Bogorad AM, Lin KY, Marintchev A. 2017. Novel mechanisms of eIF2B action and regulation by eIF2 phosphorylation. Nucleic Acids Res 45. doi:10.1093/nar/gkx845

Boivin M, Pfister V, Gaucherot A, Ruffenach F, Negroni L, Sellier C, Charlet-Berguerand N. 2020. Reduced autophagy upon C9ORF72 loss synergizes with dipeptide repeat protein toxicity in G4C2 repeat expansion disorders. EMBO J 39. doi:10.15252/embj.2018100574

Borman AM. 2000. Biochemical characterisation of cap-poly(A) synergy in rabbit reticulocyte lysates: the eIF4G-PABP interaction increases the functional affinity of eIF4E for the capped mRNA 5'-end. Nucleic Acids Res 28:4068–4075. doi:10.1093/nar/28.21.4068

Boxer AL, Mackenzie IR, Boeve BF, Baker M, Seeley WW, Crook R, Feldman H, Hsiung G-YR, Rutherford N, Laluz V, Whitwell J, Foti D, McDade E, Molano J, Karydas A,

Wojtas A, Goldman J, Mirsky J, Sengdy P, DeArmond S, Miller BL, Rademakers R. 2011. Clinical, neuroimaging and neuropathological features of a new chromosome 9p-linked FTD-ALS family. J Neurol Neurosurg Psychiatry 82:196–203. doi:10.1136/jnnp.2009.204081

Budkevich T, Giesebrecht J, Altman RB, Munro JB, Mielke T, Nierhaus KH, Blanchard SC, Spahn CMT. 2011. Structure and dynamics of the mammalian ribosomal pretranslocation complex. Mol Cell 44. doi:10.1016/j.molcel.2011.07.040

Buijsen RAM, Sellier C, Severijnen LAWFM, Oulad-Abdelghani M, Verhagen RFM, Berman RF, Charlet-Berguerand N, Willemsen R, Hukema RK. 2014. FMRpolyG-positive inclusions in CNS and non-CNS organs of a fragile X premutation carrier with fragile X-associated tremor/ataxia syndrome. Acta Neuropathol Commun. doi:10.1186/s40478-014-0162-2

Buijsen RAM, Visser JA, Kramer P, Severijnen EAWFM, Gearing M, Charlet-Berguerand N, Sherman SL, Berman RF, Willemsen R, Hukema RK. 2016. Presence of inclusions positive for polyglycine containing protein, FMRpolyG, indicates that repeat-associated non-AUG translation plays a role in fragile X-associated primary ovarian insufficiency. Human Reproduction 31:158–168. doi:10.1093/humrep/dev280

Burguete AS, Almeida S, Gao FB, Kalb R, Akins MR, Bonini NM. 2015. GGGGCC microsatellite RNA is neuritically localized, induces branching defects, and perturbs transport granule function. Elife 4. doi:10.7554/eLife.08881

Carvalho MDGDC, Carvalho JF, Merrick WC. 1984. Biological characterization of various forms of elongation factor 1 from rabbit reticulocytes. Arch Biochem Biophys 234. doi:10.1016/0003-9861(84)90310-2

Çetin B, O'Leary SE. 2022. MRNA-and factor-driven dynamic variability controls eIF4F-cap recognition for translation initiation. Nucleic Acids Res 50. doi:10.1093/nar/gkac631

Chandrasekaran V, Juszkiewicz S, Choi J, Puglisi JD, Brown A, Shao S, Ramakrishnan V, Hegde RS. 2019. Mechanism of ribosome stalling during translation of a poly(A) tail. Nat Struct Mol Biol 26. doi:10.1038/s41594-019-0331-x

Chappell SA, Edelman GM, Mauro VP. 2006. Ribosomal tethering and clustering as mechanisms for translation initiation. Proceedings of the National Academy of Sciences 103:18077–18082. doi:10.1073/pnas.0608212103

Chen F, Liu B, Zhou H, Long J. 2022. The Paf1 complex is required for RNA polymerase II removal in response to DNA damage. Proc Natl Acad Sci U S A 119. doi:10.1073/pnas.2207332119

Chen L, Muhlrad D, Hauryliuk V, Cheng Z, Lim MK, Shyp V, Parker R, Song H. 2010. Structure of the Dom34-Hbs1 complex and implications for no-go decay. Nat Struct Mol Biol 17. doi:10.1038/nsmb.1922

Cheng W, Wang S, Mestre AA, Fu C, Makarem A, Xian F, Hayes LR, Lopez-Gonzalez R, Drenner K, Jiang J, Cleveland DW, Sun S. 2018. C9ORF72 GGGGCC repeat-associated non-AUG translation is upregulated by stress through eIF2α phosphorylation. Nat Commun. doi:10.1038/s41467-017-02495-z

Choe YJ, Park SH, Hassemer T, Körner R, Vincenz-Donnelly L, Hayer-Hartl M, Hartl FU. 2016. Failure of RQC machinery causes protein aggregation and proteotoxic stress. Nature 531. doi:10.1038/nature16973

Chu D, Kazana E, Bellanger N, Singh T, Tuite MF, Von Der Haar T. 2014. Translation elongation can control translation initiation on eukaryotic mRNAs. EMBO Journal 33. doi:10.1002/embj.201385651

Chu J, Hong NA, Masuda CA, Jenkins B V., Nelms KA, Goodnow CC, Glynne RJ, Wu H, Masliah E, Joazeiro CAP, Kay SA. 2009. A mouse forward genetics screen identifies LISTERIN as an E3 ubiquitin ligase involved in neurodegeneration. Proc Natl Acad Sci U S A 106. doi:10.1073/pnas.0812819106

Cleary JD, Ranum LPW. 2013. Repeat-associated non-ATG (RAN) translation in neurological disease. Hum Mol Genet 22. doi:10.1093/hmg/ddt371

Coffee B, Zhang F, Ceman S, Warren ST, Reines D. 2002. Histone Modifications Depict an Aberrantly Heterochromatinized FMR1 Gene in Fragile X Syndrome. Am J Hum Genet 71. doi:10.1086/342931

Conlon EG, Lu L, Sharma A, Yamazaki T, Tang T, Shneider NA, Manley JL. 2016. The C9ORF72 GGGGCC expansion forms RNA G-quadruplex inclusions and sequesters hnRNP H to disrupt splicing in ALS brains. Elife 5. doi:10.7554/eLife.17820

Conlon EG, Manley JL. 2017. RNA-binding proteins in neurodegeneration: Mechanisms in aggregate. Genes Dev 31:1509–1528. doi:10.1101/gad.304055.117

Cooper-Knock J, Higginbottom A, Stopford MJ, Highley JR, Ince PG, Wharton SB, Pickering-Brown S, Kirby J, Hautbergue GM, Shaw PJ. 2015. Antisense RNA foci

in the motor neurons of C9ORF72-ALS patients are associated with TDP-43 proteinopathy. Acta Neuropathol 130. doi:10.1007/s00401-015-1429-9

Coots RA, Liu XM, Mao Y, Dong L, Zhou J, Wan J, Zhang X, Qian SB. 2017. m6A Facilitates eIF4F-Independent mRNA Translation. Mol Cell 68. doi:10.1016/j.molcel.2017.10.002

Cronister A, Schreiner R, Wittenberger M, Amiri K, Harris K, Hagerman RJ. 1991. Heterozygous fragile X female: Historical, physical, cognitive, and cytogenetic features. Am J Med Genet 38:269–274. doi:10.1002/ajmg.1320380221

Das S, Ghosh R, Maitra U. 2001. Eukaryotic Translation Initiation Factor 5 Functions as a GTPase-activating Protein. Journal of Biological Chemistry 276:6720–6726. doi:10.1074/JBC.M008863200

Davies JE, Rubinsztein DC. 2006. Polyalanine and polyserine frameshift products in Huntington's disease. J Med Genet 43:893–896. doi:10.1136/jmg.2006.044222

De Mezer M, Wojciechowska M, Napierala M, Sobczak K, Krzyzosiak WJ. 2011. Mutant CAG repeats of Huntingtin transcript fold into hairpins, form nuclear foci and are targets for RNA interference. Nucleic Acids Res 39. doi:10.1093/nar/gkq1323

Defenouillère Q, Zhang E, Namane A, Mouaikel J, Jacquier A, Fromont-Racine M. 2016. Rqc1 and ltn1 prevent c-terminal alanine-threonine tail (cat-tail)-induced protein aggregation by efficient recruitment of cdc48 on stalled 60s subunits. Journal of Biological Chemistry 291. doi:10.1074/jbc.M116.722264

DeJesus-Hernandez M, Mackenzie IR, Boeve BF, Boxer AL, Baker M, Rutherford NJ, Nicholson AM, Finch NA, Flynn H, Adamson J, Kouri N, Wojtas A, Sengdy P, Hsiung G-YR, Karydas A, Seeley WW, Josephs KA, Coppola G, Geschwind DH,

Wszolek ZK, Feldman H, Knopman DS, Petersen RC, Miller BL, Dickson DW, Boylan KB, Graff-Radford NR, Rademakers R. 2011. Expanded GGGGCC Hexanucleotide Repeat in Noncoding Region of C9ORF72 Causes Chromosome 9p-Linked FTD and ALS. Neuron 72:245–256. doi:10.1016/j.neuron.2011.09.011

Dever TE, Dinman JD, Green R. 2019. Translation Elongation and Recoding in Eukaryotes Overview of Translation Elongation HHS Public Access. Cold Spring Harb Perspect Biol 10.

Dever TE, Green R. 2012. The Elongation, Termination, and Recycling Phases of Translation in Eukaryotes. Cold Spring Harb Perspect Biol 4:a013706–a013706. doi:10.1101/cshperspect.a013706

Djumagulov M, Demeshkina N, Jenner L, Rozov A, Yusupov M, Yusupova G. 2021. Accuracy mechanism of eukaryotic ribosome translocation. Nature 600. doi:10.1038/s41586-021-04131-9

Doerfel LK, Wohlgemuth I, Kothe C, Peske F, Urlaub H, Rodnina M V. 2013. EF-P is essential for rapid synthesis of proteins containing consecutive proline residues. Science (1979) 339. doi:10.1126/science.1229017

Doerfel LK, Wohlgemuth I, Kubyshkin V, Starosta AL, Wilson DN, Budisa N, Rodnina M V. 2015. Entropic contribution of elongation factor P to proline positioning at the catalytic center of the ribosome. J Am Chem Soc 137. doi:10.1021/jacs.5b07427

Doma MK, Parker R. 2006. Endonucleolytic cleavage of eukaryotic mRNAs with stalls in translation elongation. Nature 440. doi:10.1038/nature04530

Donnelly CJ, Zhang PW, Pham JT, Heusler AR, Mistry NA, Vidensky S, Daley EL, Poth EM, Hoover B, Fines DM, Maragakis N, Tienari PJ, Petrucelli L, Traynor BJ, Wang

J, Rigo F, Bennett CF, Blackshaw S, Sattler R, Rothstein JD. 2013. RNA Toxicity from the ALS/FTD C9ORF72 Expansion Is Mitigated by Antisense Intervention. Neuron 80:415–428. doi:10.1016/j.neuron.2013.10.015

Duttler S, Pechmann S, Frydman J. 2013. Principles of cotranslational ubiquitination and quality control at the ribosome. Mol Cell 50. doi:10.1016/j.molcel.2013.03.010

Farg MA, Konopka A, Soo KY, Ito D, Atkin JD. 2017. The DNA damage response (DDR) is induced by the C9orf72 repeat expansion in amyotrophic lateral sclerosis. Hum Mol Genet 26. doi:10.1093/hmg/ddx170

Fernández IS, Bai X-C, Murshudov G, Scheres SHW, Ramakrishnan V. 2014. Initiation of Translation by Cricket Paralysis Virus IRES Requires Its Translocation in the Ribosome. Cell 157:823–831. doi:10.1016/j.cell.2014.04.015

Filbeck S, Cerullo F, Pfeffer S, Joazeiro CAP. 2022. Ribosome-associated quality-control mechanisms from bacteria to humans. Mol Cell. doi:10.1016/j.molcel.2022.03.038

Fischer N, Neumann P, Konevega AL, Bock L V., Ficner R, Rodnina M V., Stark H. 2015. Structure of the E. coli ribosome-EF-Tu complex at <3 Å resolution by Cs-corrected cryo-EM. Nature 520. doi:10.1038/nature14275

Fratta P, Mizielinska S, Nicoll AJ, Zloh M, Fisher EMC, Parkinson G, Isaacs AM. 2012. C9orf72 hexanucleotide repeat associated with amyotrophic lateral sclerosis and frontotemporal dementia forms RNA G-quadruplexes. Sci Rep. doi:10.1038/srep01016

Frolova L, Goff XLE, Zhouravleva G, Davydova E, Philippe M, Kisselev L. 1996. Eukaryotic polypeptide chain release factor eRF3 is an eRF1- and ribosome-dependent guanosine triphosphatase. RNA 2.

Frolova LY, Tsivkovskii RY, Sivolobova GF, Oparina NY, Serpinsky OI, Blinov VM, Tatkov SI, Kisselev LL. 1999. Mutations in the highly conserved GGQ motif of class I polypeptide release factors abolish ability of human eRF1 to trigger peptidyl-tRNA hydrolysis. RNA 5. doi:10.1017/S135583829999043X

Fujino Y, Mori K, Nagai Y. 2023. Repeat-associated non-AUG translation in neuromuscular diseases: mechanisms and therapeutic insights. The Journal of Biochemistry. doi:10.1093/jb/mvad012

Gao FB, Richter JD. 2017. Microsatellite Expansion Diseases: Repeat Toxicity Found in Translation. Neuron. doi:10.1016/j.neuron.2017.01.001

Garzia A, Jafarnejad SM, Meyer C, Chapat C, Gogakos T, Morozov P, Amiri M, Shapiro M, Molina H, Tuschl T, Sonenberg N. 2017. The E3 ubiquitin ligase and RNA-binding protein ZNF598 orchestrates ribosome quality control of premature polyadenylated mRNAs. Nat Commun 8. doi:10.1038/ncomms16056

Gendron TF, Bieniek KF, Zhang Y-J, Jansen-West K, Ash PEA, Caulfield T, Daughrity L, Dunmore JH, Castanedes-Casey M, Chew J, Cosio DM, van Blitterswijk M, Lee WC, Rademakers R, Boylan KB, Dickson DW, Petrucelli L. 2013. Antisense transcripts of the expanded C9ORF72 hexanucleotide repeat form nuclear RNA foci and undergo repeat-associated non-ATG translation in c9FTD/ALS. Acta Neuropathol 126:829–844. doi:10.1007/s00401-013-1192-8

Georgakopoulos-Soares I, Parada GE, Hemberg M. 2022. Secondary structures in RNA synthesis, splicing and translation. Comput Struct Biotechnol J. doi:10.1016/j.csbj.2022.05.041

Gingras AC, Gygi SP, Raught B, Polakiewicz RD, Abraham RT, Hoekstra MF, Aebersold R, Sonenberg N. 1999. Regulation of 4E-BP1 phosphorylation: A novel two step mechanism. Genes Dev 13. doi:10.1101/gad.13.11.1422

Gitler AD, Tsuiji H. 2016. There has been an awakening: Emerging mechanisms of C9orf72 mutations in FTD/ALS. Brain Res 1647:19–29. doi:10.1016/j.brainres.2016.04.004

Goodman LD, Prudencio M, Kramer NJ, Martinez-Ramirez LF, Srinivasan AR, Lan M, Parisi MJ, Zhu Y, Chew J, Cook CN, Berson A, Gitler AD, Petrucelli L, Bonini NM. 2019. Toxic expanded GGGGCC repeat transcription is mediated by the PAF1 complex in C9orf72-associated FTD. Nat Neurosci. doi:10.1038/s41593-019-0396-1

Gradi A, Imataka H, Svitkin Y V., Rom E, Raught B, Morino S, Sonenberg N. 1998. A Novel Functional Human Eukaryotic Translation Initiation Factor 4G. Mol Cell Biol 18. doi:10.1128/mcb.18.1.334

Green KM, Glineburg MR, Kearse MG, Flores BN, Linsalata AE, Fedak SJ, Goldstrohm AC, Barmada SJ, Todd PK. 2017. RAN translation at C9orf72-associated repeat expansions is selectively enhanced by the integrated stress response. Nat Commun 8. doi:10.1038/s41467-017-02200-0

Gusella JF, MacDonald ME. 1996. Trinucleotide instability: A repeating theme in human inherited disorders. Annu Rev Med. doi:10.1146/annurev.med.47.1.201

Gutierrez E, Shin BS, Woolstenhulme CJ, Kim JR, Saini P, Buskirk AR, Dever TE. 2013. eif5A promotes translation of polyproline motifs. Mol Cell 51. doi:10.1016/j.molcel.2013.04.021

Haeusler AR, Donnelly CJ, Periz G, Simko EAJ, Shaw PG, Kim M-S, Maragakis NJ, Troncoso JC, Pandey A, Sattler R, Rothstein JD, Wang J. 2014. C9orf72 nucleotide repeat structures initiate molecular cascades of disease. Nature 507:195–200. doi:10.1038/nature13124

Hanson A, Hanson G, Alhusaini N, Morris N, Sweet T, Coller J. 2018. Translation elongation and mRNA stability are coupled through the ribosomal A-site Shortened title: Ribosomal A-site decoding determines mRNA stability. Rna.

Harigaya Y, Parker R. 2010. No-go decay: A quality control mechanism for RNA in translation. Wiley Interdiscip Rev RNA. doi:10.1002/wrna.17

He F, Li X, Spatrick P, Casillo R, Dong S, Jacobson A. 2003. Genome-Wide Analysis of mRNAs Regulated by the Nonsense-Mediated and 5′ to 3′ mRNA Decay Pathways in Yeast. Mol Cell 12. doi:10.1016/S1097-2765(03)00446-5

He F, Todd P. 2011. Epigenetics in Nucleotide Repeat Expansion Disorders. Semin Neurol 31:470–483. doi:10.1055/s-0031-1299786

He L, Liang J, Chen C, Chen J, Shen Y, Sun S, Li L. 2023. C9orf72 functions in the nucleus to regulate DNA damage repair. Cell Death Differ 30. doi:10.1038/s41418-022-01074-0

Hellen CUT, Sarnow P. 2001. Internal ribosome entry sites in eukaryotic mRNA molecules. Genes Dev 15:1593–1612. doi:10.1101/gad.891101

Hertz MI, Landry DM, Willis AE, Luo G, Thompson SR. 2013. Ribosomal Protein S25 Dependency Reveals a Common Mechanism for Diverse Internal Ribosome Entry Sites and Ribosome Shunting. Mol Cell Biol 33. doi:10.1128/mcb.00879-12

Hinnebusch AG. 2014. The scanning mechanism of eukaryotic translation initiation. Annu Rev Biochem. doi:10.1146/annurev-biochem-060713-035802

Howard CJ, Frost A. 2021. Critical Reviews in Biochemistry and Molecular Biology Ribosome-associated quality control and CAT tailing. doi:10.1080/10409238.2021.1938507

Huang H, Yang X, Tao L, Xiang R, Yang H. 2023. Identification of a de novo heterozygous mutation of ANKZF1 in a Chinese patient with inflammatory bowel disease . QJM: An International Journal of Medicine. doi:10.1093/qjmed/hcad030

Huter P, Arenz S, Bock L V., Graf M, Frister JO, Heuer A, Peil L, Starosta AL, Wohlgemuth I, Peske F, Nováček J, Berninghausen O, Grubmüller H, Tenson T, Beckmann R, Rodnina M V., Vaiana AC, Wilson DN. 2017. Structural Basis for Polyproline-Mediated Ribosome Stalling and Rescue by the Translation Elongation Factor EF-P. Mol Cell 68. doi:10.1016/j.molcel.2017.10.014

Ikeuchi K, Tesina P, Matsuo Y, Sugiyama T, Cheng J, Saeki Y, Tanaka K, Becker T, Beckmann R, Inada T. 2019. Collided ribosomes form a unique structural interface to induce Hel2-driven quality control pathways. EMBO J 38. doi:10.15252/embj.2018100276

Inada T. 2019. tRNA recycling on stalled ribosomes. Nat Struct Mol Biol 26. doi:10.1038/s41594-019-0222-1

Izidoro MS, Sokabe M, Villa N, Merrick WC, Fraser CS. 2022. Human eukaryotic initiation factor 4E (eIF4E) and the nucleotide-bound state of eIF4A regulate eIF4F binding to RNA. Journal of Biological Chemistry 298. doi:10.1016/j.jbc.2022.102368

JACKSON RJ. 1991. The ATP requirement for initiation of eukaryotic translation varies according to the mRNA species. Eur J Biochem 200:285–294. doi:10.1111/j.1432-1033.1991.tb16184.x

Jackson RJ, Hellen CUT, Pestova T V. 2012. Termination and post-termination events in eukaryotic translationAdvances in Protein Chemistry and Structural Biology. doi:10.1016/B978-0-12-386497-0.00002-5

Jackson RJ, Hellen CUT, Pestova T V. 2010. The mechanism of eukaryotic translation initiation and principles of its regulation. Nat Rev Mol Cell Biol 11:113–127. doi:10.1038/nrm2838

Jacquemont S, Hagerman RJ, Leehey MA, Hall DA, Levine RA, Brunberg JA, Zhang L, Jardini T, Gane LW, Harris SW, Herman K, Grigsby J, Greco CM, Berry-Kravis E, Tassone F, Hagerman PJ. 2004. Penetrance of the Fragile X-Associated Tremor/Ataxia Syndrome in a Premutation Carrier Population. JAMA 291. doi:10.1001/jama.291.4.460

James Kent W, Sugnet CW, Furey TS, Roskin KM, Pringle TH, Zahler AM, Haussler D. 2002. The human genome browser at UCSC. Genome Res 12. doi:10.1101/gr.229102. Article published online before print in May 2002

JAN E, THOMPSON SR, WILSON JE, PESTOVA TV, HELLEN CUT, SARNOW P. 2001. Initiator Met-tRNA-independent Translation Mediated by an Internal Ribosome Entry Site Element in Cricket Paralysis Virus-like Insect Viruses. Cold Spring Harb Symp Quant Biol 66:285–292. doi:10.1101/sqb.2001.66.285

Joazeiro CAP. 2019. Mechanisms and functions of ribosome-associated protein quality control. Nat Rev Mol Cell Biol 20:368–383. doi:10.1038/s41580-019-0118-2

Joazeiro CAP. 2017. Ribosomal stalling during translation: Providing substrates for ribosome-associated protein quality control. Annu Rev Cell Dev Biol. doi:10.1146/annurev-cellbio-111315-125249

Jovičić A, Mertens J, Boeynaems S, Bogaert E, Chai N, Yamada SB, Paul JW, Sun S, Herdy JR, Bieri G, Kramer NJ, Gage FH, Van Den Bosch L, Robberecht W, Gitler AD. 2015. Modifiers of C9orf72 dipeptide repeat toxicity connect nucleocytoplasmic transport defects to FTD/ALS. Nat Neurosci 18:1226–1229. doi:10.1038/nn.4085

Juszkiewicz S, Chandrasekaran V, Lin Z, Kraatz S, Ramakrishnan V, Hegde RS. 2018. ZNF598 Is a Quality Control Sensor of Collided Ribosomes. Mol Cell 72. doi:10.1016/j.molcel.2018.08.037

Juszkiewicz S, Hegde RS. 2017. Initiation of Quality Control during Poly(A) Translation Requires Site-Specific Ribosome Ubiquitination. Mol Cell 65. doi:10.1016/j.molcel.2016.11.039

Juszkiewicz S, Slodkowicz G, Lin Z, Freire-Pritchett P, Peak-Chew SY, Hegde RS. 2020. Ribosome collisions trigger cis-acting feedback inhibition of translation initiation. Elife 9. doi:10.7554/eLife.60038

Kahvejian A. 2005. Mammalian poly(A)-binding protein is a eukaryotic translation initiation factor, which acts via multiple mechanisms. Genes Dev 19:104–113. doi:10.1101/gad.1262905

Kearse Michael G., Green KM, Krans A, Rodriguez CM, Linsalata AE, Goldstrohm AC, Todd PK. 2016. CGG Repeat-Associated Non-AUG Translation Utilizes a Cap-

Dependent Scanning Mechanism of Initiation to Produce Toxic Proteins. Mol Cell. doi:10.1016/j.molcel.2016.02.034

Kearse Michael G., Green KM, Krans A, Rodriguez CM, Linsalata AE, Goldstrohm AC, Todd PK. 2016. CGG Repeat-Associated Non-AUG Translation Utilizes a Cap-Dependent Scanning Mechanism of Initiation to Produce Toxic Proteins. Mol Cell 62:314–322. doi:10.1016/j.molcel.2016.02.034

Kedersha N, Chen S, Gilks N, Li W, Miller IJ, Stahl J, Anderson P. 2002. Evidence that ternary complex (eIF2-GTP-tRNAiMet)-Deficient preinitiation complexes are core constituents of mammalian stress granules. Mol Biol Cell 13. doi:10.1091/mbc.01-05-0221

Kessler SH, Sachs AB. 1998. RNA Recognition Motif 2 of Yeast Pab1p Is Required for Its Functional Interaction with Eukaryotic Translation Initiation Factor 4G. Mol Cell Biol 18:51–57. doi:10.1128/MCB.18.1.51

Kieft JS, Zhou K, Jubin R, Doudna JA. 2001. Mechanism of ribosome recruitment by hepatitis C IRES RNA. RNA 7. doi:10.1017/S1355838201001790

Kimball SR. 1999. Eukaryotic initiation factor eIF2. International Journal of Biochemistry and Cell Biology 31. doi:10.1016/S1357-2725(98)00128-9

Komar AA, Hatzoglou M. 2011. Cellular IRES-mediated translation: The war of ITAFs in pathophysiological states. Cell Cycle. doi:10.4161/cc.10.2.14472

Komar AA, Hatzoglou M. 2005. Internal ribosome entry sites in cellular mRNAs: Mystery of their existence. Journal of Biological Chemistry 280:23425–23428. doi:10.1074/jbc.R400041200

Koob MD, Moseley ML, Schut LJ, Benzow KA, Bird TD, Day JW, Ranum LPW. 1999. An untranslated CTG expansion causes a novel form of spinocerebellar ataxia (SCA8). Nat Genet 21. doi:10.1038/7710

Koromilas AE, Lazaris-Karatzas A, Sonenberg N. 1992. mRNAs containing extensive secondary structure in their 5' non-coding region translate efficiently in cells overexpressing initiation factor eIF-4E. EMBO Journal 11. doi:10.1002/j.1460-2075.1992.tb05508.x

Kostova KK, Hickey KL, Osuna BA, Hussmann JA, Frost A, Weinberg DE, Weissman JS. 2017. CAT-tailing as a fail-safe mechanism for efficient degradation of stalled nascent polypeptides.

Kozak M. 1986. Influences of mRNA secondary structure on initiation by eukaryotic ribosomes. Proceedings of the National Academy of Sciences 83:2850–2854. doi:10.1073/pnas.83.9.2850

Kozak M. 1978. How do eucaryotic ribosomes select initiation regions in messenger RNA? Cell. doi:10.1016/0092-8674(78)90039-9

Kramer NJ, Haney MS, Morgens DW, Jovičić A, Couthouis J, Li A, Ousey J, Ma R, Bieri G, Tsui CK, Shi Y, Hertz NT, Tessier-Lavigne M, Ichida JK, Bassik MC, Gitler AD. 2018. CRISPR-Cas9 screens in human cells and primary neurons identify modifiers of C9ORF72 dipeptide-repeat-protein toxicity. Nat Genet 50. doi:10.1038/s41588-018-0070-7

Kriachkov V, Ormsby AR, Kusnadi EP, McWilliam HEG, Mintern JD, Amarasinghe SL, Ritchie ME, Furic L, Hatters DM. 2023. Arginine-rich C9ORF72 ALS proteins stall ribosomes in a manner distinct from a canonical ribosome-associated quality

control substrate. Journal of Biological Chemistry 299. doi:10.1016/j.jbc.2022.102774

Krogan NJ, Kim M, Ahn SH, Zhong G, Kobor MS, Cagney G, Emili A, Shilatifard A, Buratowski S, Greenblatt JF. 2002. RNA Polymerase II Elongation Factors of Saccharomyces cerevisiae : a Targeted Proteomics Approach . Mol Cell Biol 22. doi:10.1128/mcb.22.20.6979-6992.2002

Kuroha K, Zinoviev A, Hellen CUT, Pestova T V. 2018. Release of Ubiquitinated and Non-ubiquitinated Nascent Chains from Stalled Mammalian Ribosomal Complexes by ANKZF1 and Ptrh1. Mol Cell 72. doi:10.1016/j.molcel.2018.08.022

Lafrenière RG, Rochefort DL, Chrétien N, Rommens JM, Cochius JI, Kälviäinen R, Nousiainen U, Patry G, Farrell K, Söderfeldt B, Federico A, Hale BR, Cossio OH, Sørensen T, Pouliot MA, Kmiec T, Uldall P, Janszky J, Pranzatelli MR, Andermann F, Andermann E, Rouleau GA. 1997. Unstable insertion in the 5' flanking region of the cystatin B gene is the most common mutation in progressive myoclonus epilepsy type 1, EPM1. Nat Genet 15. doi:10.1038/ng0397-298

Landau G, Bercovich Z, Park MH, Kahana C. 2010. The role of polyamines in supporting growth of mammalian cells is mediated through their requirement for translation initiation and elongation. Journal of Biological Chemistry 285. doi:10.1074/jbc.M110.106419

Landry DM, Hertz MI, Thompson SR. 2009. RPS25 is essential for translation initiation by the Dicistroviridae and hepatitis C viral IRESs. Genes Dev 23. doi:10.1101/gad.1832209

Lin Y, Dent SYR, Wilson JH, Wells RD, Napierala M. 2010. R loops stimulate genetic instability of CTG·CAG repeats. Proc Natl Acad Sci U S A 107. doi:10.1073/pnas.0909740107

Ling SC, Polymenidou M, Cleveland DW. 2013. Converging mechanisms in als and FTD: Disrupted RNA and protein homeostasis. Neuron. doi:10.1016/j.neuron.2013.07.033

Linsalata AE, He F, Malik AM, Glineburg MR, Green KM, Natla S, Flores BN, Krans A, Archbold HC, Fedak SJ, Barmada SJ, Todd PK. 2019. DDX 3X and specific initiation factors modulate FMR 1 repeat-associated non-AUG-initiated translation . EMBO Rep 1–18. doi:10.15252/embr.201847498

Liquori CL, Ricker K, Moseley ML, Jacobsen JF, Kress W, Naylor SL, Day JW, Ranum LPW. 2001. Myotonic dystrophy type 2 caused by a CCTG expansion in intron I of ZNF9. Science (1979) 293. doi:10.1126/science.1062125

Liu EY, Russ J, Wu K, Neal D, Suh E, McNally AG, Irwin DJ, Van Deerlin VM, Lee EB. 2014. C9orf72 hypermethylation protects against repeat expansion-associated pathology in ALS/FTD. Acta Neuropathol 128. doi:10.1007/s00401-014-1286-y

Liu H, Lu Y-N, Paul T, Periz G, Banco MT, Ferré-D'Amaré AR, Rothstein JD, Hayes LR, Myong S, Wang J. 2021. A Helicase Unwinds Hexanucleotide Repeat RNA G-Quadruplexes and Facilitates Repeat-Associated Non-AUG Translation. J Am Chem Soc 143:7368–7379. doi:10.1021/jacs.1c00131

Lozano G, Martínez-Salas E. 2015. Structural insights into viral IRES-dependent translation mechanisms. Curr Opin Virol. doi:10.1016/j.coviro.2015.04.008

Lu B. 2023. Translation stalling and ribosome collision leading to proteostasis failure: implications for neurodegenerative diseases. Neural Regen Res 18. doi:10.4103/1673-5374.340404

Lytvynenko I, Paternoga H, Thrun A, Balke A, Müller TA, Chiang CH, Nagler K, Tsaprailis G, Anders S, Bischofs I, Maupin-Furlow JA, Spahn CMT, Joazeiro CAP. 2019. Alanine Tails Signal Proteolysis in Bacterial Ribosome-Associated Quality Control. Cell 178. doi:10.1016/j.cell.2019.05.002

Lyu X, Yang Q, Zhao F, Liu Y. 2021. Codon usage and protein length-dependent feedback from translation elongation regulates translation initiation and elongation speed. Nucleic Acids Res 49. doi:10.1093/nar/gkab729

Malik I, Kelley CP, Wang ET, Todd PK. 2021a. Molecular mechanisms underlying nucleotide repeat expansion disorders. Nat Rev Mol Cell Biol 22:589–607. doi:10.1038/s41580-021-00382-6

Malik I, Tseng Y, Wright SE, Zheng K, Ramaiyer P, Green KM, Todd PK. 2021b. SRSF protein kinase 1 modulates RAN translation and suppresses CGG repeat toxicity. EMBO Mol Med 13:1–21. doi:10.15252/emmm.202114163

Margolis RL, McInnis MG, Rosenblatt A, Ross CA. 1999. Trinucleotide repeat expansion and neuropsychiatric disease. Arch Gen Psychiatry. doi:10.1001/archpsyc.56.11.1019

Matsumura K, Kawasaki Y, Miyamoto M, Kamoshida Y, Nakamura J, Negishi L, Suda S, Akiyama T. 2017. The novel G-quadruplex-containing long non-coding RNA GSEC antagonizes DHX36 and modulates colon cancer cell migration. Oncogene 36. doi:10.1038/onc.2016.282

Matsuo Y, Ikeuchi K, Saeki Y, Iwasaki S, Schmidt C, Udagawa T, Sato F, Tsuchiya H, Becker T, Tanaka K, Ingolia NT, Beckmann R, Inada T. 2017. Ubiquitination of stalled ribosome triggers ribosome-associated quality control. Nat Commun 8. doi:10.1038/s41467-017-00188-1

Matsuo Y, Tesina P, Nakajima S, Mizuno M, Endo A, Buschauer R, Cheng J, Shounai O, Ikeuchi K, Saeki Y, Becker T, Beckmann R, Inada T. 2020. RQT complex dissociates ribosomes collided on endogenous RQC substrate SDD1. Nat Struct Mol Biol 27. doi:10.1038/s41594-020-0393-9

Matsuo Y, Uchihashi T, Inada T. 2023. Decoding of the ubiquitin code for clearance of colliding ribosomes by the RQT complex. Nat Commun 14. doi:10.1038/s41467-022-35608-4

Mauger DM, Cabral BJ, Presnyak V, Su S V, Reid DW, Goodman B, Link K, Khatwani N, Reynders J, Moore MJ, McFadyen IJ. 2019. mRNA structure regulates protein expression through changes in functional half-life. Proc Natl Acad Sci U S A 116:24075–24083. doi:10.1073/pnas.1908052116

Mechanism THE, Eukaryotic OF, Initiation T, Of P, Regulation ITS. 2010. the Mechanism of Eukaryotic Translation Initiation. Nat Rev Mol Cell Biol 11:113–127. doi:10.1038/nrm2838.THE

Miller JW, Urbinati CR, Teng-Umnuay P, Stenberg MG, Byrne BJ, Thornton CA, Swanson MS. 2000. Recruitment of human muscleblind proteins to (CUG)(n) expansions associated with myotonic dystrophy. EMBO Journal 19. doi:10.1093/emboj/19.17.4439

Miller-Fleming L, Olin-Sandoval V, Campbell K, Ralser M. 2015. Remaining Mysteries of Molecular Biology: The Role of Polyamines in the Cell. J Mol Biol. doi:10.1016/j.jmb.2015.06.020

Mirkin SM. 2007. Expandable DNA repeats and human disease. Nature 447:932–940. doi:10.1038/nature05977

Mizielinska S, Lashley T, Norona FE, Clayton EL, Ridler CE, Fratta P, Isaacs AM. 2013. C9orf72 frontotemporal lobar degeneration is characterised by frequent neuronal sense and antisense RNA foci. Acta Neuropathol 126:845–857. doi:10.1007/s00401-013-1200-z

Mizuno M, Ebine S, Shounai O, Nakajima S, Tomomatsu S, Ikeuchi K, Matsuo Y, Inada T. 2021. The nascent polypeptide in the 60S subunit determines the Rqc2-dependency of ribosomal quality control. Nucleic Acids Res 49:2102–2113. doi:10.1093/nar/gkab005

Moazed D, Noller HF. 1989. Intermediate states in the movement of transfer RNA in the ribosome. Nature 342. doi:10.1038/342142a0

Mori Kohji, Arzberger T, Grässer FA, Gijselinck I, May S, Rentzsch K, Weng S-M, Schludi MH, van der Zee J, Cruts M, Van Broeckhoven C, Kremmer E, Kretzschmar HA, Haass C, Edbauer D. 2013. Bidirectional transcripts of the expanded C9orf72 hexanucleotide repeat are translated into aggregating dipeptide repeat proteins. Acta Neuropathol 126:881–893. doi:10.1007/s00401-013-1189-3

Mori K., Weng S-M, Arzberger T, May S, Rentzsch K, Kremmer E, Schmid B, Kretzschmar HA, Cruts M, Van Broeckhoven C, Haass C, Edbauer D. 2013. The C9orf72

GGGGCC Repeat Is Translated into Aggregating Dipeptide-Repeat Proteins in FTLD/ALS. Science (1979) 339:1335–1338. doi:10.1126/science.1232927

Murat P, Marsico G, Herdy B, Ghanbarian A, Portella G, Balasubramanian S. 2018. RNA G-quadruplexes at upstream open reading frames cause DHX36- and DHX9-dependent translation of human mRNAs. Genome Biol. doi:10.1186/s13059-018-1602-2

Nagafuchi S, Yanagisawa H, Ohsaki E, Shirayama T, Tadokoro K, Inoue T, Yamada M. 1994. Structure and expression of the gene responsible for the triplet repeat disorder, dentatorubral and pallidoluysian atrophy (DRPLA). Nat Genet 8. doi:10.1038/ng1094-177

Nagarajan VK, Jones CI, Newbury SF, Green PJ. 2013. XRN 5'→3' exoribonucleases: Structure, mechanisms and functions. Biochim Biophys Acta Gene Regul Mech. doi:10.1016/j.bbagrm.2013.03.005

Neary D, Snowden JS, Gustafson L, Passant U, Stuss D, Black S, Freedman M, Kertesz A, Robert PH, Albert M, Boone K, Miller BL, Cummings J, Benson DF. 1998. Frontotemporal lobar degeneration: A consensus on clinical diagnostic criteria. Neurology 51:1546–1554. doi:10.1212/WNL.51.6.1546

Negrutskii BS, Shalak VF, Novosylna O V., Porubleva L V., Lozhko DM, El'skaya A V. 2023. The eEF1 family of mammalian translation elongation factors. BBA Advances 3. doi:10.1016/j.bbadva.2022.100067

Nelson DL, Orr HT, Warren ST. 2013. The unstable repeats-Three evolving faces of neurological disease. Neuron. doi:10.1016/j.neuron.2013.02.022

Nene R V., Putnam CD, Li BZ, Nguyen KG, Srivatsan A, Campbell CS, Desai A, Kolodner RD. 2018. Cdc73 suppresses genome instability by mediating telomere homeostasis. PLoS Genet 14. doi:10.1371/journal.pgen.1007170

Ng HH, Dole S, Struhl K. 2003. The Rtf1 Component of the Paf1 Transcriptional Elongation Complex Is Required for Ubiquitination of Histone H2B. Journal of Biological Chemistry 278. doi:10.1074/jbc.C300270200

Nishimura AL, Arias N. 2021. Synaptopathy Mechanisms in ALS Caused by C9orf72 Repeat Expansion. Front Cell Neurosci. doi:10.3389/fncel.2021.660693

Orban TI, Izaurralde E. 2005. Decay of mRNAs targeted by RISC requires XRN1, the Ski complex, and the exosome. RNA 11. doi:10.1261/rna.7231505

Orr HT, Zoghbi HY. 2007. Trinucleotide Repeat Disorders. Annu Rev Neurosci 30:575–621. doi:10.1146/annurev.neuro.29.051605.113042

Park J, Lee Jongbo, Kim JH, Lee Jongbin, Park H, Lim C. 2021. ZNF598 co-translationally titrates poly(GR) protein implicated in the pathogenesis of C9ORF72-associated ALS/FTD. Nucleic Acids Res 49. doi:10.1093/nar/gkab834

Park MH, Kar RK, Banka S, Ziegler A, Chung WK. 2022. Post-translational formation of hypusine in eIF5A: implications in human neurodevelopment. Amino Acids. doi:10.1007/s00726-021-03023-6

Paulson H. 2018. Repeat expansion diseases, Handbook of Clinical Neurology. doi:10.1016/B978-0-444-63233-3.00009-9

Pavlov MY, Watts RE, Tan Z, Cornish VW, Ehrenberg M, Forster AC. 2009. Slow peptide bond formation by proline and other N-alkylamino acids in translation. Proc Natl Acad Sci U S A 106. doi:10.1073/pnas.0809211106

Pembrey ME, Winter RM, Davies KE, Opitz JM, Reynolds JF. 1985. A premutation that generates a defect at crossing over explains the inheritance of fragile X mental retardation. Am J Med Genet 21:709–717. doi:10.1002/ajmg.1320210413

Pestova T V. 2002. The roles of individual eukaryotic translation initiation factors in ribosomal scanning and initiation codon selection. Genes Dev 16:2906–2922. doi:10.1101/gad.1020902

Pestova T V., Lomakin IB, Hellen CUT. 2004. Position of the CrPV IRES on the 40S subunit and factor dependence of IRES/80S ribosome assembly. EMBO Rep 5:906–913. doi:10.1038/sj.embor.7400240

Pestova T V., Lomakin IB, Lee JH, Choi SK, Dever TE, Hellen CUT. 2000. The joining of ribosomal subunits in eukaryotes requires eIF5B. Nature 403. doi:10.1038/35002118

Pestova T V, Shatsky IN, Hellen CU. 1996. Functional dissection of eukaryotic initiation factor 4F: the 4A subunit and the central domain of the 4G subunit are sufficient to mediate internal entry of 43S preinitiation complexes. Mol Cell Biol 16. doi:10.1128/mcb.16.12.6870

Petrucelli L, Dawson TM. 2004. Mechanism of neurodegenerative disease: Role of the ubiquitin proteasome system. Ann Med 36:315–320. doi:10.1080/07853890410031948

Phan L, Zhang X, Asano K, Anderson J, Vornlocher H-P, Greenberg JR, Qin J, Hinnebusch AG. 1998. Identification of a Translation Initiation Factor 3 (eIF3) Core Complex, Conserved in Yeast and Mammals, That Interacts with eIF5. Mol Cell Biol 18. doi:10.1128/mcb.18.8.4935

Pisarev A V., Skabkin MA, Pisareva VP, Skabkina O V., Rakotondrafara AM, Hentze MW, Hellen CUT, Pestova T V. 2010. The Role of ABCE1 in Eukaryotic Posttermination Ribosomal Recycling. Mol Cell 37. doi:10.1016/j.molcel.2009.12.034

Pisareva VP, Skabkin MA, Hellen CUT, Pestova T V., Pisarev A V. 2011. Dissociation by Pelota, Hbs1 and ABCE1 of mammalian vacant 80S ribosomes and stalled elongation complexes. EMBO Journal 30:1804–1817. doi:10.1038/emboj.2011.93

Pop C, Rouskin S, Ingolia NT, Han L, Phizicky EM, Weissman JS, Koller D. 2014. Causal signals between codon bias, mRNA structure, and the efficiency of translation and elongation . Mol Syst Biol 10. doi:10.15252/msb.20145524

Preker P, Nielsen J, Kammler S, Lykke-Andersen S, Christensen MS, Mapendano CK, Schierup MH, Jensen TH. 2008. RNA exosome depletion reveals transcription upstream of active human promoters. Science (1979) 322:1851–1854. doi:10.1126/science.1164096

Puleston DJ, Buck MD, Klein Geltink RI, Kyle RL, Caputa G, O'Sullivan D, Cameron AM, Castoldi A, Musa Y, Kabat AM, Zhang Y, Flachsmann LJ, Field CS, Patterson AE, Scherer S, Alfei F, Baixauli F, Austin SK, Kelly B, Matsushita M, Curtis JD, Grzes KM, Villa M, Corrado M, Sanin DE, Qiu J, Pällman N, Paz K, Maccari ME, Blazar BR, Mittler G, Buescher JM, Zehn D, Rospert S, Pearce EJ, Balabanov S, Pearce EL. 2019. Polyamines and eIF5A Hypusination Modulate Mitochondrial Respiration and Macrophage Activation. Cell Metab 30. doi:10.1016/j.cmet.2019.05.003

Pyronnet S, Imataka H, Gingras AC, Fukunaga R, Hunter T, Sonenberg N. 1999. Human eukaryotic translation initiation factor 4G (eIF4G) recruits Mnk1 to phosphorylate eIF4E. EMBO Journal 18. doi:10.1093/emboj/18.1.270

Reddy K, Zamiri B, Stanley SYR, Macgregor RB, Pearson CE. 2013. The disease-associated r(GGGGCC)n repeat from the C9orf72 gene forms tract length-dependent uni- and multimolecular RNA G-quadruplex structures. Journal of Biological Chemistry 288. doi:10.1074/jbc.C113.452532

Renton AE, Majounie E, Waite A, Simón-Sánchez J, Rollinson S, Gibbs JR, Schymick JC, Laaksovirta H, van Swieten JC, Myllykangas L, Kalimo H, Paetau A, Abramzon Y, Remes AM, Kaganovich A, Scholz SW, Duckworth J, Ding J, Harmer DW, Hernandez DG, Johnson JO, Mok K, Ryten M, Trabzuni D, Guerreiro RJ, Orrell RW, Neal J, Murray A, Pearson J, Jansen IE, Sondervan D, Seelaar H, Blake D, Young K, Halliwell N, Callister JB, Toulson G, Richardson A, Gerhard A, Snowden J, Mann D, Neary D, Nalls MA, Peuralinna T, Jansson L, Isoviita V-M, Kaivorinne A-L, Hölttä-Vuori M, Ikonen E, Sulkava R, Benatar M, Wuu J, Chiò A, Restagno G, Borghero G, Sabatelli M, Heckerman D, Rogaeva E, Zinman L, Rothstein JD, Sendtner M, Drepper C, Eichler EE, Alkan C, Abdullaev Z, Pack SD, Dutra A, Pak E, Hardy J, Singleton A, Williams NM, Heutink P, Pickering-Brown S, Morris HR, Tienari PJ, Traynor BJ. 2011. A Hexanucleotide Repeat Expansion in C9ORF72 Is the Cause of Chromosome 9p21-Linked ALS-FTD. Neuron 72:257–268. doi:10.1016/J.NEURON.2011.09.010

Riba A, Nanni N Di, Mittal N, Arhné E, Schmidt A, Zavolan M. 2019. Protein synthesis rates and ribosome occupancies reveal determinants of translation elongation rates. Proc Natl Acad Sci U S A 116. doi:10.1073/pnas.1817299116

Rimal S, Li Y, Vartak R, Geng J, Tantray I, Li S, Huh S, Vogel H, Glabe C, Grinberg LT, Spina S, Seeley WW, Guo S, Lu B. 2021. Inefficient quality control of ribosome stalling during APP synthesis generates CAT-tailed species that precipitate hallmarks of Alzheimer's disease. Acta Neuropathol Commun 9. doi:10.1186/s40478-021-01268-6

Ringholz GM, Appel SH, Bradshaw M, Cooke NA, Mosnik DM, Schulz PE. 2005. Prevalence and patterns of cognitive impairment in sporadic ALS. Neurology 65:586–590. doi:10.1212/01.wnl.0000172911.39167.b6

Rodrigues J, Lydall D. 2018. Paf1 and Ctr9, core components of the PAF1 complex, maintain low levels of telomeric repeat containing RNA. Nucleic Acids Res 46. doi:10.1093/nar/gkx1131

Rodriguez CM, Todd PK. 2019. New pathologic mechanisms in nucleotide repeat expansion disorders. Neurobiol Dis. doi:10.1016/j.nbd.2019.104515

Russ J, Liu EY, Wu K, Neal D, Suh ER, Irwin DJ, McMillan CT, Harms MB, Cairns NJ, Wood EM, Xie SX, Elman L, McCluskey L, Grossman M, Van Deerlin VM, Lee EB. 2015. Hypermethylation of repeat expanded C9orf72 is a clinical and molecular disease modifier. Acta Neuropathol 129. doi:10.1007/s00401-014-1365-0

Saint-Léger A, Ribas De Pouplana L. 2015. The importance of codon-anticodon interactions in translation elongation. Biochimie. doi:10.1016/j.biochi.2015.04.013

Saito S, Hosoda N, Hoshino SI. 2013. The Hbs1-Dom34 protein complex functions in non-stop mRNA decay in mammalian cells. Journal of Biological Chemistry 288:17832–17843. doi:10.1074/jbc.M112.448977

Salas-Marco J, Bedwell DM. 2004. GTP Hydrolysis by eRF3 Facilitates Stop Codon Decoding during Eukaryotic Translation Termination. Mol Cell Biol 24. doi:10.1128/mcb.24.17.7769-7778.2004

Sato N, Amino T, Kobayashi K, Asakawa S, Ishiguro T, Tsunemi T, Takahashi M, Matsuura T, Flanigan KM, Iwasaki S, Ishino F, Saito Y, Murayama S, Yoshida M, Hashizume Y, Takahashi Y, Tsuji S, Shimizu N, Toda T, Ishikawa K, Mizusawa H. 2009. Spinocerebellar Ataxia Type 31 Is Associated with “Inserted” Penta-Nucleotide Repeats Containing (TGGAA)n. Am J Hum Genet 85. doi:10.1016/j.ajhg.2009.09.019

Sauer M, Juranek SA, Marks J, De Magis A, Kazemier HG, Hilbig D, Benhalevy D, Wang X, Hafner M, Paeschke K. 2019. DHX36 prevents the accumulation of translationally inactive mRNAs with G4-structures in untranslated regions. Nat Commun. doi:10.1038/s41467-019-10432-5

Schmidt C, Becker T, Heuer A, Braunger K, Shanmuganathan V, Pech M, Berninghausen O, Wilson DN, Beckmann R. 2015. Structure of the hypusinylated eukaryotic translation factor eIF-5A bound to the ribosome. Nucleic Acids Res 44. doi:10.1093/nar/gkv1517

Schnier J, Schwelberger HG, Smit-McBride Z, Kang HA, Hershey JW. 1991. Translation initiation factor 5A and its hypusine modification are essential for cell viability in the yeast Saccharomyces cerevisiae. Mol Cell Biol 11. doi:10.1128/mcb.11.6.3105

Schuller AP, Green R. 2018. Roadblocks and resolutions in eukaryotic translation. Nat Rev Mol Cell Biol. doi:10.1038/s41580-018-0011-4

Schuller AP, Wu CCC, Dever TE, Buskirk AR, Green R. 2017. eIF5A Functions Globally in Translation Elongation and Termination. Mol Cell 66. doi:10.1016/j.molcel.2017.03.003

Schwab SR, Shugart JA, Horng T, Malarkannan S, Shastri N. 2004. Unanticipated antigens: Translation initiation at CUG with leucine. PLoS Biol 2. doi:10.1371/journal.pbio.0020366

Sellier C, Buijsen RAM, He F, Natla S, Jung L, Tropel P, Gaucherot A, Jacobs H, Meziane H, Vincent A, Champy MF, Sorg T, Pavlovic G, Wattenhofer-Donze M, Birling MC, Oulad-Abdelghani M, Eberling P, Ruffenach F, Joint M, Anheim M, Martinez-Cerdeno V, Tassone F, Willemsen R, Hukema RK, Viville S, Martinat C, Todd PK, Charlet-Berguerand N. 2017. Translation of Expanded CGG Repeats into FMRpolyG Is Pathogenic and May Contribute to Fragile X Tremor Ataxia Syndrome. Neuron. doi:10.1016/j.neuron.2016.12.016

Sendoel A, Dunn JG, Rodriguez EH, Naik S, Gomez NC, Hurwitz B, Levorse J, Dill BD, Schramek D, Molina H, Weissman JS, Fuchs E. 2017. Translation from unconventional 5′ start sites drives tumour initiation. Nature 541:494–499. doi:10.1038/nature21036

Sha Z, Brill LM, Cabrera R, Kleifeld O, Scheliga JS, Glickman MH, Chang EC, Wolf DA. 2009. The eIF3 Interactome Reveals the Translasome, a Supercomplex Linking Protein Synthesis and Degradation Machineries. Mol Cell. doi:10.1016/j.molcel.2009.09.026

Shao S, Hegde RS. 2014. Reconstitution of a Minimal Ribosome-Associated Ubiquitination Pathway with Purified Factors. Mol Cell 55. doi:10.1016/j.molcel.2014.07.006

Shao S, Murray J, Brown A, Taunton J, Ramakrishnan V, Hegde RS. 2016. Decoding Mammalian Ribosome-mRNA States by Translational GTPase Complexes. Cell 167. doi:10.1016/j.cell.2016.10.046

Shao S, Von der Malsburg K, Hegde RS. 2013. Listerin-dependent nascent protein ubiquitination relies on ribosome subunit dissociation. Mol Cell 50. doi:10.1016/j.molcel.2013.04.015

Shcherbik N, Chernova TA, Chernoff YO, Pestov DG. 2016. Distinct types of translation termination generate substrates for ribosome-associated quality control. Nucleic Acids Res 44. doi:10.1093/nar/gkw566

Shen PS, Park J, Qin Y, Li X, Parsawar K, Larson MH, Cox J, Cheng Y, Lambowitz AM, Weissman JS, Brandman O, Frost A. 2015. Rqc2p and 60S ribosomal subunits mediate mRNA-independent elongation of nascent chains. Science (1979) 347. doi:10.1126/science.1259724

Shi Y, Lin S, Staats KA, Li Y, Chang WH, Hung ST, Hendricks E, Linares GR, Wang Y, Son EY, Wen X, Kisler K, Wilkinson B, Menendez L, Sugawara T, Woolwine P, Huang M, Cowan MJ, Ge B, Koutsodendris N, Sandor KP, Komberg J, Vangoor VR, Senthilkumar K, Hennes V, Seah C, Nelson AR, Cheng TY, Lee SJJ, August PR, Chen JA, Wisniewski N, Hanson-Smith V, Belgard TG, Zhang A, Coba M, Grunseich C, Ward ME, Van Den Berg LH, Pasterkamp RJ, Trotti D, Zlokovic B

V., Ichida JK. 2018. Haploinsufficiency leads to neurodegeneration in C9ORF72 ALS/FTD human induced motor neurons. Nat Med 24. doi:10.1038/nm.4490

Shoemaker CJ, Eyler DE, Green R. 2010. Dom34:Hbs1 promotes subunit dissociation and peptidyl-tRNA drop-off to initiate no-go decay. Science (1979) 330:369–372. doi:10.1126/science.1192430

Shoemaker CJ, Green R. 2011. Kinetic analysis reveals the ordered coupling of translation termination and ribosome recycling in yeast. Proc Natl Acad Sci U S A 108. doi:10.1073/pnas.1113956108

Shoji S, Walker SE, Fredrick K. 2009. Ribosomal translocation: One step closer to the molecular mechanism. ACS Chem Biol. doi:10.1021/cb8002946

Sitron CS, Brandman O. n.d. CAT tails drive degradation of stalled polypeptides on and off the ribosome. doi:10.1038/s41594-019-0230-1

Sonenberg N, Hinnebusch AG. 2009. Regulation of Translation Initiation in Eukaryotes: Mechanisms and Biological Targets. Cell. doi:10.1016/j.cell.2009.01.042

Sonenberg N, Morgan MA, Merrick WC, Shatkin AJ. 1978. A polypeptide in eukaryotic initiation factors that crosslinks specifically to the 5’-terminal cap in mRNA. Proceedings of the National Academy of Sciences 75:4843–4847. doi:10.1073/pnas.75.10.4843

Sonenberg N, Rupprecht KM, Hecht SM, Shatkin AJ. 1979. Eukaryotic mRNA cap binding protein: purification by affinity chromatography on sepharose-coupled m7GDP. Proceedings of the National Academy of Sciences 76:4345–4349. doi:10.1073/pnas.76.9.4345

Soragni E, Petrosyan L, Rinkoski TA, Wieben ED, Baratz KH, Fautsch MP, Gottesfeld JM. 2018. Repeat-associated non-ATG (RAN) translation in fuchs' endothelial corneal dystrophy. Invest Ophthalmol Vis Sci 59. doi:10.1167/iovs.17-23265

Spahn CMT, Gomez-Lorenzo MG, Grassucci RA, Jørgensen R, Andersen GR, Beckmann R, Penczek PA, Ballesta JPG, Frank J. 2004. Domain movements of elongation factor eEF2 and the eukaryotic 80S ribosome facilitate tRNA translocation. EMBO Journal 23. doi:10.1038/sj.emboj.7600102

Stoneley M, Willis AE. 2004. Cellular internal ribosome entry segments: Structures, trans-acting factors and regulation of gene expression. Oncogene. doi:10.1038/sj.onc.1207551

Stoyas CA, La Spada AR. 2018. The CAG–polyglutamine repeat diseases: a clinical, molecular, genetic, and pathophysiologic nosologyHandbook of Clinical Neurology. doi:10.1016/B978-0-444-63233-3.00011-7

Sundaramoorthy E, Leonard M, Mak R, Liao J, Fulzele A, Bennett EJ. 2017. ZNF598 and RACK1 Regulate Mammalian Ribosome-Associated Quality Control Function by Mediating Regulatory 40S Ribosomal Ubiquitylation. Mol Cell 65. doi:10.1016/j.molcel.2016.12.026

Sutcliffe JS, Nelson DL, Zhang F, Pieretti M, Caskey CT, Saxe D, Warren ST. 1992. DNA methylation represses FMR-1 transcription in fragile x syndrome. Hum Mol Genet 1. doi:10.1093/hmg/1.6.397

Swinnen B, Robberecht W, Van Den Bosch L. 2020. RNA toxicity in non-coding repeat expansion disorders. EMBO J 39. doi:10.15252/embj.2018101112

Tabet R, Schaeffer L, Freyermuth F, Jambeau M, Workman M, Lee CZ, Lin CC, Jiang J, Jansen-West K, Abou-Hamdan H, Désaubry L, Gendron T, Petrucelli L, Martin F, Lagier-Tourenne C. 2018. CUG initiation and frameshifting enable production of dipeptide repeat proteins from ALS/FTD C9ORF72 transcripts. Nat Commun 9:1–14. doi:10.1038/s41467-017-02643-5

Taneja KL, McCurrach M, Schalling M, Housman D, Singer RH. 1995. Foci of trinucleotide repeat transcripts in nuclei of myotonic dystrophy cells and tissues. Journal of Cell Biology 128. doi:10.1083/jcb.128.6.995

Tassone F, Beilina A, Carosi C, Albertosi S, Bagni C, Li L, Glover K, Bentley D, Hagerman PJ. 2007. Elevated FMR1 mRNA in premutation carriers is due to increased transcription. RNA 13:555–562. doi:10.1261/rna.280807

Taylor DJ, Nilsson J, Merrill AR, Andersen GR, Nissen P, Frank J. 2007. Structures of modified eEF2.80S ribosome complexes reveal the role of GTP hydrolysis in translocation. EMBO Journal 26. doi:10.1038/sj.emboj.7601677

Thrun A, Garzia A, Kigoshi-Tansho Y, Patil PR, Umbaugh CS, Dallinger T, Liu J, Kreger S, Patrizi A, Cox GA, Tuschl T, Joazeiro CAP. 2021. Convergence of mammalian RQC and C-end rule proteolytic pathways via alanine tailing. Mol Cell 81. doi:10.1016/j.molcel.2021.03.004

Tiburcio AF, Altabella T, Bitrián M, Alcázar R. 2014. The roles of polyamines during the lifespan of plants: From development to stress. Planta. doi:10.1007/s00425-014-2055-9

Tippana R, Chen MC, Demeshkina NA, Ferré-D'Amaré AR, Myong S. 2019. RNA G-quadruplex is resolved by repetitive and ATP-dependent mechanism of DHX36. Nat Commun. doi:10.1038/s41467-019-09802-w

Todd PK, Oh SY, Krans A, He F, Sellier C, Frazer M, Renoux AJ, Chen K chun, Scaglione KM, Basrur V, Elenitoba-Johnson K, Vonsattel JP, Louis ED, Sutton MA, Taylor JP, Mills RE, Charlet-Berguerand N, Paulson HL. 2013. CGG repeat-associated translation mediates neurodegeneration in fragile X tremor ataxia syndrome. Neuron. doi:10.1016/j.neuron.2013.03.026

Tseng YJ, Sandwith SN, Green KM, Chambers AE, Krans A, Raimer HM, Sharlow ME, Reisinger MA, Richardson AE, Routh ED, Smaldino MA, Wang YH, Vaughn JP, Todd PK, Smaldino PJ. 2021. The RNA helicase DHX36–G4R1 modulates C9orf72 GGGGCC hexanucleotide repeat–associated translation. Journal of Biological Chemistry 297:100914. doi:10.1016/j.jbc.2021.100914

Udagawa T, Seki M, Okuyama T, Adachi S, Natsume T, Noguchi T, Matsuzawa A, Inada T. 2021. Failure to Degrade CAT-Tailed Proteins Disrupts Neuronal Morphogenesis and Cell Survival. Cell Rep 34:108599. doi:10.1016/j.celrep.2020.108599

Ude S, Lassak J, Starosta AL, Kraxenberger T, Wilson DN, Jung K. 2013. Translation elongation factor EF-P alleviates ribosome stalling at polyproline stretches. Science (1979) 339. doi:10.1126/science.1228985

Umoh ME, Fournier C, Li Y, Polak M, Shaw L, Landers JE, Hu W, Gearing M, Glass JD. 2016. Comparative analysis of C9orf72 and sporadic disease in an ALS clinic population. Neurology. doi:10.1212/WNL.0000000000003067

Unbehaun A. 2004. Release of initiation factors from 48S complexes during ribosomal subunit joining and the link between establishment of codon-anticodon base-pairing and hydrolysis of eIF2-bound GTP. Genes Dev 18:3078–3093. doi:10.1101/gad.1255704

Usdin K, Kumari D. 2015. Repeat-mediated epigenetic dysregulation of the FMR1 gene in the fragile X-related disorders. Front Genet. doi:10.3389/fgene.2015.00192

Van Treeck B, Parker R. 2018. Emerging Roles for Intermolecular RNA-RNA Interactions in RNP Assemblies. Cell. doi:10.1016/j.cell.2018.07.023

Veltri AJ, D'orazio KN, Lessen LN, Loll-Krippleber R, Brown GW, Green R. 2022. Distinct elongation stalls during translation are linked with distinct pathways for mRNA degradation. Elife 11. doi:10.7554/ELIFE.76038

Verkerk AJMH, Pieretti M, Sutcliffe JS, Fu YH, Kuhl DPA, Pizzuti A, Reiner O, Richards S, Victoria MF, Zhang F, Eussen BE, van Ommen GJB, Blonden LAJ, Riggins GJ, Chastain JL, Kunst CB, Galjaard H, Thomas Caskey C, Nelson DL, Oostra BA, Warran ST. 1991. Identification of a gene (FMR-1) containing a CGG repeat coincident with a breakpoint cluster region exhibiting length variation in fragile X syndrome. Cell 65. doi:10.1016/0092-8674(91)90397-H

Verma R, Reichermeier KM, Burroughs AM, Oania RS, Reitsma JM, Aravind L, Deshaies RJ. 2018. Vms1 and ANKZF1 peptidyl-tRNA hydrolases release nascent chains from stalled ribosomes. Nature 557. doi:10.1038/s41586-018-0022-5

Vester K, Eravci M, Serikawa T, Schütze T, Weise C, Kurreck J. 2019. RNAi-mediated knockdown of the Rhau helicase preferentially depletes proteins with a Guanine-

quadruplex motif in the 5’-UTR of their mRNA. Biochem Biophys Res Commun. doi:10.1016/j.bbrc.2018.11.186

Viera Ortiz AP, Cajka G, Olatunji OA, Mikytuck B, Shalem O, Lee EB. 2022. Impaired ribosome-associated quality control of C9orf72 arginine-rich dipeptide-repeat proteins . Brain. doi:10.1093/brain/awac479

Wang Q, Chen P, Wang X, Wu Y, Xia K, Mu X, Xuan Q, Xiao J, He Y, Liu W, Song X, Sun F. 2023. piR-36249 and DHX36 together inhibit testicular cancer cells progression by upregulating OAS2. Noncoding RNA Res 8. doi:10.1016/j.ncrna.2022.12.004

Wang Z, Ursu A, Childs-disney JL, Rice JE, Petrucelli L, Disney MD, Wang Z, Ursu A, Childs-disney JL, Guertler R, Yang W, Bernat V. 2019. The Hairpin Form of r (G 4 C 2) exp in c9ALS / FTD Is Repeat-Associated Non-ATG Translated and a Target for Bioactive Small Molecules Article The Hairpin Form of r (G 4 C 2) exp in c9ALS / FTD Is Repeat-Associated Non-ATG Translated and a Target for B. Cell Chem Biol 26:179-190.e12. doi:10.1016/j.chembiol.2018.10.018

Wątor E, Wilk P, Biela A, Rawski M, Zak KM, Steinchen W, Bange G, Glatt S, Grudnik P. 2023. Cryo-EM structure of human eIF5A-DHS complex reveals the molecular basis of hypusination-associated neurodegenerative disorders. Nat Commun 14. doi:10.1038/s41467-023-37305-2

Wenninger S, Montagnese F, Schoser B. 2018. Core clinical phenotypes in Myotonic Dystrophies. Front Neurol. doi:10.3389/fneur.2018.00303

White MC, Gao R, Xu W, Mandal SM, Lim JG, Hazra TK, Wakamiya M, Edwards SF, Raskin S, Teive HAG, Zoghbi HY, Sarkar PS, Ashizawa T. 2010. Inactivation of

hnRNP K by expanded intronic AUUCU repeat induces apoptosis via translocation of PKCδ to mitochondria in spinocerebellar ataxia 10. PLoS Genet 6. doi:10.1371/journal.pgen.1000984

Wilson DN, Arenz S, Beckmann R. 2016. Translation regulation via nascent polypeptide-mediated ribosome stalling. Curr Opin Struct Biol. doi:10.1016/j.sbi.2016.01.008

Wilson Joan E, Pestova T V, Hellen CUT, Sarnow P. 2000. Initiation of Protein Synthesis from the A Site of the Ribosome. Cell 102:511–520. doi:10.1016/S0092-8674(00)00055-6

Wilson J. E., Powell MJ, Hoover SE, Sarnow P. 2000. Naturally Occurring Dicistronic Cricket Paralysis Virus RNA Is Regulated by Two Internal Ribosome Entry Sites. Mol Cell Biol 20:4990–4999. doi:10.1128/mcb.20.14.4990-4999.2000

Wohlgemuth I, Brenner S, Beringer M, Rodnina M V. 2008. Modulation of the rate of peptidyl transfer on the ribosome by the nature of substrates. Journal of Biological Chemistry 283. doi:10.1074/jbc.M805316200

Woolstenhulme CJ, Parajuli S, Healey DW, Valverde DP, Petersen EN, Starosta AL, Guydosh NR, Johnson WE, Wilson DN, Buskirk AR. 2013. Nascent peptides that block protein synthesis in bacteria. Proc Natl Acad Sci U S A 110. doi:10.1073/pnas.1219536110

Wu CCC, Zinshteyn B, Wehner KA, Green R. 2019. High-Resolution Ribosome Profiling Defines Discrete Ribosome Elongation States and Translational Regulation during Cellular Stress. Mol Cell 73. doi:10.1016/j.molcel.2018.12.009

Wu Z, Wang Y, Lim J, Liu B, Li Y, Vartak R, Stankiewicz T, Montgomery S, Lu B. 2018. Ubiquitination of ABCE1 by NOT4 in Response to Mitochondrial Damage Links

Co-translational Quality Control to PINK1-Directed Mitophagy. Cell Metab 28. doi:10.1016/j.cmet.2018.05.007

Xi Z, Zhang M, Bruni AC, Maletta RG, Colao R, Fratta P, Polke JM, Sweeney MG, Mudanohwo E, Nacmias B, Sorbi S, Tartaglia MC, Rainero I, Rubino E, Pinessi L, Galimberti D, Surace EI, McGoldrick P, McKeever P, Moreno D, Sato C, Liang Y, Keith J, Zinman L, Robertson J, Rogaeva E. 2015. The C9orf72 repeat expansion itself is methylated in ALS and FTLD patients. Acta Neuropathol 129. doi:10.1007/s00401-015-1401-8

Xi Z, Zinman L, Moreno D, Schymick J, Liang Y, Sato C, Zheng Y, Ghani M, Dib S, Keith J, Robertson J, Rogaeva E. 2013. Hypermethylation of the CpG island near the G4C2 repeat in ALS with a C9orf72 expansion. Am J Hum Genet 92. doi:10.1016/j.ajhg.2013.04.017

Xinmei W, Wenzhi T, Thomas W, Karthik K, Shamamandri MS, Yingxiao S, Shaoyu L, A. SN, John M, B. PU, Piera P, K. IJ, Davide T. 2014. Antisense Proline-Arginine RAN dipeptides linked to C9ORF72- ALS/FTD form toxic nuclear aggregates that initiate in vitro and in vivo neuronal death. Neuron 84.

Xu J, Chong J, Wang D. 2021. Strand-specific effect of Rad26 and TFIIS in rescuing transcriptional arrest by CAG trinucleotide repeat slip-outs. Nucleic Acids Res 49. doi:10.1093/nar/gkab573

Xu Y, Bernecky C, Lee CT, Maier KC, Schwalb B, Tegunov D, Plitzko JM, Urlaub H, Cramer P. 2017. Architecture of the RNA polymerase II-Paf1C-TFIIS transcription elongation complex. Nat Commun 8. doi:10.1038/ncomms15741

Yamada SB, Gendron TF, Niccoli T, Genuth NR, Grosely R, Shi Y, Glaria I, Kramer NJ, Nakayama L, Fang S, Dinger TJI, Thoeng A, Rocha G, Barna M, Puglisi JD, Partridge L, Ichida JK, Isaacs AM, Petrucelli L, Gitler AD. 2019. RPS25 is required for efficient RAN translation of C9orf72 and other neurodegenerative disease-associated nucleotide repeats. Nat Neurosci. doi:10.1038/s41593-019-0455-7

Yang H-S, Jansen AP, Komar AA, Zheng X, Merrick WC, Costes S, Lockett SJ, Sonenberg N, Colburn NH. 2003. The Transformation Suppressor Pdcd4 Is a Novel Eukaryotic Translation Initiation Factor 4A Binding Protein That Inhibits Translation. Mol Cell Biol 23. doi:10.1128/mcb.23.1.26-37.2003

Yang Y, Li W, Hoque M, Hou L, Shen S, Tian B, Dynlacht BD. 2016. PAF Complex Plays Novel Subunit-Specific Roles in Alternative Cleavage and Polyadenylation. PLoS Genet. doi:10.1371/journal.pgen.1005794

Yangyuoru PM, Bradburn DA, Liu Z, Xiao TS, Russell R. 2018. The G-quadruplex (G4) resolvase DHX36 efficiently and specifically disrupts DNA G4s via a translocation-based helicase mechanism. Journal of Biological Chemistry. doi:10.1074/jbc.M117.815076

Yip MCJ, Keszei AFA, Feng Q, Chu V, McKenna MJ, Shao S. 2019. Mechanism for recycling tRNAs on stalled ribosomes. Nat Struct Mol Biol 26. doi:10.1038/s41594-019-0211-4

Yonashiro R, Tahara EB, Bengtson MH, Khokhrina M, Lorenz H, Chen KC, Kigoshi-Tansho Y, Savas JN, Yates JR, Kay SA, Craig EA, Mogk A, Bukau B, Joazeiro CAP. 2016. The Rqc2/Tae2 subunit of the ribosome-associated quality control

(RQC) complex marks ribosome-stalled nascent polypeptide chains for aggregation. Elife 5. doi:10.7554/eLife.11794

Yoon HJ, Donahue TF. 1992. The suil suppressor locus in Saccharomyces cerevisiae encodes a translation factor that functions during tRNA(iMet) recognition of the start codon. Mol Cell Biol 12:248–260. doi:10.1128/MCB.12.1.248

Young SK, Baird TD, Wek RC. 2016. Translation Regulation of the Glutamyl-prolyl-tRNA Synthetase Gene EPRS through Bypass of Upstream Open Reading Frames with Noncanonical Initiation Codons. Journal of Biological Chemistry 291:10824–10835. doi:10.1074/JBC.M116.722256

Yu CH, Dang Y, Zhou Z, Wu C, Zhao F, Sachs MS, Liu Y. 2015. Codon Usage Influences the Local Rate of Translation Elongation to Regulate Co-translational Protein Folding. Mol Cell 59. doi:10.1016/j.molcel.2015.07.018

Zaher HS, Green R. 2009. Fidelity at the Molecular Level: Lessons from Protein Synthesis. Cell. doi:10.1016/j.cell.2009.01.036

Zeng Y, Qin T, Flamini V, Tan C, Zhang X, Cong Y, Birkin E, Jiang WG, Yao H, Cui Y. 2020. Identification of DHX36 as a tumour suppressor through modulating the activities of the stress-associated proteins and cyclin-dependent kinases in breast cancer. Am J Cancer Res 10.

Zhang K, Donnelly CJ, Haeusler AR, Grima JC, Machamer JB, Steinwald P, Daley EL, Miller SJ, Cunningham KM, Vidensky S, Gupta S, Thomas MA, Hong I, Chiu S-L, Huganir RL, Ostrow LW, Matunis MJ, Wang J, Sattler R, Lloyd TE, Rothstein JD. 2015. The C9orf72 repeat expansion disrupts nucleocytoplasmic transport. Nature 525:56–61. doi:10.1038/nature14973

Zhang N, Ashizawa T. 2017. RNA toxicity and foci formation in microsatellite expansion diseases. Curr Opin Genet Dev. doi:10.1016/j.gde.2017.01.005

Zhang Y, Glineburg MR, Basrur V, Conlon K, Wright SE, Krans A, Hall DA, Todd PK. 2022. Mechanistic convergence across initiation sites for RAN translation in fragile X associated tremor ataxia syndrome. Hum Mol Genet 31:2317–2332. doi:10.1093/hmg/ddab353

Zu T, Cleary JD, Liu Y, Bañez-Coronel M, Bubenik JL, Ayhan F, Ashizawa T, Xia G, Clark HB, Yachnis AT, Swanson MS, Ranum LPW. 2017. RAN Translation Regulated by Muscleblind Proteins in Myotonic Dystrophy Type 2. Neuron 95. doi:10.1016/j.neuron.2017.08.039

Zu T, Gibbens B, Doty NS, Gomes-Pereira M, Huguet A, Stone MD, Margolis J, Peterson M, Markowski TW, Ingram MAC, Nan Z, Forster C, Low WC, Schoser B, Somia N V., Clark HB, Schmechel S, Bitterman PB, Gourdon G, Swanson MS, Moseley M, Ranum LPW. 2011. Non-ATG-initiated translation directed by microsatellite expansions. Proceedings of the National Academy of Sciences 108:260–265. doi:10.1073/pnas.1013343108

Zu T, Liu Y, Banez-Coronel M, Reid T, Pletnikova O, Lewis J, Miller TM, Harms MB, Falchook AE, Subramony SH, Ostrow LW, Rothstein JD, Troncoso JC, Ranum LPW. 2013. RAN proteins and RNA foci from antisense transcripts in C9ORF72 ALS and frontotemporal dementia. Proceedings of the National Academy of Sciences 110:E4968–E4977. doi:10.1073/pnas.1315438110

Zu T, Pattamatta A, Ranum LPW. 2018. Repeat-associated non-ATG translation in neurological diseases. Cold Spring Harb Perspect Biol 10. doi:10.1101/cshperspect.a033019

Chapter 2: The RNA Helicase DHX36/G4R1 Modulates C9orf72 GGGGCC Hexanucleotide Repeat-associated Translation

This chapter is published as:

Tseng, Yi Ju, Siara N. Sandwith, Katelyn M. Green, Antonio E. Chambers, Amy Krans, Heather M. Raimer, Meredith E. Sharlow, Michael A. Reisinger, Adam E. Richardson, Eric D. Routh, Melissa A. Smaldino, Yuh Hwa Wang, James P. Vaughn, Peter K. Todd, and Philip J. Smaldino. 2021. “The RNA Helicase DHX36–G4R1 Modulates C9orf72 GGGGCC Hexanucleotide Repeat–Associated Translation.” Journal of Biological Chemistry 297(2):100914. doi: 10.1016/j.jbc.2021.100914.

2.1. Abstract

GGGGCC (G4C2) hexanucleotide repeat expansions (HRE) in the endosomal trafficking gene C9orf72 are the most common genetic cause of amyotrophic lateral sclerosis (ALS) and frontotemporal dementia (FTD). Repeat-associated non-AUG (RAN) translation of this expansion through near-cognate initiation codon usage and internal ribosomal entry generates toxic proteins that accumulate in patients' brains and contribute to disease pathogenesis. The helicase protein DEAH-Box Helicase 36 (DHX36/G4R1) plays active roles in RNA and DNA G-quadruplex (G4) resolution in cells. As G4C2 repeats are known to form G4 structures in vitro, we sought to determine the impact of

manipulating DHX36 expression on repeat transcription and RAN translation. Using a series of luciferase reporter assays both in cells and in vitro, we found that DHX36 depletion suppresses RAN translation in a repeat length-dependent manner, while overexpression of DHX36 enhances RAN translation from G4C2 reporter RNAs. Moreover, upregulation of RAN translation that is typically triggered by integrated stress response activation is prevented by loss of DHX36. These results suggest that DHX36 is active in regulating G4C2 repeat translation, providing potential implications for therapeutic development in nucleotide repeat expansion disorders.

2.2. Introduction

A G_4C_2 hexanucleotide repeat expansion (HRE) within the first intron of *C9orf72* is a major genetic cause of amyotrophic lateral sclerosis and frontal temporal dementia (C9 FTD/ALS) (DeJesus-Hernandez et al., 2011; Renton et al., 2011). Typically, humans have ~2-28 repeats, while disease associated alleles have >30 and often hundreds to thousands repeats (Byrne et al., 2014; Van Mossevelde et al., 2017). C9 FTD/ALS represents over 40% of the familial cases and upwards of 10% of the sporadic cases of ALS in European populations (Umoh et al., 2016). Despite intense research efforts since its discovery in 2011, C9 FTD/ALS remains a progressive and fatal condition without effective treatment (DeJesus-Hernandez et al., 2011; Haeusler et al., 2014; Renton et al., 2011).

Both DNA and RNA G_4C_2 HRE sequences are prone to folding into G-quadruplex (G4) structures *in vitro* (Conlon et al., 2016; Donnelly et al., 2013; Fratta et al., 2012; Haeusler et al., 2014; Simone et al., 2018; Su et al., 2014; Zamiri et al., 2014; Zhou et al., 2015).

G4 structures are dynamic, nucleic acid secondary structures consisting of an assembly of vertically stacked guanine-tetrad building blocks. G4 structures are stabilized by Hoogsteen hydrogen bonding and monovalent cations, especially K^+ (Maizels, 2015; Mendoza et al., 2016; Rhodes and Lipps, 2015). G4 structures have been directly observed in human cells (Biffi et al., 2013; Hänsel-Hertsch et al., 2016; Henderson et al., 2014), with >700,000 G4 motifs residing throughout the human genome (Bedrat et al., 2016; Chambers et al., 2015). G4 structures motifs are non-randomly distributed, with enrichment in gene promoters, untranslated regions, and origins of replication, suggesting functional roles in transcription, translation, and replication, respectively (Bedrat et al., 2016; Chambers et al., 2015; Huppert and Balasubramanian, 2007, 2005; Maltby et al., 2020). Taken together, G4 structures are linked to each of the major toxicities observed in C9 FTD/ALS patient neurons.

The underlying pathogenesis of the G_4C_2 HRE involves at least three inter-related pathways, each of which is foundationally linked to aberrant G4 structures. The G_4C_2 HRE as DNA impairs mRNA transcription and alters the epigenetics of the *C9orf72* locus, decreasing C9orf72 protein expression (Shi et al., 2018). Endogenous C9orf72 protein is important for endosomal trafficking and autophagy in neurons, and its loss is detrimental to neurons and impacts inflammatory pathways relevant to ALS (Shi et al., 2018). When transcribed, the resultant G_4C_2 mRNA species folds into G4 structures, which coalesce as RNA foci in complex with RNA binding proteins, impairing RNA processing (DeJesus-Hernandez et al., 2011; Haeusler et al., 2014). If transcribed G_4C_2 HRE mRNAs reach the cytoplasm, they can serve as a template for repeat-associated non-AUG initiated (RAN) translation. RAN translation from G_4C_2 repeat RNA (C9RAN) produces dipeptide

repeat proteins (DPRs) that aggregate in proteinaceous inclusions. C9RAN DPRs proteins cause proteotoxic stress and disrupt nucleocytoplasmic transport (Shi et al., 2017; Simone et al., 2018; Taylor, 2017).

The mechanisms underlying C9RAN remains enigmatic(Rodriguez and Todd, 2019). Initiation can occur at either an upstream near-AUG codon (CUG) or within the repeat itself (Cheng et al., 2018; Green et al., 2017; Sonobe et al., 2018; Tabet et al., 2018). RNA helicases such as eIF4B, eIF4H and DDX3X play active and selective roles in the translation process, as do the ribosomal accessory protein RPS25 (Cheng et al., 2019; Goodman et al., 2019; Linsalata et al., 2019; Yamada et al., 2019). RAN translation also demonstrates a selective enhancement in response to cellular stress pathways which activate stress granule formation and suppress global translation through phosphorylation of eIF2α (Cheng et al., 2018; Green et al., 2017; Tabet et al., 2018; Westergard et al., 2019; Zu et al., 2020). Consistent with this, modulation of the alternative ternary complex protein eIF2α or PKR expression can alter C9RAN translation (Sonobe et al., 2018; Zu et al., 2020).

Given their potentially central role in G_4C_2 repeats in C9 FTD/ALS pathogenesis, we explored factors responsible for G4 resolution within cells. One such enzyme, DHX36 (aliases: G4R1 and RHAU), is a member of the DExH-box family of helicases (Schult and Paeschke, 2020). DHX36 accounts for the majority of the tetramolecular G4 DNA and RNA helicase activity in HeLa cell lysates (Creacy et al., 2008; Vaughn et al., 2005). DHX36 binds to a diverse array of unimolecular DNA and RNA G4 structures with the tightest affinity of any known G4 structure binding protein and can catalytically unwind these structures in isolation (Booy et al., 2016, 2015, 2014, 2012; Giri et al., 2011;

Haeusler et al., 2014; Huang et al., 2012; Kim et al., 2011; McRae et al., 2017; Nie et al., 2015; Sexton and Collins, 2011; Smaldino et al., 2015). DHX36 associates with thousands of G4-containing DNA and mRNA sequences, facilitating both their transcription and translation (Murat et al., 2018; Sauer et al., 2019; Vester et al., 2019). Moreover, DHX36 plays an active role in stress granule dynamics, where its loss can trigger spontaneous formation of stress granules and changes in their dissolution after a transient stress exposure (Sauer et al., 2019). Thus, DHX36 has the potential to influence *C9orf72* transcription and G_4C_2-repeat RNA stability, localization, and RAN translation (Huang et al., 2012; Huppert and Balasubramanian, 2007).

Here we find that DHX36 knockdown and knockout selectively suppresses C9RAN translation as well as RAN translation at CGG repeats from reporters in human cells. In contrast, overexpression of WT DHX36, but not a mutant form of DHX36 which lacks helicase activity, enhances RAN translation. These effects are largely translational as we observe suppression of C9RAN translation in an *in vitro* DHX36 KO cell lysate translation system while observing no significant alterations in reporter RNA in response to knockdown or overexpression of DHX36. Loss of DHX36 also precludes stress-dependent upregulation of C9RAN translation consistent with its role in stress granule formation. Taken together, these results suggest modulation of G4 structures at the RNA level by candidate G4 helicases such as DHX36 impact G_4C_2 repeat expansion translation implicated in C9 FTD/ALS.

2.3. Materials and Methods

2.3.1. Electrophoretic Mobility Shift Assays

62.5 pg of 5'- IRDye 800 labeled*C9* or scrambled oligonucleotides **(Table 1)** were synthesized (Integrated DNA Technologies, Inc.) were heated in nuclease-free water in the presence of KCl (100 mM) starting at 98°C and decreasing 10°C every two min, ending at 28°C. As a control, 62.5 pg of *C9* oligonucleotides were heated and cooled as above in the absence of KCl, 3.75 pg of each oligonucleotide were incubated at 37°C for 30 min in binding buffer (75 mM EDTA, 40.6 mM Tris-Acetate pH 7.8, 40.6 mM NaCl, 1.21 mM $MgCl_2$, 8.1% glycerol, 0.0065% lactalbumin, 2-mercaptoethanol, 0.16x protease inhibitor cocktail (Roche), 0.12 mg/mL leupeptin) with varying concentrations of rDHX36 (7.4, 4.5, 1.7, 1.1, or 0 nM). Additional volumes of buffer were added to the 4.5, 1.7, 1.1, or 0 nM reactions so as to have equal buffer concentrations in all reactions. Glycerol (16% final) was added to the samples, and 3 pg of DNA were loaded per well onto a 10% non-denaturing PAGE. The samples were electrophoresed for 5 hrs at 120 V in the dark. Each EMSA was performed in triplicate and analyzed using a Li-Cor Odyssey imager. Percent bound was determined by densitometry measurements in ImageStudio using the following equation: percent bound = (bound DNA / total DNA) x 100. Triplicate values were averaged and plotted with GraphPad Prism using a non-linear regression (curve fit) function.

2.3.2. *In vitro* Transcription Assay

A HiScribe™ T7 Quick High Yield RNA Synthesis Kit (New England Bio Labs, Cat.# E2050S) was used with 1 µg of a GA_{70} or AUG-NLuc linearized plasmid as

template(Green et al., 2017). The reactions were transcribed for 15 hrs at 37°C in the presence of absence of DHX36 (0 or 6 nM). An additional volume of DHX36 storage buffer was added to reactions without DHX36 so as to have equal buffer concentrations in all reactions. The resulting transcripts were treated with DNase for 20 min at room temperature and then isolated using Micro Bio-Spin™ 6 Columns (BioRad, Cat.# 732-6221). 0.75 µg of RNA transcripts were mixed with 2X formamide buffer (95% deionized formamide, 0.025% bromophenol blue, 5 mM EDTA) and heated at 95°C for 5 min. The samples were resolved in a 7.5% denaturing-8M urea PAGE for 20 min at 2 W and then 45 minutes at 20 W. The gels were subsequently soaked in SYBR Gold nucleic acid stains (ThermoFisher, Cat.# S11494) for 20 min at RT and imaged using a BIO-Rad Gel Docs™ XR+ and quantified using densitometry software. Densitometry values for the top third of the gel were divided by total value for each lane. Values for total densitometry readings for each lane were also taken.

2.3.3. RNA Synthesis

pcDNA3.1(+)/NLuc-3xF and pcDNA3.1(+)/FF were linearized by PspOMI and XbaI restriction enzymes respectively and recovered using DNA Clean and Concentrator-25 kits (Zymo Research, Cat# D4033). m^7G-capped and poly-adenylated RNAs were transcribed in vitro from these plasmids using HiScribe T7 ARCA mRNA Kit, with polyA tailing (NEB, Cat# E2065S) following the manufacturer's instructions and recovered using RNA Clean and Concentrator-25 kits (Zymo Research, Cat# R1017). The integrity and size of all transcribed RNAs were confirmed by denaturing formaldehyde and formamide agarose gel electrophoresis.

2.3.4. Cell Culture, Transfection, qRT-PCR, and Drug Treatment

Jurkat T1-28/11 and HeLa 15/25 cells were cultured and passaged at 37°C, 5% CO_2. Jurkat T1-28/11 cells were maintained in Roswell Park Memorial Institute (RPMI) 1640 Medium supplemented with 10% fetal bovine serum (FBS). HeLa 15/25 cells were maintained in Dulbecco's modified Eagle Medium (DMEM) supplemented with 10% FBS, 1% non-essential amino acids, 3 µg/ml blasticidine, and 250 ug/ml zeocin. To induce DHX36 knockdown, HeLa 15 and HeLa 25 were both treated with daily changed media contained 1 ug/ml doxycycline (doxy.) for 4 days.

For transfection and luciferase assay in Jurkat cells, cells were plated in 24-well plates at $6x10^5$ cells/well in 500 µl media. Reverse transfection by using TransIT-Jurkat transfection reagent (Mirus, Cat.# MIR 2124) was done after cells plating. Cells were co-transfected with 250 ng/well of pcDNA(+)-NLuc-3xFLAG plasmids developed from Kearse et al. and Green et al. and 250 ng/well of pGL4.13 firefly luciferase plasmid as transfection control(Green et al., 2017; Kearse et al., 2016). Mixed plasmids and reagents were added drop-wise in cultured cells after 30 min incubation at room temperature, then the plate was gently shaken for 1 min. Luciferase assays were performed 48 hrs after plasmid transfection. Cells from each well were collected in microcentrifuge tube and media was removed after 400 rpm centrifuge for 5 min. Then cells from each tube were lysed with 60 µL of Glo Lysis Buffer 1X (Promega, Cat.# E2661) and were vortexed for 5 sec. In opaque white 96-well plates, from 60 µL of cell lysate, 25 µL of cell lysate was distributed to mix with 25 µL of Nano-Glo Luciferase Assay System (Promega, Cat.# N1120), and another 25 µL of cell lysate was mixed with 25 µL of ONE-Glo Luciferase

Assay System (Promega, Cat.# E6130). The plate was placed on a shaker for 5 min in the dark. Luciferase activity in each well was obtained by luminescence measurements. All reagents and experiments are presented at room temperature.

For transfection and luciferase assay in HeLa cells, cells were plated in 96-well plates at $2.5x10^5$ cells/well in 100 µl media. 24 hrs after plating, cells were co-transfected with 50 ng/well of pcDNA(+)-NLuc-3xFLAG plasmids, and 50 ng/well of pGL4.13 firefly luciferase plasmid as transfection control. Transfection was done by adding Viafect transfection reagent (Promega, Cat# E4981) with mixed plasmids drop-wise in cultured cells after 10 min incubation at room temperature then gently shaking the plate for 1 min. Plasmid DNA and C9-repeat RNA co-transfection were done by forward transfection of published DNA plasmid expressing empty vector, WT, or E335A DHX36(Vaughn et al., 2005) in HeLa cells seeded at $2.5x10^5$ cells/well in 100 µl media. After 24 hrs, *in vitro* synthesized C9-RNA and pcDNA-FF RNA were co-transfected at 50 ng/well each into the well by Viafect transfection reagent (Promega, Cat# E4981) as described above. Following luciferase assays were performed 24 hrs after C9-repeat DNA plasmids or RNA transfection, as described by Kearse et al(Kearse et al., 2016).

For qRT-PCR assays, after HeLa cells were plated and transfected as described above, experiments were performed as described by Linsalata et al(Linsalata et al., 2019).

For C9RAN reporter luciferase analysis following stress activation, after 4 days of doxy. treatment in HeLa 15/25 cells, cells were seeded and transfect for 19 hrs then followed by 5 hrs treatment of 2 µM Thapsigargin (Tg).

2.3.5. Immunoblot and Antibodies

In a 12-well plate, HeLa 15/25 cells were rinsed with 500 µL cold 1X PBS twice then lysed in 300 µL RIPA buffer with protease inhibitor (120 µL for 24-well plates) for 30 min at a 4°C shaker. Lysates were homogenized by passing through a 28G syringe 8 times, mixed with 6X sample buffer with a final of 2% B-ME, denatured at 95°C for 10 min, and stored at -20 °C. Protein samples were standardized by BCA assay for equal total protein loading. 20 µL of equal total protein sample was loaded in each well of a 10% SDS-PAGE. All primary antibodies applied for Western Blot were used at 1:1000 in 5% non-fat dairy milk (wt/vol) and 0.1% Tween-20 (vol/vol) in TBS except anti-puromycin at 1:5000. Monoclonal mouse anti-DHX36 antibody was generated at 2.57 µg/µl(Vaughn et al., 2005), monoclonal mouse anti-FLAG antibody was from Sigma (clone M2, Cat#F1804), mouse anti-GFP was from Roche (Cat# 11814460001), monoclonal mouse anti-GAPDH was from Santa Cruz Biotechnology (clone 6C5, Cat# sc-32233), mouse anti-puromycin 12D10 was from Millipore (Cat# MABE434).

2.3.6. Jurkat Cell Line Generation

The DHX36 gRNAs (T1, T2, and T10) were designed to target exonic regions of DHX36/G4R1 (Gene ID: 170506) in order to disrupt all the gene products (**Supplemental Figure 3**). The gRNA T1 (AAGTACGATATGACTAACAC) was evaluated to be the most effective by nucleotide mismatching assay in the cell pool examination (31.2% cleavage efficiency) and was utilized for generation of single cell clones. Cleavage efficiency was determined by sequencing trace analysis with the online tool TIDE (https://tide-calculator.nki.nl/). Clones were identified and confirmed using Sanger Sequencing of

PCR and RT-PCR productions (**Supplemental Figure 3**) and western blot analysis (**Figure 3, A**)

2.3.7. *In vitro* Translation Assays

Preparation of cell lysate, hypertonic lysis buffer, and translation buffer were followed by Linsalata et al (Linsalata et al., 2019). Jurkat cells were centrifuged, and rinsed 3 times with PBS (pH 7.4). Hypotonic lysis buffer that contained 10 mM HEPES-KOH (pH 7.6), 10 mM KOAc, 0.5 mM Mg2OAc, 5 mM DTT, and EDTA-free protease inhibitor was added to cells pellet on ice to swollen the cells for 30 minutes. Then cells were mechanically lysed by 20 strokes in a 27G syringe and followed by another 30 minutes of incubation on ice. The supernatant from the cell lysate was collected by centrifuging the cell lysate at 10,000 g for 10 min at 4°C and further diluted in lysis buffer to 8.0 ug/ul using a modified Bradford protein quantification assay (Bio-Rad), flash-frozen in liquid N_2, and stored at 80°C. The lysates were added to the translation buffer that with final concentrations of 20 mM HEPES-KOH (pH 7.6), 44 mM KOAc, 2.2 mM Mg2AOc, 2 mM DTT, 20 mM creatine phosphate (Roche), 0.1 ug/ul creatine kinase (Roche), 0.1 mM spermidine, and on average 0.1 mM of each amino acid.

For in vitro translation assays, 40 fmol of RNA was added to lysate which protein concentration at 8 ug/ul of 10 ul per reaction. After incubation at 30°C for 120 min, 25 ul room temperature Glo Lysis Buffer (Promega) was added to the reaction to incubate for 5 min at room temperature. With the Nano-Glo Dual-luciferase system, 25 ul of this mixture was added 25 ul of the ONE-Glo™ EX reagent following 25 ul of NanoDLR Stop

& Glo reagent (Promega). All mixtures were incubated in opaque white 96-well plates on a rocking shaker in the dark for 5 min before quantifying the luminescence.

2.3.8. Measuring Protein Synthesis by Puromycin Incorporation

Nascent Global translation was monitored by the surface sensing of translation (SUnSET) method(Schmidt et al., 2009). After seeding HeLa cells as described above in a 24-well plate format, 48 hrs later, cells were incubated with fresh media containing 10 µg/ml of puromycin for 10 min at room temperature. Cells were then placed on ice and washed with ice-cold PBS, prior to lysis in 100 µL RIPA buffer containing protease inhibitor.

2.3.9. Statistical Methods

Statistical analysis was performed using GraphPad Prism8. For comparison of NLuc and FFLuc reporter luciferase activity, one-way ANOVAs were performed to confirm statistical difference between control and experimental groups. Two-way ANOVA was performed to confirm the statistical difference on FFLuc signal from the treatment of Thapsigargin between different groups of control and experimental conditions. Post-hoc Student's t tests were then performed with Bonferroni correction for multiple comparisons and Welch's correction for unequal variance. All studies represent at least three independently replicated experiments. All bar graphs include a standard deviation error bar and each independent replicate. Exact N for each sample and analysis performed are noted in the figure legend.

2.3.10. Data Availability

All relevant data are available from the authors upon request.

2.4. Results

2.4.1. DHX36 Directly Binds C9-repeat G4 DNA *in vitro*

To determine if DHX36 directly binds to C9 G4 DNA structures, we performed electrophoretic mobility shift assays (EMSAs) with a DNA oligonucleotide composed of five G_4C_2-repeats with a 3' unstructured tail shown to be require for G4 binding (Chen et al., 2018; Smaldino et al., 2015) (referred to hereafter as "$(G_4C_2)_5$-DNA"). $(G_4C_2)_5$-DNA was folded into G4 structures by heating and cooling in the presence of KCl. As a negative control of non-G4 DNA, $(G_4C_2)_5$-DNA was heated and cooled in the absence of KCl. G4 $(G_4C_2)_5$-DNA and non-G4 $(G_4C_2)_5$-DNA was incubated with purified recombinant DHX36 (rDHX36) under non-catalytic conditions (-ATP, +EDTA) so that binding could be visualized on a gel **(Figure 2.1.A, C)**. As an additional control, this was repeated with scrambled C9-repeat DNA, where the C9-repeat sequence was rearranged as to prevent G4 structure formation. **(Figure 2.1.B-C)**. Following incubation, the samples were subjected to non-denaturing polyacrylamide gel electrophoresis (PAGE). In the absence of KCl, a single band is observed for $(G_4C_2)_5$-DNA. When KCl is added, slower migrating bands are observed, consistent with the formation of G4 structures. Incubation of $(G_4C_2)_5$-DNA with rDHX36 resulted in a shift of the DNA to the upper region of the gel indicating direct binding. Notably, some unstructured $(G_4C_2)_5$-DNA is present in the KCl-containing reactions and is not bound by DHX36, further suggesting selective binding to G4 structure. In the absence of KCl (i.e. non-G4 conditions), binding of rDHX36 to $(G_4C_2)_5$-

DNA is substantially reduced. Furthermore, scrambled $(G_4C_2)_5$-DNA does not form KCl-dependent higher-ordered structures and is not a strong binding substrate for rDHX36 even in the presence of KCl. Taken together, these data suggest that DHX36 directly binds to C9 HRE DNA in a G4-dependent manner *in vitro*.

2.4.2. DHX36 Enhances Transcription of C9-repeat DNA *in vitro*

G4 DNA structures impede the transcription of C9-repeat RNA and T7 elongation (Haeusler et al., 2014). Given that DHX36 is a helicase that resolves G4 structures, we hypothesized that DHX36 might facilitate the transcription of C9-repeat RNA. To test this, we performed an *in vitro* transcription assay with a plasmid containing 70 G_4C_2 repeats (pCR8-$(G_4C_2)_{70}$) driven by a T7 RNA polymerase reporter (Taylor, 2017). We incubated the plasmid with T7 polymerase in the presence and absence of rDHX36. A T7 plasmid containing a nano luciferase (NLuc) gene was used as a non-G4 control. The resulting RNA transcripts were subjected to denaturing urea gel electrophoresis. We found that rDHX36 significantly increased the length of RNA transcripts yielded from G_4C_2 repeat DNA, but not from NLuc **(Figure 2.1. D-E)**. However, the total RNA generated from G_4C_2 repeat DNA and NLuc DNA was not significantly different between rDHX36 and control reactions **(Supplemental Figure 2.1.)**. These data suggest that rDHX36 facilitates efficient and complete *in vitro* transcription of G4 C9-repeat sequences by T7 RNA polymerase, but may not impact its overall production.

2.4.3. DHX36 Depletion Modifies C9RAN Translation

We next evaluated the impact of altering DHX36 expression on C9RAN translation. To accomplish this, we utilized previously described C9RAN translation-specific nanoluciferase reporters (C9-NLuc) (Green et al., 2017). These reporters include 70 G_4C_2 repeats in the context of the first *C9orf72* intron. This sequence is inserted 5' to a nanoluciferase (NLuc) whose start codon is mutated to GGG and with a 3x FLAG tag fused to its carboxyl terminus **(Figure 2.2. A)**. Single base pair insertions between the repeat and NLuc allow for evaluation of translation in all three reading frames. An AUG-initiated NLuc serves as a positive control for canonical translation. An AUG initiated firefly luciferase (AUG-FF) is included as a transfection control (Green et al., 2017).

To study the effects of loss of DHX36, we used a previously described stable and inducible knockdown (DHX36 KD) HeLa cell line (Iwamoto et al., 2008; Vaughn et al., 2005) **(Figure 2.2. B, Supplemental Figure 2.2. A-E)**. Treatment of these cells with doxycycline for 96 hrs significantly reduced DHX36 expression as measured by immunoblot **(Figure 2.2. C)**. Comparing between control and DHX36 KD cells with transiently transfected C9-NLuc reporters, DHX36 KD selectively decreased C9RAN translation in the GA (+0), GP (+1) and GR (+2) reading frames, relative to AUG-NLuc when normalized to AUG-FF as transfection control **(Figure 2.2 D, Supplemental Figure 2.2 F)**. C9RAN translation in the GA and GR reading frames was also selectively decreased in the DHX36 KD line with doxycycline induction when compared to the DMSO vehicle treated cells, suggesting that the effect was DHX36-specific **(Supplemental Figure 2.3. A).** Either no significant transcript bias or an opposite production bias favoring DHX36 KD was observed for AUG transcripts **(Figure 2.2. D and F)**. To confirm these

findings using an orthogonal readout, we performed immunoblots to detect FLAG signal on lysates from both control and DHX36 KD cells. As we had observed in our luciferase assays, DHX36 KD led to a significant decrease in the GA C9RAN-NLuc protein without impairing AUG translation of NLuc from a separate reporter (**Figure 2.2. E**).

To determine if loss of DHX36 might have broader effects on protein translation in these cells, we performed a SUnSET assay, which measures puromycin incorporation into nascent proteins(Schmidt et al., 2009). Treatment with puromycin for 10 minutes led to a smear of proteins detectible by puromycin immunoblot. There was no difference between DHX36 Ctrl and KD cells in this assay (**Supplemental Figure 2.2. D-E**), suggesting that rates of global translation is not demonstrably affected by knockdown of DHX36 in these cell lines.

2.4.4. DHX36 Depletion Impairs RAN Translation from CGG Repeats

RAN translation occurs at multiple different GC rich repeat sequences, some of which are capable of forming G4 structures and some of which are less likely to form such structures. We therefore evaluated whether DHX36 KD impacts RAN translation at these other repeats. Expansion of a transcribed CGG repeats in the 5'UTR of *FMR1* causes Fragile X-associated Tremor/Ataxia Syndrome (FXTAS) (Krans et al., 2016; Todd et al., 2013). RAN translation from this repeat in the +1 reading frame generates a polyglycine protein (FMRpolyG) that accumulates within inclusions in patient brains and model systems (Buijsen et al., 2016, 2014; Hukema et al., 2015; Sellier et al., 2017; Todd et al., 2013). This repeat is capable of forming either a hairpin structure or a G4 structure *in vitro* (Asamitsu et al., 2021; Fry and Loeb, 1994; Kettani et al., 1995; Usdin and Woodford,

1995). Using a NLuc reporter with 100 repeats (+1CGG_{100}) (Kearse et al., 2016), we observed that KD of DHX36 significantly suppressed CGG RAN translation of FMRpolyG on a scale comparable to that of C9RAN reporters **(Figure 2.2. F)**. This decrease in CGG RAN translation was also evident by immunoblot **(Figure 2.2. E)**.

We next measured reporter mRNA levels in transfected Ctrl and DHX36 KD cells. Surprisingly, we observed only a small decrease in mRNA production that was not statistically significant **(Figure 2.2. G)**. In parallel, we also evaluated the impact of DHX36 overexpression on reporter expression. As with KD, overexpression of DHX36 did not significantly impact steady state reporter RNA expression in HeLa Cells **(Supplemental Figure 2.5.)**. These data suggest that the suppression of RAN translation in DHX36 KD cells is most likely a post-transcriptional event.

2.4.5. DHX36 KO Impairs in-cell and *in vitro* C9RAN Translation

As a second assay system in which to study the effect of DHX36, we generated a DHX36 stable knockout (DHX36 KO) Jurkat cell line using a CRISPR/Cas9 targeting approach. Wildtype Jurkat cells (WT) had no mutations at the DHX36 locus (INDEL: 0/0) while DHX36 KO Jurkat cells (DHX36 KO) had single allele KO disruption on one allele and a 6bp insertion on the other allele at the target site (INDEL: +5/+6) **(Supplemental Figure 2.4. A-B)**. Western blot analysis showed elimination of full length DHX36 protein in Jurkat DHX36 KO cell lines **(Figure 2.3.A)**. Jurkat DHX36 KO cells exhibited impaired RAN translation across all three potential G_4C_2 reading frames, similar to what we observed in HeLa DHX36 KD cells **(Figure 2.3.B)**.

The effects of DHX36KD on RAN translation product generation could theoretically be elicited by changes in RNA or protein stability or by actively impacting protein translation. To investigate this question, we utilized an *in vitro* translation assay using lysates derived from DHX36 WT or KO Jurkat cells. Previous studies in similar conditions demonstrated that we could accurately measure C9RAN translation in this context and that production from our RAN reporters is not dependent on mRNA or reporter stability (Green et al., 2017; Kearse et al., 2016). We harvested Jurkat DHX36 WT and KO cell lysates, added AUG or G_4C_2 repeat RNA in GA (+0) frame and *in vitro* translated for 2 hrs **(Figure 2.4. C, Supplemental Figure 2.4. 2C)**. AUG-NLuc translation from DHX36 KO lysates was consistently lower than that from WT Jurkat lysates. However, this effect was much larger for GA-NLuc reporters, which exhibited 36% as efficient a translation in DHX36 KO lysates compared to WT lysates over >4 independent experiments **(Supplemental Figure 2.4. C)**. Together, these results suggest that loss of DHX36 suppresses RAN translation from G_4C_2-repeats in multiple reading frames of G_4C_2-repeats and is mainly acting at the level of translation.

2.4.6. The effect of DHX36 on C9RAN translation is dependent on repeat length

Translation of C9RAN reporters in the GA reading frame initiates primarily from an upstream CUG start codon that supports translation even at small repeat sizes (Almeida et al., 2019; Green et al., 2017; Sonobe et al., 2018; Tabet et al., 2018). If DHX36 contributes to RAN translation by resolving G4 structures, then we would predict that the loss of DHX36 would selectively reduce translation for transcripts with larger repeats. In HeLa cells, expression of C9 GA frame reporters with 3x, 35x, and 70x G_4C_2 repeats was

selectively suppressed by DHX36 loss at the larger repeat sizes **(Figure 2.4. A-B, Supplemental Figure 2.3. B)**. Similar results were observed in Jurkat DHX36 stable KO cells **(Figure 2.4. C)**. These results suggest that loss of DHX36 selectively acts to reduce C9RAN translation in a repeat length dependent manner.

2.4.7. The Effect of DHX36 Overexpression on C9RAN DPRs Expression

Since depletion of DHX36 results in a significant decrease in C9RAN translation, we wondered if overexpression of DHX36 enhances C9RAN. To address this, we expressed either a DHX36 WT or a DHX36-E335A mutant which lacks the helicase activity required to unwind G4 structures in parental HeLa cells. To ascertain the impact of DHX36 on translation in particular, we conducted studies using transfected *in vitro* transcribed C9RAN reporter mRNAs. In HeLa cells, overexpression of DHX36 significantly increased C9RAN from transfected reporter RNAs in all three sense reading frames. This effect was specific to DHX36 WT, as DHX36-E335A has no effect on C9RAN DPRs production when normalized to the FFLuc mRNA reporters and western blot analysis confirmed this relationship **(Figure 2.5.).** These data suggest that DHX36 acts post-transcriptionally to enhance RAN translation.

2.4.8. Knockdown of DHX36 Prevents Stress Dependent Upregulation of RAN Translation

Activation of the integrated stress response (ISR), which triggers phosphorylation of eIF2α and formation of stress granules (SGs), suppresses global protein translation initiation by impairing ternary complex recycling (Hinnebusch et al., 2016; Jackson et al.,

2010; Starck et al., 2016; Walter and Ron, 2011; Young et al., 2016). Paradoxically, ISR activation enhances RAN translation from both CGG and G_4C_2 repeats, and repeat expression in isolation can trigger SG formation (Cheng et al., 2018; Green et al., 2017; Sonobe et al., 2018; Westergard et al., 2019). Loss of DHX36 induces spontaneous stress granule formation, suggesting that DHX36 may play a role in G4 structure-induced cellular stress(Sauer et al., 2019). We therefore wondered what impact loss of DHX36 would have on regulation of RAN translation in the setting of ISR activation. We co-transfected C9-NLuc and FFLuc into DHX36 control or DHX36 KD HeLa cells and then treated them with 2 μm of the ER stress inducer Thapsigargin (Tg) for 5 hrs. Tg treatment decreased expression of FFLuc in both Ctrl cells and in DHX36 KD cells, which is consistent with appropriate activation of the ISR in these cells **(Figure 2.6. A, right)**.

Consistent with prior studies(Green et al., 2017; Westergard et al., 2019), Tg treatment in DHX36 control cells elevated C9RAN reporter levels compared to DMSO treatment. However, depletion of DHX36 precluded this upregulation in C9RAN by Tg **(Figure 2.6. A).** Similar findings were also observed by immunoblot in studies where we co-transfected the C9RAN reporters and GFP as a control for transfection and AUG initiated translation (**Figure 2.6. B**). These data suggest that DHX36 may play a role in regulating the stress induction of RAN translation induced by the ISR.

2.5. Discussion

DNA and RNA G-quadruplex (G4) structures strongly influence both gene transcription and mRNA stability, localization and translation. Moreover, G4 structures are implicated in a number of human disorders, including C9 FTD/ALS (Schofield et al.,

2015; Simone et al., 2015). Here we find that a major human G4 helicase, DHX36, enhances C9RAN translation from expanded G_4C_2 repeat reporter RNAs in human cells. These effects on RAN translation require DHX36 helicase activity on G4 RNA. DHX36 is also required for efficient C9RAN and CGG RAN translation as knockdown or knockout of DHX36 in human cells suppressed RAN translation from both G_4C_2 and CGG repeats. We also observe a robust suppression of *in vitro* C9RAN translation in DHX36 KO cell derived lysates. Overall, these data are consistent with a model whereby DHX36 binds to and unwinds GC rich repeat RNA structures and enhances their non-AUG initiated translation with a potential secondary role in enhancing repeat transcription **(Figure 2.7.)**.

The observed effects on C9RAN reporter generation are largely post-transcriptional. While we do observe a stimulatory effect of DHX36 on T7 polymerase transcription from a C9-repeat *in vitro* **(Figure 2.1. D-E)**, we do not observe changes in C9-repeat RNA levels in cells following DHX36 KD or overexpression **(Figure 2.2. G, Supplemental Figure 2.5.).** We also show that DHX36 directly binds to C9-repeat DNA with a binding affinity of ~10-100 less than previously reported for pure G4 DNAs (Creacy et al., 2008; Giri et al., 2011; Smaldino et al., 2015) **(Figure 2.1. A-C)**. The relatively low affinity of DHX36 for C9-repeat G4 DNA might in part explain the lack of a robust effect on C9-repeat transcript levels in cells following DHX36 KD or overexpression. In addition, T7 polymerase *in vitro* is prone to early transcription termination (Brunelle and Green, 2013) and as such may be less efficient than RNA polymerase complexes at resolving RNA structures and generating complete transcripts in cells. Future work using patient-derived cells harboring greater repeat lengths (which DHX36 may have greater affinity for) will be

necessary to more fully characterize the potential for DHX36 to modulate C9-repeat transcription in patients.

DHX36 binds to C9-repeat RNA in a G4 specific manner both *in vitro* and in studies using human cell and mouse spinal cord lysates (Haeusler et al., 2014),(McRae et al., 2017)(Zu et al., 2013). Depletion of DHX36 decreases C9RAN translation and this decrease occurs across all reading frames and is dependent on the length of the repeats **(Figures 2.2-4.)**. In addition, while this manuscript was in revision, a second study was published where similar effects of DHX36 were observed on C9RAN translation(Liu et al., 2021). We further observe similar results for CGG repeats capable of supporting RAN translation and folding into G4 structures. This suggests that RAN translation initiation or elongation could be significantly influenced by both RNA binding protein recognition and resolution of repeat RNA secondary structures. This idea is supported by the finding that a helicase dead form of DHX36 failed to influence RAN translation of C9-repeat RNAs. It is also consistent with prior studies implicating RNA helicases such as DDX3X and the eIF4A helicase cofactors eIF4B and eIF4H as modifiers of RAN translation at both CGG and G_4C_2 repeats (Goodman et al., 2019; Linsalata et al., 2019).

In addition, depletion of DHX36 precluded the augmentation of RAN translation typically observed in response to stress **(Figure 2.6.)** (Cheng et al., 2018; Green et al., 2017; Westergard et al., 2016). DHX36 is a component of stress granules and plays an active role in regulating the cellular stress response (Byrd et al., 2016; Chalupníková et al., 2008; Yoo et al., 2014). Indeed, KD or KO of DHX36 is sufficient to trigger stress granule formation without application of an exogenous stressor (Sauer et al., 2019). How exactly loss of DHX36 precludes this upregulation is not clear. ISR activation augments

RAN translation at least in part by lowering initiation codon fidelity requirements (Green et al., 2017; Tabet et al., 2018). If DHX36 is specifically influencing elongation through the repeat, then its depletion may slow translation due to ribosomal stalling within the repeats despite continued enhanced initiation. Alternatively, G_4C_2 repeats also support a 5' M^7G cap independent "IRES-like" RAN initiation mechanism that is enhanced by ISR activation (Cheng et al., 2018; Komar and Hatzoglou, 2011, 2005; Stoneley and Willis, 2004). DHX36 could play an active role in generating this structure and allowing for internal ribosome entry. A deeper understanding of RNA structure/function relationships as they apply to RAN translation will be needed to determine which of these mechanisms (or both) is likely to explain how DHX36 loss impacts RAN translation at both CGG and G_4C_2 repeats.

This study has some limitations. It largely relies on reporter assays using transiently transfected plasmids or *in vitro* transcribed linear RNA. RAN translation from the endogenous locus of C9 might involve very large RNA from longer repeats and the exact nature of the RAN translated transcripts in C9 patient neurons remains unclear. In particular, endogenous RNAs may form a combination of dynamic secondary structures including hairpins and G4s, which complicate the potential effects on both RNA mediated toxicity and RAN translation. Further studies using endogenous systems such as C9 FTD/ALS patient iPSC derived neurons and rodent that harbor larger repeats will be needed to confirm the roles of DHX36 in endogenous repeat transcription, RAN translation, and toxicity derived from the endogenous repeat.

In sum, this study provides evidence that DHX36 can influence RAN translation of G_4C_2 repeats both basally and in response to stress pathways. These studies suggest

that control of G4 formation at the DNA and RNA levels and modulation of G4 resolving helicases such as DHX36 are candidate therapeutic strategies and targets for G rich repeat-associated neurological diseases.

2.6. Chapter-specific Acknowledgements

We thank everyone in the Todd lab and the Smaldino lab for thoughtful feedback and discussion on this project. Jiou Wang provided initial G_4C_2 repeat plasmids to the Smaldino Lab.

This work was funded by the NIH (R15 AG067291 to PJS, T32GM008136 to HMR, RO1GM101192 to Y-HW, P50HD104463, R01NS099280 and R01NS086810 to PKT), VA (BLRD BX004842 and BX003231 to PKT), the University of Michigan (Cellular and Molecular Biology Graduate program and the Chia-Lun Lo Fellowship to Y-JT), Ball State University (Startup Funds and Junior Faculty ASPIRE grant to PJS, Graduate Student ASPIRE grant to AER), and Amyotrophic Lateral Sclerosis Association Grant 18-IIA-406 to PJS.

2.7. Figures

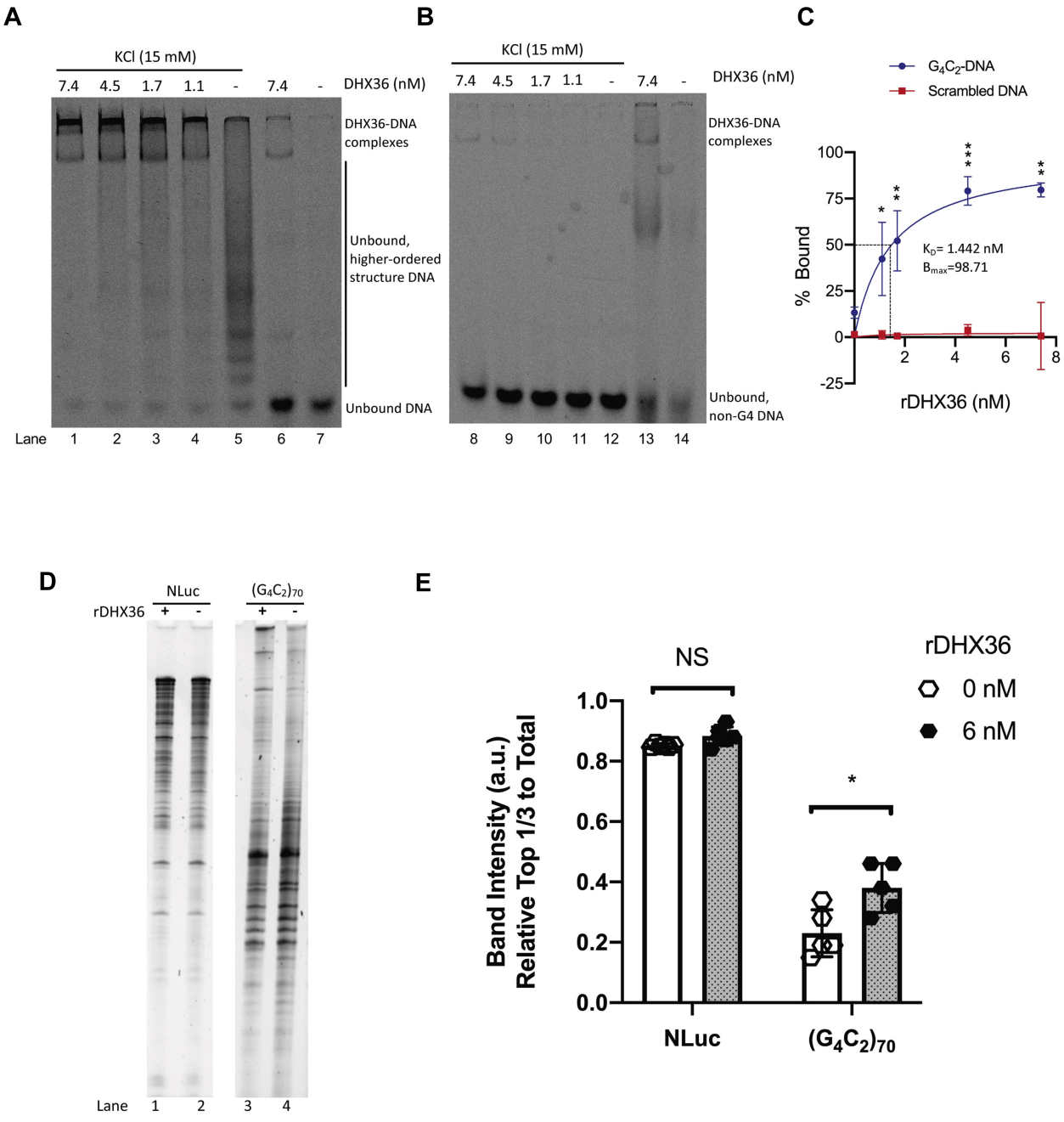

Figure 2-1. DHX36 binds and enhances transcription of C9-DNA *in vitro.*

(A) Representative electrophoretic mobility shift assay (EMSA) image. *C9* repeat DNA oligonucleotides were heated and cooled in the presence (lanes 1-5) and absence (lanes 6-7) of KCl to induce or prevent G4 formation, respectively. DNA was incubated with increasing concentrations of recombinant DHX36, analyzed with non-denaturing PAGE, and imaged. (B) Representative EMSA image. Scrambled control DNA oligonucleotides were heated and cooled in the presence (lanes 1-5) and absence (lanes 6-7) of KCl. DNA was incubated with increasing concentrations of recombinant DHX36, analyzed with non-denaturing PAGE, and imaged. (C) Densiometric quantification of panels A and B. The percent bound for each lane was graphed versus the concentration of DHX36. Data in are presented as mean ±SD, n=3. Multiple t-tests for each concentration of protein, *p=<0.05, **p<0.01, ***p<0.001. (D) T7 polymerase transcript products generated from equal amounts of linearized nanoLuciferase (lanes 1-2) or $(G_4C_2)_{70}$ plasmids (lanes 3-4) resolved by denaturing PAGE. The gel was stained with SYBR gold nucleic acid stain and imaged. (E) Densiometric quantification of panel D. All signals were first subtracted by the background. Then signal from the top third of the gel was divided by the total signal per lane. Data are presented as ±SD, n=5(NLuc)-6$(G_4C_2)_{70}$. Two-tailed pair t-test, N.S. = not-significant, *$P < 0.05$.

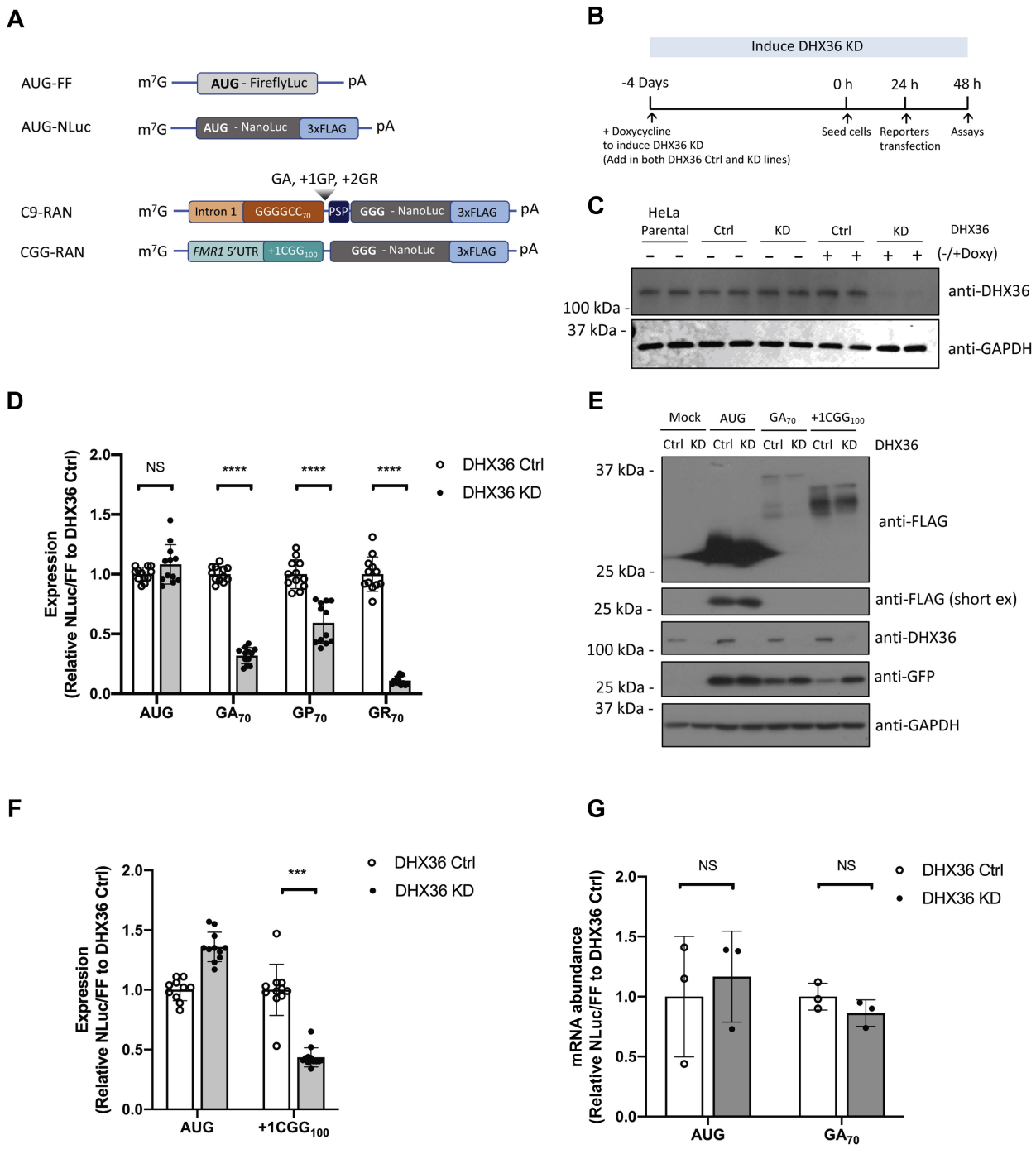

Figure 2-2. The effect of DHX36 knockdown on C9-RNA and C9RAN reporter expression.

(A) Schematic of AUG-FF, AUG-NLuc control, C9-RAN and CGG-RAN luciferase reporters. (B) Experimental timeline for doxycycline treatment and reporter transfection.

(C) Immunoblots detecting DHX36 in parental, Ctrl and DHX36 KD HeLa cells with and without doxycycline treatment. (D) Relative expression of AUG and C9-RAN translation in GA (+0), GP (+1), and GR (+2) frames with 70 repeats between Ctrl and DHX36 KD HeLa cells. NLuc signal were normalized to AUG-FFluc translation. (E) Immunoblot of RAN translation products from 70 repeats of G_4C_2 in GA frame and 100 repeats of CGG in +1 reading frame in Ctrl and DHX36 KD HeLa cells. GFP was blotted as transfection control and GAPDH was blotted as loading control. (F) Expression of $+1CGG_{100}$ RAN translation reporters measured by luciferase assay. NLuc signals were normalized to AUG-FFluc signals to compare between Ctrl and DHX36 KD HeLa cells. (G) Abundance of NLuc mRNA from AUG and GA_{70} in DHX36 Ctrl and KD HeLa cells. NLuc mRNA were normalized to FF mRNA and compared to DHX36 Ctrl. Data in (D) and (F) are represented as mean ±SD, n=9-12. Data in (G) are mean ±SD, n=3. Two-tailed Student's t-test with Bonferroni and Welch's correction, N.S. = not-significant, $*P < 0.05$; $**P < 0.01$; $***P < 0.001$; $****P < 0.0001$.

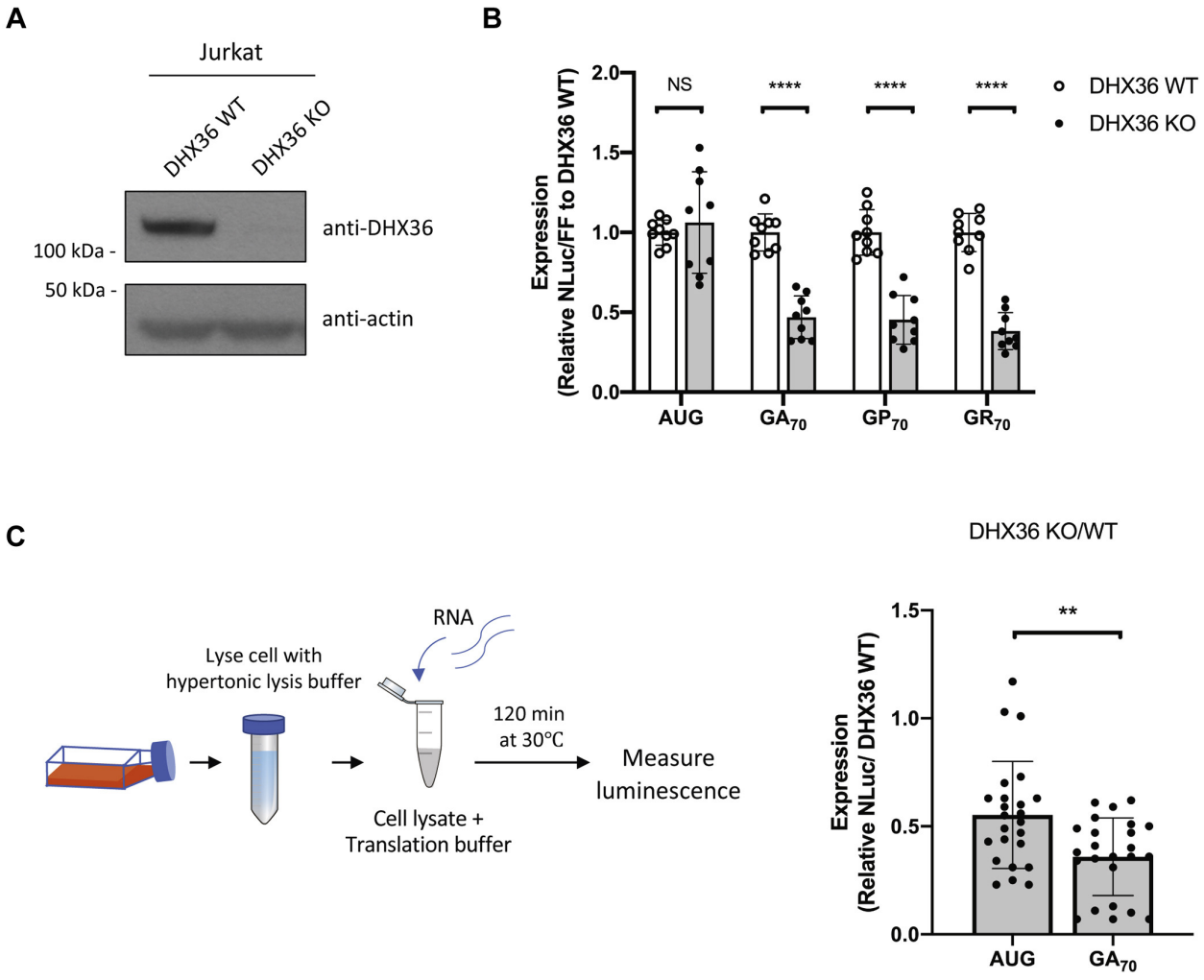

Figure 2-3. C9RAN reporter expression in DHX36 knockout Jurkat cell lines and *in vitro* cell lysates.

(A) Immunoblots to DHX36 from WT and DHX36 KO Jurkat cells. (B) Relative expression of AUG and C9-RAN translation from GA(+0), GP(+1), and GR(+2) reading frames in WT and DHX36 KO Jurkat cells. NLuc signal were normalized to AUG-FF and compared between WT and DHX36 KO Jurkat cells. Data are represented as mean ±SD, n=9. (C) *In vitro* translation using lysates derived from DHX36 WT and KO Jurkat cells for AUG-NLuc RNA and C9-RAN in GA frame RNA. NLuc signals were normalized to signal from

DHX36 WT. Data are represented as mean ±SD, n=24. Two-tailed Student's t-test with Bonferroni and Welch's correction, *$P < 0.05$; ***$P < 0.001$; ****$P < 0.0001$.

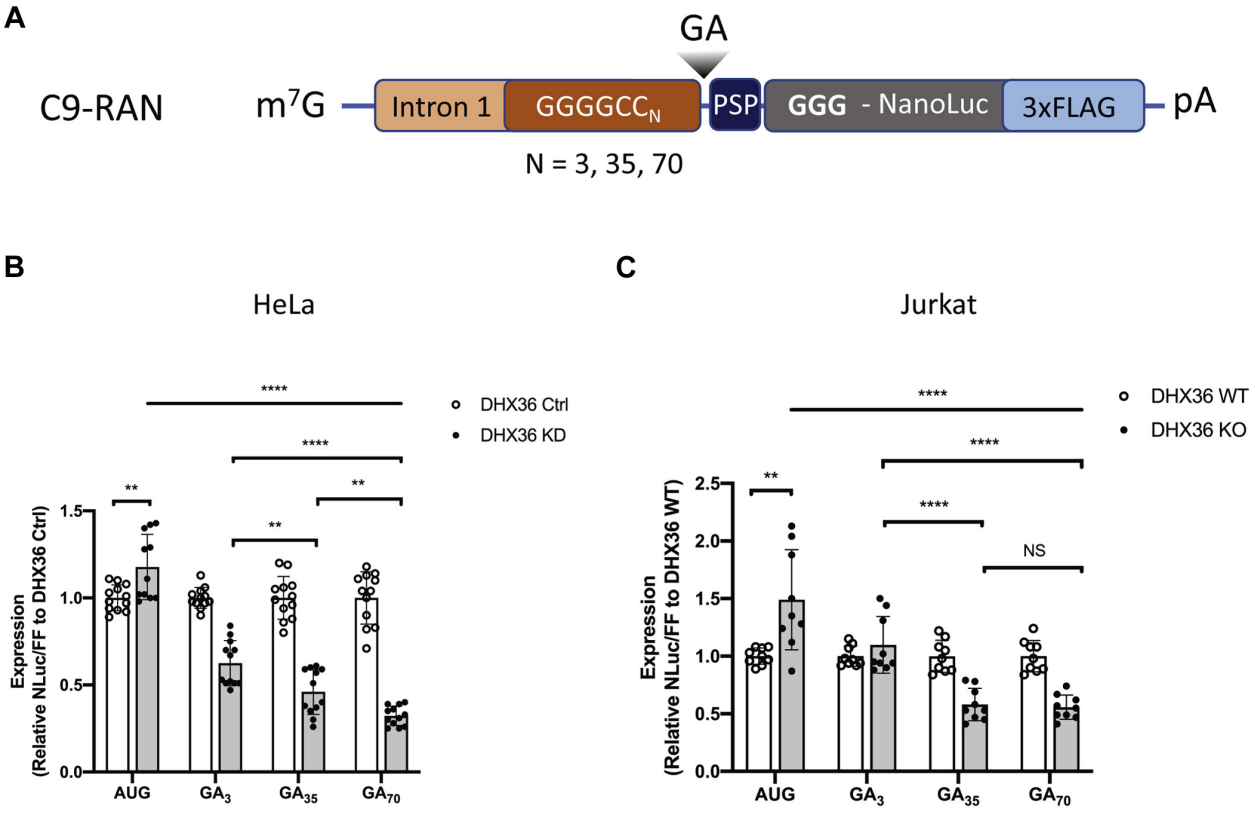

Figure 2-4. The effect of decreased DHX36 on C9RAN reporter expression is G_4C_2 repeat length dependent.

(A) Schematic of previously published luciferase reporters of C9-RAN in GA frame harboring different repeat sizes. (B)-(C) Relative expression of AUG and C9-RAN translation from GA frames with 3, 35, and 70 repeats in Ctrl and DHX36 KD HeLa cells (B), and DHX36 WT and KO Jurkat cells. NLuc signal were normalized to AUG-FF. Data are represented as mean ±SD, n=9-12. One-way ANOVA were performed to compare the statistical differences between repeat length in DHX36 KD or KO cell lines. Two-tailed Student's t-test with Bonferroni and Welch's correction were then perform to confirm the differences between multiple comparison, *$P < 0.05$; **$P < 0.01$; ****$P < 0.0001$.

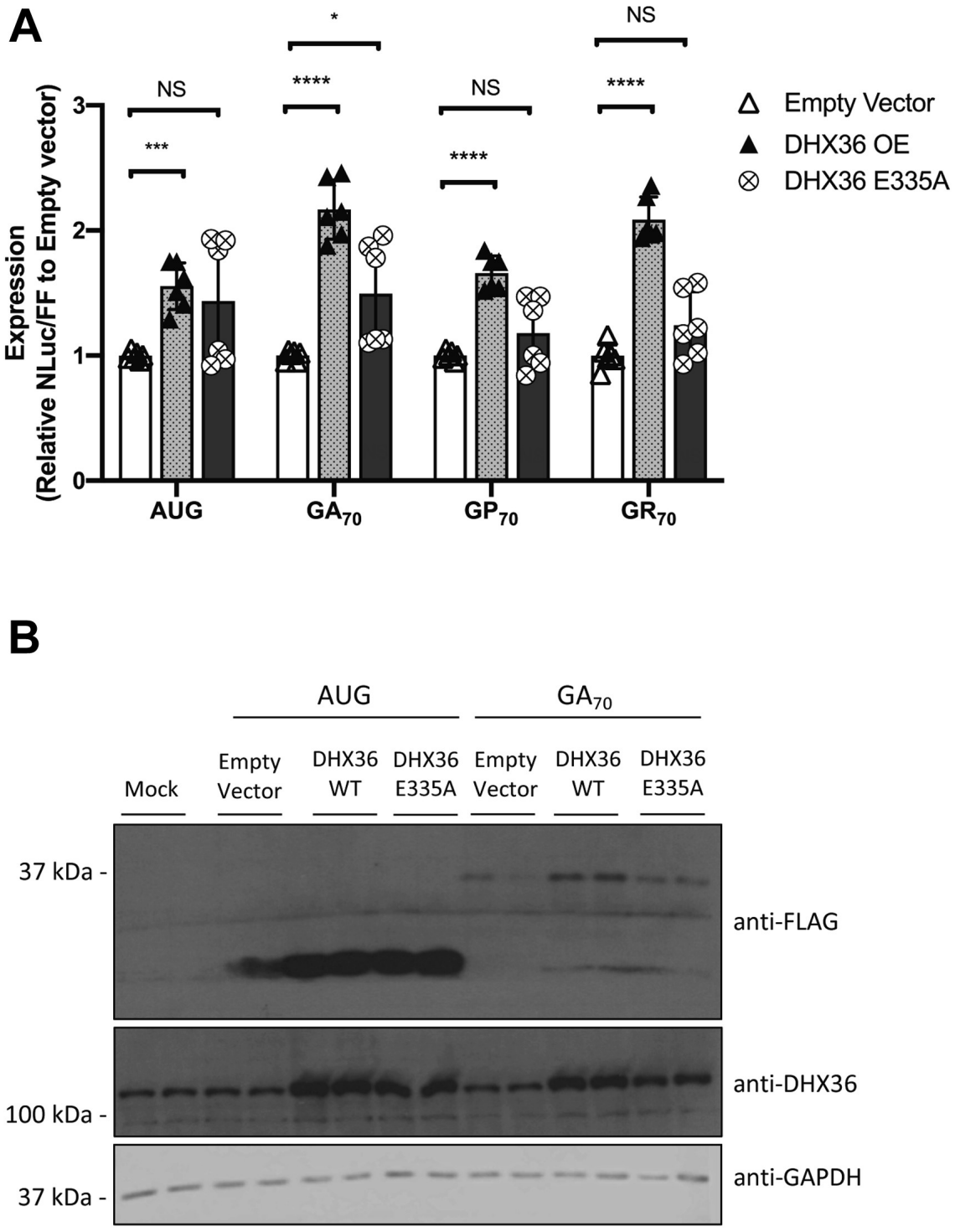

Figure 2-5. DHX36 overexpression enhances C9RAN reporter expression from G_4C_2 repeat RNA.

(A) Relative expression of AUG and C9-RAN translation when co-transfecting reporter RNA and overexpression of empty vector, WT or E335A DHX36 DNA plasmids in HeLa cells. Data are represented as mean ±SD, n=9. Two-tailed Student's t-test with Bonferroni and Welch's correction, *$P < 0.05$; ***$P < 0.001$; ****$P < 0.0001$. (B) Western blots analysis of co-transfected AUG and C9-RAN luciferase reporters in RNA and empty vector, DHX36 WT or DHX36 E335A DNA plasmids in HeLa cells. GAPDH was blotted as internal control.

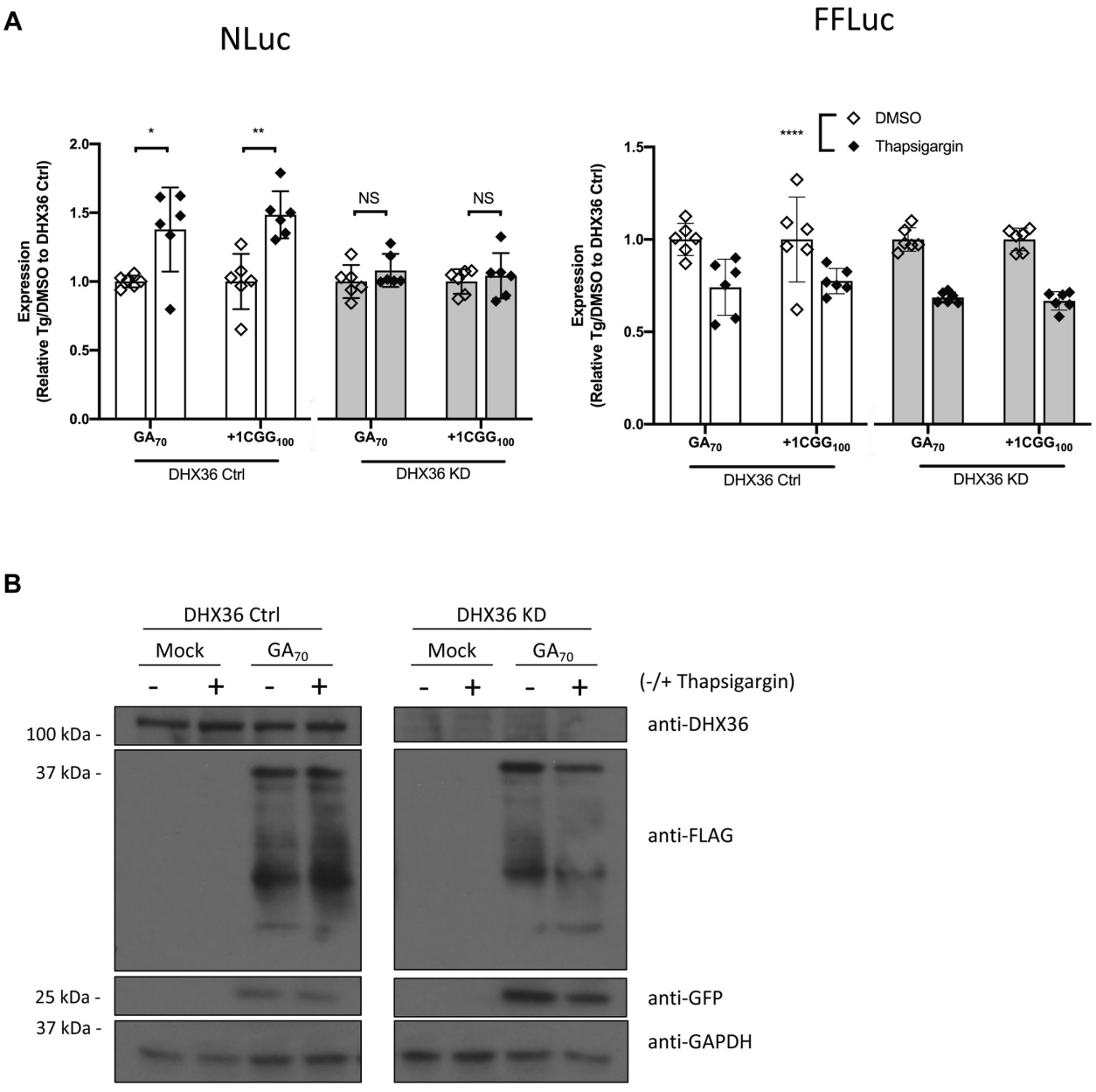

Figure 2-6. Knockdown of DHX36 prevents stress dependent upregulation of C9RAN reporter expression.

(A) Relative expression of RAN translation in G_4C_2 and CGG repeat treated with 2 μM thapsigargin or DMSO in Ctrl and DHX36 KD HeLa cells. NLuc (left) and FF (right) signal were represented as ratio of Thapsigargin treated cells to DMSO treated cells and

compared between Ctrl and DHX36 KD HeLa cells. (B) Immunoblots of G_4C_2 and CGG RAN luciferase reporters in Ctrl and DHX36 KD HeLa cells treated with 2 μM Thapsigargin. GFP was blotted as a transfection control and GAPDH was blotted as internal control. For panel A, data are represented as mean ±SD, n=6. two-way ANOVA was performed to discern effect of thapsigargin treatment across cell types. Two-tailed Student's t-test with Bonferroni and Welch's correction were performed to assess differences between individual groups. *$P < 0.05$; **$P < 0.01$; ****$P < 0.0001$.

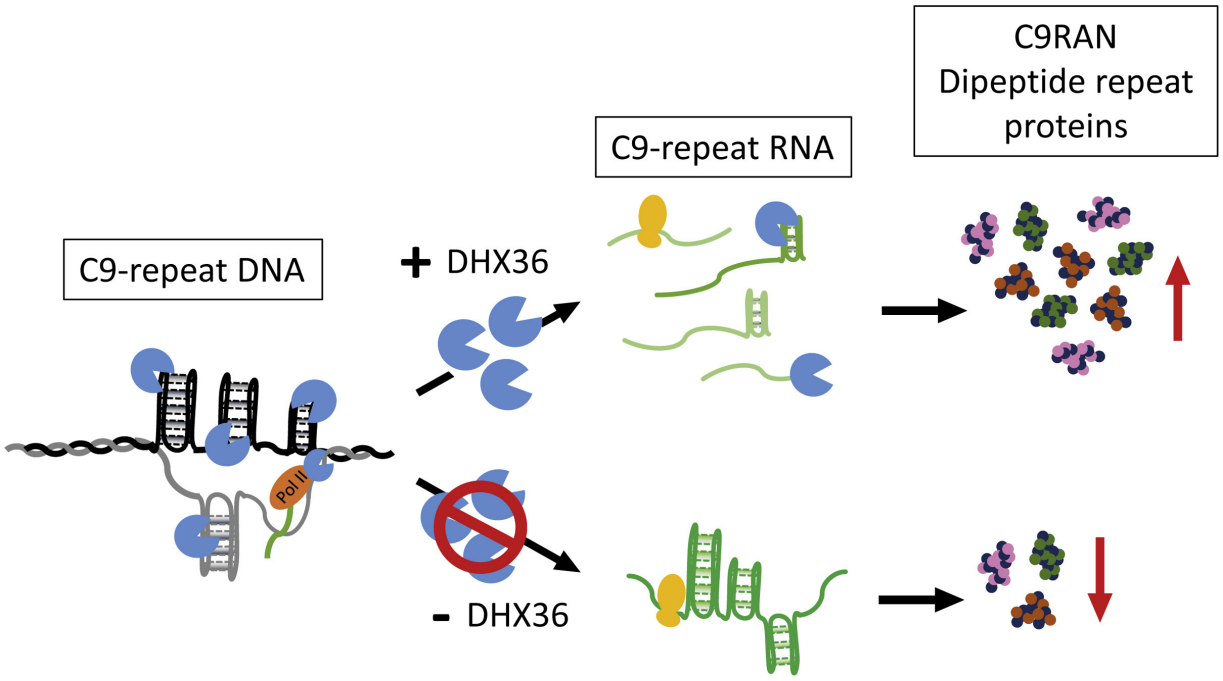

Figure 2-7. Model of DHX36 modulation of C9 RAN translation

DHX36 binds to G-quadruplex DNA and RNA structures. DHX36 aids transcription through large stretches of G_4C_2 repeat RNA *in vitro* but its effects in human cells with large repeats are unclear. Depletion of DHX36 decreases RAN translation from both CGG and C9-repeat reporters- both of which are capable of forming G-quadruplex structures- while increased DHX36 expression enhances C9RAN translation. These findings suggest a direct role for DHX36 in RAN translation of GC rich repeats.

Supplemental Figure 1

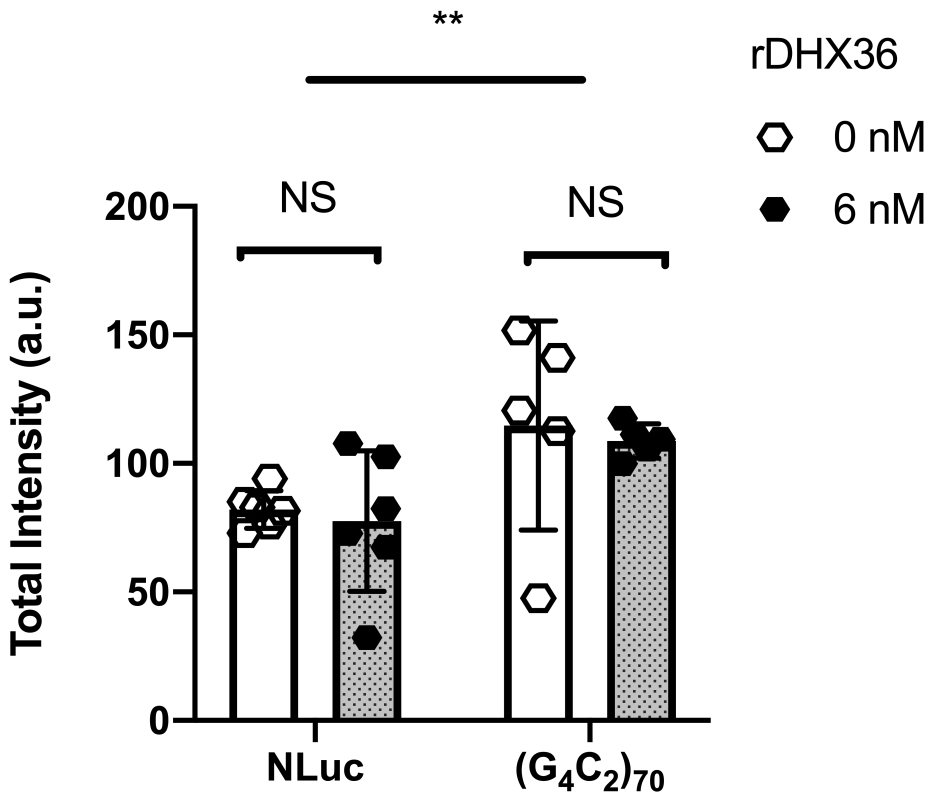

Supplemental Figure 2-8. Total RNA quantification of in vitro transcription.

The total density of each lane were quantified after subtraction to the background signal. Data are presented as ±SD, n=5(NLuc) - 6 $(G_4C_2)_{70}$. Two-tailed pair t-test was performed to compared between with or without rDHX36, N.S. = not-significant. Two-way ANOVA was performed to compare differences between NLuc and $(G_4C_2)_{70}$ experimental groups, $^{**}P < 0.005$

Supplemental Figure 2

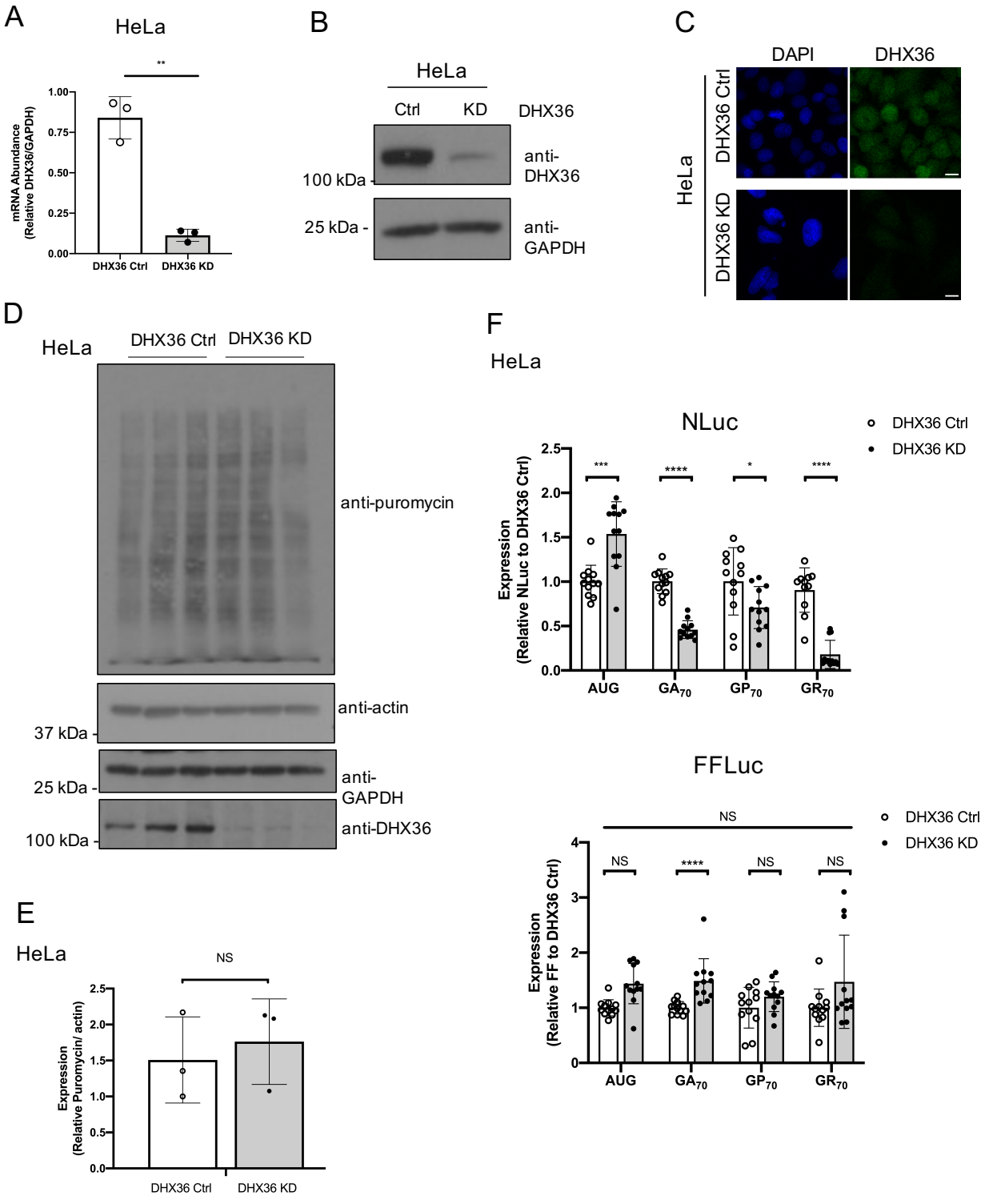

Supplemental Figure 2-9. Characterization of Control and DHX36 KD in HeLa cells.

(A) Relative abundance of DHX36 mRNA in Ctrl and DHX36 KD HeLa cells as measured by qRT-PCR (normalized to GAPDH mRNA). Data are represented as mean ±SD, n=3. Two-tailed Student's t-test with Bonferroni and Welch's correction, $^{**}P < 0.01$ (B) Western blots of DHX36 in Ctrl and DHX36 KD HeLa cells. GAPDH was blotted as internal control. (C) Immuno-fluorescent images of Ctrl and DHX36 KD HeLa cells expressing DHX36, scale bar = 10 μm. (D&E) Translation was monitored by puromycin incorporation and quantification was performed by normalizing puromycin to actin. Data are represented as mean ±SD, n=3. (F) Relative NLuc or FF signal normalized to DHX36 WT. One-way ANOVA comparing FF signal between DHX36 control and KD groups in different treatment conditions. Then two-tailed Student's t-test with Bonferroni and Welch's correction was further performed to test for statistical difference between AUG and C9-RAN translation groups, N.S. = not-significant; $^{*}P < 0.05$; $^{***}P < 0.001$; $^{****}P < 0.0001$.

Supplemental Figure 3

A

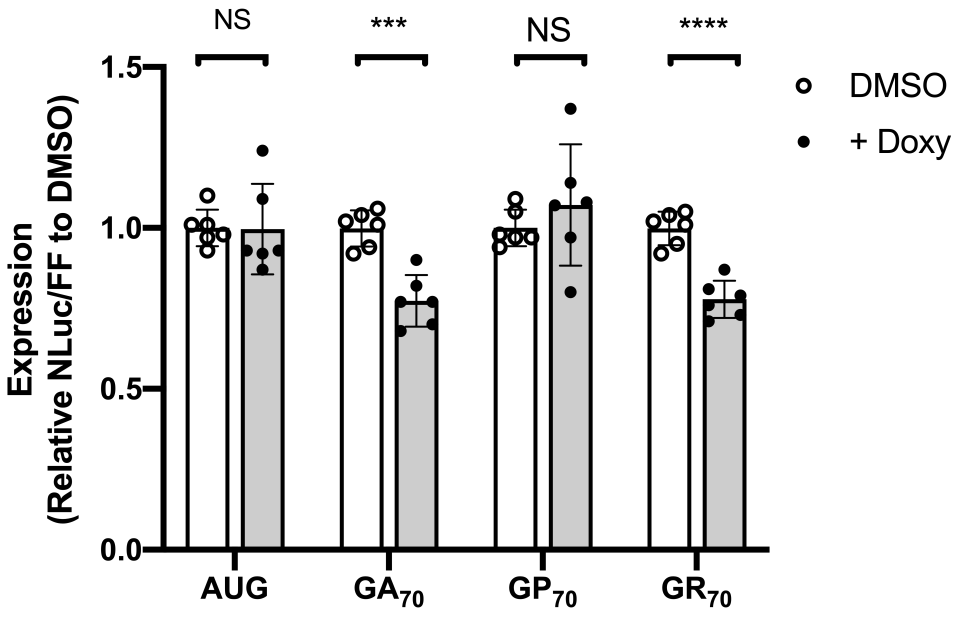

B

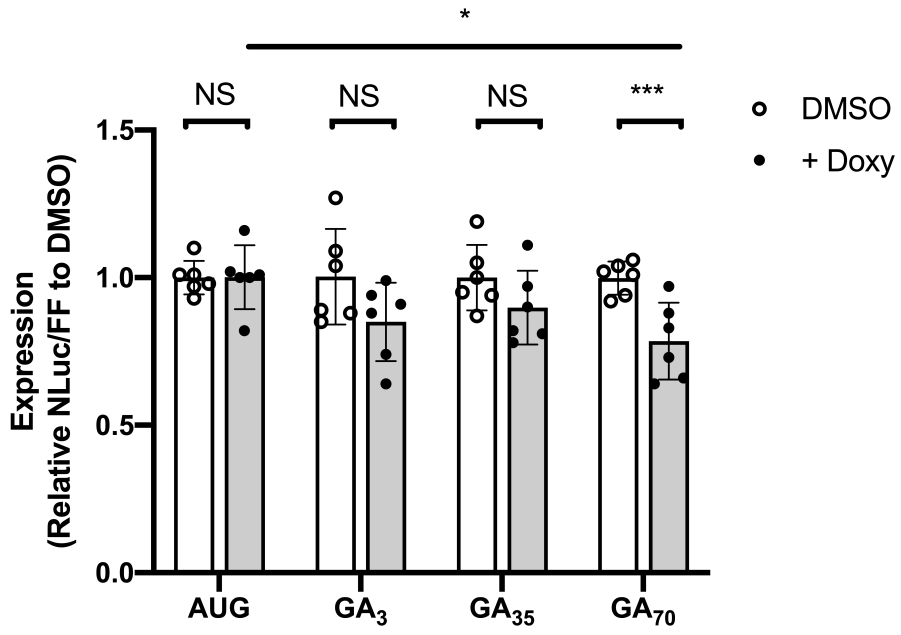

Supplemental Figure 2-1. C9RAN reporter expression in DHX36 KD inducible HeLa cells. treated with DMSO or Doxycycline.

Inducible DHX36 KD HeLa cells were treated with DMSO or Doxy prior plasmids transfection. (A) Relative expression of AUG and C9-RAN translation in GA (+0), GP (+1), and GR (+2) frames with 70 repeats. (B) Relative expression of AUG and C9-RAN translation from GA frames with 3, 35, and 70 repeats. NLuc signal were normalized to AUG-FF translation. Data are represented as mean ±SD, n=6. One-way ANOVA was performed to compare the statistical differences between repeat length in treatment of Doxycycline. Two-tailed Student's t-test with Bonferroni and Welch's correction, $*P < 0.05$; $***P < 0.001$; $****P < 0.0001$.

Supplemental Figure 4

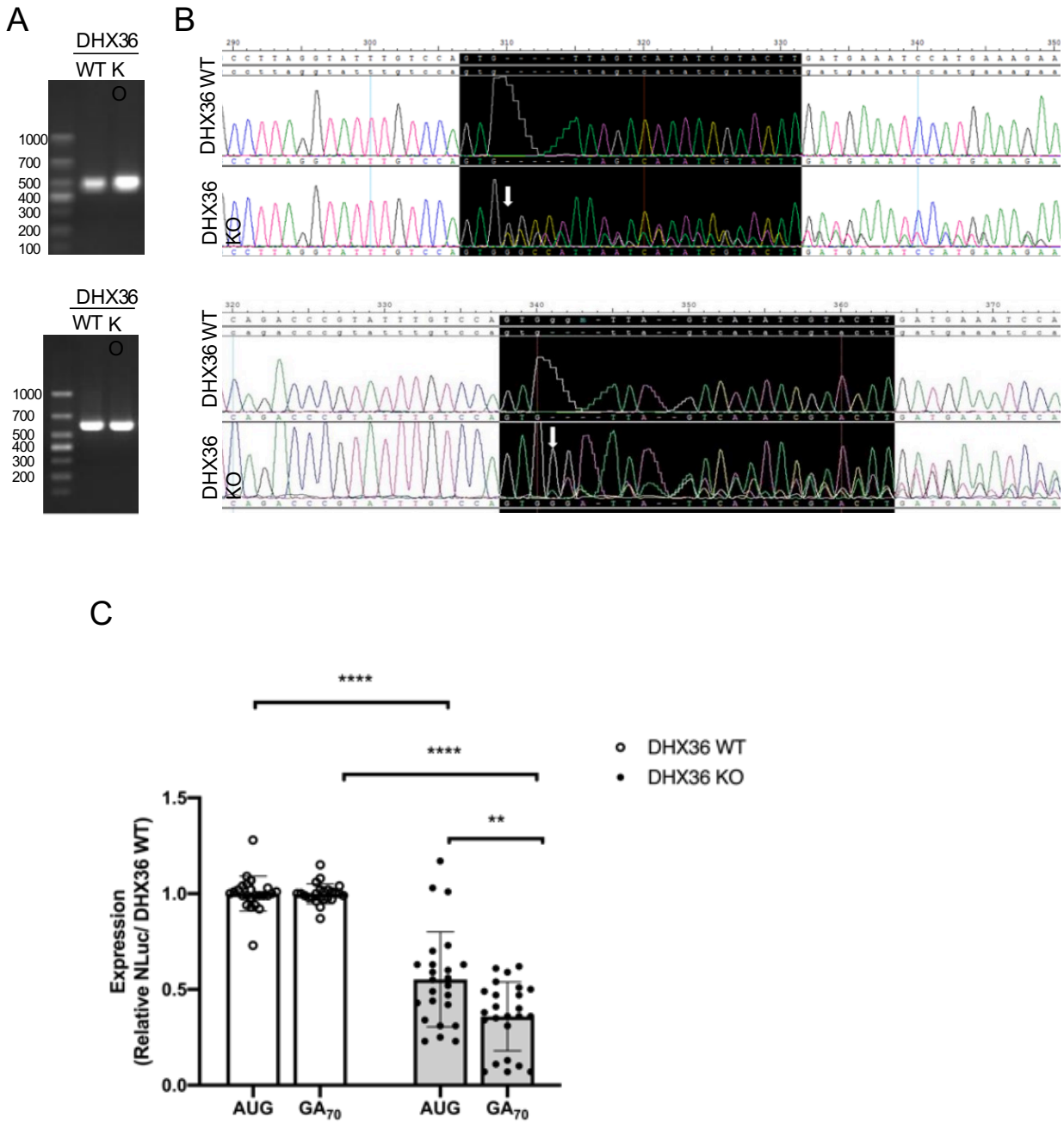

Supplemental Figure 2-2. Generation of DHX36 Knockout Jurkat cell lines.

(A) PCR (top) and RT-PCR products (bottom) from primers flanking the DHX36 gRNA site (B) Alignment of Sanger sequencing data from PCR (top) and RT-PCR (bottom) products. gRNA targeting site was shaded in black. Arrow indicates the site of INDEL mutation. The DHX36 WT clone was identified and confirmed as a negative KO clone with genotype of the target gene identical to the parental cell line (INDEL:0/0). The DHX36 KO clone was identified and confirmed with a 5 bp insertion on one allele and 6 bp insertion on the other allele at the targeted site (INDEL: +5/+6). (C) *In vitro* translation assay demonstrates knockout of DHX36 preferentially decreases C9-RAN translation compared to AUG-NLUC control. NLuc signal were normalized to DHX36 WT. Data are represented as mean ±SD, n=24. Two-tailed Student's t-test with Bonferroni and Welch's correction, $^{**}P < 0.01$; $^{****}P < 0.0001$.

Supplemental Figure 5

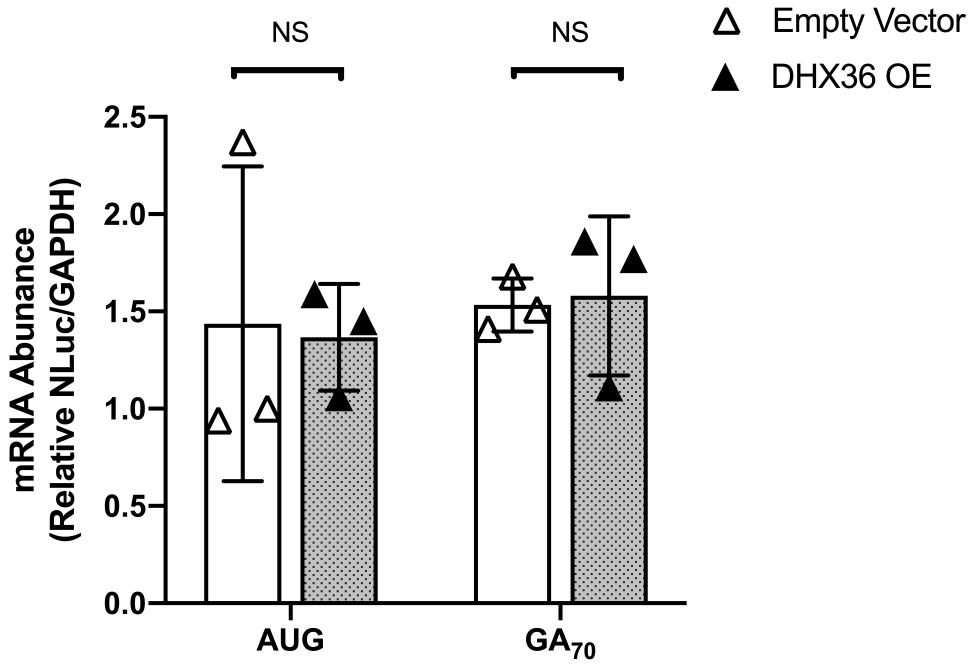

Supplemental Figure 2-3. DHX36 overexpression effect on C9RAN mRNA abundance from transfected plasmids.

Relative expression of AUG and C9-RAN translation when co-transfecting reporter DNA and overexpression of empty vector, DHX36 WT or DHX36 E335A DNA plasmids in HeLa cells. Data are represented as mean ±SD, n=9. Two-tailed Student's t-test with Bonferroni and Welch's correction, *$P < 0.05$; **$P < 0.01$; ***$P < 0.001$. (B) qRT-PCR detecting NLuc mRNA from cells transfected with empty vector or DHX36 overexpression in HeLa cells. Data are represented as mean ±SD, n=3. Two-tailed Student's t-test with Bonferroni and Welch's correction, not significant.

Supplemental Figure 6

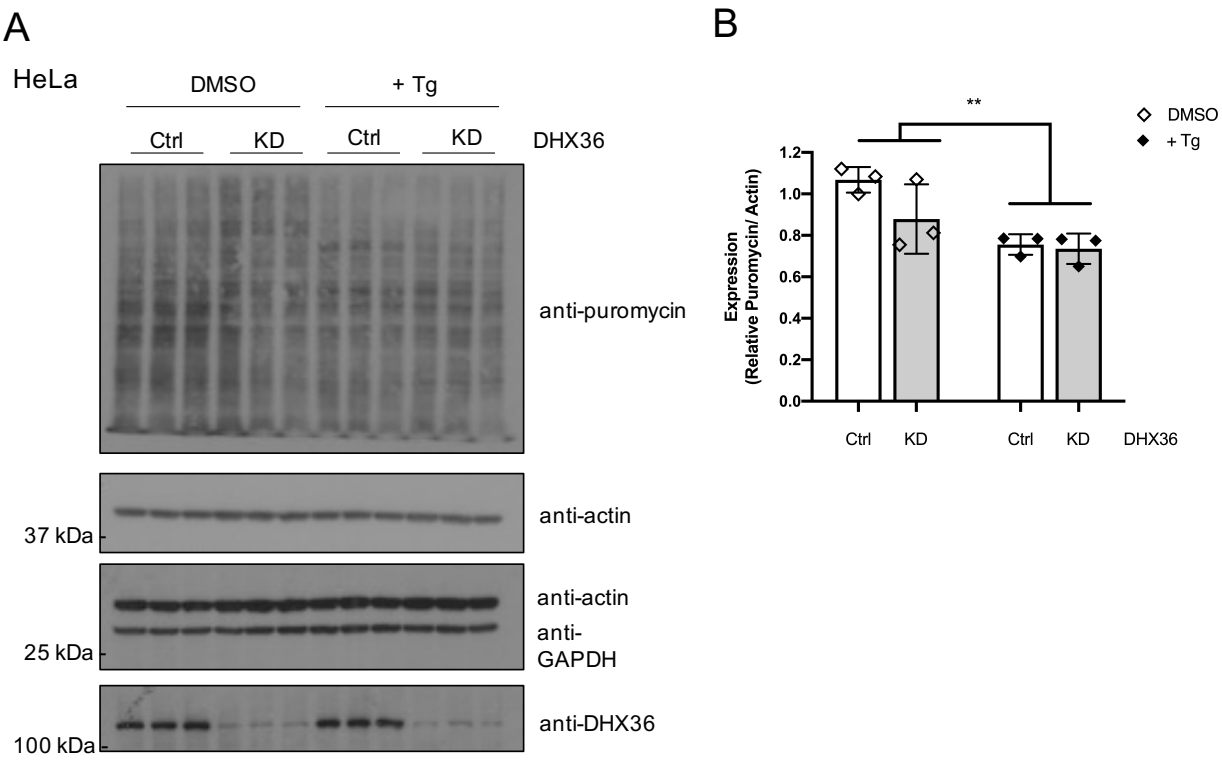

Supplemental Figure 2-4. Global protein translation in DHX36 KD HeLa cells under Thapsigargin stress.

(A-B) Effect on protein synthesis under Tg stress was monitored by puromycin incorporation and quantification was performed by normalizing puromycin to actin. With treatment of Tg, there is a decrease on global translation. Data are represented as mean ±SD, n=3. One-way ANOVA compared between DMSO and Tg treated groups, $^{**}P < 0.01$.

2.8. References

Almeida S, Krishnan G, Rushe M, Gu Y, Kankel MW, Gao FB. 2019. Production of poly(GA) in C9ORF72 patient motor neurons derived from induced pluripotent stem cells. Acta Neuropathologica. doi:10.1007/s00401-019-02083-z

Asamitsu S, Yabuki Y, Ikenoshita S, Kawakubo K, Kawasaki M, Usuki S, Nakayama Y, Adachi K, Kugoh H, Ishii K, Matsuura T, Nanba E, Sugiyama H, Fukunaga K, Shioda N. 2021. CGG repeat RNA G-quadruplexes interact with FMRpolyG to cause neuronal dysfunction in fragile X-related tremor/ataxia syndrome. Sci Adv. doi:10.1126/sciadv.abd9440

Bedrat A, Lacroix L, Mergny JL. 2016. Re-evaluation of G-quadruplex propensity with G4Hunter. Nucleic Acids Research. doi:10.1093/nar/gkw006

Biffi G, Tannahill D, McCafferty J, Balasubramanian S. 2013. Quantitative visualization of DNA G-quadruplex structures in human cells. Nature Chemistry. doi:10.1038/nchem.1548

Booy EP, Howard R, Marushchak O, Ariyo EO, Meier M, Novakowski SK, Deo SR, Dzananovic E, Stetefeld J, Mckenna SA. 2014. The RNA helicase RHAU (DHX36) suppresses expression of the transcription factor PITX1. Nucleic Acids Research. doi:10.1093/nar/gkt1340

Booy EP, McRae EKS, Howard R, Deo SR, Ariyo EO, Dzananovic E, Meier M, Stetefeld J, McKenna SA. 2016. RNA helicase associated with AU-rich element (RHAU/DHX36) interacts with the 3′-tail of the long non-coding RNA BC200 (BCYRN1). Journal of Biological Chemistry 291:5355–5372. doi:10.1074/jbc.M115.711499

Booy EP, McRae EKS, McKenna SA. 2015. Biochemical characterization of G4 Quadruplex Telomerase RNA unwinding by the RNA helicase RHAU. Methods in Molecular Biology. doi:10.1007/978-1-4939-2214-7_9

Booy EP, Meier M, Okun N, Novakowski SK, Xiong S, Stetefeld J, McKenna SA. 2012. The RNA helicase RHAU (DHX36) unwinds a G4-quadruplex in human telomerase RNA and promotes the formation of the P1 helix template boundary. Nucleic Acids Research. doi:10.1093/nar/gkr1306

Brunelle JL, Green R. 2013. In vitro transcription from plasmid or PCR-amplified DNA, 1st ed, Methods in Enzymology. Elsevier Inc. doi:10.1016/B978-0-12-420037-1.00005-1

Buijsen RAM, Sellier C, Severijnen LAWFM, Oulad-Abdelghani M, Verhagen RFM, Berman RF, Charlet-Berguerand N, Willemsen R, Hukema RK. 2014. FMRpolyG-positive inclusions in CNS and non-CNS organs of a fragile X premutation carrier with fragile X-associated tremor/ataxia syndrome. Acta Neuropathol Commun. doi:10.1186/s40478-014-0162-2

Buijsen RAM, Visser JA, Kramer P, Severijnen EAWFM, Gearing M, Charlet-Berguerand N, Sherman SL, Berman RF, Willemsen R, Hukema RK. 2016. Presence of inclusions positive for polyglycine containing protein, FMRpolyG, indicates that repeat-associated non-AUG translation plays a role in fragile X-associated primary ovarian insufficiency. Human Reproduction 31:158–168. doi:10.1093/humrep/dev280

Byrd AK, Zybailov BL, Maddukuri L, Gao J, Marecki JC, Jaiswal M, Bell MR, Griffin WC, Reed MR, Chib S, Mackintosh SG, MacNicol AM, Baldini G, Eoff RL, Raney KD.

2016. Evidence that G-quadruplex DNA accumulates in the cytoplasm and participates in stress granule assembly in response to oxidative stress. Journal of Biological Chemistry. doi:10.1074/jbc.M116.718478

Byrne S, Heverin M, Elamin M, Walsh C, Hardiman O. 2014. Intermediate repeat expansion length in C9orf72 may be pathological in amyotrophic lateral sclerosis. Amyotrophic Lateral Sclerosis and Frontotemporal Degeneration. doi:10.3109/21678421.2013.838586

Chalupníková K, Lattmann S, Selak N, Iwamoto F, Fujiki Y, Nagamine Y. 2008. Recruitment of the RNA helicase RHAU to stress granules via a unique RNA-binding domain. Journal of Biological Chemistry. doi:10.1074/jbc.M804857200

Chambers VS, Marsico G, Boutell JM, Di Antonio M, Smith GP, Balasubramanian S. 2015. High-throughput sequencing of DNA G-quadruplex structures in the human genome. Nature Biotechnology. doi:10.1038/nbt.3295

Chen MC, Tippana R, Demeshkina NA, Murat P, Balasubramanian S, Myong S, Ferré-D'amaré AR. 2018. Structural basis of G-quadruplex unfolding by the DEAH/RHA helicase DHX36. Nature 558:465–483. doi:10.1038/s41586-018-0209-9

Cheng W, Wang S, Mestre AA, Fu C, Makarem A, Xian F, Hayes LR, Lopez-Gonzalez R, Drenner K, Jiang J, Cleveland DW, Sun S. 2018. C9ORF72 GGGGCC repeat-associated non-AUG translation is upregulated by stress through eIF2α phosphorylation. Nat Commun. doi:10.1038/s41467-017-02495-z

Cheng W, Wang S, Zhang Z, Morgens DW, Hayes LR, Lee S, Portz B, Xie Y, Nguyen B V., Haney MS, Yan S, Dong D, Coyne AN, Yang J, Xian F, Cleveland DW, Qiu Z, Rothstein JD, Shorter J, Gao FB, Bassik MC, Sun S. 2019. CRISPR-Cas9 Screens

Identify the RNA Helicase DDX3X as a Repressor of C9ORF72 (GGGGCC)n Repeat-Associated Non-AUG Translation. Neuron 104:885-898.e8. doi:10.1016/j.neuron.2019.09.003

Conlon EG, Lu L, Sharma A, Yamazaki T, Tang T, Shneider NA, Manley JL. 2016. The C9ORF72 GGGGCC expansion forms RNA G-quadruplex inclusions and sequesters hnRNP H to disrupt splicing in ALS brains. Elife 5. doi:10.7554/eLife.17820

Creacy SD, Routh ED, Iwamoto F, Nagamine Y, Akman SA, Vaughn JP. 2008. G4 resolvase 1 binds both DNA and RNA tetramolecular quadruplex with high affinity and is the major source of tetramolecular quadruplex G4-DNA and G4-RNA resolving activity in HeLa cell lysates. Journal of Biological Chemistry. doi:10.1074/jbc.M806277200

DeJesus-Hernandez M, Mackenzie IR, Boeve BF, Boxer AL, Baker M, Rutherford NJ, Nicholson AM, Finch NA, Flynn H, Adamson J, Kouri N, Wojtas A, Sengdy P, Hsiung G-YR, Karydas A, Seeley WW, Josephs KA, Coppola G, Geschwind DH, Wszolek ZK, Feldman H, Knopman DS, Petersen RC, Miller BL, Dickson DW, Boylan KB, Graff-Radford NR, Rademakers R. 2011. Expanded GGGGCC Hexanucleotide Repeat in Noncoding Region of C9ORF72 Causes Chromosome 9p-Linked FTD and ALS. Neuron 72:245–256. doi:10.1016/j.neuron.2011.09.011

Donnelly CJ, Zhang PW, Pham JT, Heusler AR, Mistry NA, Vidensky S, Daley EL, Poth EM, Hoover B, Fines DM, Maragakis N, Tienari PJ, Petrucelli L, Traynor BJ, Wang J, Rigo F, Bennett CF, Blackshaw S, Sattler R, Rothstein JD. 2013. RNA Toxicity

from the ALS/FTD C9ORF72 Expansion Is Mitigated by Antisense Intervention. Neuron 80:415–428. doi:10.1016/j.neuron.2013.10.015

Fratta P, Mizielinska S, Nicoll AJ, Zloh M, Fisher EMC, Parkinson G, Isaacs AM. 2012. C9orf72 hexanucleotide repeat associated with amyotrophic lateral sclerosis and frontotemporal dementia forms RNA G-quadruplexes. Sci Rep. doi:10.1038/srep01016

Fry M, Loeb LA. 1994. The fragile X syndrome d(CGG)(n) nucleotide repeats form a stable tetrahelical structure. Proc Natl Acad Sci U S A. doi:10.1073/pnas.91.11.4950

Giri B, Smaldino PJ, Thys RG, Creacy SD, Routh ED, Hantgan RR, Lattmann S, Nagamine Y, Akman SA, Vaughn JP. 2011. G4 Resolvase 1 tightly binds and unwinds unimolecular G4-DNA. Nucleic Acids Research. doi:10.1093/nar/gkr234

Goodman LD, Prudencio M, Srinivasan AR, Rifai OM, Lee VMY, Petrucelli L, Bonini NM. 2019. eIF4B and eIF4H mediate GR production from expanded G4C2 in a Drosophila model for C9orf72-associated ALS. Acta neuropathologica communications. doi:10.1186/s40478-019-0711-9

Green KM, Glineburg MR, Kearse MG, Flores BN, Linsalata AE, Fedak SJ, Goldstrohm AC, Barmada SJ, Todd PK. 2017. RAN translation at C9orf72-associated repeat expansions is selectively enhanced by the integrated stress response. Nat Commun 8. doi:10.1038/s41467-017-02200-0

Haeusler AR, Donnelly CJ, Periz G, Simko EAJ, Shaw PG, Kim M-S, Maragakis NJ, Troncoso JC, Pandey A, Sattler R, Rothstein JD, Wang J. 2014. C9orf72

nucleotide repeat structures initiate molecular cascades of disease. Nature 507:195–200. doi:10.1038/nature13124

Hänsel-Hertsch R, Beraldi D, Lensing S V., Marsico G, Zyner K, Parry A, Di Antonio M, Pike J, Kimura H, Narita M, Tannahill D, Balasubramanian S. 2016. G-quadruplex structures mark human regulatory chromatin. Nature Genetics. doi:10.1038/ng.3662

Henderson A, Wu Y, Huang YC, Chavez EA, Platt J, Johnson FB, Brosh RM, Sen D, Lansdorp PM. 2014. Detection of G-quadruplex DNA in mammalian cells. Nucleic Acids Research. doi:10.1093/nar/gkt957

Hinnebusch AG, Ivanov IP, Sonenberg N. 2016. Translational control by 5′-untranslated regions of eukaryotic mRNAs. Science 352:1413–1416. doi:10.1126/science.aad9868

Huang W, Smaldino PJ, Zhang Q, Miller LD, Cao P, Stadelman K, Wan M, Giri B, Lei M, Nagamine Y, Vaughn JP, Akman SA, Sui G. 2012. Yin Yang 1 contains G-quadruplex structures in its promoter and 5′-UTR and its expression is modulated by G4 resolvase 1. Nucleic Acids Research. doi:10.1093/nar/gkr849

Hukema RK, Buijsen RAM, Schonewille M, Raske C, Severijnen L-AWFM, Nieuwenhuizen-Bakker I, Verhagen RFM, van Dessel L, Maas A, Charlet-Berguerand N, De Zeeuw CI, Hagerman PJ, Berman RF, Willemsen R. 2015. Reversibility of neuropathology and motor deficits in an inducible mouse model for FXTAS. Human Molecular Genetics 24:4948–4957. doi:10.1093/hmg/ddv216

Huppert JL, Balasubramanian S. 2007. G-quadruplexes in promoters throughout the human genome. Nucleic Acids Research. doi:10.1093/nar/gkl1057

Huppert JL, Balasubramanian S. 2005. Prevalence of quadruplexes in the human genome. Nucleic Acids Research. doi:10.1093/nar/gki609

Iwamoto F, Stadler M, Chalupníková K, Oakeley E, Nagamine Y. 2008. Transcription-dependent nucleolar cap localization and possible nuclear function of DExH RNA helicase RHAU. Experimental Cell Research. doi:10.1016/j.yexcr.2008.01.006

Jackson RJ, Hellen CUT, Pestova T V. 2010. The mechanism of eukaryotic translation initiation and principles of its regulation. Nat Rev Mol Cell Biol 11:113–127. doi:10.1038/nrm2838

Kearse MG, Green KM, Krans A, Rodriguez CM, Linsalata AE, Goldstrohm AC, Todd PK. 2016. CGG Repeat-Associated Non-AUG Translation Utilizes a Cap-Dependent Scanning Mechanism of Initiation to Produce Toxic Proteins. Mol Cell 62:314–322. doi:10.1016/j.molcel.2016.02.034

Kettani A, Kumar RA, Patel DJ. 1995. Solution structure of a DNA quadruplex containing the fragile X syndrome triplet repeat. Journal of Molecular Biology. doi:10.1006/jmbi.1995.0644

Kim HN, Lee JH, Bae SC, Ryoo HM, Kim HH, Ha H, Lee ZH. 2011. Histone deacetylase inhibitor MS-275 stimulates bone formation in part by enhancing Dhx36-mediated TNAP transcription. Journal of Bone and Mineral Research. doi:10.1002/jbmr.426

Komar AA, Hatzoglou M. 2011. Cellular IRES-mediated translation: The war of ITAFs in pathophysiological states. Cell Cycle. doi:10.4161/cc.10.2.14472

Komar AA, Hatzoglou M. 2005. Internal ribosome entry sites in cellular mRNAs: Mystery of their existence. Journal of Biological Chemistry 280:23425–23428. doi:10.1074/jbc.R400041200

Krans A, Kearse MG, Todd PK. 2016. Repeat-associated non-AUG translation from antisense CCG repeats in fragile X tremor/ataxia syndrome. Ann Neurol. doi:10.1002/ana.24800

Linsalata AE, He F, Malik AM, Glineburg MR, Green KM, Natla S, Flores BN, Krans A, Archbold HC, Fedak SJ, Barmada SJ, Todd PK. 2019. DDX 3X and specific initiation factors modulate FMR 1 repeat-associated non-AUG-initiated translation . EMBO Rep 1–18. doi:10.15252/embr.201847498

Liu H, Lu Y-N, Paul T, Periz G, Banco MT, Ferré-D'amaré AR, Rothstein JD, Hayes LR, Myong S, Wang J. 2021. A Helicase Unwinds Hexanucleotide Repeat RNA G-Quadruplexes and Facilitates Repeat-Associated Non-AUG Translation. Cite This: J Am Chem Soc 143:7368–7379. doi:10.1021/jacs.1c00131

Maizels N. 2015. G4-associated human diseases. EMBO reports. doi:10.15252/embr.201540607

Maltby CJ, Schofield JPR, Houghton SD, O'Kelly I, Vargas-Caballero M, Deinhardt K, Coldwell MJ. 2020. A 5' UTR GGN repeat controls localisation and translation of a potassium leak channel mRNA through G-quadruplex formation. Nucleic Acids Research. doi:10.1093/nar/gkaa699

McRae EKS, Booy EP, Moya-Torres A, Ezzati P, Stetefeld J, McKenna SA. 2017. Human DDX21 binds and unwinds RNA guanine quadruplexes. Nucleic Acids Research. doi:10.1093/nar/gkx380

Mendoza O, Bourdoncle A, Boulé JB, Brosh RM, Mergny JL. 2016. G-quadruplexes and helicases. Nucleic Acids Research. doi:10.1093/nar/gkw079

Murat P, Marsico G, Herdy B, Ghanbarian A, Portella G, Balasubramanian S. 2018. RNA G-quadruplexes at upstream open reading frames cause DHX36- and DHX9-dependent translation of human mRNAs. Genome Biol. doi:10.1186/s13059-018-1602-2

Nie J, Jiang M, Zhang X, Tang H, Jin H, Huang X, Yuan B, Zhang C, Lai JC, Nagamine Y, Pan D, Wang W, Yang Z. 2015. Post-transcriptional Regulation of Nkx2-5 by RHAU in Heart Development. Cell Reports. doi:10.1016/j.celrep.2015.09.043

Renton AE, Majounie E, Waite A, Simón-Sánchez J, Rollinson S, Gibbs JR, Schymick JC, Laaksovirta H, van Swieten JC, Myllykangas L, Kalimo H, Paetau A, Abramzon Y, Remes AM, Kaganovich A, Scholz SW, Duckworth J, Ding J, Harmer DW, Hernandez DG, Johnson JO, Mok K, Ryten M, Trabzuni D, Guerreiro RJ, Orrell RW, Neal J, Murray A, Pearson J, Jansen IE, Sondervan D, Seelaar H, Blake D, Young K, Halliwell N, Callister JB, Toulson G, Richardson A, Gerhard A, Snowden J, Mann D, Neary D, Nalls MA, Peuralinna T, Jansson L, Isoviita V-M, Kaivorinne A-L, Hölttä-Vuori M, Ikonen E, Sulkava R, Benatar M, Wuu J, Chiò A, Restagno G, Borghero G, Sabatelli M, Heckerman D, Rogaeva E, Zinman L, Rothstein JD, Sendtner M, Drepper C, Eichler EE, Alkan C, Abdullaev Z, Pack SD, Dutra A, Pak E, Hardy J, Singleton A, Williams NM, Heutink P, Pickering-Brown S, Morris HR, Tienari PJ, Traynor BJ. 2011. A Hexanucleotide Repeat Expansion in C9ORF72 Is the Cause of Chromosome 9p21-Linked ALS-FTD. Neuron 72:257–268. doi:10.1016/J.NEURON.2011.09.010

Rhodes D, Lipps HJ. 2015. Survey and summary G-quadruplexes and their regulatory roles in biology. Nucleic Acids Research. doi:10.1093/nar/gkv862

Rodriguez CM, Todd PK. 2019. New pathologic mechanisms in nucleotide repeat expansion disorders. Neurobiol Dis. doi:10.1016/j.nbd.2019.104515

Sauer M, Juranek SA, Marks J, De Magis A, Kazemier HG, Hilbig D, Benhalevy D, Wang X, Hafner M, Paeschke K. 2019. DHX36 prevents the accumulation of translationally inactive mRNAs with G4-structures in untranslated regions. Nat Commun. doi:10.1038/s41467-019-10432-5

Schmidt EK, Clavarino G, Ceppi M, Pierre P. 2009. SUnSET, a nonradioactive method to monitor protein synthesis. Nature Methods 6:275–277. doi:10.1038/nmeth.1314

Schofield JPR, Cowan JL, Coldwell MJ. 2015. G-quadruplexes mediate local translation in neurons. Biochemical Society Transactions. doi:10.1042/BST20150053

Schult P, Paeschke K. 2020. The DEAH helicase DHX36 and its role in G-quadruplex-dependent processes. Biological Chemistry 402:581–591. doi:10.1515/hsz-2020-0292

Sellier C, Buijsen RAM, He F, Natla S, Jung L, Tropel P, Gaucherot A, Jacobs H, Meziane H, Vincent A, Champy MF, Sorg T, Pavlovic G, Wattenhofer-Donze M, Birling MC, Oulad-Abdelghani M, Eberling P, Ruffenach F, Joint M, Anheim M, Martinez-Cerdeno V, Tassone F, Willemsen R, Hukema RK, Viville S, Martinat C, Todd PK, Charlet-Berguerand N. 2017. Translation of Expanded CGG Repeats into FMRpolyG Is Pathogenic and May Contribute to Fragile X Tremor Ataxia Syndrome. Neuron. doi:10.1016/j.neuron.2016.12.016

Sexton AN, Collins K. 2011. The 5’ Guanosine Tracts of Human Telomerase RNA Are Recognized by the G-Quadruplex Binding Domain of the RNA Helicase DHX36

and Function To Increase RNA Accumulation. Molecular and Cellular Biology. doi:10.1128/mcb.01033-10

Shi KY, Mori E, Nizami ZF, Lin Y, Kato M, Xiang S, Wu LC, Ding M, Yu Y, Gall JG, McKnight SL. 2017. Toxic PRn poly-dipeptides encoded by the C9orf72 repeat expansion block nuclear import and export. Proceedings of the National Academy of Sciences of the United States of America. doi:10.1073/pnas.1620293114

Shi Y, Lin S, Staats KA, Li Y, Chang WH, Hung ST, Hendricks E, Linares GR, Wang Y, Son EY, Wen X, Kisler K, Wilkinson B, Menendez L, Sugawara T, Woolwine P, Huang M, Cowan MJ, Ge B, Koutsodendris N, Sandor KP, Komberg J, Vangoor VR, Senthilkumar K, Hennes V, Seah C, Nelson AR, Cheng TY, Lee SJJ, August PR, Chen JA, Wisniewski N, Hanson-Smith V, Belgard TG, Zhang A, Coba M, Grunseich C, Ward ME, Van Den Berg LH, Pasterkamp RJ, Trotti D, Zlokovic B V., Ichida JK. 2018. Haploinsufficiency leads to neurodegeneration in C9ORF72 ALS/FTD human induced motor neurons. Nat Med 24. doi:10.1038/nm.4490

Simone R, Balendra R, Moens TG, Preza E, Wilson KM, Heslegrave A, Woodling NS, Niccoli T, Gilbert-Jaramillo J, Abdelkarim S, Clayton EL, Clarke M, Konrad M, Nicoll AJ, Mitchell JS, Calvo A, Chio A, Houlden H, Polke JM, Ismail MA, Stephens CE, Vo T, Farahat AA, Wilson WD, Boykin DW, Zetterberg H, Partridge L, Wray S, Parkinson G, Neidle S, Patani R, Fratta P, Isaacs AM. 2018. G-quadruplex-binding small molecules ameliorate C9orf72 FTD / ALS pathology in vitro and in vivo . EMBO Molecular Medicine 10:22–31. doi:10.15252/emmm.201707850

Simone R, Fratta P, Neidle S, Parkinson GN, Isaacs AM. 2015. G-quadruplexes: Emerging roles in neurodegenerative diseases and the non-coding transcriptome. FEBS Lett. doi:10.1016/j.febslet.2015.05.003

Smaldino PJ, Routh ED, Kim JH, Giri B, Creacy SD, Hantgan RR, Akman SA, Vaughn JP. 2015. Mutational dissection of telomeric DNA binding requirements of G4 Resolvase 1 shows that G4-structure and certain 3′-tail sequences are sufficient for tight and complete binding. PLoS ONE. doi:10.1371/journal.pone.0132668

Sonobe Y, Ghadge G, Masaki K, Sendoel A, Fuchs E, Roos RP. 2018. Translation of dipeptide repeat proteins from the C9ORF72 expanded repeat is associated with cellular stress. Neurobiol Dis. doi:10.1016/j.nbd.2018.05.009

Starck SR, Tsai JC, Chen K, Shodiya M, Wang L, Yahiro K, Martins-Green M, Shastri N, Walter P. 2016. Translation from the 5' untranslated region shapes the integrated stress response. Science 351. doi:10.1126/science.aad3867

Stoneley M, Willis AE. 2004. Cellular internal ribosome entry segments: Structures, trans-acting factors and regulation of gene expression. Oncogene. doi:10.1038/sj.onc.1207551

Su Z, Zhang Y, Gendron TF, Bauer PO, Chew J, Yang WY, Fostvedt E, Jansen-West K, Belzil V V., Desaro P, Johnston A, Overstreet K, Oh SY, Todd PK, Berry JD, Cudkowicz ME, Boeve BF, Dickson D, Floeter MK, Traynor BJ, Morelli C, Ratti A, Silani V, Rademakers R, Brown RH, Rothstein JD, Boylan KB, Petrucelli L, Disney MD. 2014. Discovery of a Biomarker and Lead Small Molecules to Target r(GGGGCC)-Associated Defects in c9FTD/ALS. Neuron. doi:10.1016/j.neuron.2014.07.041

Tabet R, Schaeffer L, Freyermuth F, Jambeau M, Workman M, Lee CZ, Lin CC, Jiang J, Jansen-West K, Abou-Hamdan H, Désaubry L, Gendron T, Petrucelli L, Martin F, Lagier-Tourenne C. 2018. CUG initiation and frameshifting enable production of dipeptide repeat proteins from ALS/FTD C9ORF72 transcripts. Nat Commun 9:1–14. doi:10.1038/s41467-017-02643-5

Taylor JP. 2017. A PR plug for the nuclear pore in amyotrophic lateral sclerosis. Proceedings of the National Academy of Sciences of the United States of America. doi:10.1073/pnas.1621085114

Todd PK, Oh SY, Krans A, He F, Sellier C, Frazer M, Renoux AJ, Chen K chun, Scaglione KM, Basrur V, Elenitoba-Johnson K, Vonsattel JP, Louis ED, Sutton MA, Taylor JP, Mills RE, Charlet-Berguerand N, Paulson HL. 2013. CGG repeat-associated translation mediates neurodegeneration in fragile X tremor ataxia syndrome. Neuron. doi:10.1016/j.neuron.2013.03.026

Umoh ME, Fournier C, Li Y, Polak M, Shaw L, Landers JE, Hu W, Gearing M, Glass JD. 2016. Comparative analysis of C9orf72 and sporadic disease in an ALS clinic population. Neurology. doi:10.1212/WNL.0000000000003067

Usdin K, Woodford KJ. 1995. CGG repeats associated with DNA instability and chromosome fragility form structures that block DNA synthesis in vitro. Nucleic Acids Research. doi:10.1093/nar/23.20.4202

Van Mossevelde S, van der Zee J, Cruts M, Van Broeckhoven C. 2017. Relationship between C9orf72 repeat size and clinical phenotype. Current Opinion in Genetics and Development. doi:10.1016/j.gde.2017.02.008

Vaughn JP, Creacy SD, Routh ED, Joyner-Butt C, Jenkins GS, Pauli S, Nagamine Y, Akman SA. 2005. The DEXH protein product of the DHX36 gene is the major source of tetramolecular quadruplex G4-DNA resolving activity in HeLa cell lysates. Journal of Biological Chemistry. doi:10.1074/jbc.C500348200

Vester K, Eravci M, Serikawa T, Schütze T, Weise C, Kurreck J. 2019. RNAi-mediated knockdown of the Rhau helicase preferentially depletes proteins with a Guanine-quadruplex motif in the 5'-UTR of their mRNA. Biochem Biophys Res Commun. doi:10.1016/j.bbrc.2018.11.186

Walter P, Ron D. 2011. The unfolded protein response: From stress pathway to homeostatic regulation. Science. doi:10.1126/science.1209038

Westergard T, Jensen BK, Wen X, Cai J, Kropf E, Iacovitti L, Pasinelli P, Trotti D. 2016. Cell-to-Cell Transmission of Dipeptide Repeat Proteins Linked to C9orf72-ALS/FTD. Cell Reports 17:645–652. doi:10.1016/j.celrep.2016.09.032

Westergard T, McAvoy K, Russell K, Wen X, Pang Y, Morris B, Pasinelli P, Trotti D, Haeusler A. 2019. Repeat-associated non- AUG translation in C9orf72- ALS / FTD is driven by neuronal excitation and stress . EMBO Molecular Medicine. doi:10.15252/emmm.201809423

Yamada SB, Gendron TF, Niccoli T, Genuth NR, Grosely R, Shi Y, Glaria I, Kramer NJ, Nakayama L, Fang S, Dinger TJI, Thoeng A, Rocha G, Barna M, Puglisi JD, Partridge L, Ichida JK, Isaacs AM, Petrucelli L, Gitler AD. 2019. RPS25 is required for efficient RAN translation of C9orf72 and other neurodegenerative disease-associated nucleotide repeats. Nat Neurosci. doi:10.1038/s41593-019-0455-7

Yoo JS, Takahasi K, Ng CS, Ouda R, Onomoto K, Yoneyama M, Lai JC, Lattmann S, Nagamine Y, Matsui T, Iwabuchi K, Kato H, Fujita T. 2014. DHX36 Enhances RIG-I Signaling by Facilitating PKR-Mediated Antiviral Stress Granule Formation. PLoS Pathogens. doi:10.1371/journal.ppat.1004012

Young SK, Baird TD, Wek RC. 2016. Translation Regulation of the Glutamyl-prolyl-tRNA Synthetase Gene EPRS through Bypass of Upstream Open Reading Frames with Noncanonical Initiation Codons. Journal of Biological Chemistry 291:10824–10835. doi:10.1074/JBC.M116.722256

Zamiri B, Reddy K, Macgregor RB, Pearson CE. 2014. TMPyP4 porphyrin distorts RNA G-quadruplex structures of the disease-associated r(GGGGCC)n repeat of the C9orf72 gene and blocks interaction of RNAbinding proteins. Journal of Biological Chemistry. doi:10.1074/jbc.C113.502336

Zhou B, Liu C, Geng Y, Zhu G. 2015. Topology of a G-quadruplex DNA formed by C9orf72 hexanucleotide repeats associated with ALS and FTD. Scientific Reports. doi:10.1038/srep16673

Zu T, Guo S, Bardhi O, Ryskamp DA, Li J, Tusi SK, Engelbrecht A, Klippel K, Chakrabarty P, Nguyen L, Golde TE, Sonenberg N, Ranum LPW. 2020. Metformin inhibits RAN translation through PKR pathway and mitigates disease in C9orf72 ALS/FTD mice. Proceedings of the National Academy of Sciences of the United States of America 117:18591–18599. doi:10.1073/pnas.2005748117

Zu T, Liu Y, Banez-Coronel M, Reid T, Pletnikova O, Lewis J, Miller TM, Harms MB, Falchook AE, Subramony SH, Ostrow LW, Rothstein JD, Troncoso JC, Ranum LPW. 2013. RAN proteins and RNA foci from antisense transcripts in C9ORF72

ALS and frontotemporal dementia. Proceedings of the National Academy of Sciences 110:E4968–E4977. doi:10.1073/pnas.1315438110

Chapter 3: Ribosomal Quality Control Factors Inhibit Repeat-Associated Non-AUG Translation from GC-Rich Repeats

This chapter is published as:

Tseng, Yi-Ju, Indranil Malik, Xiexiong Deng, Amy Krans, Karen Jansen-West, Elizabeth M. H. Tank, Nicolas B. Gomez, Roger Sher, Leonard Petrucelli, Sami J. Barmada, and Peter Todd. 2023. “Ribosomal Quality Control Factors Inhibit Repeat-Associated Non-AUG Translation from GC-Rich Repeats.” BioRxiv 2023.06.07.544135. doi: 10.1101/2023.06.07.544135.

3.1. Abstract

A GGGGCC (G4C2) hexanucleotide repeat expansion in *C9ORF72* causes amyotrophic lateral sclerosis and frontotemporal dementia (C9ALS/FTD), while a CGG trinucleotide repeat expansion in *FMR1* leads to the neurodegenerative disorder Fragile X-associated tremor/ataxia syndrome (FXTAS). These GC-rich repeats form RNA secondary structures that support repeat-associated non-AUG (RAN) translation of toxic proteins that contribute to disease pathogenesis. Here we assessed whether these same repeats might trigger stalling and interfere with translational elongation. We find that depletion of ribosome-associated quality control (RQC) factors NEMF, LTN1, and ANKZF1 markedly boost RAN translation product accumulation from both G4C2 and

CGG repeats while overexpression of these factors reduces RAN production in both reporter cell lines and C9ALS/FTD patient iPSC-derived neurons. We also detected partially made products from both G4C2 and CGG repeats whose abundance increased with RQC factor depletion. Repeat RNA sequence, rather than amino acid content, is central to the impact of RQC factor depletion on RAN translation - suggesting a role for RNA secondary structure in these processes. Together, these findings suggest that ribosomal stalling and RQC pathway activation during RAN translation elongation inhibits the generation of toxic RAN products. We propose augmenting RQC activity as a therapeutic strategy in GC-rich repeat expansion disorders.

3.2. Introduction

Short Tandem Repeat (STR) expansions cause more than 50 human neurodegenerative, neurodevelopmental, and neuromuscular disorders (Koob et al., 1999; Lander et al., 2001; Liquori et al., 2001; Malik et al., 2021a; Nelson et al., 2013; Verkerk et al., 1991). Several STR expansions trigger a process known as repeat-associated non-AUG (RAN) translation, which is a non-canonical initiation process whereby proteins are generated from repeats without an AUG start codon (Bañez-Coronel et al., 2015; Cleary and Ranum, 2014, 2013; Gao and Richter, 2017; Green et al., 2016; Kohji Mori et al., 2013; Zu et al., 2018, 2011). RAN translation-generated proteins accumulate within neurons and in patient tissues and elicit toxicity in both cellular and animal disease models (Buijsen et al., 2016, 2014; Cleary and Ranum, 2013; Freibaum et al., 2015; Sellier et al., 2017; Todd et al., 2013; Xinmei et al., 2014). As at least 10 different neurodegenerative disease-associated STRs support RAN translation,

there is significant interest in identifying selective inhibitors and regulators of this non-canonical translation process (Ash et al., 2013; Bañez-Coronel et al., 2015; Fujino et al., 2023; Goodman et al., 2019; Ishiguro et al., 2017; Jovičić et al., 2015; Kong et al., 2022; Malik et al., 2021a; K. Mori et al., 2013; Soragni et al., 2018; Todd et al., 2013; Yamada et al., 2019; Zu et al., 2017). However, to date, the precise mechanisms that regulate RAN translation remain largely unknown.

Amyotrophic lateral sclerosis (ALS) and frontotemporal dementia (FTD) are inexorably progressive and fatal neurodegenerative disorders. The most common genetic cause of FTD and ALS is an expanded GGGGCC (G4C2) hexanucleotide repeat within the first intron of *C9ORF72* (C9FTD.ALS)(DeJesus-Hernandez et al., 2011; Majounie et al., 2012; van der Zee et al., 2013). Fragile X-associated tremor/ataxia syndrome (FXTAS) is similarly a progressive adult-onset neurodegenerative disorder without effective treatments. FXTAS results from a transcribed CGG repeat expansion in the 5' UTR of *FMR1* that affects about 1/5000 people worldwide (F et al., 2012; Hagerman and Hagerman, 2021; Hagerman et al., 2001; Jacquemont et al., 2004). The repeats that cause both C9ALS/FTD and FXTAS are highly GC-rich and are thought to form strong secondary structures as RNA, including RNA hairpins and G quadruplexes (Asamitsu et al., 2021; Conlon et al., 2016; Fratta et al., 2012; Haeusler et al., 2014; Wang et al., 2019; Zamiri et al., 2014). Moreover, both repeat sequences support RAN translation (Ash et al., 2013; Cheng et al., 2018; Gendron et al., 2013; Green et al., 2017; Kohji Mori et al., 2013; Sellier et al., 2017; Todd et al., 2013; Zu et al., 2013). Without an AUG start codon, RAN translation can occur in all possible reading frames from both sense and antisense transcripts (Krans et al., 2016; Zu et al., 2013). For example, G4C2 repeats in *C9ORF72*

generate GA (glycine-alanine, GA; +0 frame), GP (glycine-proline, GP; +1 frame), and GR (glycine arginine, GR; +2 frame) dipeptide repeat proteins (DPRs) while CGG repeats in *FMR1* generate polyG (glycine; +1 frame), polyA (alanine; +2 frame), and polyR (arginine; +0 frame) homopolymeric peptides from the sense transcripts (Kearse et al., 2016; Zu et al., 2013). However, the efficiency of RAN translation differs significantly across reading frames for each repeat, such that GA DPRs are produced more readily than GP or GR from G4C2 repeats, and polyG and polyA are more efficiently generated than polyR peptides from CGG repeats (Cheng et al., 2018; Green et al., 2017; Kearse et al., 2016; Sellier et al., 2017; Todd et al., 2013). While initial studies suggested that these differences might be due solely to near-cognate initiation sites in the sequences surrounding the repeats, more recent work suggests that these differences in translational efficiency persist even when each product is generated from an AUG codon in an ideal Kozak context (Green et al., 2017; Kearse et al., 2016; Schwab et al., 2004; Tabet et al., 2018; Zhang et al., 2022). This suggests that differences in translational elongation efficiency may be critically important to RAN translation efficiency and as such could represent a therapeutic target.

Ribosomes stall during translational elongation in response to many cues, including RNA damage, mRNA secondary structures, the charge of the nascent polypeptide chain, and cellular stress (Brandman and Hegde, 2016; Buskirk and Green, 2017; Ikeuchi et al., 2019a; Inada, 2020; Matsuo et al., 2023; Wolin and Walter, 1988). Stalled ribosomes trigger a series of mRNA and protein surveillance pathways known collectively as ribosome-associated protein quality control (RQC) (Filbeck et al., 2022; Ikeuchi et al., 2019b; Joazeiro, 2019; Lyumkis et al., 2014; Matsuo et al., 2017; Shao et al., 2015;

Shoemaker and Green, 2012). These quality control pathways ensure the fidelity of protein synthesis and degrade incompletely generated polypeptides and the mRNAs from which they are derived. Stalled ribosomes are sensed by RING-domain E3 ubiquitin ligase, zinc finger protein 598 (ZNF598, yeast Hel2), and receptor for activated C kinase 1 (RACK1, yeast Asc1) to dissociate the 80S ribosome (Garzia et al., 2017; Sitron et al., 2017; Sundaramoorthy et al., 2017). Alternatively, stalling at the 3' end of mRNA is detected by the mRNA surveillance and ribosome rescue factor Pelota (PELO, yeast Dom34) and HBS1-like translational GTPase (HBS1L, yeast Hbs1) (Guydosh and Green, 2014; Saito et al., 2013; Shoemaker et al., 2010). The PELO:HBS1L complex subsequently recruits ATP binding cassette subfamily E member 1 (ABCE1, yeast Rli1) to disassemble the ribosome (Pisarev et al., 2010; Pisareva et al., 2011). Separation of 80S subunits releases 40S and 60S subunits. The 40S subunits contain the truncated mRNA, which is degraded by 5' - 3' exoribonuclease (XRN1) and the exosome complex (Orban and Izaurralde, 2005). 60S subunits entrapped with tRNA-bound nascent polypeptide leads are engaged by the ribosomal quality control (RQC) complex, which targets partially made nascent polypeptides for proteasomal degradation (Brandman et al., 2012; Defenouillère and Fromont-Racine, 2017; Hashimoto et al., 2020; Lyumkis et al., 2014; Matsuo et al., 2020; Shao et al., 2015; Yonashiro et al., 2016). Assembly of the RQC complex is initiated by the binding of nuclear export mediated factor (NEMF, yeast Rqc2), which recruits and stabilizes binding by the E3 ligase listerin (LTN1, yeast Ltn1) (Bengtson and Joazeiro, 2010; Doamekpor et al., 2016; Mizuno et al., 2021; Shen et al., 2015; Yonashiro et al., 2016). NEMF also synthesizes carboxy-terminal alanine and threonine tails (CAT-tails) on partially made polypeptide chains (Kostova et al., 2017;

Lytvynenko et al., 2019; Sitron and Brandman, n.d.; Thrun et al., 2021). This pushes amino acids on the nascent chain out from the ribosomal exit tunnel and triggers their ubiquitination by LTN1 (Brandman et al., 2012; Juszkiewicz and Hegde, 2017; Shao et al., 2013; Shao and Hegde, 2014; Udagawa et al., 2021). The ubiquitin chains signal for recruitment of the valosin-containing protein (VCP, yeast Cdc48) (Defenouillère et al., 2013; Verma et al., 2013). The nascent polypeptide chain is then released by ankyrin repeat and zinc finger peptidyl tRNA hydrolase 1 (ANKZF1, yeast Vms1) and VCP targets the ubiquitylated polypeptide chain for proteasomal degradation (Su et al., 2019; Verma et al., 2018; Zurita Rendón et al., 2018).

Previous studies demonstrated that ribosomes stall during the synthesis of C9 ALS/FTD-associated GR and PR dipeptide proteins (Kriachkov et al., 2023; Park et al., 2021; Radwan et al., 2020). These stalling events were not seen on similarly sized but uncharged DPR repeats such as GA and were therefore ascribed to positively charged arginine residues within these nascent polypeptide chains. Further studies suggest that the GR protein may also interact with protein surveillance pathways through other means than its directed translation (Li et al., 2020; Park et al., 2021; Viera Ortiz et al., 2022). However, these studies were not done in the context of the GC-rich RNA repeats or in the absence of AUG start codons as occurs in RAN translation. As such, whether the dynamics of translation and/or the potential for repeat RNA structures to elicit ribosomal stalling and RQC pathway engagement remains largely unexplored.

In this study, we performed a targeted RAN translation modifier screen at two different GC-rich short tandem repeats with factors involved in the mRNA and protein surveillance pathways. We find that NEMF, LTN1, and ANKZF1 from the RQC pathway all act as

significant modifiers of RAN translation from GC-rich repeat RNAs. This is true for the generation of both GA and polyG polypeptides, even though both products contain no runs of charged amino acids. Consistent with translational stalling in these reading frames, we detected partially made N-terminal peptides containing GA from G4C2 repeats and polyG from CGG repeats, and depletion of these RQC factors enhance the accumulation of these truncated repeat peptides. We see a similar effect that the RQC factor impacts on the accumulation of RAN products in patient-derived neurons and find that altering NEMF directly impacts repeat-associated toxicity in a *Drosophila* model system. Taken together, our results suggest that RQC factor engagement during translational elongation through GC-rich short tandem repeats directly impacts both RAN translation efficiency and product generation through a repeat RNA structure-dependent mechanism. Moreover, as modulating RQC factor abundance modulates RAN product abundance, targeted augmentation of RQC activity is an intriguing target for further therapeutic evaluation.

3.3. Materials and methods

3.3.1. Plasmids

Plasmids and cloning primers used in this study and their sources are listed in **Table 1**. Primers and synthesized fragments used for cloning are listed in **Table 2**. ATG-V5-GA_{69}-NLuc-3xFLAG was generated by the insertion of an ATG-V5 fragment flanked with NheI/EcoRV upstream of Intron-$(GGGGCC)_{70}$-NLuc-3xFLAG (GA frame). ATG-V5-+1$(CGG)_{101}$-NLuc-3xFLAG was generated by the insertion of an ATG-V5 sequence flanked by EcoRI and NarI upstream of +1$(CGG)_{100}$-NLuc-3xFLAG (polyG frame). ATG-

V5-$(GGN)_{103}$ sequence was synthesized by GeneWiz with flanking restriction enzymes of EcoRI (5') and XhoI (3'). The synthesized sequence was inserted into the ATG-V5-+1$(CGG)_{101}$-NLuc-3xFLAG plasmid with EcoRI/XhoI to replace the ATG-V5-+1$(CGG)_{101}$ sequence. pBI-dsRED/hNEMF R86S was a gift from Roger Sher. WT hNEMF was generated by mutating the serine at site 86 to an arginine using Q5 site-directed mutagenesis (NEB, E0554S). pBI-dsRED empty vector was cloned using annealing primers flanked by NheI and EcoRV. pCMV3TAG8li-hRNF160-3FLAG was a gift from Martin Dorf (Addgene plasmid #159138). pCMV6-hANKZF1-Myc-FLAG was purchased from Origene, RC201054. All other reporter sequences have been previously published (Green et al., 2017; Kearse et al., 2016).

Table 1. Plasmids information

Plasmid	Source	Cat#
pcDNA3.1-ATG-NLuc-3xFLAG	Kearse et al., 2016	N/A
pcDNA3.1-Intron-$(GGGGCC)_3$-NLuc-3xFLAG (+0 polyGA frame)	Green et al., 2017	N/A
pcDNA3.1-Intron-$(GGGGCC)_{35}$-NLuc-3xFLAG (+0 polyGA frame)	Green et al., 2017	N/A
pcDNA3.1-Intron-$(GGGGCC)_{70}$-NLuc-3xFLAG (+0 polyGA frame)	Green et al., 2017	N/A
pcDNA3.1-Intron-$(GGGGCC)_{70}$-NLuc-3xFLAG (+1 polyGP frame)	Green et al., 2017	N/A

pcDNA3.1-Intron-$(GGGGCC)_{70}$-NLuc-3xFLAG (+2 polyGR frame)	Green et al., 2017	N/A
pcDNA3.1-$(CGG)_{100}$-NLuc-3xFLAG (+0 polyR frame)	Kearse et al., 2016	N/A
pcDNA3.1-$(CGG)_{100}$-NLuc-3xFLAG (+1 polyG frame)	Kearse et al., 2016	N/A
pcDNA3.1-$(CGG)_{100}$-NLuc-3xFLAG (+2 polyA frame)	Kearse et al., 2016	N/A
pcDNA3.1-ATG-V5-NLuc-3xFLAG	Kearse et al., 2016	N/A
pcDNA3.1-ATG-V5-$(GGGGCC)_{69}$-NLuc-3xFLAG (polyGA frame)	This paper	N/A
pcDNA3.1-ATG-V5-$(CGG)_{101}$-NLuc-3xFLAG (polyG frame)	This paper	N/A
pcDNA3.1-ATG-V5-$(GGN)_{103}$-NLuc-3xFLAG (polyG peptides)	This paper	N/A
pBI-CMV2-dsRED	This paper	N/A
pBI-CMV4-hNEMF/CMV2-dsRED	This paper	N/A
pCMV-FLAG	Sigma	E7908
pCMV-3TAG8li-hRNF160-3xFLAG (hLTN1)	Addgene	159138
pCMV6-hANKZF1-Myc-FLAG	Origene	RC201054

Table 2. Primers and fragments for cloning

Plasmid	Forward	Reverse
ATG-V5-GA_{69}-NLuc-3xFLAG	5’-ctagctagctagtagatgggtaagcctatccctaaccctctcctcggtctcgattctacggat-3’	5’-cgtagaatcgagaccgaggagagggttaggataggcttacccatctactagctag-3’
ATG-V5-+1$(CGG)_{101}$-NLuc-3xFLAG	5’-aattcgtagtatgggtaagcctatccctaacctctcctcggtctcgattctacgg-3’	5’-cgccgtagaatcgagaccgaggagaggg ttagggataggcttacccatactacg-3’
ATG-V5-$(GGN)_{103}$-NLuc-3xFLAG	5’-aattcgtagtatgggtaagcctatccctaaccctctcctcggtctcgattctacggcgccgctgccaggggcgtgcggcagcgcggtggcggaggaggtgggggtggtggaggaggaggcggtggtggaggtggtgggggaggaggcggaggaggggtggtggtggcggcggtggaggaggaggcggtggtggtggaggaggcggaggaggaggggtggaggaggaggtggcggtggtggtggaggaggcggaggaggaggtggcggtggtggaggtggcggtggaggggcggtggtgtggtggaggtgggggaggtggtggaggaggtggtggcggtggaggtggaggcggtggaggaggaggtggcggaggcggtggtggaggaggaggttgggcc-3’	
pBI-dsRED	5’-taggcggccgcatcgata-3’	5’-ggtggctggatccctagc-3’
pBI-dsRED/hNEMF	5’-gaagagtcggagattagtcagtg-3’	5’-aaatgttttcggcacttc-3’

3.3.2. RNA T7 synthesis

pcDNA3.1(+) plasmids containing nano-luciferase and 3xFLAG (NLuc-3xFLAG) reporters were linearized after the 3' FLAG tag with PspOMI. The efficiency of restriction enzyme digestion was confirmed with a DNA agarose gel. Linearized DNA plasmids were cleaned and concentrated with DNA Clean & Concentrator-25 (Zymo Research, D4033). RNAs were *in vitro* transcribed with HiScribe T7 ARCA mRNA Kit with tailing (NEB, E2060S) following the manufacturer's recommended protocol. mRNAs were then cleaned and concentrated with RNA Clean & Concentrator-25 Kit (Zymo Research, R1017) and run on a denaturing glyoxal RNA gel to verify mRNA size and integrity. Transcribed RNA sequences are shown in **Table 3**.

Table 3. DNA plasmid sequence used to synthesize RNA transcript

Reporter name	Sequence from T7 to PspOMI cut site
ATG-V5-NLuc-3xFLAG	GGAGACCCAAGCTGGCTAGCGTTTAAACTTAAGCTTGGCAATC CGGTACTGTTGGTAAAGCCACCATGGGTAAGCCTATCCCTAAC CCTCTCCTCGGTCTCGATTCTACGGTCTTCACACTCGAAGATTT CGTTGGGGACTGGCGACAGACAGCCGGCTACAACCTGGACCA AGTCCTTGAACAGGGAGGTGTGTCCAGTTTGTTTCAGAATCTCG GGGTGTCCGTAACTCCGATCCAAAGGATTGTCCTGAGCGGTGA AAATGGGCTGAAGATCGACATCCATGTCATCATCCCGTATGAAG GTCTGAGCGGCGACCAAATGGGCCAGATCGAAAAAATTTTTAA GGTGGTGTACCCTGTGGATGATCATCACTTTAAGGTGATCCTGC

	ACTATGGCACACTGGTAATCGACGGGGTTACGCCGAACATGAT CGACTATTTCGGACGGCCGTATGAAGGCATCGCCGTGTTCGAC GGCAAAAAGATCACTGTAACAGGGACCCTGTGGAACGGCAACA AAATTATCGACGAGCGCCTGATCAACCCCGACGGCTCCCTGCT GTTCCGAGTAACCATCAACGGAGTGACCGGCTGGCGGCTGTGC GAACGCATTCTGGCGGACTACAAAGACCATGACGGTGATTATAA AGATCATGACATCGATTACAAGGATGACGATGACAAGTAAGGCC GCGACTCTAGAG
ATG-V5-GA$_{69}$- NLuc-3xFLAG	GGGAGACCCAAGCTGGCTAGCTAGCTAGTAGATGGGTAAGCCT ATCCCTAACCCTCTCCTCGGTCTCGATTCTACGGGATATCAAGA TAGCGCCGGGGCCGGGGCCGGGGCCGGGGCCGGGGCCGGG GCCGGGGCCGGGGCCGGGGCCGGGGCCGGGGCCGGGGCCG GGGCAGGGGCCGGGGCCGGGGCCGGGGCCGGGGCCGGGGC CGGGGCCGGGGCCGGGGCCGGGGCCGGGGCCGGGGCCGGG GCCGGGGCCGGGGCCGGGGCCGGGGCCGGGGCCGGGGCCG GGGCCGGGGCCGGGGCCGGGGCCGGGGCCGGGGCCGGGGC CGGGGCCGGGGCCGGGGCCGGGGCCGGGGCCGGGGCCGGG GCCGGGGCCGGGGCCGGGGCCGGGGCCGGGGCCGGGGCCG GGGCCGGGGCCGGGGCCGGGGCCGGGGCCGGGGCCGGGGC CGGGGCCGGGGCCGGGGCCGGGGCCGGGGCCGGGGCCGGG GCCGGGGCCGGGGCCGGGGCCGGGCTGGAAGCTTGGCAATC CGGTACTGTTGGTAAAGCCACCGGGGTCTTCACACTCGAAGAT TTCGTTGGGGACTGGCGACAGACAGCCGGCTACAACCTGGACC

	AAGTCCTTGAACAGGGAGGTGTGTCCAGTTTGTTTCAGAATCTC GGGGTGTCCGTAACTCCGATCCAAAGGATTGTCCTGAGCGGTG AAAATGGGCTGAAGATCGACATCCATGTCATCATCCCGTATGAA GGTCTGAGCGGCGACCAAATGGGCCAGATCGAAAAAATTTTTA AGGTGGTGTACCCTGTGGATGATCATCACTTTAAGGTGATCCTG CACTATGGCACACTGGTAATCGACGGGGTTACGCCGAACATGA TCGACTATTTCGGACGGCCGTATGAAGGCATCGCCGTGTTCGA CGGCAAAAAGATCACTGTAACAGGGACCCTGTGGAACGGCAAC AAAATTATCGACGAGCGCCTGATCAACCCCGACGGCTCCCTGC TGTTCCGAGTAACCATCAACGGAGTGACCGGCTGGCGGCTGTG CGAACGCATTCTGGCGGACTACAAAGACCATGACGGTGATTAT AAAGATCATGACATCGATTACAAGGATGACGATGACAAGTAAGG CCGCGACTCGAGAG
ATG-V5- +1(CGG)$_{101}$- NLuc-3xFLAG	GGAGACCCAAGCTGGCTAGCGTTTAAACTTAAGCTTGGTACCG AGCTCGGATCCACTAGTCCAGTGTGGTGGAATTCGTAGTATGG GTAAGCCTATCCCTAACCCTCTCCTCGGTCTCGATTCTACGGCG CCGCTGCCAGGGGGCGTGCGGCAGCGCGGCGGCGGCGGCGG CGGCGGCGGAGGCGGCGGCGGCGGCGGCGGCGGCGGCGGC GGCGGCGGCGGCGGCGGCGGCGGCGGCGGCGGCGGCGGCG GCGGCGGCGGCGGCGGCGGCGGCGGCGGCGGCGGCGGCGG CGGCGGCGGCGGCGGCGGCGGCGGCGGCGGCGGCGGCGGC GGCGGCGGCGGCGGCGGCGGCGGCGGCGGCGGCGGCGGCG GCGGCGGCGGCGGCGGCGGCGGCGGCGGCGGCGGCGGCGG

	CGGCGGCGGCGGCGGCGGCGGCGGCGGCGGCGGCGGCGGC GGCGGCGGCTGGGCCTCGAGGATATCAAGATCTGGCCTCGGC GGCCAAGCTTGGCAATCCGGTACTGTTGGTAAAGCCACCGGGG TCTTCACACTCGAAGATTTCGTTGGGGACTGGCGACAGACAGC CGGCTACAACCTGGACCAAGTCCTTGAACAGGGAGGTGTGTCC AGTTTGTTTCAGAATCTCGGGGTGTCCGTAACTCCGATCCAAAG GATTGTCCTGAGCGGTGAAAATGGGCTGAAGATCGACATCCAT GTCATCATCCCGTATGAAGGTCTGAGCGGCGACCAAATGGGCC AGATCGAAAAAATTTTTAAGGTGGTGTACCCTGTGGATGATCAT CACTTTAAGGTGATCCTGCACTATGGCACACTGGTAATCGACGG GGTTACGCCGAACATGATCGACTATTTCGGACGGCCGTATGAA GGCATCGCCGTGTTCGACGGCAAAAAGATCACTGTAACAGGGA CCCTGTGGAACGGCAACAAAATTATCGACGAGCGCCTGATCAA CCCCGACGGCTCCCTGCTGTTCCGAGTAACCATCAACGGAGTG ACCGGCTGGCGGCTGTGCGAACGCATTCTGGCGGACTACAAA GACCATGACGGTGATTATAAAGATCATGACATCGATTACAAGGA TGACGATGACAAGTAAGGCCGCGACTCTAGAG
ATG-V5- $(GGN)_{103}$- NLuc-3xFLAG	GGAGACCCAAGCTGGCTAGCGTTTAAACTTAAGCTTGGTACCG AGCTCGGATCCACTAGTCCAGTGTGGTGGAATTCGTAGTATGGG GTAAGCCTATCCCTAACCCTCTCCTCGGTCTCGATTCTACGGCG CCGCTGCCAGGGGGCGTGCGGCAGCGCGGTGGCGGAGGAGG TGGGGGTGGTGGAGGAGGAGGCGGTGGTGGAGGTGGTGGGG GAGGAGGCGGAGGAGGGGGTGGTGGTGGCGGCGGTGGAGGA

	GGAGGCGGTGGTGGTGGAGGAGGCGGAGGAGGAGGGGGTGG AGGAGGAGGTGGCGGTGGTGGTGGAGGAGGCGGAGGAGGAG GTGGCGGTGGTGGAGGTGGCGGTGGAGGGGGCGGTGGTGGT GGAGGTGGGGGAGGTGGTGGAGGAGGTGGTGGCGGTGGAGG TGGAGGCGGTGGAGGAGGAGGTGGCGGAGGCGGTGGTGGAG GAGGAGGTTGGGCCTCGAGGATATCAAGATCTGGCCTCGGCG GCCAAGCTTGGCAATCCGGTACTGTTGGTAAAGCCACCGGGGT CTTCACACTCGAAGATTTCGTTGGGGACTGGCGACAGACAGCC GGCTACAACCTGGACCAAGTCCTTGAACAGGGAGGTGTGTCCA GTTTGTTTCAGAATCTCGGGGTGTCCGTAACTCCGATCCAAAGG ATTGTCCTGAGCGGTGAAAATGGGCTGAAGATCGACATCCATG TCATCATCCCGTATGAAGGTCTGAGCGGCGACCAAATGGGCCA GATCGAAAAAATTTTTAAGGTGGTGTACCCTGTGGATGATCATC ACTTTAAGGTGATCCTGCACTATGGCACACTGGTAATCGACGG GGTTACGCCGAACATGATCGACTATTTCGGACGGCCGTATGAA GGCATCGCCGTGTTCGACGGCAAAAAGATCACTGTAACAGGGA CCCTGTGGAACGGCAACAAAATTATCGACGAGCGCCTGATCAA CCCCGACGGCTCCCTGCTGTTCCGAGTAACCATCAACGGAGTG ACCGGCTGGCGGCTGTGCGAACGCATTCTGGCGGACTACAAA GACCATGACGGTGATTATAAAGATCATGACATCGATTACAAGGA TGACGATGACAAGTAAGGCCGCGACTCTAGAG

3.3.3. Cell Culture and Transfections

HEK293 cells were maintained at 37°C, 5% CO_2 in DMEM with high glucose (Gibco, 11965118) supplemented with 9% fetal bovine serum (50 mL FBS added to 500 mL DMEM; Bio-Techne, S11150). For siRNA transfection, HEK293 cells were seeded at $2x10^5$ cells/mL with 100 µL in 96-well or 500 µL in 24-well plates. Cells were then transfected with siRNA at 1 nM/well in a mixture with Lipofectamine RNAiMax (Thermo Fisher, 13778075) following the manufacturer's recommended protocol on the same day while seeding the cells. siRNA used for this paper are listed in **Table 4**. For effector plasmid transfection, 24 hr after seeding the cells at 50-60% confluency, 100 ng and 500 ng of effectors were transfected in each well of 96-well and 24-well plate, respectively, with FuGeneHD (Promega, E2312), at a 3:1 ratio of FuGeneHD to DNA. Plasmid reporters were transfected into 70-80% confluent cells 48 hr post-seeding. Each well of a 96-well and 24-well plate was transfected with 50 ng and 500 ng NL reporter DNA, respectively, with FuGeneHD as described above. Cells were harvested 24 hr post-transfection for analysis. For mRNA transfection, T7 synthesized mRNA was transfected in cells at 70-80% confluency with TransIT-mRNA Transfection Kit (Mirus, MIR 2256) following the manufacturer's recommended protocol. Cells were harvested 24 hr post-transfection for analysis.

Table 4. siRNA Information

siRNA target	Source	Sequence/ Cat#/ siRNA ID
NanoLuc #2 Custom (NLuc)	Horizon	F: 5'-gguuacgccgaacaugaucgacuuu-3'

		R: 5’-Pagucgaucauguucggcguaaccuu-3’
Negative Control No. 1	Thermo silencer select	4390843
PELO		s28807
HBS1L		s21151
ABCE1		s12088
XRN1		s29016
RACK1		s20340
ZNF598		s40509
NEMF #1		s17483
NEMF #2		s17484
LTN1 #1		s25003
LTN1 #2		s25002
VCP		s14765
ANKZF1 #1		s30259
ANKZF1 #2		s30260

3.3.4. Luminescent Assays

From a 96-well plate, cells were lysed with 60 µL Glo Lysis Buffer (Promega, E2661) for 5 min at room temperature with constant rocking. NanoGlo Substrate (Promega, N113B) was freshly diluted 1:50 in NanoGlo Buffer (Promega, N112A). For a nano-luciferase assay, 25 µL of the diluted NanoGlo substrate was added to 25 µL of cell lysate. To test cell viability, 25 µL of CellTiter-Glo (Promega, G7573) was added to

another 25 µL of lysate. Both assays were mixed for 5 min in a covered opaque 96-well plate then luminescence was measured on a GloMax 96 Microplate Luminometer.

3.3.5. Immunoblotting

For HEK293, each well of cells from 24-well plates was lysed with 120 µL of RIPA buffer with protease inhibitor (Roche, 11836153001). All protein lysates were denatured with 12% β-mercapto-ethanol in 6x SDS-loading dye, boiled at 95°C for 5 min. 20 µL lysate for each sample was loaded per well on 12% sodium dodecyl sulfate-polyacrylamide gels. To detect stalling products between 10-15 kDa, those samples were loaded on 15% sodium dodecyl sulfate-polyacrylamide gels. Gels were then transferred to PVDF membranes either overnight at 40 V at 4°C, or for 2.5 hr at 320 mAmps in the ice bucket at 4°C. Membranes were blocked with 5% non-fat dry milk for 30-60 min, and all antibodies were diluted in 5% non-fat dry milk. All primary antibody information and probing conditions are listed in **Table 5**. Washes were performed with 1x TBST 3 times, 5 min each. Horseradish peroxidase secondary antibodies were applied at 1:10,000, for 2 hr at room temperature. Bands were then visualized on film. Mild stripping (1.5% Glycine, 0.1% SDS, 1% Tween 20, pH to 2.2 with HCl) was performed with two 10 min incubations at room temperature.

Table 5. Antibody Information

Item	WB Conc.	Species	Company	Catalog number

FLAG M2	1:1000	mouse	Sigma	F1804
V5	1:2000	mouse	Abcam	ab27671
Tubulin	1:1000	mouse	DSHB	E7
PELO	1:1000	rabbit	Abcam	ab154335
HBS1L	1:1000	rabbit	Thermo Fisher	PIPA556241
ABCE1	1:1000	rabbit	Abcam	ab32270
XRN1	1:1000	rabbit	Thermo Fisher	PA5-41888
RACK1	1:1000	rabbit	Thermo Fisher	MA5-34809
ZNF598	1:1000	rabbit	Sigma	HPA041760
NEMF	1:1000	rabbit	Proteintech	11840-1-AP
LTN1	1:2000	rabbit	Proteintech	28452-1-AP
ANKZF1	1:2000	rabbit	Proteintech	20447-1-AP
VCP	1:5000	rabbit	Proteintech	10736-1-AP

3.3.6. Immunoprecipitation

Cells were lysed with NP40 lysis buffer (50 mM HEPES-KOH, 150 mM KCl, 0.5% NP40, 0.5 mM DTT, 2 mM EDTA, 1 mM PMSF, protease inhibitors) on ice and incubated at 4°C for 30 min. Lysates were cleared by centrifugation at 20,000 xg for 10 min at 4°C, and the supernatant was transferred into a new tube. Protein concentration for each sample was measured by BCA assay (Thermo Fisher, 23227). 1 mg of total protein was used for each immunoprecipitation. Each lysate was first incubated with 20 µL pre-washed FLAG M2magnetic beads (Sigma, M8823), rotating at 4°C for 2 hr. Next, flow-through was collected and incubated with pre-washed 20 µL of V5-Trap magnetic beads

(Proteintech, v5tma) rotating at 4°C for 2 hr. 10% of input and 20% of the supernatant from each step was saved for immunoblot. Afterward, FLAG and V5 beads were washed with NP-40 lysis buffer until the absorbance of the wash supernatant at 280 nm is below 0.05. After the final wash, beads were resuspended with 2x SDS dye and boiled at 95°C for 5 min. The supernatant was collected for immunoblot.

3.3.7. Drosophila Studies

Drosophila were crossed and maintained at 25°C on SY10 food supplemented with dry yeast. For eye phenotyping at a higher temperature, flies were crossed and maintained at 29°C. To measure G4C2 repeat RNA toxicity in flies, a previously characterized GMR-GAL4-driven UAS-$(GGGGCC)_{28}$-EGFP reporter containing fly was used (He et al., 2020). NEMF knockdown flies were obtained from Bloomington Drosophila Stock Center (BDSC) with stock numbers BDSC 36955 and BDSC 25214. Rough eye phenotyping was performed as described earlier (Malik et al., 2021b). In brief, 5-6 virgin female flies expressing the GMR-GAL4-driven UAS-$(GGGGCC)_{28}$-EGFP transgene were crossed with male flies carrying a germline mutation (insertion/disruption) of the fly homolog of NEMF gene (Dmel\Clbn). The rough eye phenotype of flies in F1 progenies was determined at 1-2 days post-eclosion. Rough eye scores were given based on the following eye abnormalities: orientation of bristles, presence of supernumerary bristles, ommatidial fusion, and disarray, presence of necrosis, and shrinkage of the whole eye. Eye images were captured using a Leica M125 stereomicroscope with a Leica DFC425 digital camera. Eye images were scored and analyzed with ImageJ in a blinded manner.

3.3.8. Maintenance of iPSCs and Differentiation into Forebrain-like Neurons (iNs)

C9 patient-derived induced pluripotent stem cells (iPSCs; CS52iALS-C9n6) and isogenic controls (CS52iALS-C9n6.ISOC3) were obtained from the Cedars-Sinai iPSC Core. iPSCs were maintained in TeSR-E8 media (Stemcell Technologies, 05990) on vitronectin-coated plates, and passaged every 4-5 days using EDTA as described in Weskamp et al. (Weskamp et al., 2020). A doxycycline-inducible cassette for induced expression of Ngn1/2 was integrated into the *CLYBL* safe harbor locus of each line, as per Weskamp et al, enabling directed differentiation into forebrain-like glutamatergic iNeurons (iNs) (Busskamp et al., 2014; Cerbini et al., 2015; Habibey et al., 2022; Weskamp et al., 2020). Neural progenitor cells (NPCs) were frozen on day 2 of differentiation and stored in liquid N_2 until needed. One day before plating NPCs ($1x10^6$ cells/well in a 6-well plate), each well was coated overnight at 37°C with 1 mL of 100 µg/mL poly-L-ornithine hydrobromide (PLO, Sigma, P3655) prepared in filter sterilized 0.1 M borate buffer (Fisher Chemical, A73-500) at pH 8.4. PLO was removed by washing with sterile water 3x and air-dried for at least 1 hr. The remainder of the iNs differentiation procedure was as described in Weskamp et al. (Weskamp et al., 2020).

3.3.9. Lentivirus Transduction

Lentiviral shRNA plasmids against NEMF, LTN1, and ANKZF1 were purchased from Horizon Discovery. Lentiviral overexpression of NEMF and ANKZF1 was purchased from VectorBuilder (**Table 6**). Lentiviral overexpression of LTN1 was cloned with NEBuilder Gibson Assembly. In brief, the RPL22 sequence from the plasmid pLV-Ef1a-

RPL22-3XHA-P2A-EGFP-T2A-Puro (gift from Hemali Phatnani, Addgene plasmid # 170317) was removed by restriction enzymes digestion with EcoRI-HF and AgeI-HF. The human LTN1 was amplified from pCMV-3TAG8li-hRNF160-3xFLAG with primers (forward: 5'- tttgccgccagaacacaggaccggttaatctgcgctgccaccatgggcggz-3', Reverse 5'-aattcgtggcgccagatccgggctcgacatcgatgaaaaacg-3') designed using NEBuilder Assembly Tool v2.7.1. pLV-Ef1a-hLTN1-3XHA-P2A-EGFP-T2A-Puro was generated by Gibson cloning with the hLTN1 fragment generated as described above. Lentiviruses were packed at the University of Michigan Vector Core with HIV lentivirus and then 10x concentrated in 10 mL of DMEM. A GFP vector control was purchased from the University of Michigan Vector Core. Transduction efficiencies as measured by GFP fluorescence were tested in HEK293 cells with 10 µg/mL polybrene following the lentiviral transduction protocol provided by the Vector Core. Knockdown and overexpression of the gene were confirmed with immunoblot. C9 and its isogenic control iNeurons were transduced with lentivirus on Day 6 post differentiation. Cell media were replaced with fresh B27 media on Day 8, and cells were harvested on Day 14.

Table 6. Lentiviral Constructs

Plasmid	Source	Cat#
Lenti-EV-GFP-VSVG	UM Vector Core	UMICHVC-YT-4612
SMARTvector Lentiviral Human NEMF hEF1a-TurboGFP shRNA	Horizon	V3SH11240-224809840
SMARTvector Lentiviral Human LTN1 hEF1a-TurboGFP shRNA	Horizon	V3SH11240-226558312

SMARTvector Lentiviral Human ANKZF1 hEF1a-TurboGFP shRNA	Horizon	V3SH11240-224939332
pLV-EGFP-EF1A-hNEMF [NM_004713.6]	VectorBuilder	VB221216-1307gkc
pLV-EF1A-hLTN1-3XHA-P2A-EGFP-T2A-Puro	This paper	N/A
pLV-EGFP-EF1A-hANKZF1 [NM_001042410.2]	VectorBuilder	VB900124-1663tuj

3.3.10. GP MSD

From a 6-well plate, cells were washed with 1x PBS on ice and then harvested by scraping with 200 µL of Co-IP buffer (50 mM Tris-HCl, 300 mM NaCl, 5 mM EDTA, 0.1% triton-X 100, 2% SDS, protease inhibitors, phosphoSTOP) on ice. Lysates were passed through a 28.5G syringe 10 times, spun at 16,000 xg for 20 min at 15°C, and then the supernatant was collected. Levels of polyGP proteins in cell lysates were measured using the Meso Scale Discovery (MSD) electrochemiluminescence detection technology as previously described (Andrade et al., 2020). Briefly, a purified mouse monoclonal polyGP antibody was used as both the capture and detection antibody (Target ALS Foundation, TALS 828.179). For capture, the antibody was biotinylated and used to coat a 96-well MSD Small Spot Streptavidin plate (Meso Scale Discovery, L45SA-2), whereas the detection antibody was tagged with an electro-chemiluminescent label (MSD GOLD SULFO-TAG). An equal amount of each lysate was diluted in TBS and tested in duplicate in a blinded fashion. For each well, the intensity of emitted light, which is reflective of GP

abundance and presented as arbitrary units, was acquired upon electrochemical stimulation of the plate.

3.3.11. Quantitative Real-time Reverse Transcription PCR (qRT-PCR)

RNA from iN lysates was isolated and collected using Quick-RNA MiniPrep Kit (Zymo Research, R1054). 2 µg of RNA per sample was treated with 2 U of TURBO DNase (Thermo Fisher Scientific, AM2238) for 30 min at 37°C twice to remove contaminating genomic and plasmid DNA, and then recovered using the RNA Clean & Concentrator-5 Kit (Zymo Research, R1015). cDNA from each sample was generated from 250 ng of RNA from the previous step with a mixture of oligo(dT) and random hexamer primers (iScript cDNA Synthesis Kit, Bio-Rad, 1708891). Finally, cDNA abundance was measured using iQ SYBR Green Supermix (Bio-Rad, 1708882) from an iQ5 qPCR system (Bio-Rad), and the appropriate primers at 100 nM. Primer information is listed in **Table 7**. cDNA abundance was quantified using a modified ΔΔCt method recommended by the manufacturer.

Table 7. Primer sets for qRT-PCR

Primer name	Sequence	Source
C9 Intron-F	5’-ctccccactacttgctctcacagta-3’	Rodriguez et al., 2021
C9 Intron-R	5’-tagcgcgcgactcctgagttcca-3’	Rodriguez et al., 2021
NEMF-F	5’-aacttgcggtagtgaccctc-3’	This paper
NEMF-R	5’-attcagctccgcgagtacg-3’	This paper

LTN1-F	5’-tgtccaagccaaacctcttga-3’	This paper
LTN1-R	5’-ggacatgccttggttaga-3’	This paper
ANKZF1-F	5’-gcagaaatccggcaatcgac-3’	This paper
ANKZF1-R	5’-gcccttagaagacgcaccaa-3’	This paper
GAPDH-F	5’-aaggtgaaggtcggagtcaa-3’	Tseng et al., 2021
GAPDH-R	5’-ggaagatggtgatgggattt-3’	Tseng et al., 2021

3.3.12. Polysome Profiling

HEK293 cells at 85-95% confluency in a 15 cm culture dish were treated with 100 µg/mL cycloheximide (CHX) for 5 min at 37°C. The culture dish was placed on ice, washed with 5 mL ice-cold PBS containing 100 µg/mL CHX, harvested by scraping with another 5 mL cold PBS + CHX, and centrifuged at 1200 xg at 4°C for 5 min. PBS was aspirated and the pellet was resuspended in polysome-profiling lysis buffer (20 mM Tris-HCl (pH 7.5), 150 mM NaCl, 15 mM MgCl2, 8% (vol/vol) glycerol, 20 U/mL SUPERase, 80 U/ml murine RNase inhibitor, 0.1 mg/mL heparin, 100 µg/mL CHX, 1 mM DTT,1x EDTA-free protease inhibitor cocktail, 20 U/mL Turbo DNase, 1% Triton X-100). Lysates were vortexed for 30 sec, passed through a 21G needle 10 times, and incubated on ice for 5 min. Cellular debris was pelleted at 14,000 xg at 4°C for 10 min, and the supernatant was transferred to a pre-cooled tube. Total lysate RNA was estimated by NanoDrop. Lysates were flash-frozen in liquid nitrogen and stored at -80°C until fractionation.

Sucrose gradients were prepared by sequentially freezing 2.7 mL of 50, 36.7, 23.3, and 10% sucrose (wt/vol) in 13.2 mL thin wall polypropylene tubes (Beckman Coulter, 331372). Sucrose-gradient buffer consisted of 20 mM Tris-HCl (pH 7.5), 150 mM NaCl,

15 mM MgCl2, 10 U/mL SUPERase, 20 U/mL murine RNase inhibitor, 100 µg/mL CHX, and 1 mM DTT. Before use, gradients were thawed and linearized overnight at 4°C. For fractionation, approximately 50 µg total RNA was applied to the top of the sucrose gradient. Gradients were spun at 35,000 rpm at 4°C for 3 hr using a Beckman Coulter Optima L-90 K ultracentrifuge and SW 41 Ti swinging-bucket rotor. Gradients were fractionated with Brandel's Gradient Fractionation System, measuring absorbance at 254 nm. The detector was baselined with 60% sucrose chase solution and its sensitivity was set to 0.05. For fractionation, 60% sucrose was pumped at a rate of 1.5 mL/min. Brandel's PeakChart software was used to collect the profile data.

3.3.13. Data Analysis

Prediction of RNA structure and calculation of the minimum free energy was computed by The Vienna RNA Websuite, RNAfold 2.5.1. (Gruber et al., 2008). Statistical analyses were performed with GraphPad Prism9.5.1. All luciferase activity was calculated by normalizing the nano-luciferase signal with cell titer. For comparison of NLuc reporter luciferase activity assays, GP MSD response, and fly eye phenotype quantification, we used two-tailed unpaired Student's t-tests with Welch's correction for multiple comparisons to confirm the statistical difference between control and multiple experimental groups within each sample. To assess group effects, we used a two-way ANOVA with Sidak's multiple comparison tests to compare the differences between groups within different samples. Fly eye necrosis and width measurements were done with reviewer genotype- blinded analysis by at least two independent investigators to avoid subjective bias. Fly eye width measurement was performed with ImageJ

(www.imagej.nih.gov/ij/). Experiments were performed with a minimum of three independent biological samples (n > 3) with technical replication of results from each sample. Fly experiments were done using multiple crosses with a minimum of 10 flies analyzed per group per cross. Further statistical analysis details are included in figure legends including the numbers of analyzed samples, statistical tests, and P values.

3.3.14. Data Availability

All data points are included in the main figures or supplementary data. Raw data used for figure generation are available upon request.

3.4. Results

3.4.1. RQC Pathway Factor Depletion Enhances RAN Translation from GC-Rich Repeat Sequences

Slowing or stalling of translational elongation can result in ribosomal collisions and engagement of ribosomal quality control pathways. He hypothesized that GC-rich repetitive elements would be prone to such events. We therefore performed a targeted modifier screen at two disease-associated repetitive elements (G4C2 hexanucleotide or CGG trinucleotide repeats) for factors involved in mRNA and protein surveillance pathways to evaluate their role in regulating RAN translation **(Figure 3.1A)**. Specifically, we assessed the impact of lowering expression of RNA degradation pathway factors PELO, HBS1L, ABCE1, and XRN1; ribosome stalling sensing factors RACK1 and ZNF598, or RQC pathway factors NEMF, LTN1, VCP, and ANKZF1. Our group previously generated a series of RAN translation-specific nano-luciferase reporters for both G4C2

repeats and CGG repeats **(Figure 3.1B)** (Green et al., 2017; Kearse et al., 2016). We used those well-characterized reporters for the screen. Validation of gene knockdown for each factor was confirmed by immunoblotting **(Figure S3.1)**. For factors involved in Ribosome associated RNA degradation, depletion of XRN1 increased RAN translation at both G4C2 and CGG repeats, while depletion of HSB1L selectively increased RAN translation from CGG repeats **(Figure 3.1C)**. However, the largest effect was observed for factors involved in the RQC pathway that classically engages the ribosomes after stall detection and ribosome splitting. Depletion of NEMF, LTN1, or ANKZF1 markedly and selectively increased the accumulation of RAN translation products from both G4C2 and CGG repeats, with increases between 2 and 5-fold compared to a non-targeting siRNA control. We, therefore, focused our attention on these RQC pathway factors and their effect on RAN translation.

3.4.2. NEMF, LTN1, and ANKZF1 Effects on RAN Translation are Repeat Length-dependent

Previous studies found that knockdown of NEMF and LTN1 can increase the production of GR and PR DPRs from non-GC-rich sequences (Park et al., 2021; Viera Ortiz et al., 2022). This difference was thought to result from the positively charged arginine residues in PR and GR DPR tracks, which can interact with the ribosome exit tunnel to elicit ribosomal stalling (Kriachkov et al., 2023; Loveland et al., 2022; Radwan et al., 2020). However, RNA secondary structures can also elicit ribosomal stalling (Kumari et al., 2007; Schaeffer et al., 2001; Wieland and Hartig, 2007). As GC-rich repeats form stable secondary structures and the RNA helicases that resolve these structures are implicated in RAN translation (Cheng et al., 2019; Linsalata et al., 2019;

Liu et al., 2021; Tseng et al., 2021), we hypothesized that ribosome stalling would occur during RAN translation from GC-rich repeats, leading to RQC pathway activation. To assess this, we first validated the effects of NEMF, LTN1, and ANKZF1 on RAN translation with a second set of siRNAs. Knockdown of NEMF, LTN1, or ANKZF1 with this second set of siRNAs elicited similar increases in GA DPR RAN production from G4C2 and CGG repeats **(Figure 3.2, Figure S3.2A-C)**. We next assessed whether this impact by RQC factors was dependent on the length of the G4C2 repeat. At 35 G4C2 repeats, we did not see any effect of NEMF knockdown on GA frame RAN translation, suggesting repeat-length dependence **(Figure 3.2A, 2B)**. Similarly, the depletion of LTN1 significantly increased RAN translation from both GA35 and GA70 repeat reporters, but the effect on the larger repeat was greater **(Figure 3.2C)**. As NEMF helps recruit LTN1 to assemble the RQC complex, we asked if there is a synergetic effect of NEMF and LTN1 knockdown on RAN translation. When we performed the knockdown of both NEMF and LTN1 together, we observed a mild additive effect, with slightly more RAN translation production from GA35, GA70, GP70, and GR70 reporters **(Figure 3.2D)**. Similarly, the depletion of ANKZF1 had a modest effect on translation from an AUG reporter with no repeat and from our GA35 reporter, but a larger effect on product generation from the GA70 reporter **(Figure 3.2E)**.

If RNA secondary structure contributes to ribosomal stalling, then the effect of knockdown of RQC factors should influence RAN translation production from all 3 potential reading frames. To address this, we utilized (G4C2)70 RAN translation reporters, where the NLuc tag was in the GP (+1) or GR (+2) reading frames **(Figure 3.2A)**. Knockdown of NEMF increased RAN from (G4C2)70 sequences in all 3 reading

frames **(Figure 3.2B)**. Similarly, the knockdown of LTN1 increased RAN product accumulation from (G4C2)70 sequences in GA, GP, and GR frames **(Figure 3.2C)**. When we knocked down both NEMF and LTN1 together, we observed a mild additive effect, with more production from GA35, GA70, GP70, and GR70 RAN reporters compared to controls **(Figure 3.2D)**. This suggests that NEMF and LTN1 are functioning on the same pathway in RAN translation. Knockdown of ANKZF1 significantly increased RAN production from (G4C2)70 sequences in all three reading frames, with greater effects on the GR frame **(Figure 3.2E)**. Taken together, these data suggest that depleting RQC factors increase RAN translation in a repeat length-dependent but repeat reading-frame independent fashion.

3.4.3. Detection of Short/truncated Translation Products from G4C2 and CGG Transcripts

RQC pathway activation typically triggers the degradation of partially made translation products through a proteosome-dependent process. Prior studies utilized a dual fluorescent tagging system with GFP and RFP bracketing a ribosome-stall inducing sequence coupled with flow cytometry to measure stalling during translation (Juszkiewicz and Hegde, 2017). In this set up 'stalling' events are measured by detecting the signal of one (stalled/truncated) or both reporters (full-length). However, such truncated products would not be detectable by either carboxyl-terminal nano-luciferase (NLuc) signal or FLAG tag western blots. We, therefore, generated a new set of reporter constructs with an AUG-initiated V5 tag at the amino-terminus of 69 G4C2 repeats in the GA frame or 100 CGG in the polyG frame. For each construct, we retained an in-frame NLuc and 3xFLAG at the carboxyl-terminus **(Figure 3.3A)**. To avoid the generation of potentially

aberrant RNA products from plasmids that might complicate our data interpretation, we transfected in vitro synthesized mRNAs with either G4C2 repeats or CGG repeats into HEK293 cells. We then performed a dual IP experiment where we first used FLAG magnetic beads to pull down the full-length products and then performed a second IP with V5 on the flowthrough to enrich for partially made products that only have the amino terminus of the protein **(Figure 3.3B)**. We detected partially made products, approximately 10-15 kDa in size, only with the V5 antibody for both GA **(Figure 3.3C)** and polyG **(Figure 3.3D)**. In contrast, constructs lacking the GC-rich repeats did not generate any partially made products **(Figure S3.3A-C)**. These data suggest that ribosome stalling presumably occurs during translational elongation from GC-rich repeats - even when the protein products from those repeats lack arginine or similarly charged amino acids.

To assess whether NEMF, LTN1, or ANKZF1 might affect the generation or accumulation of these truncated repeat products, we repeated the studies as above after depletion of NEMF + LTN1 or ANKZF1. From immunoblot analysis, we detected an increase in both the abundance of the full-length products and the truncated products after double knockdown of NEMF + LTN1 or after knockdown of ANKZF1 from both (G4C2)69 and (CGG)100 repeats **(Figure 3.4A-D)**. However, we do not see any change in the expression or generation of products from a no-repeat control **(Figure S3.3B-C)**. These observations suggest that short/stalled products are generated normally during translation through GC-rich repeats and that their abundance is impacted by RQC factor abundance.

3.4.4. Repeat RNA Sequence Determines the Impact of RQC Factor Depletion.

Prior studies are conflicted as to whether GA DPRs generated from non-repetitive mRNA sequences induce ribosomal stalls (Park et al., 2021; Viera Ortiz et al., 2022). Our data suggests that the repeat RNA sequence and structure may be sufficient to elicit ribosomal stalling and RQC activation **(Figure 3.3, 4)**. To assess this more formally, we took advantage of the redundant nature of RNA codons to generate a reporter that would make a polyG product but lack the CGG repeat RNA structure **(Figure 3.5A-B)**. Glycine is encoded by GGN, where N is any nucleotide. Therefore, we generated constructs with identical AUG initiation codons above either a GGC repeat or a GGN repeat that should not form a strong hairpin structure **(Figures 3 5A-C)**. Both constructs will generate the same polyG-containing protein that we can measure using NLuc **(Figure 3.5C)**. Compared to a non-targeting siRNA control, depletion of NEMF, LTN1, or ANKZF1 significantly enhanced the production of the polyG protein from the AUG-V5-(CGG)101 reporter, which suggests that the modulation of these factors is acting primarily at the stage of translational elongation rather than RAN translational initiation. In contrast, depletion of either NEMF or LTN1 had no impact on polyG protein generation from the AUG-V5-(GGN)103 construct or an AUG-V5-NLuc no-repeat control **(Figure 3.5D)**. Depletion of ANKZF1 did modestly enhance polyG production from the AUG-V5-(GGN)103 construct, but the effect was significantly weaker than that seen for polyG protein production from the AUG-V5-(CGG)101 reporter **(Figure 3.5D)**. Together, these results suggest that the repeat sequence plays a key role in eliciting ribosomal stalling and the interplay of RQC factors with CGG repeat translation.

3.4.5. Depletion of NEMF and ANKZF1 Aggravates Toxicity in *Drosophila* Model of C9 FTD/ALS.

A prior study demonstrated a worsening of rough eye phenotypes with depletion of NEMF in *Drosophila* expressing dipeptide GR or PR from constructs lacking a G4C2 repeat, which again suggested a direct role for serial arginine translation in RQC pathway activation (Li et al., 2020; Park et al., 2021). To assess the impact of modulating RQC factor expression on G4C2 repeat-associated phenotypes in vivo, we utilized an established *Drosophila* model of C9ALS/FTD that supports RAN translation from G4C2 repeats and elicits significant toxicity resulting in a rough eye phenotype when expressed using a GMR-GAL4 driver (He et al., 2020). Genetic ablation of NEMF led to a more severe rough eye phenotype compared to the control cross in both NEMF depletion lines **(Figure 3.6A)**. Rearing the G4C2 repeat-expressing flies at a higher temperature (29°C) led to more severe eye degeneration as marked by physical constriction of eye width (Green et al., 2022; Malik et al., 2021b). Depletion of NEMF mitigated this decrease in eye width **(Figure 3.6B)**. Together these data suggest that depletion of NEMF enhances G4C2 repeat elicited toxicity in *Drosophila*.

3.4.6. Depletion of NEMF and ANKZF1 Enhances RAN Translation in C9ORF72 Human Neurons

We next assessed whether modulating RQC factors also influence RAN translation product accumulation from the endogenous repeat locus in *C9ORF72* ALS patient-derived neurons. To this end, we utilized a well-characterized pair of C9 patient iPSC-derived iNeurons (iN) with an accompanied isogenic control line (Sareen et al., 2013). These iN lines contain a doxycycline-inducible Ngn1/2 cassette that allows for rapid

neuronal differentiation (Busskamp et al., 2014). After two weeks of differentiation, we harvested cell lysates and performed an MSD assay to measure GP DPR product abundance **(Figure 3.6C)**. In parallel, we performed a qRT-PCR analysis of RNA abundance for different RQC factors. We observed a significant increase of NEMF and ANKZF1 transcript expression in C9ALS iNeurons compared to isogenic controls differentiated in parallel, suggesting that there could be a compensatory upregulation of RQC machinery elicited by the repeat expansion **(Figure 3.6D, E)**. There was no change in LTN1 transcript abundance between these C9ALS iNeurons and their isogenic control **(Figure 3.6F)**.

As expected, we were able to reliably measure GP DPR abundance in C9ALS iNeurons but not in isogenic control neurons across multiple differentiations **(Figure 3.6G-I).** To assess whether altering RQC factor abundance could impact endogenous RAN product abundance, we utilized lentiviral delivery of shRNAs against each factor. In line with our reporter assays, we observed a significant increase in GP DPR abundance following the depletion of NEMF or ANKZF1 in C9 iN compared to iNeurons treated with a lentiviral control **(Figure 3.6G, H)**. However, the depletion of LTN1 did not significantly impact GP DPR abundance **(Figure 3.6I)**. The RQC pathway typically pairs with the mRNA surveillance pathway after the separation of 80S ribosomes into 40S and 60S subunits to degrade the template mRNA. Therefore, we assessed whether endogenous C9 RNA abundance might be impacted by the depletion of NEMF, LTN1, and ANKZF1. Using primers that specifically target the first intron of C9RNA that contains the repeat, we observed a modest increase of C9 transcript abundance with depletion of NEMF or LTN1 **(Figure S3.4A-B)**. However, we observed no effect on the depletion of ANKZF1

compared to a lentiviral control **(Figure S3.4C)**. Taking our data together with the previous study, whether the activation of RQC degraded the C9 RNA is still unclear (Park et al., 2021).

3.4.7. Enhancing the Expression of RQC Factors Suppresses RAN Product Accumulation

As depletion of NEMF, LTN1, and ANKZF1 increase GA and polyG product accumulation from GC-rich repeats, we wondered if boosting NEMF, LTN1, or ANKZF1 expression in cells might suppress RAN translation or lower RAN product accumulation. To assess this, we overexpressed each of the RQC factors (NEMF, LTN1, and ANKZF1) in conjunction with the AUG-driven no repeat control, G4C2 GA reporter, or the CGG polyG reporter. Overexpression of NEMF and LTN1 decreased both GA and polyG RAN product accumulations **(Figure 3.7A-B)**. Overexpression of ANKZF1 decreased the accumulation of RAN products from all three (GA, GP, and GR) reading frames from G4C2 repeats without impacting an AUG-driven no-repeat control **(Figure 3.7C)**. In contrast, overexpression of ANKZF1 did not significantly decrease polyG RAN product abundance **(Figure 3.7D)**. Next, we transduced C9 patient iPSC-derived iNeurons (iN) with lentivirus expressing hNEMF, hLTN1, or hANKZF1 and subsequently measured the GP DPR abundance **(Figure 3.6C)**. Overexpression of either NEMF or ANKZF1 in C9 iN significantly decreased GP abundance compared to a lentiviral control **(Figure 7E, F)**. However, there was no significant increase in GP abundance seen with hLTN1 expression **(Figure 3.7G)**. Notably, overexpression of NEMF, LTN1, or ANKZF1 did not affect C9 intronic transcript abundance **(Figure S3.4D-F)**. Taken together, these data

suggest modulation of RQC factors can directly impact RAN product accumulation from both reporters and endogenous loci in patient-derived neurons.

3.5. Discussion

Transcribed GC-rich short tandem repeat expansions in *C9ORF72* and *FMR1* form strong RNA secondary structures as either RNA hairpins or G-quadruplexes (Asamitsu et al., 2021; Fratta et al., 2012; Fry and Loeb, 1994; Haeusler et al., 2014; Wang et al., 2019). These structures are critical for repeat-associated non-AUG (RAN) translation (Cheng et al., 2018; Chiang et al., 2001; Green et al., 2017; Kearse and Todd, 2014; Sonobe et al., 2018; Todd et al., 2013; Zu et al., 2011). mRNA secondary structures can impede elongating ribosomes leading to stalling or collision, and activation of? ribosome-associated quality-control pathways (Hashimoto et al., 2020; Ikeuchi et al., 2019b; Inada, 2020; Joazeiro, 2019). To understand how these pathways interplay with RAN translation across GC-rich repeat RNAs, we performed a targeted screen on factors from the mRNA and protein surveillance pathways associated with ribosomal stalling. We identified NEMF, LTN1, and ANKZF1 from the RQC pathway as robust inhibitors of RAN translation on G4C2 mRNA repeats in the GA frame and CGG repeats in the polyG frame. Depletion of NEMF, LTN1, and ANKZF1 increased the abundance of RAN products while overexpression decreased detectable RAN products, with similar genetic compensation effects at endogenous loci in human C9 patient-derived neurons (iNs). Intriguingly, these same factors are upregulated in C9 iNs, suggesting that these pathways may be activated by the translation of expanded repeats. With an N-terminal tagging system, we observed that both G4C2 and CGG repeat sequences generate partially made truncated products,

suggesting peptide release associated with RQC degradation pathways activated during repeat translation. Importantly, these effects are mediated not by alterations in the initiation rates (as they persist even when initiation is driven with an AUG initiation codon) or by the charge of the amino acids associated with the peptides (both GA and polyG are uncharged), but by the mRNA structures themselves, as we can abrogate this genetic interaction by changing the repeat sequence to diminish the predicted RNA hairpin structures formed by the CGG repeat element. These data suggest a role for RQC pathways in both RAN translation and AUG-initiated translation of GC-rich structured repeat RNAs, with implications for disease pathogenesis and therapeutic development in this currently untreatable class of disorders.

Several studies implicate RQC activation as associated with neuronal death and human neurodegenerative diseases(Li et al., 2023; Lu, 2023; Rimal et al., 2021; Udagawa et al., 2021; Wu et al., 2019, 2018). NEMF mutations in mice are sufficient to trigger neurodegenerative phenotypes and variants of NEMF in humans are associated with neuromuscular disease (Ahmed et al., 2021; Martin et al., 2020). LTN1 mutations in mice also trigger movement disorder phenotypes and motor neuron degeneration (Chu et al., 2009). Factors from protein surveillance pathways directly associate with ALS/FTD-causing toxic arginine-rich dipeptide repeat (DPR) proteins, GR, and PR (Li et al., 2020; Loveland et al., 2022; Park et al., 2021; Viera Ortiz et al., 2022). AUG-initiated arginine-rich proteins from GR and PR encoding RNAs induce ribosomal stalling in an RNA-independent and DPR protein length-dependent manner in both mammalian cells and GR and PR DPR protein-expressing flies (Kriachkov et al., 2023; Mizielinska et al., 2014). In these cases, ZNF598, NEMF, and LTN1 regulate the expression of GR protein in a

fashion that does not require the G4C2 repeat RNA sequence or structure, and these effects are thought to be due to interactions of the charged DPR protein due to the charged arginine residue. Importantly, in these studies, AUG-initiated translation of a GA or GP sequence from a non-repetitive sequence was insufficient to elicit ribosomal stalling. In contrast, here, we observe evidence for ribosomal stalling impacting the expression of GA, GP, and GR generated through RAN translation on G4C2 repeat transcripts that include the native upstream endogenous intronic sequence of *C9ORF72*. We also demonstrate that polyG RAN translation from CGG repeats but not AUG-initiated translation of polyG from a non-repetitive sequence is highly sensitive to RQC factor expression manipulation. As such, our findings suggest that RNA secondary structure formed by GC-rich STRs contributes to ribosomal stalling and activation of downstream surveillance mechanisms. As RAN translation can proceed in multiple reading frames on the same repeat simultaneously, our data cannot rule out a second contribution to ribosomal stalling by rare polyGR translation events on G4C2 or polyR CGG repeats as a stall trigger in other reading frames.

Prior studies utilized P2A-based polycistronic reporter systems encoding two fluorescent proteins to assess translation elongation stalling (Juszkiewicz and Hegde, 2017). In these assays, the efficiency of the translation is measured by the ratio of two fluorescent proteins by flow cytometry. However, on GC-rich repeats, the relative loss of expression from a C-terminal tagged fluorescent protein could also result from translational frameshifting, which occurs on both CGG and G4C2 repeats (Tabet et al., 2018; Wright et al., 2022). In addition, fluorescent protein systems cannot exclude a contribution to C-terminal tag fluorescent protein expression from internal ribosome entry

site (IRES) initiation within these GC-rich repeats as is proposed as a potential mechanism for RAN translation at both CGG and G4C2 repeats (Cheng et al., 2018; Chiang et al., 2001; Sonobe et al., 2018). To overcome these limitations, we used an N-terminal AUG-V5 tag above G4C2 and CGG repeats to successfully detect short, truncated V5-tagged peptides, which are likely to be released from stalled ribosomes and are resistant to degradation. We also observed that the accumulation of these short peptides is modulated by genetic manipulation of RQC factor expression. Future studies will be needed to see if such peptides are independently toxic and contribute to disease.

Among the modifiers studied, loss of ANKZF1 (yeast Vms1) had the greatest impact on RAN translation product accumulation from both CGG and G4C2 repeats. This factor was not previously assessed with PR or GR-elicited ribosome stalling, presumably because it was thought to act at a very late stage in the RQC pathway. Overexpression of ANKZF1 in mammalian cells selectively decreased expression of GA, GP, and GR from G4C2 repeats and we see a similar of this effect in C9 patient iPSC-derived iNeurons. ANKZF1 is conserved from yeast to humans, where it is thought to act as a hydrolase and/or nuclease to release the nascent peptide chain from the peptidyl-tRNA on the 60S ribosome (Inada, 2019; Izawa et al., 2017; Kuroha et al., 2018; Verma et al., 2018; Yip et al., 2019; Zurita Rendón et al., 2018). In addition, Vms1 in yeast may have additional roles related to ribosomal stalling that are independent of the canonical RQC pathway, as it can cleave peptidyl-tRNA chains on the leading stalled ribosome independent of 40S and 60S subunit splitting (Verma et al., 2018). Consistent with this earlier role in stall resolution, Vms1 is found across the entire gradient in yeast polysome profiles, suggesting an association with polysomes as well as isolated and split 60S subunits

(Verma et al., 2018). In the absence of ANKZF1, as with other RQC factors, 60S subunits cannot be recycled for further rounds of translation, leading to a decrease in global translation **(Figure S5)**.

In this work, we highlight NEMF, LTN1, and ANKZF1 as regulators of RAN translation product accumulation from G4C2 and CGG repeats. By detecting truncated products generated from GC-rich transcripts, we suggest that translational stalling occurs within the short tandem repeat region of these mRNAs. We propose that these stalled ribosomes are triggered by the mRNA repeat secondary structure and that they recruit RQC complexes to assist with ribosomal recycling and clearance of aberrant mRNA and proteins (Joazeiro, 2019). How exactly this ribosomal recycling and clearance would work on repeats, however, is somewhat unclear. Classically, the RQC pathway degrades nascent peptide chains after ribosomal splitting and disassembly through a process that is CAT-tailing and NEMF-dependent (Lytvynenko et al., 2019; Sitron and Brandman, n.d.). This CAT-tailing is thought to allow for lysine residues to exit the ribosome and then be (Kostova et al., 2017; Sitron and Brandman, n.d.) ubiquitinated in an LTN1-dependent fashion to allow for targeting of nascent peptide chain to proteasomal degradation (Juszkiewicz and Hegde, 2017; Kuroha et al., 2018; Matsuo et al., 2023, 2017; Shao et al., 2013). However, there is no lysine available for ubiquitination in either of the sequences that serve as RAN translation templates from C9orf72-associated GA, GP, and GR reading frames from the sense transcript or the upstream endogenous 5'UTR, including the CGG repeat, of the FMR1 sequence. Without available lysine, we hypothesize that even when RQC pathways are triggered during RAN translation, the truncated products generated by RQC processing will likely be resistant to ubiquitination

and degradation. What roles such truncated degradation-resistant products might play in repeat-associated toxicity will be an important future research direction.

Carboxyl-terminal reporters are often used to measure the efficiency of RAN translation initiation in different settings (Cheng et al., 2018; Green et al., 2017; Kearse et al., 2016). These approaches face a limitation in that they assume translational elongation is held constant across reporters. As RAN translation potentially happens in multiple reading frames of the same transcript with different rates for both initiation and elongation, interpretation of results from the use of such carboxyl terminal tags as their sole readouts will need to be re-evaluated. Here, we observed largely similar results from both reporters using such a C-terminal tag reporter system as well as from MSD-based assays that directly measure DPR product generation (and as such are not reliant on translation elongation extending completely through the repeat to the NLuc reporter). The increase in generation of both partially made products from stalled ribosomes and complete protein products which contain the C-terminal reporter in the absence of key RQC factors (**Figure 4**) suggests that ribosomal stalling triggers one of two possible events. First, the surveillance pathway might still be triggered, leading to removal of stalled or collided ribosomes from the repeat mRNA but a failure to clear the nascent peptides from the 60S subunit. This would result in accumulation of those stall products and their detection on a denaturing gel. If the repeat mRNA is not degraded during this process, then removal of stalled ribosomes would also allow trailing ribosomes to complete translation through the entire repeat at increased rates, resulting in greater C-terminal reporter signal. Alternatively, the lack of RQC factors may create a longer time window during which stalled ribosomes can resume elongation through the repeat without

engagement of the RQC machinery. As such, more ribosomes would make it to the C-terminal reporter and generate complete products.

In summary, we find that RQC pathways inhibit accumulation of RAN translation products generated from GC-rich transcripts. Depletion of NEMF, LTN1, and ANKZF1 increases the accumulation of proteins made via RAN translation from GC-rich transcripts while overexpression of NEMF, LTN1, and ANKZF1 decreases the production of these proteins. These data suggest that augmenting RQC activity could have therapeutic benefits in GC-rich nucleotide repeat expansion diseases and that translational elongation needs to be considered in studies of RAN translation and other initiation-dependent processes.

3.6. Chapter-specific Acknowledgements

We thank current and former members of the Todd lab and the Barmada lab for critical discussions, and technical advice in the pursuit of this study. We thank the University of Michigan Vector Core for packaging lentivirus for this study. We thank Dr. Claudio Joazeiro for sharing cell lines and materials for the initial studies and Dr. James Bardwell for his generous support. We thank the University of Michigan Mass Spectrometry-Based Proteomics Resource Facility, especially Dr. Venkatesha Basrur, for the assistance and use of equipment.

Y-J.T., I.M., R. S., and P.K.T. conceived the project. Y-J.T. and I.M. designed the experiments. Y-J.T. performed, optimized, and visualized experiments with help from A.K. on plasmid construct and validation; K.J-W and L.P. on GP MSD assay; E.M.H.T. and S.J.B. on patient-derived iPSC iN. I.M. performed Drosophila experiments and assisted with the design and analysis of these studies. X.D. performed polysome

profiling experiments. N.B.G. performed initial studies. Y-J.T. wrote the draft of the manuscript with critics from I.M. along with P.K.T., and all authors reviewed and edited the manuscript.

This work was funded by grants from the NIH to P.K.T. (P50HD104463, R01NS099280, and R01NS086810), S.J.B. (R01 NS097542, R01 NS113943, and R56 NS128110) and L.P. (RF1AG062171, R35NS097273, P01NS084974, AG062077). P.K.T. and A.K. were also supported by the VA (BLRD BX004842). Y-J.T. was supported by the Cellular and Molecular Biology Graduate Program, University of Michigan. IM was supported by an Alzheimer's Association Research Fellowship.

3.7. Figures

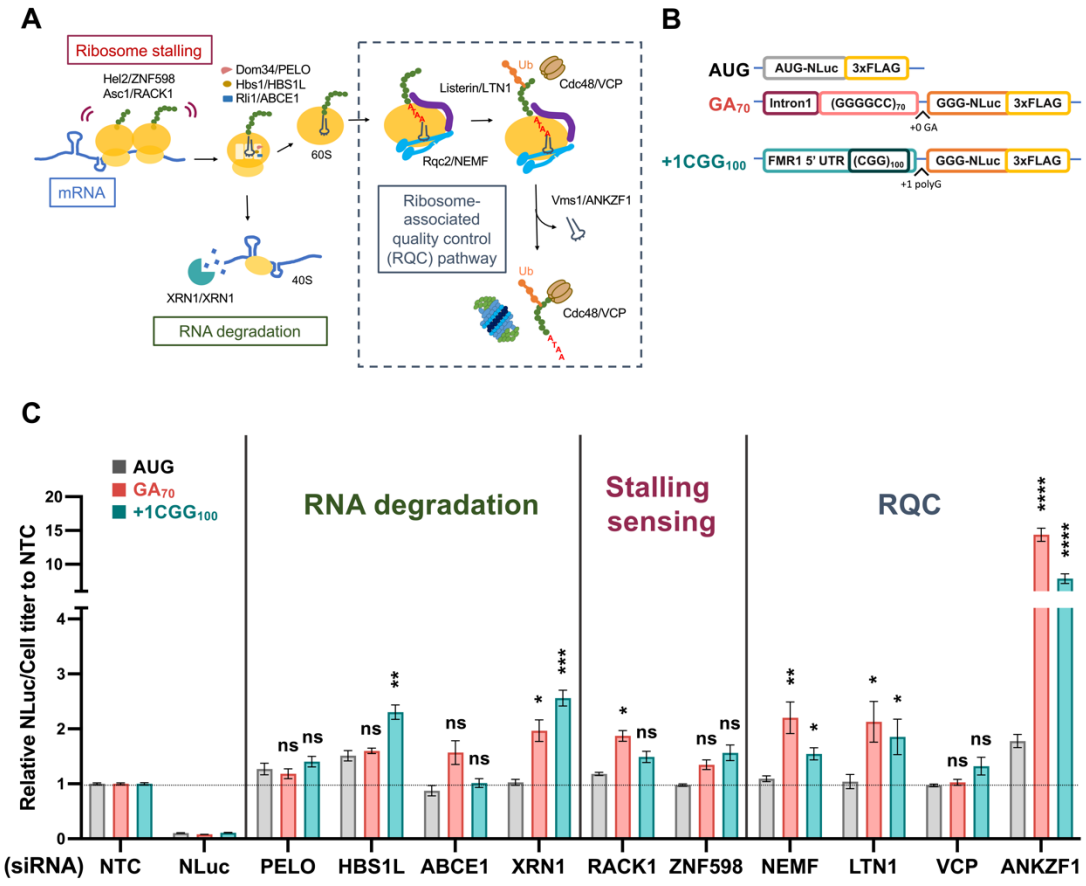

Figure 3-1. NEMF, LTN1, and ANKZF1 act as genetic modifiers of RAN translation from G4C2 and CGG repeats.

(**A**) Schematic of mRNA and protein surveillance pathways(Joazeiro, 2019).(**B**) Schematic of luciferase reporters used to assess RAN translation product abundance. (**C**) Targeted screen of factors involved in mRNA and protein surveillance pathways. The relative expression of NLuc to cell titer was compared to a non-targeting siRNA control (NTC). Data represent mean with error bars ± SEM of n = 6 cross at least 2 independent

experiments ns = not significant; *P < 0.05; **P ≤ 0.01; ***P ≤ 0.001; ****P ≤ 0.0001, multiple unpaired t-test after Welch's correction.

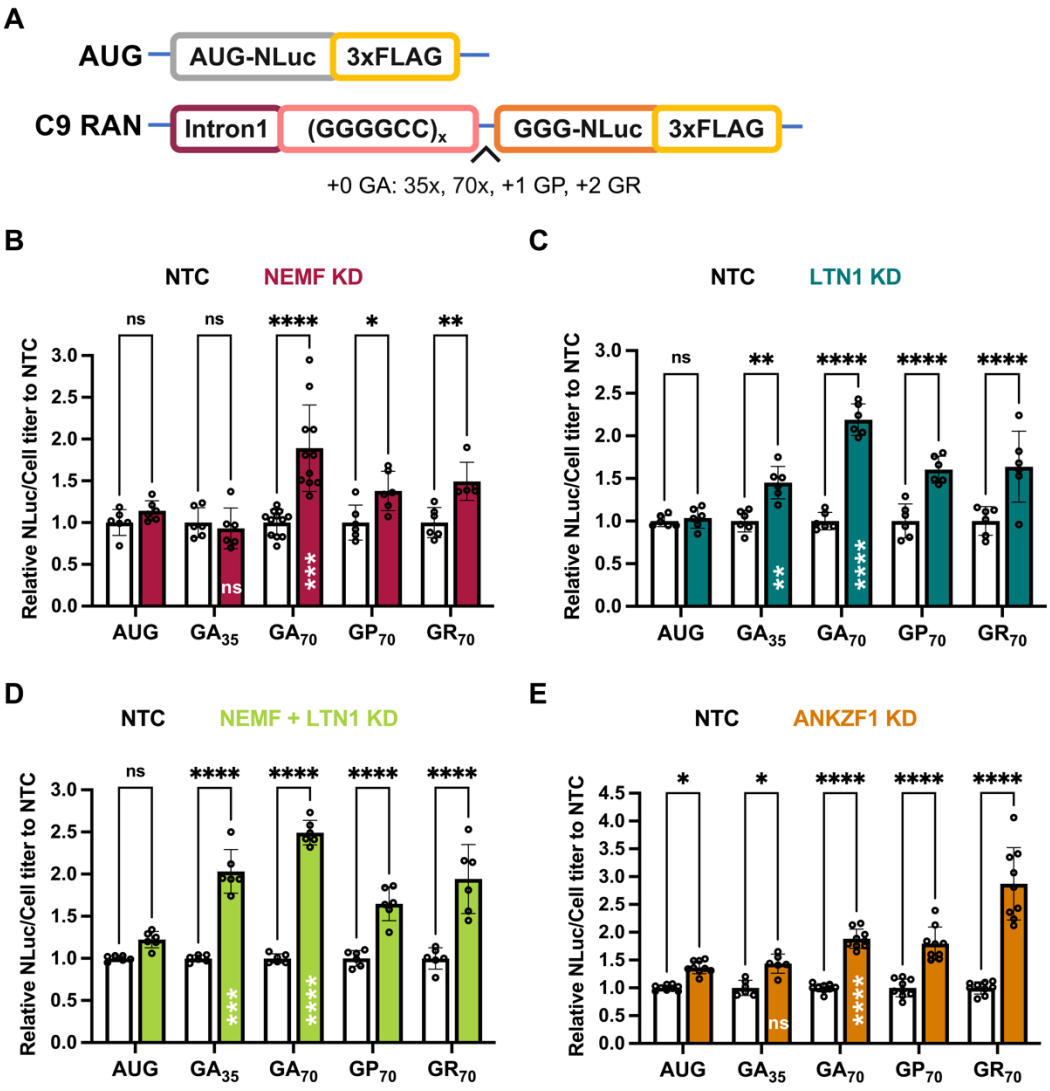

Figure 3-2. Depletion of NEMF, LTN1, and ANKZF1 enhances G4C2 C9 RAN translation in a repeat length-dependent manner across all reading frames.

(**A**) Schematic AUG-driven NLuc-3xFLAG and C9 RAN G4C2 repeat length and reading frame reporters. (**B-E**) Luciferase assays after NEMF, LTN1, both NEMF and LTN1 or ANKZF1 depletion. All graphs show mean with error bars ± SD. Each N is shown as an open circle (n=6-9/group). Asterisks above each bar are comparisons of expression between NTC and gene(s) knockdown. ns = not significant; *$P < 0.05$; **$P \leq 0.01$; ***$P \leq$

0.001; ****$P \leq 0.0001$, as determined with two-way ANOVA with Sidak's multiple comparison test. Asterisks placed inside each bar are comparisons between AUG-driven no-repeat control and different repeat lengths of the GA frame of cells treated with gene(s) knockdown. ns = not significant; **$P \leq 0.01$; ***$P \leq 0.001$; ****$P \leq 0.0001$, represent unpaired t-tests with Welch's correction for multiple comparisons.

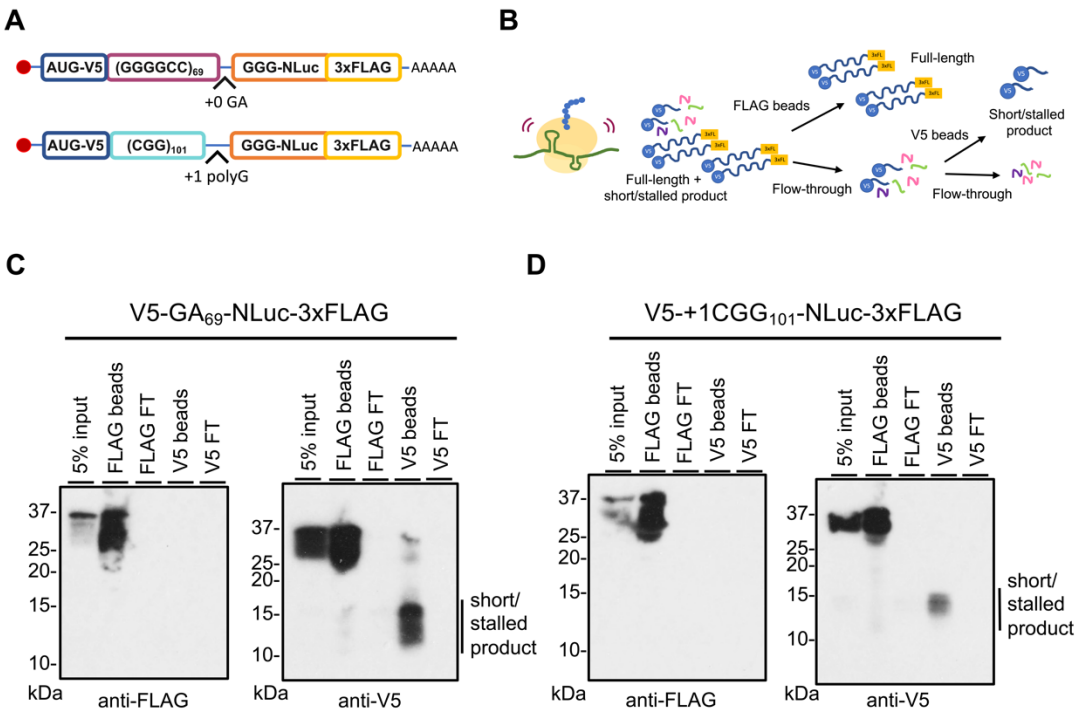

Figure 3-3. Detection of partially made products translated from GC-rich transcripts.

(**A**) Schematic of AUG-V5-(G4C2)$_{69}$-NLuc-3xFLAG in GA frame and AUG-V5-+1(CGG)$_{101}$-NLuc-3xFLAG in polyG frame. (**B**) FLAG and V5 IP workflow to enrich for incomplete products generated from GC-rich transcripts. 3xFL: 3xFLAG (**C-D**) V5 antibody IP reveals short/stalled products (line next to the blot) that are generated from G4C2 (panel C) or CGG repeats (panel D) that do not contain the carboxyl-terminal FLAG tag. FT: Flow-through.

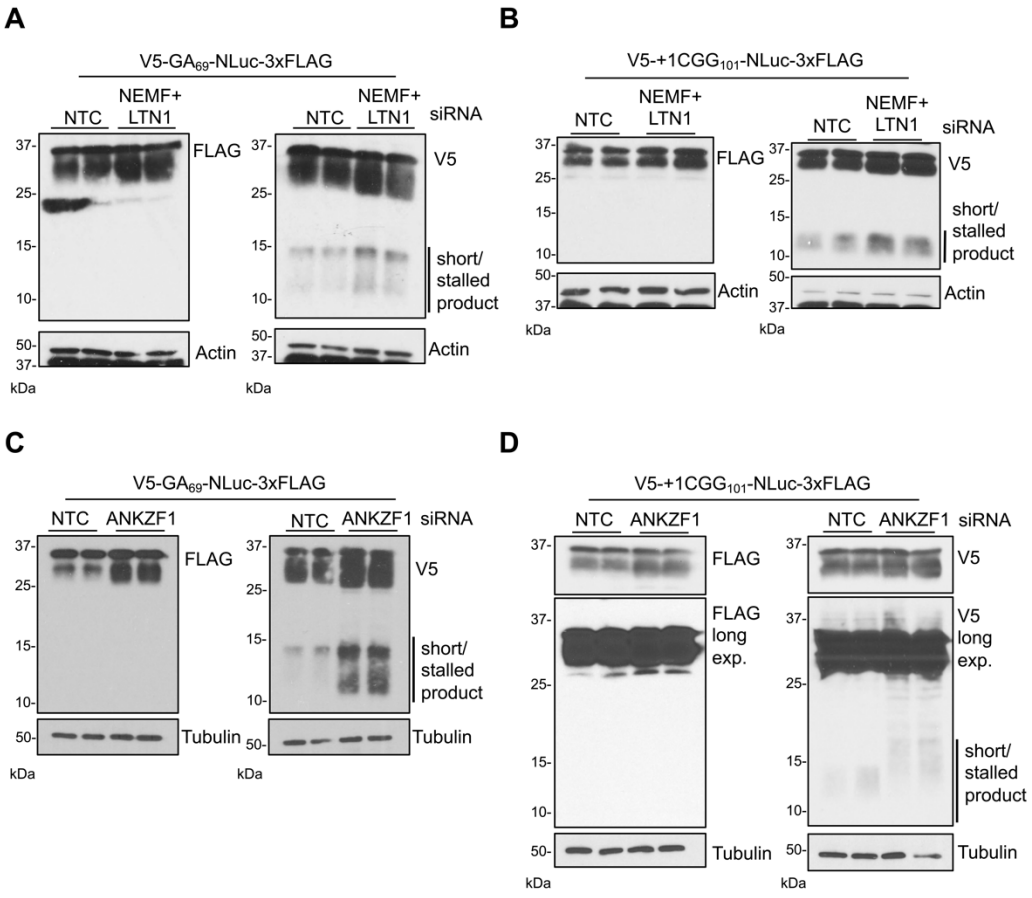

Figure 3-4. Depletion of NEMF, LTN1, and ANKZF1 enhances the generation of both full-length and partially made GA and polyG products from GC-rich transcripts.

(**A-D**) Immunoblots of HEK293 cells transfected with in vitro synthesized G4C2 (GA frame) and CGG repeat RNA reporters (polyG frame) in the presence and absence of NEMF + LTN1, and ANKZF1. Samples were processed as in Figure 3B. Blots represent two biological replicates. Lines next to the blots indicate short/stalled product products.

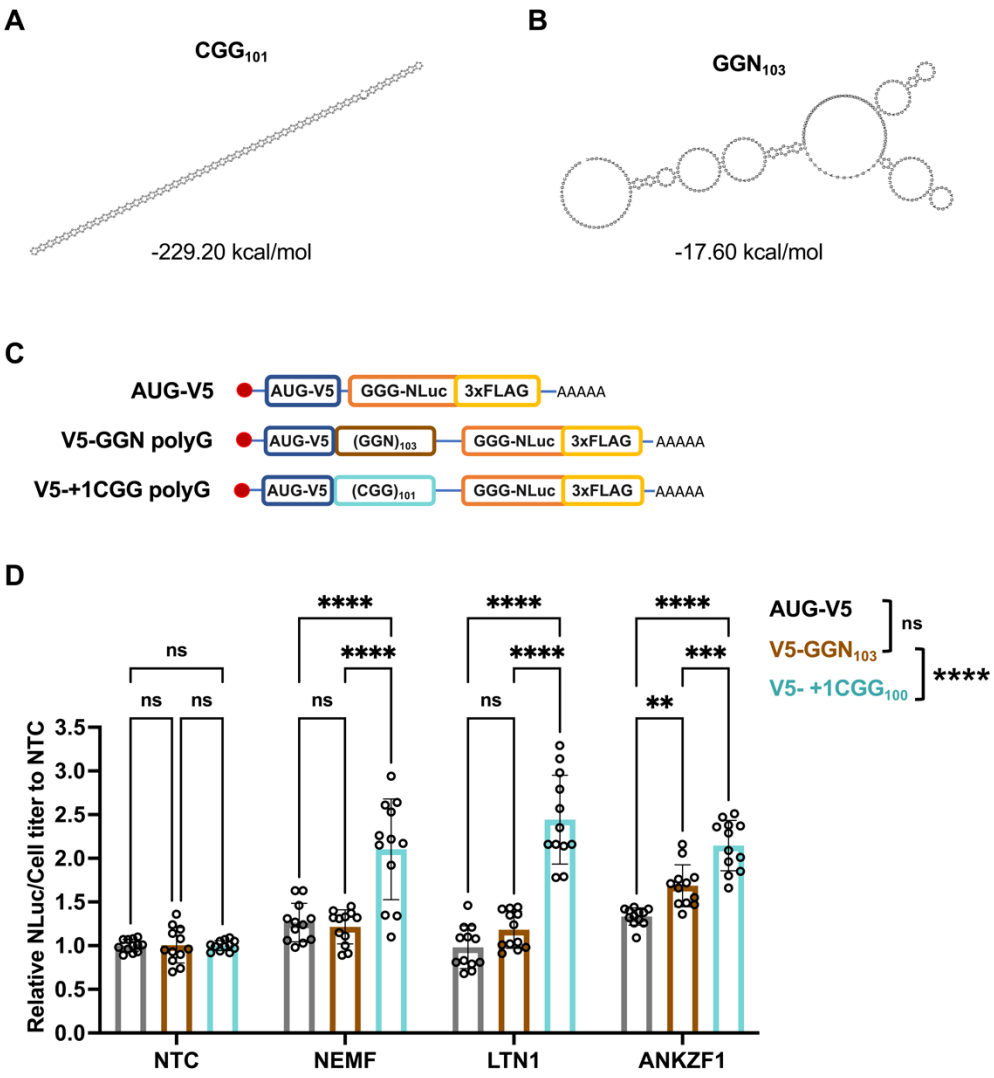

Figure 3-5. Enhancement of polyG production with NEMF, LTN1, and ANKZF1 depletion requires the CGG repeat RNA structure.

(**A-B**) Prediction of the optimal RNA secondary structure and calculation of the minimum free energy in CGG_{101} and GGN_{103} repeats. Only the repeat region from each repeat was used to predict the RNA secondary structure and calculate the minimum free energy. The results were computed by RNAfold 2.5.1. (**C**)Schematics of AUG-V5-NLuc-3xFLAG, AUG-V5-+1$(CGG)_{101}$-NLuc-3xFLAG, and AUG-V5-$(GGN)_{103}$-NLuc-3xFLAG transcripts.

(**D**) Knockdown of NEMF, LTN1, and ANKZF1 in HEK293 with no-repeat control, polyG from GGN repeats, and CGG repeats RNA transfection. Data represent means with error bars ±SD of n = 12, ns = not significant; ** $P \leq 0.01$; *** $P \leq 0.001$; **** $P \leq 0.0001$ by Tukey's multiple comparisons tests. The statistic result placed in the legend is group comparisons by two-way ANOVA Sidak’s multiple comparisons tests.

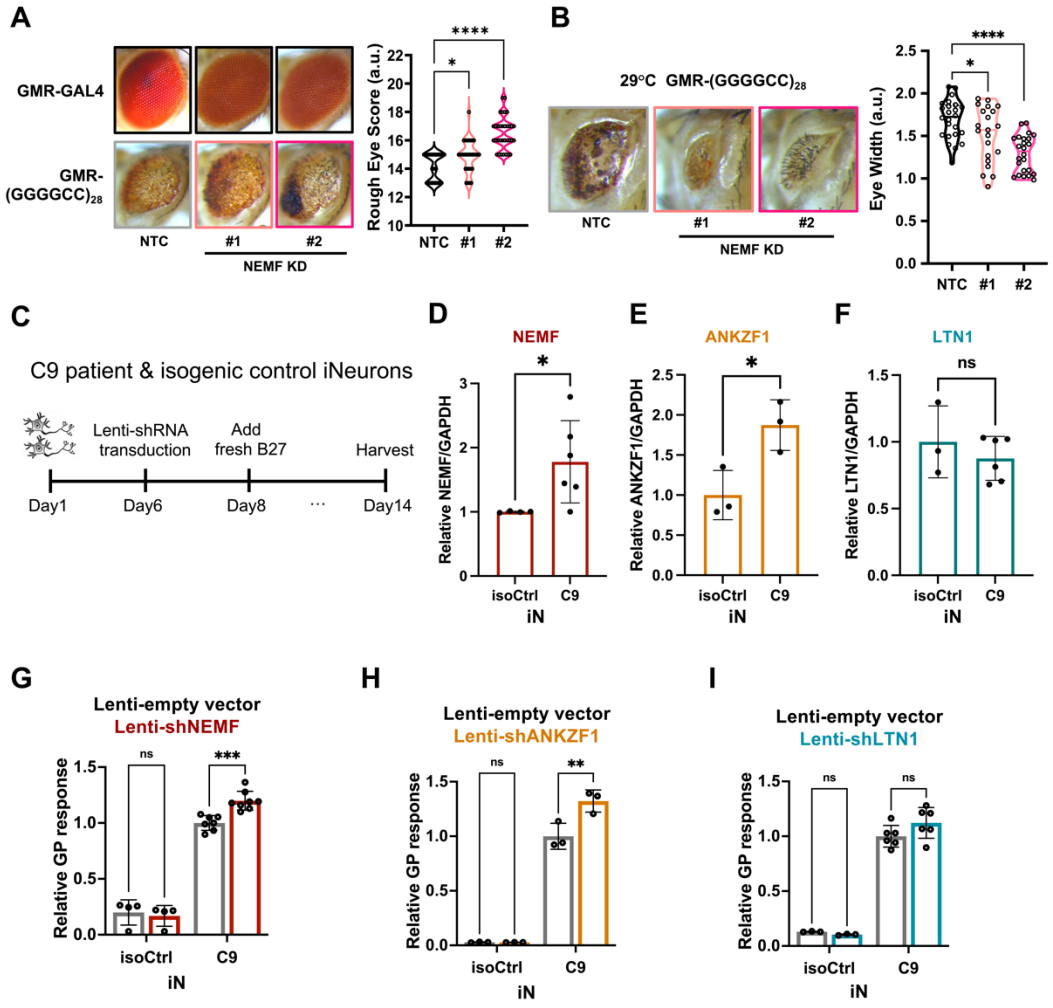

Figure 3-6. Depletion of NEMF enhances repeat-associated toxicity in a fly model of C9 ALS/FTD and DPR accumulation in human neurons.

(**A)** Representative images of *Drosophila* eyes expressing (G4C2)28 repeats under the GMR-GAL4 driver in the presence or absence of NEMF at 25°C [BDSC36955 #1 and BDSC25214 #2]. Rough eye phenotypes quantified using a nominal scoring system are shown as violin plots on the right. Individual flies are represented by single data points. n= 30-33/genotype. (**B**) (G4C2)28 repeats expressed with a GMR-GAL4 driver at 29°C show decreased eye width that is enhanced by the depletion of NEMF, as quantified on

the right. Graphs represent the mean with error bars ±SD, n = 21-24. For A and B, *P < 0.05; ****P ≤ 0.0001 by one-way ANOVA with Dunnett's multiple comparison test. (**C**) Schematic workflow for studies with C9ALS patient-derived iNeurons (iN). (**D-F**) RNA Expression of NEMF, LTN1, and ANKZF1 transcripts from C9ALS and isogenic control iN lysates. Data represent means with error bars ±SD. n = 3-6/gene, ns = not significant; *P < 0.05 by Student's t-test. (**G-I**) Quantification of GP by MSD assay from C9ALS and isogenic control iNs treated with lenti-empty vector or lenti-shRNA of NEMF, LTN1, or ANKZF1. Data represent mean ±SD; n = 3-6, ns = not significant; **P ≤ 0.01; ***P ≤ 0.001 by two-way ANOVA with Sidak's multiple comparison test.

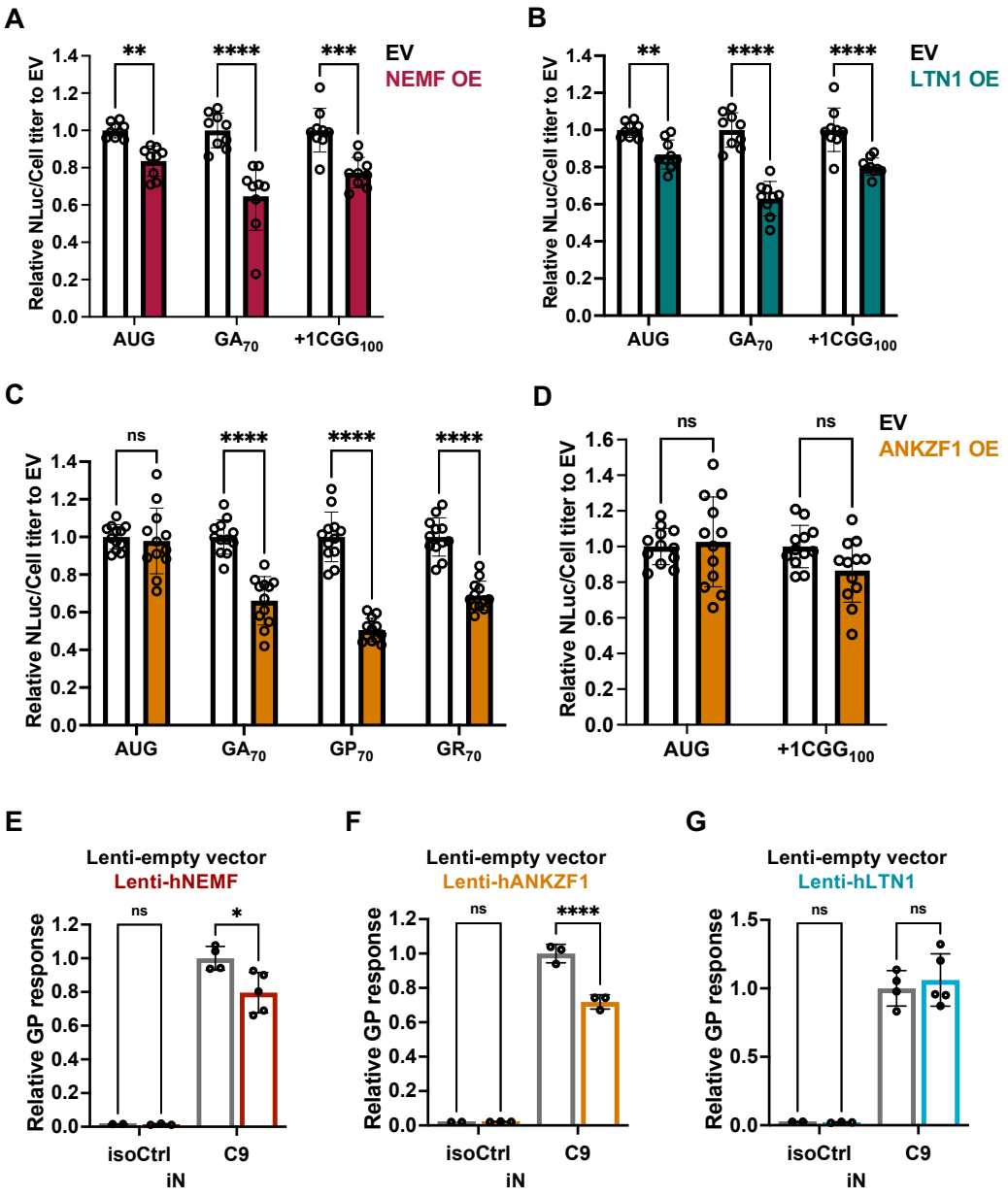

Figure 3-7. Overexpression of NEMF, LTN1, and ANKZF1 decreases RAN translation from G4C2 and CGG repeats.

(**A-B**) Relative expression of AUG-driven no repeats, (G4C2)70 repeats in the GA frame, and (CGG)100 repeats in the polyG frame when overexpressing empty vector (EV) versus hNEMF or hLTN1. (**C**) Relative expression of AUG-driven no-repeat control and

(G4C2)70 repeats in the GA, GP, and GR frames when overexpressing empty vector (EV) versus hANKZF1. (**D**) Relative expression of AUG-driven no-repeat control and (CGG)100 repeats in the polyG frame when overexpressing empty vector (EV) versus hANKZF1. Data represent means with error bars ±SD of n = 9-12, ns = not significant; $^{**}P \leq 0.01$; $^{***}P \leq 0.001$; $^{****}P \leq 0.0001$ by two-way ANOVA with Sidak's multiple comparison test. (**E-G**) Relative GP response of C9 and isogenic control iN treated with lenti-empty vector or lenti-hNEMF, hLTN1, and hANKZF1. The level of GP was measured by MSD. Data represent means with error bars ±SD of n = 3-5, ns = not significant; $^{*}P < 0.05$; $^{****}P \leq 0.0001$ by two-way ANOVA with Sidak's multiple comparison test.

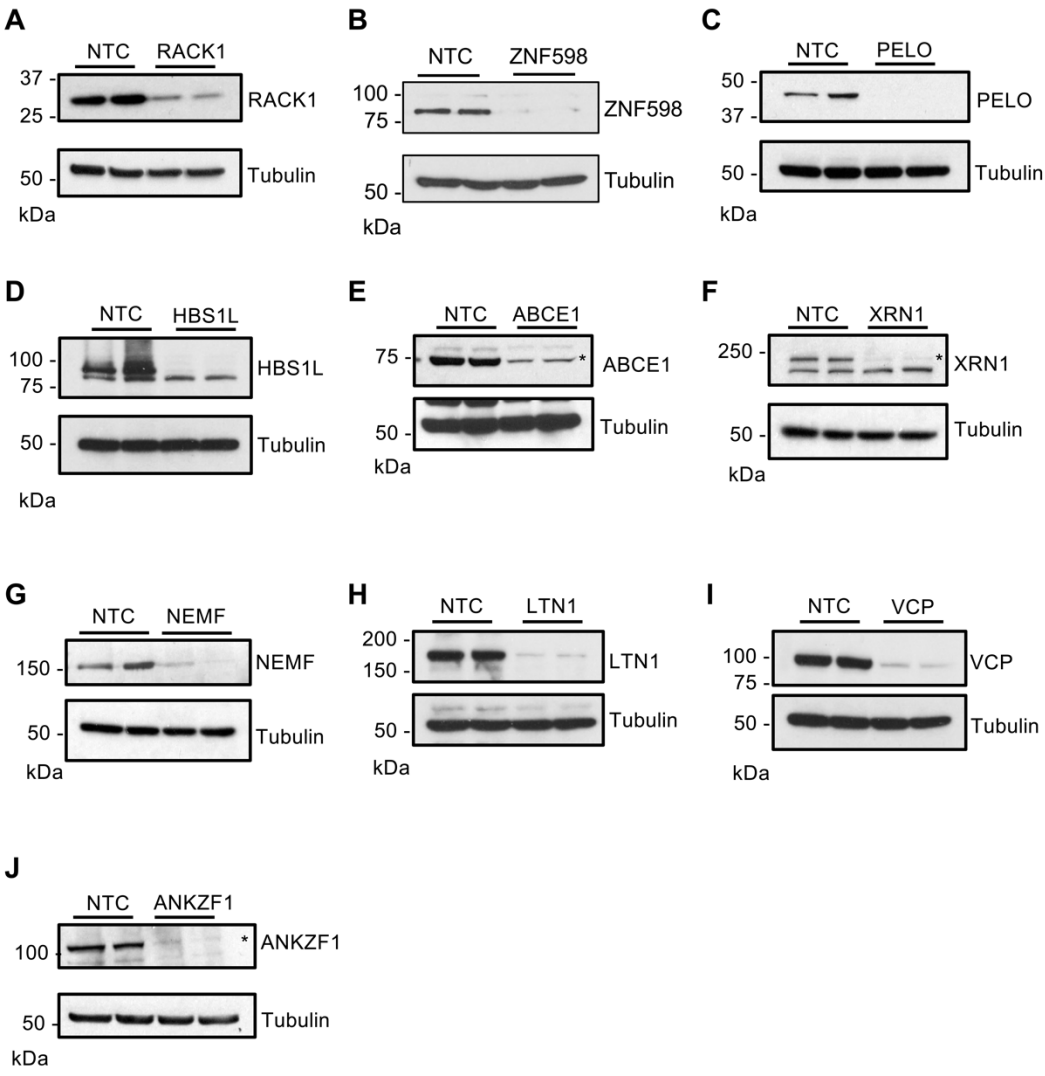

Supplemental Figure 3-8. Validation of siRNAs used in targeted screening

(**A-J**) 1nM siRNA transfected in HEK293 of each non-targeting (NTC) control and knockdown of ZNF598, RACK1, PELO, HBS1L, ABCE1, XRN1, NEMF, LTN1, VCP, and ANKZF1

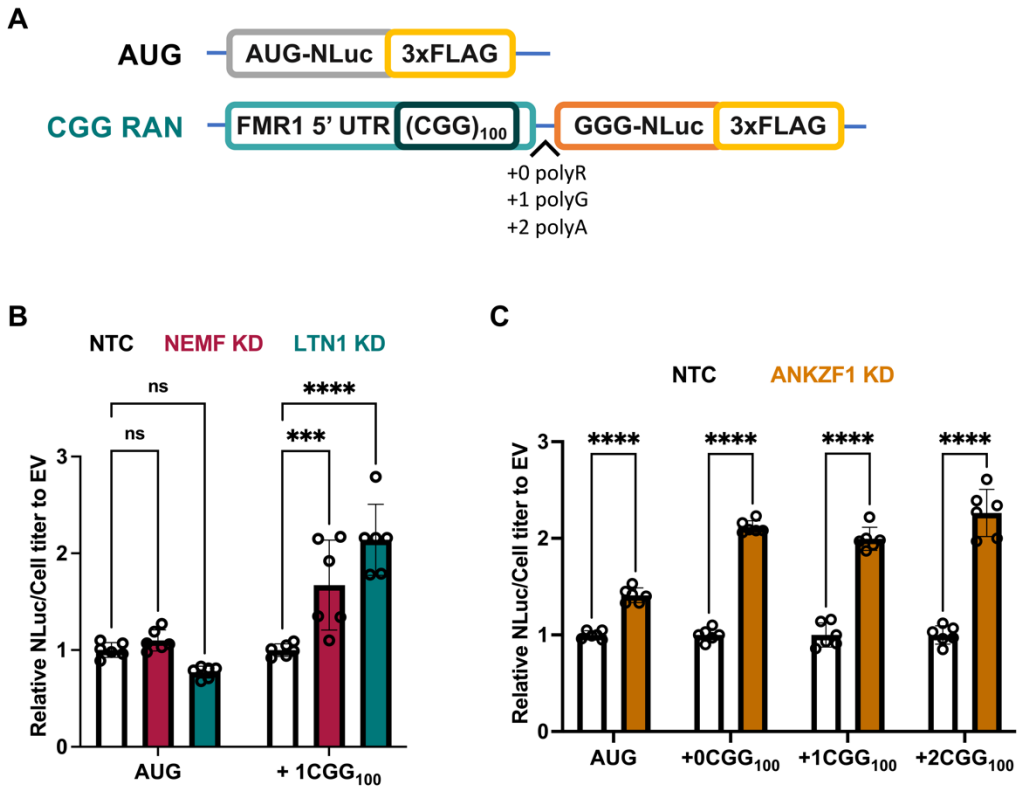

Supplemental Figure 3-9. Depletion of NEMF, LTN1, and ANKZF1 enhances CGG RAN translation

(**A**) Schematic AUG-driven and CGG RAN at different reading frame reporters. (**B-C**) Luciferase assays of RAN translation after NEMF, LTN1, or ANKZF1 depletion. All graphs show mean with error bars ± SD. Each N is shown as an open circle (n=6/group). Asterisks above each bar are comparisons of expression between NTC and gene(s) knockdown. ns = not significant; ***$P \leq 0.001$; ****$P \leq 0.0001$, as determined with one-way ANOVA with Sidak's multiple comparison test.

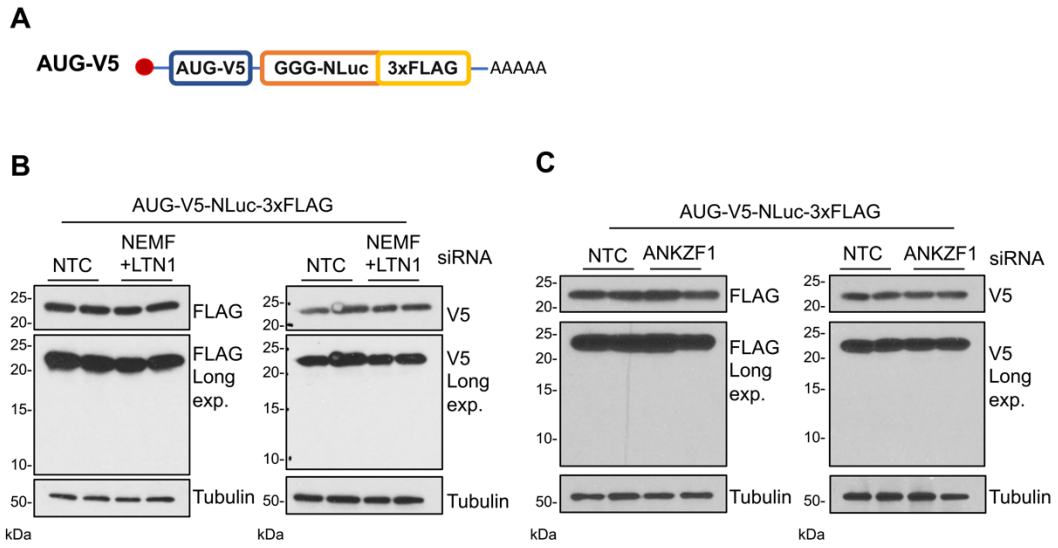

Supplemental Figure 3-10. No detection of stall products from constructs lacking GC repeats

(**A**)Schematic of AUG-V5-NLuc-3xFLAG. (**B-C**) Knockdown of NEMF + LTN1, and ANKZF1 in HEK293 with AUG-V5-NLuc-3xFLAG RNA transfection.

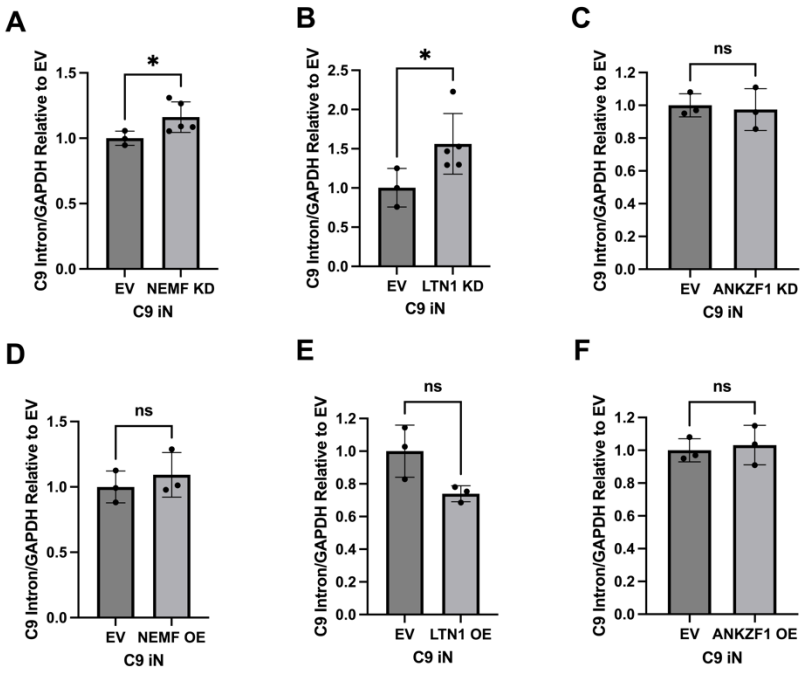

Supplemental Figure 3-11. Effect of NEMF, LTN1, and ANKZF1 knockdown and overexpression on C9 transcripts

(**A-F**) Quantification of RNA abundance targeting the C9 intronic region normalized to GAPDH. C9 iN was treated with lentiviruses of empty vector, NEMF, LTN1, or ANKZF1 knockdown or overexpression. Leftover lysates from GP MSD were collected for RNA extraction and qRT-PCR analysis. Data represent means with error bars ±SD of n = 3-5, ns = not significant; *$P \leq 0.05$ by Student's t-test.

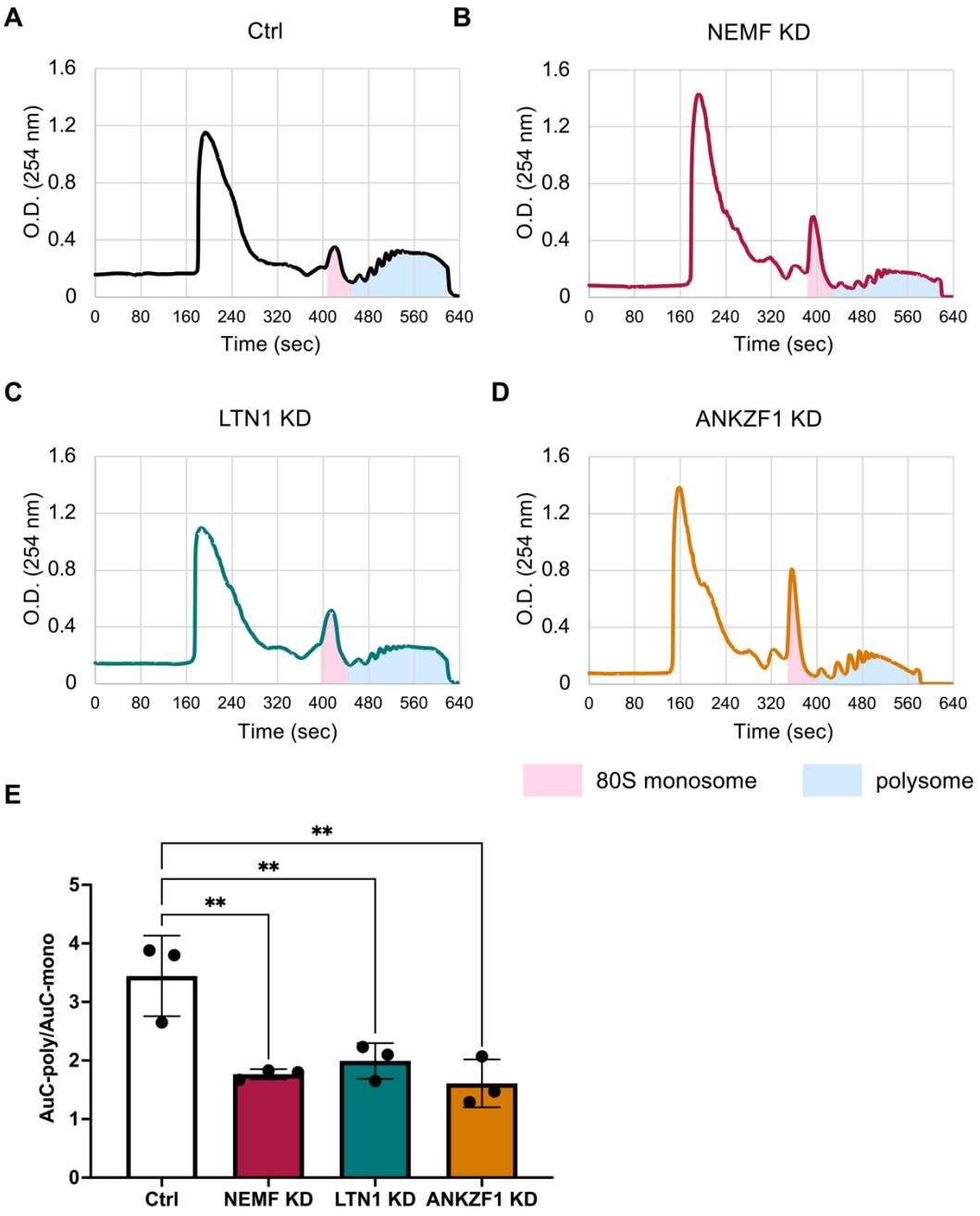

Supplemental Figure 3-12. Knockdown of NEMF, LTN1, and ANKZF1 inhibit global translation

(**A-D**) Representative polysome-fractionation profiles of HEK293 lysates transduced with lentivirus of Ctrl KD, NEMF KD, LTN1 KD, or ANKZF1 KD. (**E**) The areas-under-the-curve

(AuC) for monosomes and polysomes are shaded pink and blue, respectively. Global translation activity is calculated by normalizing AuC-polysome/AuC-monosome. Data represent means with error bars ±SD of n = 3, $^{**}P \leq 0.001$ as determined with one-way ANOVA with Sidak's multiple comparison test.

3.8. References

Ahmed A, Wang M, Bergant G, Maroofian R, Zhao R, Alfadhel M, Nashabat M, AlRifai MT, Eyaid W, Alswaid A, Beetz C, Qin Y, Zhu T, Tian Q, Xia L, Wu H, Shen L, Dong S, Yang X, Liu C, Ma L, Zhang Q, Khan R, Shah AA, Guo J, Tang B, Leonardis L, Writzl K, Peterlin B, Guo H, Malik S, Xia K, Hu Z. 2021. Biallelic loss-of-function variants in NEMF cause central nervous system impairment and axonal polyneuropathy. Hum Genet 140. doi:10.1007/s00439-020-02226-3

Andrade NS, Ramic M, Esanov R, Liu W, Rybin MJ, Gaidosh G, Abdallah A, Del'olio S, Huff TC, Chee NT, Anatha S, Gendron TF, Wahlestedt C, Zhang Y, Benatar M, Mueller C, Zeier Z. 2020. Dipeptide repeat proteins inhibit homology-directed DNA double strand break repair in C9ORF72 ALS/FTD. Mol Neurodegener 15. doi:10.1186/s13024-020-00365-9

Asamitsu S, Yabuki Y, Ikenoshita S, Kawakubo K, Kawasaki M, Usuki S, Nakayama Y, Adachi K, Kugoh H, Ishii K, Matsuura T, Nanba E, Sugiyama H, Fukunaga K, Shioda N. 2021. CGG repeat RNA G-quadruplexes interact with FMRpolyG to cause neuronal dysfunction in fragile X-related tremor/ataxia syndrome. Sci Adv. doi:10.1126/sciadv.abd9440

Ash PEA, Bieniek KF, Gendron TF, Caulfield T, Lin W-L, DeJesus-Hernandez M, van Blitterswijk MM, Jansen-West K, Paul JW, Rademakers R, Boylan KB, Dickson DW, Petrucelli L. 2013. Unconventional Translation of C9ORF72 GGGGCC Expansion Generates Insoluble Polypeptides Specific to c9FTD/ALS, Neuron. doi:10.1016/j.neuron.2013.02.004

Bañez-Coronel M, Ayhan F, Tarabochia AD, Zu T, Perez BA, Tusi SK, Pletnikova O, Borchelt DR, Ross CA, Margolis RL, Yachnis AT, Troncoso JC, Ranum LPW. 2015. RAN Translation in Huntington Disease. Neuron 88:667–677. doi:10.1016/j.neuron.2015.10.038

Bengtson MH, Joazeiro CAP. 2010. Role of a ribosome-associated E3 ubiquitin ligase in protein quality control. Nature 467. doi:10.1038/nature09371

Brandman O, Hegde RS. 2016. Ribosome-associated protein quality control. Nat Struct Mol Biol. doi:10.1038/nsmb.3147

Brandman O, Stewart-Ornstein J, Wong D, Larson A, Williams CC, Li GW, Zhou S, King D, Shen PS, Weibezahn J, Dunn JG, Rouskin S, Inada T, Frost A, Weissman JS. 2012. A Ribosome-Bound Quality Control Complex Triggers Degradation of Nascent Peptides and Signals Translation Stress. Cell 151. doi:10.1016/j.cell.2012.10.044

Buijsen RAM, Sellier C, Severijnen LAWFM, Oulad-Abdelghani M, Verhagen RFM, Berman RF, Charlet-Berguerand N, Willemsen R, Hukema RK. 2014. FMRpolyG-positive inclusions in CNS and non-CNS organs of a fragile X premutation carrier with fragile X-associated tremor/ataxia syndrome. Acta Neuropathol Commun. doi:10.1186/s40478-014-0162-2

Buijsen RAM, Visser JA, Kramer P, Severijnen EAWFM, Gearing M, Charlet-Berguerand N, Sherman SL, Berman RF, Willemsen R, Hukema RK. 2016. Presence of inclusions positive for polyglycine containing protein, FMRpolyG, indicates that repeat-associated non-AUG translation plays a role in fragile X-

associated primary ovarian insufficiency. Human Reproduction 31:158–168. doi:10.1093/humrep/dev280

Buskirk AR, Green R. 2017. Ribosome pausing, arrest and rescue in bacteria and eukaryotes. Philosophical Transactions of the Royal Society B: Biological Sciences. doi:10.1098/rstb.2016.0183

Busskamp V, Lewis NE, Guye P, Ng AH, Shipman SL, Byrne SM, Sanjana NE, Murn J, Li Y, Li S, Stadler M, Weiss R, Church GM. 2014. Rapid neurogenesis through transcriptional activation in human stem cells. Mol Syst Biol 10. doi:10.15252/msb.20145508

Cerbini T, Funahashi R, Luo Y, Liu C, Park K, Rao M, Malik N, Zou J. 2015. Transcription activator-like effector nuclease (TALEN)-mediated CLYBL targeting enables enhanced transgene expression and one-step generation of dual reporter human induced pluripotent stem cell (iPSC) and neural stem cell (NSC) lines. PLoS One 10. doi:10.1371/journal.pone.0116032

Cheng W, Wang S, Mestre AA, Fu C, Makarem A, Xian F, Hayes LR, Lopez-Gonzalez R, Drenner K, Jiang J, Cleveland DW, Sun S. 2018. C9ORF72 GGGGCC repeat-associated non-AUG translation is upregulated by stress through eIF2α phosphorylation. Nat Commun. doi:10.1038/s41467-017-02495-z

Cheng W, Wang S, Zhang Z, Morgens DW, Hayes LR, Lee S, Portz B, Xie Y, Nguyen B V., Haney MS, Yan S, Dong D, Coyne AN, Yang J, Xian F, Cleveland DW, Qiu Z, Rothstein JD, Shorter J, Gao FB, Bassik MC, Sun S. 2019. CRISPR-Cas9 Screens Identify the RNA Helicase DDX3X as a Repressor of C9ORF72

(GGGGCC)n Repeat-Associated Non-AUG Translation. Neuron 104:885-898.e8. doi:10.1016/j.neuron.2019.09.003

Chiang PW, Carpenter LE, Hagerman PJ. 2001. The 5′-Untranslated Region of the FMR1 Message Facilitates Translation by Internal Ribosome Entry. Journal of Biological Chemistry 276. doi:10.1074/jbc.m105584200

Chu J, Hong NA, Masuda CA, Jenkins B V., Nelms KA, Goodnow CC, Glynne RJ, Wu H, Masliah E, Joazeiro CAP, Kay SA. 2009. A mouse forward genetics screen identifies LISTERIN as an E3 ubiquitin ligase involved in neurodegeneration. Proc Natl Acad Sci U S A 106. doi:10.1073/pnas.0812819106

Cleary JD, Ranum LPW. 2014. Repeat associated non-ATG (RAN) translation: New starts in microsatellite expansion disorders. Curr Opin Genet Dev. doi:10.1016/j.gde.2014.03.002

Cleary JD, Ranum LPW. 2013. Repeat-associated non-ATG (RAN) translation in neurological disease. Hum Mol Genet 22. doi:10.1093/hmg/ddt371

Conlon EG, Lu L, Sharma A, Yamazaki T, Tang T, Shneider NA, Manley JL. 2016. The C9ORF72 GGGGCC expansion forms RNA G-quadruplex inclusions and sequesters hnRNP H to disrupt splicing in ALS brains. Elife 5. doi:10.7554/eLife.17820

Defenouillère Q, Fromont-Racine M. 2017. The ribosome-bound quality control complex: from aberrant peptide clearance to proteostasis maintenance. Curr Genet. doi:10.1007/s00294-017-0708-5

Defenouillère Q, Yao Y, Mouaikel J, Namane A, Galopier A, Decourty L, Doyen A, Malabat C, Saveanu C, Jacquier A, Fromont-Racine M. 2013. Cdc48-associated

complex bound to 60S particles is required for the clearance of aberrant translation products. Proc Natl Acad Sci U S A 110. doi:10.1073/pnas.1221724110

DeJesus-Hernandez M, Mackenzie IR, Boeve BF, Boxer AL, Baker M, Rutherford NJ, Nicholson AM, Finch NA, Flynn H, Adamson J, Kouri N, Wojtas A, Sengdy P, Hsiung G-YR, Karydas A, Seeley WW, Josephs KA, Coppola G, Geschwind DH, Wszolek ZK, Feldman H, Knopman DS, Petersen RC, Miller BL, Dickson DW, Boylan KB, Graff-Radford NR, Rademakers R. 2011. Expanded GGGGCC Hexanucleotide Repeat in Noncoding Region of C9ORF72 Causes Chromosome 9p-Linked FTD and ALS. Neuron 72:245–256. doi:10.1016/j.neuron.2011.09.011

Doamekpor SK, Lee JW, Hepowit NL, Wu C, Charenton C, Leonard M, Bengtson MH, Rajashankar KR, Sachs MS, Lima CD, Joazeiro CAP. 2016. Structure and function of the yeast listerin (Ltn1) conserved N-terminal domain in binding to stalled 60S ribosomal subunits. Proc Natl Acad Sci U S A 113. doi:10.1073/pnas.1605951113

F T, KP I, T T, J Lo, LW G, E B-K, D N, LY M, J Laffin, DB B, RJ H. 2012. FMR1 CGG allele size and prevalence ascertained through newborn screening in the United States. Genome Med 4.

Filbeck S, Cerullo F, Pfeffer S, Joazeiro CAP. 2022. Ribosome-associated quality-control mechanisms from bacteria to humans. Mol Cell. doi:10.1016/j.molcel.2022.03.038

Fratta P, Mizielinska S, Nicoll AJ, Zloh M, Fisher EMC, Parkinson G, Isaacs AM. 2012. C9orf72 hexanucleotide repeat associated with amyotrophic lateral sclerosis and

frontotemporal dementia forms RNA G-quadruplexes. Sci Rep. doi:10.1038/srep01016

Freibaum BD, Lu Y, Lopez-Gonzalez R, Kim NC, Almeida S, Lee K-H, Badders N, Valentine M, Miller BL, Wong PC, Petrucelli L, Kim HJ, Gao F-B, Taylor JP. 2015. GGGGCC repeat expansion in C9orf72 compromises nucleocytoplasmic transport. Nature 525:129–133. doi:10.1038/nature14974

Fry M, Loeb LA. 1994. The fragile X syndrome d(CGG)(n) nucleotide repeats form a stable tetrahelical structure. Proc Natl Acad Sci U S A. doi:10.1073/pnas.91.11.4950

Fujino Y, Mori K, Nagai Y. 2023. Repeat-associated non-AUG translation in neuromuscular diseases: mechanisms and therapeutic insights. The Journal of Biochemistry. doi:10.1093/jb/mvad012

Gao FB, Richter JD. 2017. Microsatellite Expansion Diseases: Repeat Toxicity Found in Translation. Neuron. doi:10.1016/j.neuron.2017.01.001

Garzia A, Jafarnejad SM, Meyer C, Chapat C, Gogakos T, Morozov P, Amiri M, Shapiro M, Molina H, Tuschl T, Sonenberg N. 2017. The E3 ubiquitin ligase and RNA-binding protein ZNF598 orchestrates ribosome quality control of premature polyadenylated mRNAs. Nat Commun 8. doi:10.1038/ncomms16056

Gendron TF, Bieniek KF, Zhang Y-J, Jansen-West K, Ash PEA, Caulfield T, Daughrity L, Dunmore JH, Castanedes-Casey M, Chew J, Cosio DM, van Blitterswijk M, Lee WC, Rademakers R, Boylan KB, Dickson DW, Petrucelli L. 2013. Antisense transcripts of the expanded C9ORF72 hexanucleotide repeat form nuclear RNA

foci and undergo repeat-associated non-ATG translation in c9FTD/ALS. Acta Neuropathol 126:829–844. doi:10.1007/s00401-013-1192-8

Goodman LD, Prudencio M, Kramer NJ, Martinez-Ramirez LF, Srinivasan AR, Lan M, Parisi MJ, Zhu Y, Chew J, Cook CN, Berson A, Gitler AD, Petrucelli L, Bonini NM. 2019. Toxic expanded GGGGCC repeat transcription is mediated by the PAF1 complex in C9orf72-associated FTD. Nat Neurosci. doi:10.1038/s41593-019-0396-1

Green KM, Glineburg MR, Kearse MG, Flores BN, Linsalata AE, Fedak SJ, Goldstrohm AC, Barmada SJ, Todd PK. 2017. RAN translation at C9orf72-associated repeat expansions is selectively enhanced by the integrated stress response. Nat Commun 8. doi:10.1038/s41467-017-02200-0

Green KM, Linsalata AE, Todd PK. 2016. RAN translation—What makes it run? Brain Res 1647:30–42. doi:10.1016/j.brainres.2016.04.003

Green KM, Miller SL, Malik I, Todd PK. 2022. Non-canonical initiation factors modulate repeat-associated non-AUG translation. Hum Mol Genet 31. doi:10.1093/hmg/ddac021

Gruber AR, Lorenz R, Bernhart SH, Neuböck R, Hofacker IL. 2008. The Vienna RNA websuite. Nucleic Acids Res 36. doi:10.1093/nar/gkn188

Guydosh NR, Green R. 2014. Dom34 rescues ribosomes in 3′ untranslated regions. Cell 156:950–962. doi:10.1016/j.cell.2014.02.006

Habibey R, Striebel J, Schmieder F, Czarske J, Busskamp V. 2022. Long-term morphological and functional dynamics of human stem cell-derived neuronal

networks on high-density micro-electrode arrays. Front Neurosci 16. doi:10.3389/fnins.2022.951964

Haeusler AR, Donnelly CJ, Periz G, Simko EAJ, Shaw PG, Kim M-S, Maragakis NJ, Troncoso JC, Pandey A, Sattler R, Rothstein JD, Wang J. 2014. C9orf72 nucleotide repeat structures initiate molecular cascades of disease. Nature 507:195–200. doi:10.1038/nature13124

Hagerman R, Hagerman P. 2021. Fragile X-associated tremor/ataxia syndrome: pathophysiology and management. Curr Opin Neurol. doi:10.1097/WCO.0000000000000954

Hagerman RJ, Leehey M, Heinrichs W, Tassone F, Wilson R, Hills J, Grigsby J, Gage B, Hagerman PJ. 2001. Intention tremor, parkinsonism, and generalized brain atrophy in male carriers of fragile X. Neurology 57:127–130. doi:10.1212/WNL.57.1.127

Hashimoto S, Sugiyama T, Yamazaki R, Nobuta R, Inada T. 2020. Identification of a novel trigger complex that facilitates ribosome-associated quality control in mammalian cells. Sci Rep 10. doi:10.1038/s41598-020-60241-w

He F, Flores BN, Krans A, Frazer M, Natla S, Niraula S, Adefioye O, Barmada SJ, Todd PK. 2020. The carboxyl termini of RAN translated GGGGCC nucleotide repeat expansions modulate toxicity in models of ALS/FTD. Acta Neuropathol Commun 8. doi:10.1186/s40478-020-01002-8

Ikeuchi K, Izawa T, Inada T. 2019a. Recent progress on the molecular mechanism of quality controls induced by ribosome stalling. Front Genet. doi:10.3389/fgene.2018.00743

Ikeuchi K, Tesina P, Matsuo Y, Sugiyama T, Cheng J, Saeki Y, Tanaka K, Becker T, Beckmann R, Inada T. 2019b. Collided ribosomes form a unique structural interface to induce Hel2-driven quality control pathways. EMBO J 38. doi:10.15252/embj.2018100276

Inada T. 2020. Quality controls induced by aberrant translation. Nucleic Acids Res 48. doi:10.1093/NAR/GKZ1201

Inada T. 2019. tRNA recycling on stalled ribosomes. Nat Struct Mol Biol 26. doi:10.1038/s41594-019-0222-1

Ishiguro T, Sato N, Ueyama M, Fujikake N, Sellier C, Kanegami A, Tokuda E, Zamiri B, Gall-Duncan T, Mirceta M, Furukawa Y, Yokota T, Wada K, Taylor JP, Pearson CE, Charlet-Berguerand N, Mizusawa H, Nagai Y, Ishikawa K. 2017. Regulatory Role of RNA Chaperone TDP-43 for RNA Misfolding and Repeat-Associated Translation in SCA31. Neuron 94. doi:10.1016/j.neuron.2017.02.046

Izawa T, Park SH, Zhao L, Hartl FU, Neupert W. 2017. Cytosolic Protein Vms1 Links Ribosome Quality Control to Mitochondrial and Cellular Homeostasis. Cell 171. doi:10.1016/j.cell.2017.10.002

Jacquemont S, Hagerman RJ, Leehey MA, Hall DA, Levine RA, Brunberg JA, Zhang L, Jardini T, Gane LW, Harris SW, Herman K, Grigsby J, Greco CM, Berry-Kravis E, Tassone F, Hagerman PJ. 2004. Penetrance of the Fragile X-Associated Tremor/Ataxia Syndrome in a Premutation Carrier Population. JAMA 291. doi:10.1001/jama.291.4.460

Joazeiro CAP. 2019. Mechanisms and functions of ribosome-associated protein quality control. Nat Rev Mol Cell Biol 20:368–383. doi:10.1038/s41580-019-0118-2

Jovičić A, Mertens J, Boeynaems S, Bogaert E, Chai N, Yamada SB, Paul JW, Sun S, Herdy JR, Bieri G, Kramer NJ, Gage FH, Van Den Bosch L, Robberecht W, Gitler AD. 2015. Modifiers of C9orf72 dipeptide repeat toxicity connect nucleocytoplasmic transport defects to FTD/ALS. Nat Neurosci 18:1226–1229. doi:10.1038/nn.4085

Juszkiewicz S, Hegde RS. 2017. Initiation of Quality Control during Poly(A) Translation Requires Site-Specific Ribosome Ubiquitination. Mol Cell 65. doi:10.1016/j.molcel.2016.11.039

Kearse MG, Green KM, Krans A, Rodriguez CM, Linsalata AE, Goldstrohm AC, Todd PK. 2016. CGG Repeat-Associated Non-AUG Translation Utilizes a Cap-Dependent Scanning Mechanism of Initiation to Produce Toxic Proteins. Mol Cell. doi:10.1016/j.molcel.2016.02.034

Kearse MG, Todd PK. 2014. Repeat-Associated Non-AUG Translation and Its Impact in Neurodegenerative Disease. Neurotherapeutics 11:721–731. doi:10.1007/s13311-014-0292-z

Kong HE, Lim J, Linsalata A, Kang Y, Malik I, Allen EG, Cao Y, Shubeck L, Johnston R, Huang Y, Gu Y, Guo X, Zwick ME, Qin Z, Wingo TS, Juncos J, Nelson DL, Epstein MP, Cutler DJ, Todd PK, Sherman SL, Warren ST, Jin P. 2022. Identification of PSMB5 as a genetic modifier of fragile X–associated

tremor/ataxia syndrome. Proc Natl Acad Sci U S A 119. doi:10.1073/pnas.2118124119

Koob MD, Moseley ML, Schut LJ, Benzow KA, Bird TD, Day JW, Ranum LPW. 1999. An untranslated CTG expansion causes a novel form of spinocerebellar ataxia (SCA8). Nat Genet 21. doi:10.1038/7710

Kostova KK, Hickey KL, Osuna BA, Hussmann JA, Frost A, Weinberg DE, Weissman JS. 2017. CAT-tailing as a fail-safe mechanism for efficient degradation of stalled nascent polypeptides.

Krans A, Kearse MG, Todd PK. 2016. Repeat-associated non-AUG translation from antisense CCG repeats in fragile X tremor/ataxia syndrome. Ann Neurol. doi:10.1002/ana.24800

Kriachkov V, Ormsby AR, Kusnadi EP, McWilliam HEG, Mintern JD, Amarasinghe SL, Ritchie ME, Furic L, Hatters DM. 2023. Arginine-rich C9ORF72 ALS proteins stall ribosomes in a manner distinct from a canonical ribosome-associated quality control substrate. Journal of Biological Chemistry 299. doi:10.1016/j.jbc.2022.102774

Kumari S, Bugaut A, Huppert JL, Balasubramanian S. 2007. An RNA G-quadruplex in the 5′ UTR of the NRAS proto-oncogene modulates translation. Nat Chem Biol 3. doi:10.1038/nchembio864

Kuroha K, Zinoviev A, Hellen CUT, Pestova T V. 2018. Release of Ubiquitinated and Non-ubiquitinated Nascent Chains from Stalled Mammalian Ribosomal Complexes by ANKZF1 and Ptrh1. Mol Cell 72. doi:10.1016/j.molcel.2018.08.022

Lander ES, Linton LM, Birren B, Nusbaum C, Zody MC, Baldwin J, Devon K, Dewar K, Doyle M, Fitzhugh W, Funke R, Gage D, Harris K, Heaford A, Howland J, Kann L, Lehoczky J, Levine R, McEwan P, McKernan K, Meldrim J, Mesirov JP, Miranda C, Morris W, Naylor J, Raymond Christina, Rosetti M, Santos R, Sheridan A, Sougnez C, Stange-Thomann N, Stojanovic N, Subramanian A, Wyman D, Rogers J, Sulston J, Ainscough R, Beck S, Bentley D, Burton J, Clee C, Carter N, Coulson A, Deadman R, Deloukas P, Dunham A, Dunham I, Durbin R, French L, Grafham D, Gregory S, Hubbard T, Humphray S, Hunt A, Jones M, Lloyd C, McMurray A, Matthews L, Mercer S, Milne S, Mullikin JC, Mungall A, Plumb R, Ross M, Shownkeen R, Sims S, Waterston RH, Wilson RK, Hillier LW, McPherson JD, Marra MA, Mardis ER, Fulton LA, Chinwalla AT, Pepin KH, Gish WR, Chissoe SL, Wendl MC, Delehaunty KD, Miner TL, Delehaunty A, Kramer JB, Cook LL, Fulton RS, Johnson DL, Minx PJ, Clifton SW, Hawkins T, Branscomb E, Predki P, Richardson P, Wenning S, Slezak T, Doggett N, Cheng JF, Olsen A, Lucas S, Elkin C, Uberbacher E, Frazier M, Gibbs RA, Muzny DM, Scherer SE, Bouck JB, Sodergren EJ, Worley KC, Rives CM, Gorrell JH, Metzker ML, Naylor SL, Kucherlapati RS, Nelson DL, Weinstock GM, Sakaki Y, Fujiyama A, Hattori M, Yada T, Toyoda A, Itoh T, Kawagoe C, Watanabe H, Totoki Y, Taylor T, Weissenbach J, Heilig R, Saurin W, Artiguenave F, Brottier P, Bruls T, Pelletier E, Robert C, Wincker P, Rosenthal A, Platzer M, Nyakatura G, Taudien S, Rump A, Smith DR, Doucette-Stamm L, Rubenfield M, Weinstock K, Hong ML, Dubois J, Yang H, Yu J, Wang J, Huang G, Gu J, Hood L, Rowen L, Madan A, Qin S, Davis RW, Federspiel NA, Abola AP, Proctor MJ, Roe BA, Chen F, Pan H,

Ramser J, Lehrach H, Reinhardt R, McCombie WR, De La Bastide M, Dedhia N, Blöcker H, Hornischer K, Nordsiek G, Agarwala R, Aravind L, Bailey JA, Bateman A, Batzoglou S, Birney E, Bork P, Brown DG, Burge CB, Cerutti L, Chen HC, Church D, Clamp M, Copley RR, Doerks T, Eddy SR, Eichler EE, Furey TS, Galagan J, Gilbert JGR, Harmon C, Hayashizaki Y, Haussler D, Hermjakob H, Hokamp K, Jang W, Johnson LS, Jones TA, Kasif S, Kaspryzk A, Kennedy S, Kent WJ, Kitts P, Koonin E V., Korf I, Kulp D, Lancet D, Lowe TM, McLysaght A, Mikkelsen T, Moran J V., Mulder N, Pollara VJ, Ponting CP, Schuler G, Schultz J, Slater G, Smit AFA, Stupka E, Szustakowki J, Thierry-Mieg D, Thierry-Mieg J, Wagner L, Wallis J, Wheeler R, Williams A, Wolf YI, Wolfe KH, Yang SP, Yeh RF, Collins F, Guyer MS, Peterson J, Felsenfeld A, Wetterstrand KA, Myers RM, Schmutz J, Dickson M, Grimwood J, Cox DR, Olson M V., Kaul R, Raymond Christopher, Shimizu N, Kawasaki K, Minoshima S, Evans GA, Athanasiou M, Schultz R, Patrinos A, Morgan MJ, de Jong P, Catanese JJ, Osoegawa K, Shizuya H, Choi S, Chen YJ. 2001. Erratum: Initial sequencing and analysis of the human genome: International Human Genome Sequencing Consortium (Nature (2001) 409 (860-921)). Nature 412:565–566. doi:10.1038/35087627

Li S, Wu Z, Tantray I, Li Y, Chen S, Dong J, Glynn S, Vogel H, Snyder M, Lu B. 2020. Quality-control mechanisms targeting translationally stalled and C-terminally extended poly(GR) associated with ALS/FTD. Proc Natl Acad Sci U S A 117. doi:10.1073/pnas.2005506117

Li Y, Geng J, Rimal S, Wang H, Liu X, Lu B, Li S. 2023. The mTORC2/AKT/VCP axis is associated with quality control of the stalled translation of poly(GR) dipeptide

repeats in C9-ALS/FTD. Journal of Biological Chemistry 299. doi:10.1016/j.jbc.2023.102995

Linsalata AE, He F, Malik AM, Glineburg MR, Green KM, Natla S, Flores BN, Krans A, Archbold HC, Fedak SJ, Barmada SJ, Todd PK. 2019. DDX 3X and specific initiation factors modulate FMR 1 repeat-associated non-AUG-initiated translation . EMBO Rep 1–18. doi:10.15252/embr.201847498

Liquori CL, Ricker K, Moseley ML, Jacobsen JF, Kress W, Naylor SL, Day JW, Ranum LPW. 2001. Myotonic dystrophy type 2 caused by a CCTG expansion in intron I of ZNF9. Science (1979) 293. doi:10.1126/science.1062125

Liu H, Lu Y-N, Paul T, Periz G, Banco MT, Ferré-D'Amaré AR, Rothstein JD, Hayes LR, Myong S, Wang J. 2021. A Helicase Unwinds Hexanucleotide Repeat RNA G-Quadruplexes and Facilitates Repeat-Associated Non-AUG Translation. J Am Chem Soc 143:7368–7379. doi:10.1021/jacs.1c00131

Loveland AB, Svidritskiy E, Susorov D, Lee S, Park A, Zvornicanin S, Demo G, Gao FB, Korostelev AA. 2022. Ribosome inhibition by C9ORF72-ALS/FTD-associated poly-PR and poly-GR proteins revealed by cryo-EM. Nat Commun 13. doi:10.1038/s41467-022-30418-0

Lu B. 2023. Translation stalling and ribosome collision leading to proteostasis failure: implications for neurodegenerative diseases. Neural Regen Res 18. doi:10.4103/1673-5374.340404

Lytvynenko I, Paternoga H, Thrun A, Balke A, Müller TA, Chiang CH, Nagler K, Tsaprailis G, Anders S, Bischofs I, Maupin-Furlow JA, Spahn CMT, Joazeiro

CAP. 2019. Alanine Tails Signal Proteolysis in Bacterial Ribosome-Associated Quality Control. Cell 178. doi:10.1016/j.cell.2019.05.002

Lyumkis D, Dos Passosb DO, Tahara EB, Webb K, Bennett EJ, Vinterbo S, Potter CS, Carragher B, Joazeiro CAP. 2014. Structural basis for translational surveillance by the large ribosomal subunit-associated protein quality control complex. Proc Natl Acad Sci U S A 111. doi:10.1073/pnas.1413882111

Majounie E, Renton AE, Mok K, Dopper EGP, Waite A, Rollinson S, Chiò A, Restagno G, Nicolaou N, Simon-Sanchez J, van Swieten JC, Abramzon Y, Johnson JO, Sendtner M, Pamphlett R, Orrell RW, Mead S, Sidle KC, Houlden H, Rohrer JD, Morrison KE, Pall H, Talbot K, Ansorge O, Hernandez DG, Arepalli S, Sabatelli M, Mora G, Corbo M, Giannini F, Calvo A, Englund E, Borghero G, Floris GL, Remes AM, Laaksovirta H, McCluskey L, Trojanowski JQ, Van Deerlin VM, Schellenberg GD, Nalls MA, Drory VE, Lu CS, Yeh TH, Ishiura H, Takahashi Y, Tsuji S, Le Ber I, Brice A, Drepper C, Williams N, Kirby J, Shaw P, Hardy J, Tienari PJ, Heutink P, Morris HR, Pickering-Brown S, Traynor BJ, Adamson G, Bayer AJ, Beck J, Callister JB, Blake DJ, Blumen SC, Collinge J, Dunckley T, Ealing J, East S, Elman L, Gerhard A, Guerreiro RJ, Gwinn K, Halliwell N, Hamdalla HH, Hewitt C, Ince P, Jablonka S, James C, Kent L, Knock JC, Lynch T, Mahoney C, Mann D, Neal J, Norris D, O'Dowd S, Richardson A, Rossor M, Rothstein J, Scholz SW, Snowden J, Stephan DA, Toulson G, Turner MR, Warren JD, Young K, Weng YH, Kuo HC, Lai SC, Huang CL, Camuzat A, Entraingues L, Guillot-Noël, Verpillat P, Clerget-Darpoux F, Corcia P, Couratier P, Didic M, Dubois B, Duyckaerts C, Guedj E, Golfier V, Habert MO, Hannequin D, Lacomblez L, Meininger V,

Salachas F, Levy R, Michel BF, Pasquier F, Puel M, Thomas-Anterion C, Sellal F, Vercelletto M, Moglia C, Cammarosano S, Canosa A, Gallo S, Brunetti M, Ossola I, Marinou K, Papetti L, Pisano F, Pinter GL, Conte A, Luigetti M, Zollino M, Lattante S, Marangi G, la Bella V, Spataro R, Colletti T, Battistini S, Ricci C, Caponnetto C, Mancardi G, Mandich P, Salvi F, Bartolomei I, Mandrioli J, Sola P, Lunetta C, Penco S, Monsurrò MR, Tedeschi G, Conforti FL, Gambardella A, Quattrone A, Volanti P, Cannas A, Piras V, Marrosu F, Marrosu MG, Murru MR, Pugliatti M, Parish LD, Sotgiu A, Solinas G, Ulgheri L, Ticca A, Simone I, Logroscino G. 2012. Frequency of the C9orf72 hexanucleotide repeat expansion in patients with amyotrophic lateral sclerosis and frontotemporal dementia: A cross-sectional study. Lancet Neurol 11. doi:10.1016/S1474-4422(12)70043-1

Malik I, Kelley CP, Wang ET, Todd PK. 2021a. Molecular mechanisms underlying nucleotide repeat expansion disorders. Nat Rev Mol Cell Biol 22:589–607. doi:10.1038/s41580-021-00382-6

Malik I, Tseng Y, Wright SE, Zheng K, Ramaiyer P, Green KM, Todd PK. 2021b. SRSF protein kinase 1 modulates RAN translation and suppresses CGG repeat toxicity. EMBO Mol Med 13:1–21. doi:10.15252/emmm.202114163

Martin PB, Kigoshi-Tansho Y, Sher RB, Ravenscroft G, Stauffer JE, Kumar R, Yonashiro R, Müller T, Griffith C, Allen W, Pehlivan D, Haral T, Zenker M, Howting D, Schanze D, Faqeih EA, Almontashiri NAM, Maroofian R, Houlden H, Mazaheri N, Galehdari H, Douglas G, Posey JE, Ryan M, Lupski JR, Laing NG, Joazeiro CAP, Cox GA. 2020. NEMF mutations that impair ribosome-associated quality

control are associated with neuromuscular disease. Nat Commun 11. doi:10.1038/s41467-020-18327-6

Matsuo Y, Ikeuchi K, Saeki Y, Iwasaki S, Schmidt C, Udagawa T, Sato F, Tsuchiya H, Becker T, Tanaka K, Ingolia NT, Beckmann R, Inada T. 2017. Ubiquitination of stalled ribosome triggers ribosome-associated quality control. Nat Commun 8. doi:10.1038/s41467-017-00188-1

Matsuo Y, Tesina P, Nakajima S, Mizuno M, Endo A, Buschauer R, Cheng J, Shounai O, Ikeuchi K, Saeki Y, Becker T, Beckmann R, Inada T. 2020. RQT complex dissociates ribosomes collided on endogenous RQC substrate SDD1. Nat Struct Mol Biol 27. doi:10.1038/s41594-020-0393-9

Matsuo Y, Uchihashi T, Inada T. 2023. Decoding of the ubiquitin code for clearance of colliding ribosomes by the RQT complex. Nat Commun 14. doi:10.1038/s41467-022-35608-4

Mizielinska S, Gronke S, Niccoli T, Ridler CE, Clayton EL, Devoy A, Moens T, Norona FE, Woollacott IOC, Pietrzyk J, Cleverley K, Nicoll AJ, Pickering-Brown S, Dols J, Cabecinha M, Hendrich O, Fratta P, Fisher EMC, Partridge L, Isaacs AM. 2014. C9orf72 repeat expansions cause neurodegeneration in Drosophila through arginine-rich proteins. Science (1979) 345:1192–1194. doi:10.1126/science.1256800

Mizuno M, Ebine S, Shounai O, Nakajima S, Tomomatsu S, Ikeuchi K, Matsuo Y, Inada T. 2021. The nascent polypeptide in the 60S subunit determines the Rqc2-dependency of ribosomal quality control. Nucleic Acids Res 49:2102–2113. doi:10.1093/nar/gkab005

Mori Kohji, Arzberger T, Grässer FA, Gijselinck I, May S, Rentzsch K, Weng S-M, Schludi MH, van der Zee J, Cruts M, Van Broeckhoven C, Kremmer E, Kretzschmar HA, Haass C, Edbauer D. 2013. Bidirectional transcripts of the expanded C9orf72 hexanucleotide repeat are translated into aggregating dipeptide repeat proteins. Acta Neuropathol 126:881–893. doi:10.1007/s00401-013-1189-3

Mori K., Weng S-M, Arzberger T, May S, Rentzsch K, Kremmer E, Schmid B, Kretzschmar HA, Cruts M, Van Broeckhoven C, Haass C, Edbauer D. 2013. The C9orf72 GGGGCC Repeat Is Translated into Aggregating Dipeptide-Repeat Proteins in FTLD/ALS. Science (1979) 339:1335–1338. doi:10.1126/science.1232927

Nelson DL, Orr HT, Warren ST. 2013. The unstable repeats-Three evolving faces of neurological disease. Neuron. doi:10.1016/j.neuron.2013.02.022

Orban TI, Izaurralde E. 2005. Decay of mRNAs targeted by RISC requires XRN1, the Ski complex, and the exosome. RNA 11. doi:10.1261/rna.7231505

Park J, Lee Jongbo, Kim JH, Lee Jongbin, Park H, Lim C. 2021. ZNF598 co-translationally titrates poly(GR) protein implicated in the pathogenesis of C9ORF72-associated ALS/FTD. Nucleic Acids Res 49. doi:10.1093/nar/gkab834

Pisarev A V., Skabkin MA, Pisareva VP, Skabkina O V., Rakotondrafara AM, Hentze MW, Hellen CUT, Pestova T V. 2010. The Role of ABCE1 in Eukaryotic Posttermination Ribosomal Recycling. Mol Cell 37. doi:10.1016/j.molcel.2009.12.034

Pisareva VP, Skabkin MA, Hellen CUT, Pestova T V., Pisarev A V. 2011. Dissociation by Pelota, Hbs1 and ABCE1 of mammalian vacant 80S ribosomes and stalled elongation complexes. EMBO Journal 30. doi:10.1038/emboj.2011.93

Radwan M, Ang CS, Ormsby AR, Cox D, Daly JC, Reid GE, Hatters DM. 2020. Arginine in C9ORF72 dipolypeptides mediates promiscuous proteome binding and multiple modes of toxicity. Molecular and Cellular Proteomics 19. doi:10.1074/mcp.RA119.001888

Rimal S, Li Y, Vartak R, Geng J, Tantray I, Li S, Huh S, Vogel H, Glabe C, Grinberg LT, Spina S, Seeley WW, Guo S, Lu B. 2021. Inefficient quality control of ribosome stalling during APP synthesis generates CAT-tailed species that precipitate hallmarks of Alzheimer's disease. Acta Neuropathol Commun 9. doi:10.1186/s40478-021-01268-6

Saito S, Hosoda N, Hoshino SI. 2013. The Hbs1-Dom34 protein complex functions in non-stop mRNA decay in mammalian cells. Journal of Biological Chemistry 288:17832–17843. doi:10.1074/jbc.M112.448977

Sareen D, O'Rourke JG, Meera P, Muhammad AKMG, Grant S, Simpkinson M, Bell S, Carmona S, Ornelas L, Sahabian A, Gendron T, Petrucelli L, Baughn M, Ravits J, Harms MB, Rigo F, Frank Bennett C, Otis TS, Svendsen CN, Baloh RH. 2013. Targeting RNA foci in iPSC-derived motor neurons from ALS patients with a C9ORF72 repeat expansion. Sci Transl Med 5. doi:10.1126/scitranslmed.3007529

Schaeffer C, Bardoni B, Mandel JL, Ehresmann B, Ehresmann C, Moine H. 2001. The fragile X mental retardation protein binds specifically to its mRNA via a purine quartet motif. EMBO Journal 20. doi:10.1093/emboj/20.17.4803

Schwab SR, Shugart JA, Horng T, Malarkannan S, Shastri N. 2004. Unanticipated antigens: Translation initiation at CUG with leucine. PLoS Biol 2. doi:10.1371/journal.pbio.0020366

Sellier C, Buijsen RAM, He F, Natla S, Jung L, Tropel P, Gaucherot A, Jacobs H, Meziane H, Vincent A, Champy MF, Sorg T, Pavlovic G, Wattenhofer-Donze M, Birling MC, Oulad-Abdelghani M, Eberling P, Ruffenach F, Joint M, Anheim M, Martinez-Cerdeno V, Tassone F, Willemsen R, Hukema RK, Viville S, Martinat C, Todd PK, Charlet-Berguerand N. 2017. Translation of Expanded CGG Repeats into FMRpolyG Is Pathogenic and May Contribute to Fragile X Tremor Ataxia Syndrome. Neuron. doi:10.1016/j.neuron.2016.12.016

Shao S, Brown A, Santhanam B, Hegde RS. 2015. Structure and assembly pathway of the ribosome quality control complex. Mol Cell 57. doi:10.1016/j.molcel.2014.12.015

Shao S, Hegde RS. 2014. Reconstitution of a Minimal Ribosome-Associated Ubiquitination Pathway with Purified Factors. Mol Cell 55. doi:10.1016/j.molcel.2014.07.006

Shao S, Von der Malsburg K, Hegde RS. 2013. Listerin-dependent nascent protein ubiquitination relies on ribosome subunit dissociation. Mol Cell 50. doi:10.1016/j.molcel.2013.04.015

Shen PS, Park J, Qin Y, Li X, Parsawar K, Larson MH, Cox J, Cheng Y, Lambowitz AM, Weissman JS, Brandman O, Frost A. 2015. Rqc2p and 60S ribosomal subunits mediate mRNA-independent elongation of nascent chains. Science (1979) 347. doi:10.1126/science.1259724

Shoemaker CJ, Eyler DE, Green R. 2010. Dom34:Hbs1 promotes subunit dissociation and peptidyl-tRNA drop-off to initiate no-go decay. Science (1979) 330:369–372. doi:10.1126/science.1192430

Shoemaker CJ, Green R. 2012. Translation drives mRNA quality control. Nat Struct Mol Biol 19:594–601. doi:10.1038/nsmb.2301

Sitron CS, Brandman O. n.d. CAT tails drive degradation of stalled polypeptides on and off the ribosome. doi:10.1038/s41594-019-0230-1

Sitron CS, Park JH, Brandman O. 2017. Asc1, Hel2, and Slh1 couple translation arrest to nascent chain degradation. RNA 23. doi:10.1261/rna.060897.117

Sonobe Y, Ghadge G, Masaki K, Sendoel A, Fuchs E, Roos RP. 2018. Translation of dipeptide repeat proteins from the C9ORF72 expanded repeat is associated with cellular stress. Neurobiol Dis. doi:10.1016/j.nbd.2018.05.009

Soragni E, Petrosyan L, Rinkoski TA, Wieben ED, Baratz KH, Fautsch MP, Gottesfeld JM. 2018. Repeat-associated non-ATG (RAN) translation in fuchs' endothelial corneal dystrophy. Invest Ophthalmol Vis Sci 59. doi:10.1167/iovs.17-23265

Su T, Izawa T, Thoms M, Yamashita Y, Cheng J, Berninghausen O, Hartl FU, Inada T, Neupert W, Beckmann R. 2019. Structure and function of Vms1 and Arb1 in RQC and mitochondrial proteome homeostasis. Nature 570:538–542. doi:10.1038/s41586-019-1307-z

Sundaramoorthy E, Leonard M, Mak R, Liao J, Fulzele A, Bennett EJ. 2017. ZNF598 and RACK1 Regulate Mammalian Ribosome-Associated Quality Control Function by Mediating Regulatory 40S Ribosomal Ubiquitylation. Mol Cell 65. doi:10.1016/j.molcel.2016.12.026

Tabet R, Schaeffer L, Freyermuth F, Jambeau M, Workman M, Lee CZ, Lin CC, Jiang J, Jansen-West K, Abou-Hamdan H, Désaubry L, Gendron T, Petrucelli L, Martin F, Lagier-Tourenne C. 2018. CUG initiation and frameshifting enable production of dipeptide repeat proteins from ALS/FTD C9ORF72 transcripts. Nat Commun 9:1–14. doi:10.1038/s41467-017-02643-5

Thrun A, Garzia A, Kigoshi-Tansho Y, Patil PR, Umbaugh CS, Dallinger T, Liu J, Kreger S, Patrizi A, Cox GA, Tuschl T, Joazeiro CAP. 2021. Convergence of mammalian RQC and C-end rule proteolytic pathways via alanine tailing. Mol Cell 81. doi:10.1016/j.molcel.2021.03.004

Todd PK, Oh SY, Krans A, He F, Sellier C, Frazer M, Renoux AJ, Chen K chun, Scaglione KM, Basrur V, Elenitoba-Johnson K, Vonsattel JP, Louis ED, Sutton MA, Taylor JP, Mills RE, Charlet-Berguerand N, Paulson HL. 2013. CGG repeat-associated translation mediates neurodegeneration in fragile X tremor ataxia syndrome. Neuron. doi:10.1016/j.neuron.2013.03.026

Tseng YJ, Sandwith SN, Green KM, Chambers AE, Krans A, Raimer HM, Sharlow ME, Reisinger MA, Richardson AE, Routh ED, Smaldino MA, Wang YH, Vaughn JP, Todd PK, Smaldino PJ. 2021. The RNA helicase DHX36–G4R1 modulates C9orf72 GGGGCC hexanucleotide repeat–associated translation. Journal of Biological Chemistry 297:100914. doi:10.1016/j.jbc.2021.100914

Udagawa T, Seki M, Okuyama T, Adachi S, Natsume T, Noguchi T, Matsuzawa A, Inada T. 2021. Failure to Degrade CAT-Tailed Proteins Disrupts Neuronal Morphogenesis and Cell Survival. Cell Rep 34:108599. doi:10.1016/j.celrep.2020.108599

van der Zee J, Gijselinck I, Dillen L, Van Langenhove T, Theuns J, Engelborghs S, Philtjens S, Vandenbulcke M, Sleegers K, Sieben A, Bäumer V, Maes G, Corsmit E, Borroni B, Padovani A, Archetti S, Perneczky R, Diehl-Schmid J, de Mendonça A, Miltenberger-Miltenyi G, Pereira S, Pimentel J, Nacmias B, Bagnoli S, Sorbi S, Graff C, Chiang HH, Westerlund M, Sanchez-Valle R, Llado A, Gelpi E, Santana I, Almeida MR, Santiago B, Frisoni G, Zanetti O, Bonvicini C, Synofzik M, Maetzler W, vom Hagen JM, Schöls L, Heneka MT, Jessen F, Matej R, Parobkova E, Kovacs GG, Ströbel T, Sarafov S, Tournev I, Jordanova A, Danek A, Arzberger T, Fabrizi GM, Testi S, Salmon E, Santens P, Martin JJ, Cras P, Vandenberghe R, De Deyn PP, Cruts M, Van Broeckhoven C, Ramirez A, Kurzwelly D, Sachtleben C, Mairer W, Firmo C, Antonell A, Molinuevo J, Forsell C, Lillius L, Kinhult Ståhlbom A, Thonberg H, Nennesmo I, Börjesson-Hanson A, Bessi V, Piaceri I, Helena Ribeiro M, Oliveira C, Massano J, Garret C, Pires P, Danel A, Ferrari S, Cavallaro T. 2013. A Pan-European Study of the C9orf72 Repeat Associated with FTLD: Geographic Prevalence, Genomic Instability, and Intermediate Repeats. Hum Mutat 34:363–373. doi:10.1002/humu.22244

Verkerk AJMH, Pieretti M, Sutcliffe JS, Fu YH, Kuhl DPA, Pizzuti A, Reiner O, Richards S, Victoria MF, Zhang F, Eussen BE, van Ommen GJB, Blonden LAJ, Riggins GJ, Chastain JL, Kunst CB, Galjaard H, Thomas Caskey C, Nelson DL,

Oostra BA, Warran ST. 1991. Identification of a gene (FMR-1) containing a CGG repeat coincident with a breakpoint cluster region exhibiting length variation in fragile X syndrome. Cell 65. doi:10.1016/0092-8674(91)90397-H

Verma R, Oania RS, Kolawa NJ, Deshaies RJ. 2013. Cdc48/p97 promotes degradation of aberrant nascent polypeptides bound to the ribosome. Elife 2013. doi:10.7554/eLife.00308

Verma R, Reichermeier KM, Burroughs AM, Oania RS, Reitsma JM, Aravind L, Deshaies RJ. 2018. Vms1 and ANKZF1 peptidyl-tRNA hydrolases release nascent chains from stalled ribosomes. Nature 557. doi:10.1038/s41586-018-0022-5

Viera Ortiz AP, Cajka G, Olatunji OA, Mikytuck B, Shalem O, Lee EB. 2022. Impaired ribosome-associated quality control of C9orf72 arginine-rich dipeptide-repeat proteins . Brain. doi:10.1093/brain/awac479

Wang Z, Ursu A, Childs-disney JL, Rice JE, Petrucelli L, Disney MD, Wang Z, Ursu A, Childs-disney JL, Guertler R, Yang W, Bernat V. 2019. The Hairpin Form of r (G 4 C 2) exp in c9ALS / FTD Is Repeat-Associated Non-ATG Translated and a Target for Bioactive Small Molecules Article The Hairpin Form of r (G 4 C 2) exp in c9ALS / FTD Is Repeat-Associated Non-ATG Translated and a Target for B. Cell Chem Biol 26:179-190.e12. doi:10.1016/j.chembiol.2018.10.018

Weskamp K, Tank EM, Miguez R, McBride JP, Gómez NB, White M, Lin Z, Gonzalez CM, Serio A, Sreedharan J, Barmada SJ. 2020. Shortened TDP43 isoforms upregulated by neuronal hyperactivity drive TDP43 pathology in ALS. Journal of Clinical Investigation 130. doi:10.1172/JCI130988

Wieland M, Hartig JS. 2007. RNA Quadruplex-Based Modulation of Gene Expression. Chem Biol 14. doi:10.1016/j.chembiol.2007.06.005

Wolin SL, Walter P. 1988. Ribosome pausing and stacking during translation of a eukaryotic mRNA. EMBO J 7. doi:10.1002/j.1460-2075.1988.tb03233.x

Wright SE, Rodriguez CM, Monroe J, Xing J, Krans A, Flores BN, Barsur V, Ivanova MI, Koutmou KS, Barmada SJ, Todd PK. 2022. CGG repeats trigger translational frameshifts that generate aggregation-prone chimeric proteins. Nucleic Acids Res 50. doi:10.1093/nar/gkac626

Wu Z, Tantray I, Lim J, Chen S, Li Y, Davis Z, Sitron C, Dong J, Gispert S, Auburger G, Brandman O, Bi X, Snyder M, Lu B. 2019. MISTERMINATE Mechanistically Links Mitochondrial Dysfunction with Proteostasis Failure. Mol Cell 75. doi:10.1016/j.molcel.2019.06.031

Wu Z, Wang Y, Lim J, Liu B, Li Y, Vartak R, Stankiewicz T, Montgomery S, Lu B. 2018. Ubiquitination of ABCE1 by NOT4 in Response to Mitochondrial Damage Links Co-translational Quality Control to PINK1-Directed Mitophagy. Cell Metab 28. doi:10.1016/j.cmet.2018.05.007

Xinmei W, Wenzhi T, Thomas W, Karthik K, Shamamandri MS, Yingxiao S, Shaoyu L, A. SN, John M, B. PU, Piera P, K. IJ, Davide T. 2014. Antisense Proline-Arginine RAN dipeptides linked to C9ORF72- ALS/FTD form toxic nuclear aggregates that initiate in vitro and in vivo neuronal death. Neuron 84.

Yamada SB, Gendron TF, Niccoli T, Genuth NR, Grosely R, Shi Y, Glaria I, Kramer NJ, Nakayama L, Fang S, Dinger TJI, Thoeng A, Rocha G, Barna M, Puglisi JD, Partridge L, Ichida JK, Isaacs AM, Petrucelli L, Gitler AD. 2019. RPS25 is required

for efficient RAN translation of C9orf72 and other neurodegenerative disease-associated nucleotide repeats. Nat Neurosci. doi:10.1038/s41593-019-0455-7

Yip MCJ, Keszei AFA, Feng Q, Chu V, McKenna MJ, Shao S. 2019. Mechanism for recycling tRNAs on stalled ribosomes. Nat Struct Mol Biol 26. doi:10.1038/s41594-019-0211-4

Yonashiro R, Tahara EB, Bengtson MH, Khokhrina M, Lorenz H, Chen KC, Kigoshi-Tansho Y, Savas JN, Yates JR, Kay SA, Craig EA, Mogk A, Bukau B, Joazeiro CAP. 2016. The Rqc2/Tae2 subunit of the ribosome-associated quality control (RQC) complex marks ribosome-stalled nascent polypeptide chains for aggregation. Elife 5. doi:10.7554/eLife.11794

Zamiri B, Reddy K, Macgregor RB, Pearson CE. 2014. TMPyP4 porphyrin distorts RNA G-quadruplex structures of the disease-associated r(GGGGCC)n repeat of the C9orf72 gene and blocks interaction of RNAbinding proteins. Journal of Biological Chemistry. doi:10.1074/jbc.C113.502336

Zhang Y, Glineburg MR, Basrur V, Conlon K, Wright SE, Krans A, Hall DA, Todd PK. 2022. Mechanistic convergence across initiation sites for RAN translation in fragile X associated tremor ataxia syndrome. Hum Mol Genet 31:2317–2332. doi:10.1093/hmg/ddab353

Zu T, Cleary JD, Liu Y, Bañez-Coronel M, Bubenik JL, Ayhan F, Ashizawa T, Xia G, Clark HB, Yachnis AT, Swanson MS, Ranum LPW. 2017. RAN Translation Regulated by Muscleblind Proteins in Myotonic Dystrophy Type 2. Neuron 95. doi:10.1016/j.neuron.2017.08.039

Zu T, Gibbens B, Doty NS, Gomes-Pereira M, Huguet A, Stone MD, Margolis J, Peterson M, Markowski TW, Ingram MAC, Nan Z, Forster C, Low WC, Schoser B, Somia N V., Clark HB, Schmechel S, Bitterman PB, Gourdon G, Swanson MS, Moseley M, Ranum LPW. 2011. Non-ATG-initiated translation directed by microsatellite expansions. Proceedings of the National Academy of Sciences 108:260–265. doi:10.1073/pnas.1013343108

Zu T, Liu Y, Banez-Coronel M, Reid T, Pletnikova O, Lewis J, Miller TM, Harms MB, Falchook AE, Subramony SH, Ostrow LW, Rothstein JD, Troncoso JC, Ranum LPW. 2013. RAN proteins and RNA foci from antisense transcripts in C9ORF72 ALS and frontotemporal dementia. Proceedings of the National Academy of Sciences 110:E4968–E4977. doi:10.1073/pnas.1315438110

Zu T, Pattamatta A, Ranum LPW. 2018. Repeat-associated non-ATG translation in neurological diseases. Cold Spring Harb Perspect Biol 10. doi:10.1101/cshperspect.a033019

Zurita Rendón O, Fredrickson EK, Howard CJ, Van Vranken J, Fogarty S, Tolley ND, Kalia R, Osuna BA, Shen PS, Hill CP, Frost A, Rutter J. 2018. Vms1p is a release factor for the ribosome-associated quality control complex. Nat Commun 9. doi:10.1038/s41467-018-04564-3

Chapter 4 : A High-Throughput Genome-Wide siRNA Screen Identifies Modifiers of C9ORF72- and FMR1-Associated RAN Translation

4.1. Abstract

A GGGGCC (G4C2) hexanucleotide repeat expansion in the first intron of *C9orf72* is the most common genetic cause of amyotrophic lateral sclerosis and frontotemporal dementia (ALS/FTD). One of the mechanisms by which G4C2 repeat transcripts elicit toxicity is by generating toxic dipeptide repeat (DPR) proteins without an AUG start codon upstream of the repeat region. This non-canonical translation event is called repeat-associated non-AUG (RAN) translation, generating toxic peptides as RAN products. RAN translation also is also related to at least 10 other nucleotide repeat expansion-associated neurodegenerative disorders. However, the exact mechanism of RAN translation remains unclear. To elucidate the mechanism of RAN translation, we conducted a genome-wide siRNA screen to evaluate specific modulators of this process. We utilized luciferase-based reporters that express poly-Glycine-Alanine (GA) from the +0 reading frame in (G4C2)70 repeats of C9orf72 (C9RAN) for the initial screen. Later, we performed a validation screen together with poly-Glycine (polyG) from the +1 reading frame of (CGG)100 repeats which CGG repeat expansion from the FMR1 5' UTR is another RAN-associated neurodegenerative disease (FMR1RAN). We analyzed top candidate hits with gene ontology and KEGG pathway to identify potential targets for further studies. From

the analysis, we identified a group of 20S core proteasome subunits showing depletion of their function decrease the expression of RAN products. Meanwhile, we also identified genes from the hypusination pathway as potential enzymatic targets, with hypusination loss-of-function increasing RAN translation. Identifying regulatory nodes of RAN translation from C9RAN and FMR1RAN can improve our understanding of the underlying mechanism of RAN translation and discover potential therapeutic targets for RAN translation-related diseases. Nevertheless, additional work will be required to further validate and prioritize RAN translation modifiers.

4.2. Introduction

Amyotrophic lateral sclerosis (ALS) is a fatal motor neuron degeneration disease that causes by neuronal death. ALS is characterized by motor dysfunction, respiratory failure, and progressive paralysis that could lead to death within two to three years after disease onset (Luukkainen et al., 2015; Onyike and Diehl-Schmid, 2013). Frontotemporal dementia (FTD) is caused by progressive neuronal loss in the brain's frontal or temporal lobes. FTD presents heterogeneously and is divided into three clinical syndromes: behavioral variant, semantic dementia, and progressive non-fluent aphasia (Neary et al., 1998). The *C9orf72* G4C2 repeat expansions are frequently associated with both ALS and FTD (DeJesus-Hernandez et al., 2011; Gijselinck et al., 2012; Renton et al., 2011). Despite ALS and FTD showing distinct symptoms and some pathology hallmarks, they also constitute two ends of a single disease spectrum. They share disease-causing mutations, histopathological hallmarks, and some clinical features (Lomen-Hoerth et al., 2003, 2002; Neumann et al., 2006; Ringholz et al., 2005).

Extensive studies are focusing on a shared mutation of ALS/FTD, which is the G4C2 hexanucleotide repeat expansion in *C9orf72* that was identified in 2011 (DeJesus-Hernandez et al., 2011; Majounie et al., 2012; Renton et al., 2011). This G4C2 hexanucleotide repeat expansion is the most common genetic cause of ALS/FTD (DeJesus-Hernandez et al., 2011; Renton et al., 2011). The G4C2 repeat RNA element is one of the mechanisms that cause toxicity by showing an accumulation of peptides in patients' brain tissue (Zu et al., 2013). However, there is no AUG start codon upstream of the repeat locus. Protein production is through a non-canonical translation process called repeat-associated non-AUG (RAN) translation (Zu et al., 2011). Nucleotide repeat expansion causes more than 50 human neuronal disorders, while RAN translation is involved in at least 10 of the diseases (Fujino et al., 2023; Malik et al., 2021; Rodriguez and Todd, 2019). There is currently no effective treatment for neurodegenerative diseases. However, the mechanism of RAN translation is still unclear. Elucidating the mechanism of RAN translation can advance our understanding of this novel process and provide insight into potential therapeutic targets for RAN translation-related diseases.

To address this, we design a high-throughput reporter-based whole genome siRNA screen in HEK293 cells to identify factors and pathways that modulate RAN translation. Previous studies of RAN modifiers include hypothesis-driven approaches (see Chapter 1), targeted candidate-based screens (see Chapter 2), and unbiased genome-wide screens. An unbiased genome-wide screen could potentially comprehensively interrogates the mechanism of RAN translation. In this screen, we utilized a luciferase-based reporter system expressing poly-Glycine-Alanine (GA) from the +0 reading frame of the G4C2 repeats (C9 RAN). Since a CGG repeat expansion

from the 5'UTR of FMR1 also generates toxic peptides by RAN translation (FMR1 RAN), we include FMR1 RAN in a subset of the initial screen and validation screens. We expressed poly-Glycine (polyG) from the +1 reading frame of CGG repeats with a PEST tag, a signal peptide that triggers protein degradation. The PEST tag leads to a slightly lower plain luciferase signal to create a greater range to quantify the increase of luciferase signal with gene knockdown and eliminate the degradation rate given that the initial polyG luciferase signal is around 5 times higher than the GA luciferase signal.

We screened a total of 16,851 genes for the primary screen and 2,175 genes for the validation screen. We performed gene ontology and KEGG pathway with the top candidates showing either an increase or decrease of RAN products. We identified a group of 20S proteasome subunits showing knockdown of them decrease RAN products from the C9RAN product with later in-house validation in FMR1RAN given that there is a PEST tag on FMR1 reporter from the screen. On the other hand, we identified a pathway, hypusination, showing knockdown of DOHH from the pathway increases both C9 and FMR1 RAN products.

The ubiquitin-proteasome system (UPS) degrades misfolded, damaged, and unassembled proteins as a mechanism of protein quality control (Bence et al., 2001; Ciechanover et al., 2000). The pathogenesis of neurodegenerative diseases is linked to UPS dysfunction, which leads to aberrant protein aggregation in the cell (Petrucelli and Dawson, 2004). Previous studies have demonstrated that C9RAN products can interact and regulate proteasome function (Guo et al., 2018; May et al., 2014; Oh et al., 2015; Yamakawa et al., 2015; Zhang et al., 2014; Zhao et al., 2018). Previous studies also demonstrated connections between RNA polymerase II (RNA pol II) and the UPS during

translation, including a physical interaction of RNA pol II and 26S proteasome and an eIF3 interactome coupling with proteasome translatome model (Aravind and Ponting, 1998; Baugh and Pilipenko, 2004; Gillette et al., 2004; Sha et al., 2009). However, in our siRNA screen, the depletion of proteasome subunits decreased RAN products. This paradoxical result implies that the proteasome can function in opposition to its typical role in degrading RAN products.

Hypusination is a post-translational modification pathway unique for eIF5A (Park et al., 2022; Schmidt et al., 2015; Wątor et al., 2023). eIF5A is initially identified as a translation initiation factor but also demonstrates an important role as a translation elongation factor. eIF5A is highly abundant and essential in cells. Hypusination is a polyamine biosynthetic pathway that functionally activates eIF5A. The first step of hypusination is a deoxyhypusine synthase (DHPS) that cleaves the 4-aminobutyl moiety of spermidine. It then transfers to the ε-amino group of a specific lysine residue of the eIF5A precursor protein to form an intermediate, deoxyhypusined-eIF5A [Nε-(4-aminobutyl)lysine]. Finally, deoxyhypusine hydroxylase (DOHH) forms hypusine by subsequently hydroxylating the eIF5A precursor into mature eIF5A (Landau et al., 2010; Miller-Fleming et al., 2015; Puleston et al., 2019; Schnier et al., 1991; Tiburcio et al., 2014). Identifying DOHH as a candidate hit from the hypusination pathway showing depleted the function of DOHH increase RAN products implies that eIF5A could play a critical role in RAN translation that differs from regular AUG-driven translation.

Identifying RAN modifiers with a whole genome screen from two different RAN-associated repeat sequences can further understand the RAN mechanisms' common factors and pathways and generate therapeutic strategies for C9ALS/FTD and other RAN

translation-associated neurodegenerative disorders.

4.3. Materials and Methods

4.3.1. Plasmids

pcDNA3.1(+) C9orf72-(GGGCC)70-NLuc-3xFLAG (GA frame) and pGL4.13 (AUG-FireFly, FF) are published plasmids from Green et al. (Green et al., 2017). pcDNA3.1(+) AUG-NLuc-3xFLAG-PEST was generated from pcDNA3.1(+) AUG-NLuc-3xFLAG using Q5 Site-Directed Mutagenesis (New England BioLabs) and the primers detailed in **Table.** pcDNA3.1(+) *FMR1*-+1$(CGG)_{100}$-NLuc-3xFLAG-PEST was generated from pcDNA3.1(+) *FMR1*-+1$(CGG)_{100}$-NLuc-3xFLAG which is published from Kearse et al (Kearse et al., 2016). using the same method as described above (Kearse et al., 2016). All plasmids used throughout the screen were purified from *E. coli* cultures using the Maxiprep Plasmid DNA Purification Kit (Qiagen).

4.3.2. C9RAN and FMR1 RAN High-Throughput Screens

HEK293 cells (ATCC, CRL-1573) were maintained and passaged at 37°C, 5% CO_2 in DMEM supplemented with 9% (vol/vol) FBS. The use of Human siGENOME SMART*pool* siRNA Libraries (Dharmacon) are from the Center for Chemical Genomics at the University of Michigan, Ann Arbor. We first reconstituted siRNAs in 1x siRNA Buffer (Dharmacon) in 384-well stock plates (Thermo Fisher Scientific, AB-0781), sealed the plate, and stored under RNase-free conditions at -20°C. The day before siRNA transfection, we moved the siGENOME siRNAs library plates to 4°C and allowed to thaw at least 24 hours. Before diluting siRNA to desire working concentration, we mixed and spun down each library plate after thawing overnight. siRNA from each well were transferred to white 384-well assay plates (Greiner Bio-One, cat. # 781080) in triplicate.

Next, we use a Biomek FXP (Beckman-Coulter) automated liquid handler to transfer siRNAs to white 384-well assay plates (Greiner Bio-One, cat. # 781080) in triplicate. We diluted to 13.17 nM of siRNA in OptiMEM Reduced Serum Medium (Thermo Fisher Scientific) containing 450 nL/well of Lipofectamine RNAiMAX Transfection Reagent (Thermo Fisher Scientific; final volume of 10.4 µL/well), centrifuged at 200xg for 1 min, and incubated at room temperature for 30 minutes. siNTC, siNLuc, and siPLK1 were added to each assay plate and each plate is handled identically. We applied a MultiDrop Dispenser (Thermo Fisher Scientific) to reverse transfect 6,000 of HEK293 in 20 µL into each well with a final concentration of concentrations of 9% FBS, 100 U/mL penicillin, 100 µg/mL streptomycin (Thermo Fisher Scientific), and 39.5 nM siRNA. 48 hours post-transfection of siRNA, we transfected 15 ng/well firefly luciferase plasmid (pGL4.13) and 15 ng/well either pcDNA3.1(+)-*C9ORF72*-GA_{70}-NLuc-3xFLAG plasmid or pcDNA3.1(+)-*FMR1*-+1 CGG_{100}-NLuc-3xFLAG-PEST plasmid using Viafect (Promega) according to manufacturer's instructions.

24 hour post-transfection of luciferase reporter, we aspirated excess media using a 405 Select Microplate Washer (BioTek) and leave 10 µl media/well. The Nano-Glo Dual Luciferase Reporter Assay System (Promega) and Envision 2104 Multilabel Reader (Perkin-Elmer) were used per manufacturer's instructions to quantify expression of GA_{70}-NLuc-3xFLAG (or +1CGG_{100}-NLuc-3xFLAG-PEST) and AUG-FF reporters independently. We read 6 plates at a time to ensure we measure all luciferase signals before they started to decay.

4.3.3. Original Data Analysis of Primary Screen and Validation Screen

The original data analysis applied calculation function from Excel (Microsoft 365).

We normalized NLuc and FF signal of each gene to the mean of NLuc and FF signal of siNTC control. We then repeat the same steps for every triplicate (64 triplicates with a total of 192 plates, from primary screen and 8 triplicates with a total of 24 plates from validation screen). Later, we average the signal of NLuc and FF of each gene knockdown from triplicate experiments. We also calculated the average and standard deviation of siNTC from both NLuc and FF signals. We determined primary hits for a secondary validation screen by building an algorithm to filter candidate hits from the screen. The rule is that we first excluded genes from further analysis if the gene knockdown resulted in reduced cell viability when comparing the signal with FF of siPLK, i.e., genes with FF signal < $\mu_{PLK1}+\sigma_{PLK1}$. Second, we counted as primary hits that any genes which met the following criteria. Genes were included as suppressors of *C9ORF72* RAN translation if:

1) knockdown reduced NLuc/FF values to less than the mean NLuc/FF of siNTC-treated cells minus 3 standard deviations ($NLuc/FF_{siX} \leq \mu_{siNTC}-3\sigma_{siNTC}$) in at least 2 of 3 replicates;

2) knockdown reduced the mean NLuc value to below 50% of the mean NLuc value of siNTC-transfected cells ($NLuc_{siX}/NLuc_{siNTC} \leq 0.50$);

3) knockdown *did not* reduce the mean FF value to below 75% of the mean FF value of siNT-transfected cells ($FF_{siX}/FF_{siNTC} \geq 0.75$).

In contrast, genes were included as enhancers of *C9ORF72* RAN translation if:

1) $NLuc/FF_{siX} \geq \mu_{siNTC}+3\sigma_{siNTC}$ in at least 2 of 3 replicates;

2) $NLuc_{siX}/NLuc_{siNTC} \geq 2.0$;

3) $FF_{siX}/FF_{siNTC} \leq 1.25$.

Data analysis for validation screen is less stringent:

NLuc/FF-suppressing siRNAs were included if $NLuc_{siX}/NL_{siNTC} \leq 0.75$, and NLuc/FF-enhancing siRNAs were included if $NLuc_{siX}/NLuc_{siNT} \geq 1.5$. All other criteria remained identical.

4.3.4. Reperformed Data Analysis of Primary Screen and Validation Screen

We acknowledge that with the previous analysis, we are not accounting the variability of each gene knockdown from plate to plate, we did not look at the significant of each decrease or increase of the NLuc or FF signal. We did not account batch to batch variant of the experiments since we simply normalized all NLuc and FF signals of siNTC to compare with. Therefore, with better computational skill, we reanalyzed the screen data, both primary and secondary validation screen, with Python 3.7.0 applying pandas, numpy, and scipy.

We first clean up each plate by calculating the mean of NLuc and FF from siNTC in each single plate. We then normalized each gene knockdown's NLuc and FF signals to their siNTC's NLuc and FF within the same plate. We then calculate the Z-score of each NLuc and FF value of each gene from each plate and transform the Z-score to P-value. Next, we account the variability of each triplicate. We applied Fisher's method to combine three P-value from each gene from three different plate. We then calculated the adjusted *P*-value (*P*-adj) by false discovery rate (FDR) method. This allows us to declare the statistically significant adjusting multiple comparison. We then graph a volcano plot to filter top candidate hits as both RAN enhancer and inhibitor. To do this, we calculated -log10 (P-adj) and the average of fold change (FC) then transform to log2(FC). We then took top hits for gene ontology and KEGG pathway analysis by g:profiler.

4.3.5. C9RAN and FMR1 RAN Low-throughput Validation

All cell plating, siRNA transfections, DMSO vehicle versus drug treatment, plasmid transfections, and luminescence assays in low-throughput format from 96 or 24-well plates were performed as previously described (Chapter 2 and 3).

4.3.6. Immunoblotting

Immunoblotting was performed as described previously (Chapter 2 and 3). All antibodies used for blotting were list in **Table**

4.3.7. qRT-PCR Experiments

All qRT-PCR experiments were performed as described previously (Chapter 2 and 3).

4.4. Results

4.4.1. Design and Results of C9RAN Genome-wide High-throughput siRNA Screen

We plated HEK293 cells and transfected them with a genome-wide library of siRNAs (the human siGENOME SMARTpool library, Dharmacon) on the first day of the experiment. For each plate, other than siRNA from the genome library, we have 6-10 wells of non-targeting siRNAs (siNCT; Dharmacon) as negative control from both side columns of the plate. We also included 6-10 wells of siRNA targeting the ORF of NLuc (siNLuc) served as positive control from both side columns of the plate. In addition, we added an siRNA against *PLK1* (siPLK1) that causes mitotic arrest as a positive biological control for loss of cell viability. At 48h hours after siRNA transfection, we co-transfected two plasmids:

1. A 3xFLAG-tagged nano-luciferase reporter (NLuc-3xFLAG) downstream of the

human *C9ORF72* with the first intronic region harboring 70 repeats of the G4C2 sequences from the GA reading frame (GA_{70}-NLuc-3xFLAG). In this reporter the AUG of NLuc is mutated to GGG, so that NLuc or FLAG signal represents RAN translation of the GA C9RAN product.

2. An AUG-initiated FF luciferase reporter used for normalization and to assess for nonselective effects on general protein translation or cell viability.

24 hours after plasmids transfection, we measure the luminescence of NLuc and FF. We used GA frame among other available C9 DPR proteins for the screen because the GA expresses at the highest signal, which provides a wider dynamic range. Moreover, the GA RAN product is the most abundant DPR protein in C9ALS/FTD patient tissues. Performing dual luminescence assays by co-transfecting two independent luciferase plasmids provide an approach to measure the different effect of a gene knockdown on both RAN translation (NLuc-3xFLAG) and AUG-driven translation (AUG-FF) **(Figure 4.1.)**.

Our primary screening statistic was the C9RAN NLuc signal normalized to the AUG-FF signal to identify hits. For any modifiers of C9 RAN, we checked additional values from negative, positive, and biological controls. For the entire primary screen of C9RAN, from the NLuc signal, comparing siNTC to siNLuc, there is a dramtic decrease of siNLuc, indicating that the transfection process of siRNA and plasmid worked. From the FF signal, comparing siNTC to siPLK, there is around 40% signal remaining from surviving cells. We performed the same controls check with the validation screen **(Figure 4.2. B-E)**.

For the primary screen of GA C9RAN, we ran 24 plates from the druggable library with

5,892 genes and 40 plates from the human genome library with 10,959 genes. These together add up to a total of 16,851 genes. Since we did triplicates (n=3) of each library plate, we screened a total of 192 plates. The average Z-score of the entire C9RAN primary screen is 0.663 by calculating the NLuc/FF values from siNTC and siNLuc control cells **(Figure 4.2. F)**.

With the original algorithm (describe in the method and **Figure 4.4**), we made an 8 plate validation library with 2,175 genes selected as potential candidate hits. The C9RAN validation screened a total of 24 plates (n=3) with an average Z-score of 0.606 with the same calculation method as the primary screen. From the validation screen, we confirmed 760 (34.9%) genes for which selective knockdown selectively decreased C9RAN while confirming 121 genes (5.56%) for which selective knockdown selectively increased C9RAN **(Figure 4.2. A, right panel, F)**.

4.4.2. Design and Results of FMR1RAN Subset siRNA Screen

In parallel, we conducted a series of screens to identify specific modifiers of FMR1RAN translation. We replaced the GA_{70}-NLuc-3xFLAG reporter of the C9RAN screens with +1$(CGG)_{100}$-NLuc-3xFLAG with the CGG repeats from the 5'UTR of the FMR1 gene. Translation of this construct yields the poly-glycine (polyG) RAN product FMRpolyG.

We used the polyG frame among other available FMR1RAN products for the screen because the polyG expresses the highest signal. Moreover, the FMRpolyG product is the most abundant FMR1RAN protein in FXTAS patient tissue. From the first batch of the experiment, we saw extremely few hits showing an increase of FMR1RAN. We realized that the NLuc signal from FMR1RAN is 3-5 times higher than C9RAN.

Because of concerns that this was limiting our dynamic range, we added a PEST tag downstream of the 3xFLAG to allow for more rapid turnover of FMR1RAN protein.

In the primary FMR1 screen, we screened only the Drug Target and Druggable Genome subsets of the siGENOME siRNA library (Dharmacon). This library identifies targets of pharmacologic agents and kinases, phosphatases, proteases, ion channels, and others potentially amenable to pharmacological inhibition. For the validation screen of FMR1RAN we used the same validation screen library that we used for C9RAN. FMR1 screens followed the same high-throughput format, hit-detection algorithm, and validation/counter-screen design described above for C9orf72 screens. **(Figure 4.3. A).**

We checked luciferase signals from each control as we did for the C9RAN screen. Comparing the NLuc signal of siNLuc to siNTC, the transfection process is efficient by showing decrease of NLuc signal from siNLuc condition. Comparing the FF signal of siNTC and siPLK, there is around 40-50% FF signal from the survived cells. **(Figure 4.3. B-E)**.

We tested 5,892 siRNAs from 24 plates as the primary screen of the druggable library, and we tested 2,175 siRNA together aside with C9RAN as the validation screen. From the primary druggable library screen, the average Z-score from a total of 72 plates (n=3) was 0.630. The average Z-score from the validation screen among 24 plates (n=3) was 0.550. From the validation screen, we identified 201 (9.24%) genes whose knockdown selectively decreased FMR1RAN while knockdown of 275 (12.6%) genes selectively increased FMR1RAN **(Figure 4.3. F)**.

4.4.3. Design and Results of AUG-driven Counter Screen

To make sure that the selective modifiers we identified were not different solely

due to selective effects on intrinsic NLuc versus FFLuc activity, we conducted an AUG-initiated NLuc-3xFLAG reporter counter-screen with a short, unstructured 5' UTR (AUG-NLuc-3xFLAG) representing general translation. In the AUG counter screen, we transfected cells with AUG-NLuc-3xFLAG and AUG-FF plasmids and siRNAs against all primary hits. The entire screening setting is the same as the C9RAN and FMR1RAN validation screens. Despite filtering our primary screen data using AUG-FF, numerous modifiers of general gene expression had escaped elimination in the C9RAN and FMR1RAN screens.

C9RAN suppressors that also suppressed AUG-NLuc-3xFLAG ($NLuc_{siX}/NLuc_{siNTC} \leq 0.80$) and C9RAN enhancers that also enhanced AUG-NLuc-3xFLAG ($NLuc_{siX}/NLuc_{siNTC} \geq 1.2$) were eliminated, leaving 739 suppressors and 14 enhancers, representing 4.1% and 0.08% of the genome, respectively. And for FMR1RAN, 100 (1.28% of the siRNA library) suppressors and 0 enhancers remained when we filtered the hits with the results from the AUG counter screen.

In reviewing the outcomes of the C9RAN validation and AUG counter screens, we noted that the frequency of validated C9RAN modifiers that also validated for FMR1RAN would have been higher had non-specific modulators not been eliminated from the datasets by the AUG counter screen. The most potent suppressors of both C9RAN and FMR1RAN reporters also suppressed AUG-NLuc-3xFLAG, resulting in their elimination, and the correlation between relative GA_{70}-NLuc-3xFLAG expression and relative AUG-NLuc-3xFLAG expression among all C9RAN-validated siRNAs, including those the counter screen would eliminate, was significant. Our screen design nevertheless permitted the identification of siRNAs that modified both C9ORF72 and FMR1 reporters

without affecting AUG-NL-3xF. This perspective supports our decision to construct and conduct these screens as we did.

4.4.4. Gene Ontology and Pathway Analysis

We next performed gene ontology and KEGG pathway analysis with lists of genes using two different data-sorting algorithms. With the previous algorithm **(Figure 4.4)**, we identify proteasome subunits as a strong C9RAN modifier of the screen. Depletion of proteasome function decreases the expression of the C9RAN product. However, because of the PEST tag on the FMR1RAN reporter, we cannot identify whether the knockdown of these proteasome subunits also suppresses the FMR1RAN product. For common suppressor genes that are shared between C9RAN and FMR1RAN, we do not find any significant group of genes from gene ontology analysis. Given that few RAN inhibitors were identified, we did not perform a gene ontology analysis. Therefore, we decided to update the data sorting algorithm to account for the variability between triplicate plates and account for statistical significance in the study **(Figure 4.5)**. We performed gene ontology and KEGG pathway analysis with updated data analysis by g:Profiler.

We assessed gene ontology and common pathways using g:profiler from all C9RAN suppressors showing both adjusted *P*-values (*P*-adj) <0.001 and fold-change (FC) greater than 2 **(Figure 4.6)**. From the results, we found nuclear division, proteasome **(Figure 4.7.B)**, and organelle fission as three of the top enriched groups of genes. When we narrow the list to include just the top 100 hits **(Figure 4.7.C)** from the suppressor genes, cytoplasmic vesicle membrane and small GTPase binding categories are apparent. With the same criteria described above, we looked at all enhancers and the top 100 hits **(Figure 4.8.A)** with g:Profiler. Catalytic activity **(Figure 4.8.B)** was the leading

enriched group of genes. From the narrowed top 100 hits **(Figure 4.8.C),** we found genes related to cerebral lipofuscin as the most enriched group of genes.

We next performed the same analysis with g:Profiler for the FMR1RAN screen. As no enriched pathways emerged from the top 100 hits, we performed gene ontology with all 201 candidates **(Figure 4.9)**. We found chemical carcinogenesis – DNA adduct as the top enriched gene group from FMR1RAN suppressors **(Figure 4.10)**. On the other hand, catalytic activity was among the top enhanced group of genes for FMR1RAN enhancers **(Figure 4.11.B)**. Interestingly, the proteasome is one of the top enriched hits from the KEGG pathway analysis **(Figure 4.11.C)**. This result is opposite from the C9RAN screen, potentially due to the presence of PEST tag in FMR1RAN. The proteasome is one of the pathways that mediate the degradation of the PEST-tagged protein. Therefore, depleting proteasome function leads to an increase of PEST-tagged FMR1RAN. However, we can also see this as a biological control showing the expected results of PEST-tagged protein.

Next, we look at hits that share between C9RAN and FMR1RAN from both suppressor and enhancers **(Figure 4.12-13.)**.

4.4.5. Proteasome Subunits as RAN Modifiers

Our C9RAN screen identified multiple subunits of the proteasome, where knockdown of proteasome subunits selectively suppressed the expression of *C9ORF72* RAN reporters. This included PSMD11, PSMD7, PSMC1, PSMC2, PSMA7, and PSMB5. We next validated the effect in a low-throughput format in GA repeats using a second and distinct set of siRNAs targeting PSMA7, PSMD7, PSMC1, and PSMC2 **(Figure 4.14.)**. With immunoblotting, we observed a selective decrease in GA RAN products when the

expression of PSMA7, PSMD7, PSMC1, or PSMC2 is depleted **(Figure 4.15.)**. Importantly, we observe mild changes in AUG-NLuc or AUG-FF with these manipulations. Next, we assessed whether pharmacological inhibition of the proteasome would have the same effect on generation of RAN translation products. We tested MG132, lactacystin (Lac.), and bortezomib (BTZ) using T7 synthesized G4C2 RNA in an RRL *in vitro* translation system. This approach excludes transcription events and focuses on how proteasome inhibitors affect C9RAN translation. When we treat RRL lysate with 30 uM of MG132, we see a general decrease in AUG and C9RAN products with a greater decrease in the GP frame (**Figure 4.16. A)**. A similar effect is shown in Lac. treated RRL (**Figure 4.16. B)**. However, when we treat RRL with BTZ, we do not see any effect on AUG and C9RAN translation (**Figure 4.16. C)**.

DOHH as a Selective RAN Translation Modifier

DOHH, deoxyhypusine hydroxylase, is one of the genes from the list of enhancer hits. It is a RAN enhancer for both C9RAN and FMR1RAN **(Figure 4.17.A)**. When we validated the effect in-house with immunoblotting and a second set of siRNA, we confirmed that the knockdown of DOHH increases the production of GA RAN product **(Figure 4.17.B)**. DOHH hydroxylates deoxyhypusine to form hypusine as the last step of post-translation modification of the initiation factor 5A (eIF5A) protein. This entire hypusination pathway starts with the polyamine synthesis pathway. The polyamine synthesis pathway generates spermidine, which joins inactive eIF5A to begin the hypusination pathway. Next, deoxyhypusine synthase (DHPS) catalyzes the precursor eIF5A by transferring the butylamine moiety of spermidine to its specific lysine residue.

DHSP helps form intermediate deoxyhypusinated eIF5A. DOHH then encoded a metalloenzyme that catalyzes the conversion of lysine to hypusin of eIF5A. This produces mature hypusinated eIF5A **(Figure 4.17C)**.

GC7 is a small molecule that inhibits the function of DHPS, while multiple small molecule inhibitors impede the function of DOHH, including Ciclopirox (CPX). Therefore, after validating the result of DOHH siRNA from the screen, we assessed whether we could recapitulate these effects with CPX. We first confirmed the efficiency of CPX in the cell on depleting DOHH expression and the level of hypusination. After treatment 5, 10, and 15 uM of CPX for 48 hours, we see a decrease in DOHH and hypusination levels **(Figure 4.18.A)**. We next treated cells with 10 uM of CPX, which has less toxicity and expressed either C9RAN in the GA frame or FMR1RAN in the polyG frame **(Figure 4.18.B-C)**. When we depleted the function of DOHH and hypusination, we saw an increase in RAN products from both GA and polyG without affecting AUG-driven translation.

4.5. Discussion

RAN translation selective modifiers have the potential to both advance our understanding of non-canonical translation initiation mechanisms and reveal novel therapeutic targets for nucleotide repeat expansion diseases. To this end, we performed a non-biased high-throughput siRNA screen of the whole human genome in C9RAN and FMR1RAN. This screen highlights a group of proteasome subunits as selective C9RAN suppressors, while DOHH, from the unique eIF5A hypusination pathway, is a C9RAN and FMR1RAN enhancer. Here, I will discuss potential directions to study proteasomal

function and hypusination in RAN translation and what we should do better for future screens of this novel disease mechanism.

The ubiquitin-proteasome system (UPS) degrades misfolded, damaged, and unassembled proteins as a mechanism of protein quality control (Bence et al., 2001; Ciechanover et al., 2000). The pathogenesis of neurodegenerative diseases has been linked to UPS dysfunction (Petrucelli and Dawson, 2004), which leads to aberrant protein aggregation in the cell. Previous studies have demonstrated that C9RAN DPRs can interact and regulate proteasome function (Guo et al., 2018; May et al., 2014; Yamakawa et al., 2015; Zhang et al., 2014; Zhao et al., 2018). In our screen, we identified and then validated a group of 6 proteasome subunits - *PSMD11, PSMD7, PSMC2, PSMC1, PSMA7*, and *PSMB5* -as C9RAN suppressers, where depletion of each proteasomal subunits leads to a selective decrease in RAN product accumulation. Meanwhile, a similar result has been shown by another group's C9RAN genome-wide CRISPR knockout screen, demonstrating that the knockdown of *PSMA6* decreases the accumulation of C9RAN DPRs (Cheng et al., 2018; Kong et al., 2022). The GO analysis of a mass spectrometry dataset from *C9orf72* ALS and sporadic ALS patient-derived iPSCs revealed significant enrichment of ubiquitin-mediated proteolysis pathways, which could explain a genetic compensation effect in disease (Tank et al., 2018). Kramer et al. performed genome-wide CRISPR knockout screens in K562 cells with synthetic PR20 and GR20 proteins which found 9 different proteasome subunits that suppress PR20 and GR20 cytotoxicity (Kramer et al., 2018). Thus, endogenously elevated proteasome levels in C9ALS patients could be physiologically relevant to disease pathogenesis. However, the mechanism by which proteasome impairment might selectively downregulate

accumulation of DPRs is unclear. Previous studies demonstrated interactions between the 26S proteasome and RNA polymerase II (RNA pol II), eukaryotic initiation factors, and eukaryotic elongation factors (Aravind and Ponting, 1998; Baugh and Pilipenko, 2004; Gillette et al., 2004; Sha et al., 2009). These findings suggested that the proteasome could play a role in regulating RNA toxicity. If the former is accurate, and the depletion of the proteasome affects the abundance of C9 repeat RNA, then we would anticipate that selective knockdown of these factors would lead to differences in the stability of repeat RNAs or impact specific RNA decay pathways that are part of the mRNA quality control cascade. Alternatively depletion of the proteasome might directly impact C9RAN translational efficiency through either altering RAN translational initiation and/or translation elongation through GC rich repeats. In contrast, results from Kramer et al. showing that proteasomal knockouts surprisingly exhibit decreased toxicity from C9 DPRs implies that the proteasome may play roles in toxicity elicited by RAN product itself. This screen used a very short DPR sequence (only 20 repeats) so whether these findings translate to the human disease context is unclear. It is also worth noting that translation of PR and GR DPRs - even in the absence of the repeat element – can trigger ribosomal stalling and collisions and activate the Ribosomal Quality control pathway which utilizes the proteosome for degradation of key products. Further studies will be needed to discern the mechanism by which loss of proteosomal subunits impacts translation and the disconnect between this and the expected roles of the UPS system in degradation of aggregated proteins.

Hypusination is a unique post-translational modification pathway that acts on only one protein: the eukaryotic initiation factor 5A (eIF5A). Hypusinated eIF5A is the mature

and functional form of eIF5A that is active in translation machinery. eIF5A was initially identified as a translation factor that assists the formation of the first peptide bond between Met-tRNA and puromycin (Kemper et al., 1976; Schreier et al., 1977). Later studies from yeast revealed a more general function of eIF5A in translation elongation (Henderson and Hershey, 2011; Saini et al., 2009; Schreier et al., 1977). During elongation, eIF5A binds to the ribosome's E site, stabilizing the peptidyl-tRNA on the P site. This prevents nucleophilic attack by the incoming amino acid on the A-site tRNA when forming the peptide bond (Gutierrez et al., 2013; Melnikov et al., 2016; Schmidt et al., 2015). Recently, studies also demonstrated a role for eIF5A in translation termination (Pelechano and Alepuz, 2017; Schuller et al., 2017). Therefore, eIF5A is globally active in translation with tasks at all key translation stages. In eukaryotic cells, eIF5A is essential and highly abundant (Kulak et al., 2014; von der Haar, 2008). Therefore, functional studies of eIF5A directly in RAN translation are challenging in cells. A complete CRISPR knockout of eIF5A is too toxic, while a partial knockdown with siRNA might not be enough. This makes the hypusination pathway a better approach to studying eIF5A effects indirectly. We validated the screen results with a second set of siRNAs to knockdown DOHH. When we depleted DOHH, there was a large and selective increase in the C9RAN product. We later treated HEK293 with CPX, a drug that inhibits DOHH. This drug recapitulate the effects of DOHH knockdown with siRNA in both C9RAN and FMR1RAN. Multiple diseases, disorders, and aging are related to deficiencies in eIF5A and the hypusination pathway (Barba-Aliaga and Alepuz, 2022; Faundes et al., 2021; Liang et al., 2021; Tauc et al., 2021). This includes effects of depleting hypusination function on aging in the fly brain and dysfunction of mitochondria while feeding flies with spermidine can

correct the degenerative phenotype (Liang et al., 2021). Heterozygous variants in EIF5A cause a novel craniofacial-neurodevelopmental disorder while treating with spermidine in yeast harboring those variants can rescue the survival phenotype (Faundes et al., 2021). Future studies with DOHH should include other factors in the polyamine pathway aside from the hypusination pathway and eIF5A, as the polyamine pathway is the pathway that generates spermidine and is a critical molecule to initiate the hypusination pathway.

Tesina et al. recently solved the cryo-EM structure of the ribosomal-associated quality control (RQC) complex, which is a complex involves NEMF and LTN1 that NEMF form to CAT-tail (C-terminal addition of alanine and threonine) and LTN1 target falsely made short nascent chain for proteasomal degradation (Joazeiro, 2019; Tesina et al., 2023). In this cryo-EM structure of the RQC complex, they surprisingly found that eIF5A attached to LTN1 at the RQC complex (Tesina et al., 2023). With the findings from Chapter 2 suggesting that defects in RQC elicited by knockdown of LTN1 or NEMF1 can increase RAN product accumulation, it is possible that incomplete hypusination of eIF5A might also lead increased production of RAN products through RQC impairment. However, more studies of eIF5A in the RQC pathway and CAT-tailing will help elucidate this cross-functional mechanism and how RAN translation is involved in this process. Other studies will required to further understand the role of eIF5A in RAN translation in terms of the specific stage of RAN translation where eIF5A is critically involved whether there might be a different and novel function of eIF5A in RAN translation.

After we completed our initial genome-wide screen from the 384-well format, we tried but failed many times to validate screen results in a 96-well low-throughput format in our lab. Being unable to validate so many results from the screen was problematic and

suggests that different approaches should be taken in any future screen. This includes choosing the proper method for gene silencing, designing the ideal RAN reporter system to express RAN products, and performing the screen in a manner that would better control for or eliminate batch effects.

siRNAs (short interfering RNAs) are a powerful tool that interrogates gene functions by blocking gene expression and analyzing its effect on phenotype, which this process is referred to as RNA interference (RNAi). Comparing siRNA and CRISPR, there are pros and cons for each of them. The main difference between siRNA and CRISPR is that siRNA lower gene expression by knocking down mRNA expression while CRISPR completely and permanently knocks out the expression of a gene at the DNA level. This is the main reason we chose to perform siRNA knockdown instead of CRISPR knockout- knocking out essential genes can be lethal, which we thought would be problematic for studying translation initiation processes given their centrality to life.

HEK293 is an useful mammalian cell line for transient transfection studies. It is relatively easy to transfect with high expression levels. Previous graduate students utilized 4 different RNA-seq datasets from HEK293 to find genes that barely or do not express in HEK293. We applied that list of genes from RNA-seq to filter the list of genes from the validation screen that could be false positive effects. Hence, if the gene is not expressed in HEK293 cells, then the knockdown of the gene should not affect RAN translation. This strategy eliminated 23% of genes from the C9RAN and 25% from the FMR1RAN screen. However, the RNA seq libraries may not capture low-abundant mRNAs whose further knockdown might still effect RAN translation in this context.

Given the surprisingly high number of candidates, we could have applied this strategy when designing the validation screen library. As it is, these data suggests that 23~25% of genes identified were false positive effects. This raises an issue with siRNA screens that the potential for off-target effects from siRNAs is much higher than CRISPR. Therefore, silencing unintended mRNA sequence targets may have resulted in misinformation about the cause of RAN expression modification in some contexts, significantly misleading what genes we should advance in our screen. Comparing the main cons of CRISPR, that complete knockout of the gene function versus siRNA has a high off-target effect, if I were conducting this screen again I would instead investigate the impact of knockout of genes. This could provide a more efficient method to focus on the natural effect of the gene and save time in validating off-target effects.

In this study, we co-transfected AUG-FF and RAN-NLuc constructs into cells after reverse transfection of the siRNAs. This approcha could potentially lead to errant results. The primary method we applied to filter the effect of genes was normalization of the signal of RAN-NLuc to AUG-FF. However, we found that the AUG-FF signal usually fluctuates for multiple reasons, including cell viability, global translation affected by the gene knockdown but not RAN translation, and competition between ribosomes when RAN translation is exceptionally high or low. Therefore, when the NLuc/FF is below one, it can be caused by a relatively high signal of FF instead of actual decrease in NLuc, while when NLuc/FF is above one, it can cause by a relatively low FF signal instead real increases of NLuc.

An additional limitation came from the use of transient transfection. By transfecting in two plasmids – one for NLuc and one for FFLuc – the screen was potentially impacted

by differences in transfection of the two plasmids and by transfection efficiency impacts associated with siRNA knockdown. Ideally one could use stable cell lines which carry reporters for RAN translation. Indeed, we have since established stable cell lines that carry RAN translation specific reporters, but these have issues related to maintenance of the repat size. Given that repat size is a potential effector on RAN translation efficiency, we initially avoided use of this tool for our studies Alternatively we could use plasmids harboring a bidirectional promotor to drive NLuc and FF from the same construct or use a separate control.

NLuc tags tend to stabilize the products to which they are attached. To try to increase the dynamic range for expression of our RAN constructs, we inserted a PEST tag on our FMR1RAN reporters. However, we did not account for the biological effects of this PEST tag. For example, while we found that knockdown of a group of proteasome subunits suppressed the expression of C9RAN, we saw the opposite impact on FMR1RAN in our screen, with knockdown of proteasome subunits increasing FMR1RAN. We now know that this is a false posiive, as we and others have now observed that knockdown of PSMB5, in particular, leads to a reduction in FMR1RAN and was actually found to be a suppressor of FXTAS development in patients with premutation sized repeats (Kong et al., 2022).

When we reanalyzed the data and generated volcano plots - especially in the validation screen, where there are fewer genes from the library - we see a feather-like pattern on the volcano plot. We hypothesize that this is due to differences in batch-to-batch transfection efficiency. We ran the validation screen in 4 batches of experiments. Each set of transfections is in a triplicate of 2 library plates, with 2 different RAN

constructs, so 12 plates in total, and this pattern of 4 lines of feathers aligns with clear batch effects as a driver of these differences. This batch effect has a number of consequences. We can partly account for the variability of triplicates by further grouping each batch of experiments closer to each other. This eventually led to the 4 lines of the volcano plots. As we see, the feather pattern affects the suppressor genes more than the enhancer genes, and we hypothesize this is because there is a greater dynamic range to increase the signal than to show a decrease of the signal since we tend to start with a lower expression level to minimize early degradation of the signal. I would proposed that if we conduct a future screen that we should do n=1 for all libraries simultaneously, then repeat it for n=2 and 3. This can help eliminate the batch effect induced by subtle differences in the plasmid preps, transection efficiency, or differences in the read quality from NLuc or FF assays.

In summary, while the genome-wise siRNA screen that we performed has limitations, it provides some meaningful and surprising insights into RAN translation. While depleting proteasomal subunits may not be a viable therapeutic target, this surprising finding coupled with previously published work suggests an undiscovered role of the proteosome in RAN translation that may reveal key insights in the future. While depleting DOHH increases RAN product accumulation and its elimination is not likely to be of therapeutic benefit, it remains unknown whether overexpression of DOHH or augmentation of polyamine signaling might suppress RAN translation and repeat associated phenotypes (*of note- in preliminary studies spermidine supplementation was not beneficial*). In addition, the role of eIF5A in RAN translation machinery is also unclear and worth further investigation. Future studies using these novel new targets will hopefully

identify factors of disease relevance that can be assessed in appropriate model systems, including *Drosophila and* patient-derived iPSCs or iNeurons.

4.6. Chapter-specific Acknowledgement

We thank everyone at the Center for Chemical Genomics at the University of Michigan, Ann Arbor for many hours of technical assistance and even more hours of thoughtful high-throughput design. We thank the Todd lab member for critical discussion and input to this project. We apologize to future generations for the tonnage of plastic consumed by this and other high-throughput screens.

4.7. Figures

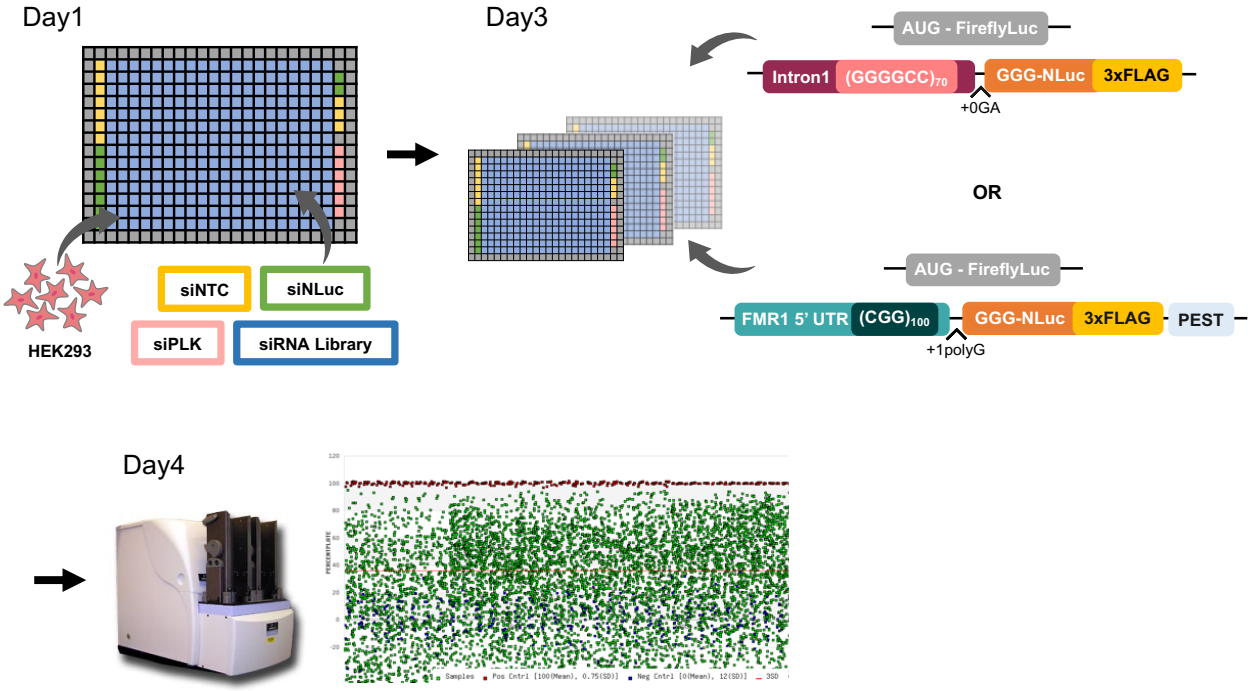

Figure 4-1. A screen for RAN translation modifiers

All experiments were performed in 384-well plates. siNTC, siNLuc, and siPLK are negative, positive, and biological controls, respectively, that are included in each plate at both sides of the column of the plate. The siRNA library is in the center of the plate. On Day 1, we reverse-transfected all siRNAs at 39.5 nM in HEK293 cells. After 48 hours, we co-transfected either AUG-FireflyLuc-3xFLAG with (G4C2)70-NLuc-3xFLAG with Nluc in the GA reading frame or AUG-FireflyLuc-3xFLAG with (CGG)100-NLuc-3xFLAG-PEST with NLuc in the polyG reading frame. 24 hours after luciferase plasmid transfection, we measured the luminescence from both nano-luciferase (NLuc) and Firefly luciferase (FF).

A

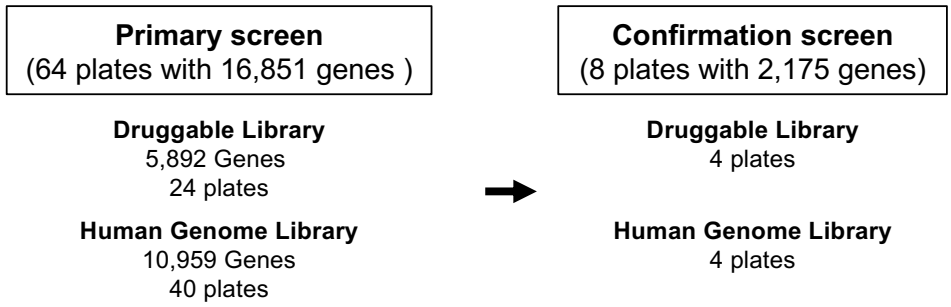
Primary screen
(64 plates with 16,851 genes)
Druggable Library
5,892 Genes
24 plates
Human Genome Library
10,959 Genes
40 plates
Confirmation screen
(8 plates with 2,175 genes)
Druggable Library
4 plates
Human Genome Library
4 plates

B

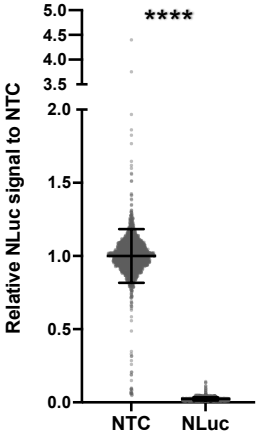
Relative NLuc signal to NTC
****
NTC
NLuc

C

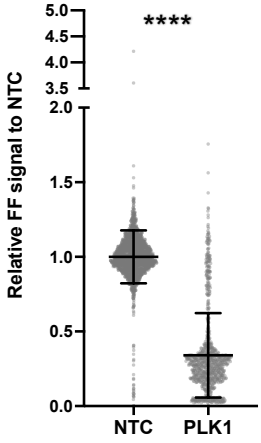
Relative FF signal to NTC
****
NTC
PLK1

D

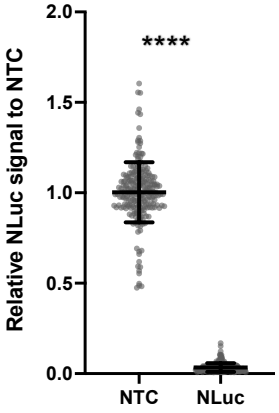
Relative NLuc signal to NTC
****
NTC
NLuc

E

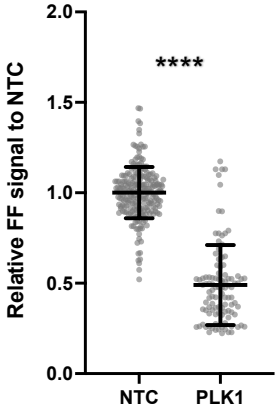
Relative FF signal to NTC
****
NTC
PLK1

F

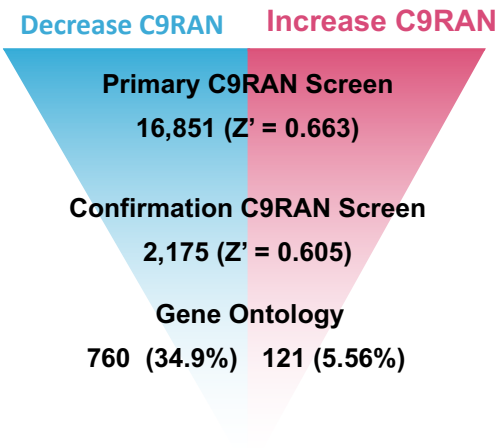
Decrease C9RAN
Increase C9RAN
Primary C9RAN Screen
16,851 (Z' = 0.663)
Confirmation C9RAN Screen
2,175 (Z' = 0.605)
Gene Ontology
760 (34.9%)
121 (5.56%)

Figure 4-2. Primary and validation screens for modifiers of C9RAN

(A) 16,851 genes were divided into two libraries: a druggable library, and a human genome library. The primary C9RAN screen started with 16,851 genes from both libraries (left panel). Next, we filtered and selected 2,175 genes as candidate hits from the primary C9RAN screen with the previous algorithm and performed a C9RAN validation screen (right panel). **(B)** Relative NLuc signal of siNLuc to siNTC from the C9RAN primary screen. **(C)** Relative FF signal of siPLK to siNTC from the C9RAN primary screen. For **(B)** and **(C)** from the C9 RAN primary screen, data points were from 192 plates with triplicates of 64 library plates. Each N is shown as a dot. NTC: N=1830; NLuc: N = 1769; PLK: N = 878. **(D)** Relative NLuc signal of siNLuc to siNTC from the C9RAN validation screen. **(E)** Relative FF signal of siPLK to siNTC from the C9RAN validation screen. For **(D)** and **(E)** from the C9 RAN validation screen, data points were from 24 plates with triplicates of 8 library plates. Each N is shown as a dot. NTC: N=237; NLuc: N = 235; PLK: N = 112. Asterisks above each data group are comparisons of expression between NTC and NLuc or PLK knockdown. ****$P \leq 0.0001$, represent unpaired t-tests with Welch's correction. **(F)** The average Z-score of each screen and the number and percentage of the final hits from the C9RAN validated screen. The number and percentage of hits are shown in two categories as C9RAN suppressors and C9RAN enhancers. Asterisks above each data group are comparisons of expression between NTC and NLuc or PLK knockdown. ****$P \leq 0.0001$, represent unpaired t-tests with Welch's correction.

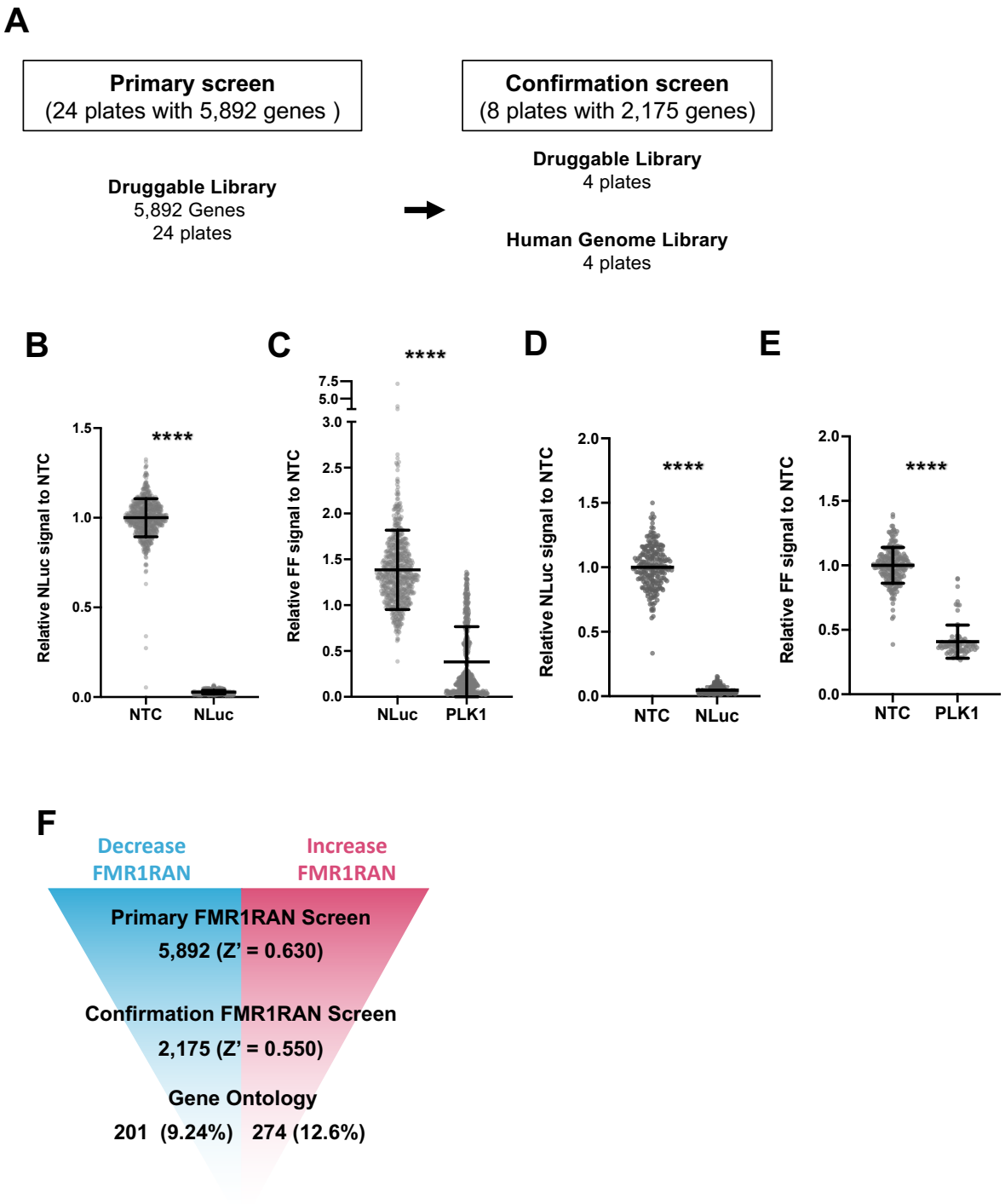

Figure 4-3. Primary and validation screen for FMR1RAN translation modifiers

(A) The primary FMR1RAN screen started with 5,892 genes from only the druggable library (left panel). Then we performed the FMR1RAN validation screen together with

C9RAN using the same library with 2,175 genes from both libraries (right panel). **(B)** Relative NLuc signal of siNLuc to siNTC from the FMR1RAN primary screen. **(C)** Relative FF signal of siPLK to siNTC from the FMR1RAN primary screen. For **(B)** and **(C)** from the FMR1 RAN primary screen, data points were from 72 plates with triplicates of 24 library plates. Each N is shown as a dot. NTC: N=698; NLuc: N = 684; PLK: N = 878. **(D)** Relative NLuc signal of siNLuc to siNTC from the FMR1RAN validation screen. **(E)** Relative FF signal of siPLK to siNTC from the FMR1RAN validation screen. For **(D)** and **(E)** from the C9 RAN validation screen, data points were from 24 plates with triplicates of 8 library plates. Each N is shown as a dot. NTC: N=220; NLuc: N = 230; PLK: N = 88. Asterisks above each data group are comparisons of expression between NTC and NLuc or PLK knockdown. ****$P \leq 0.0001$, represent unpaired t-tests with Welch's correction. **(F)** The average Z-score of each screen and the number and percentage of the final hits from the FMR1RAN validated screen. The number and percentage of hits are shown in two categories as FMR1RAN suppressors and FMR1RAN enhancers.

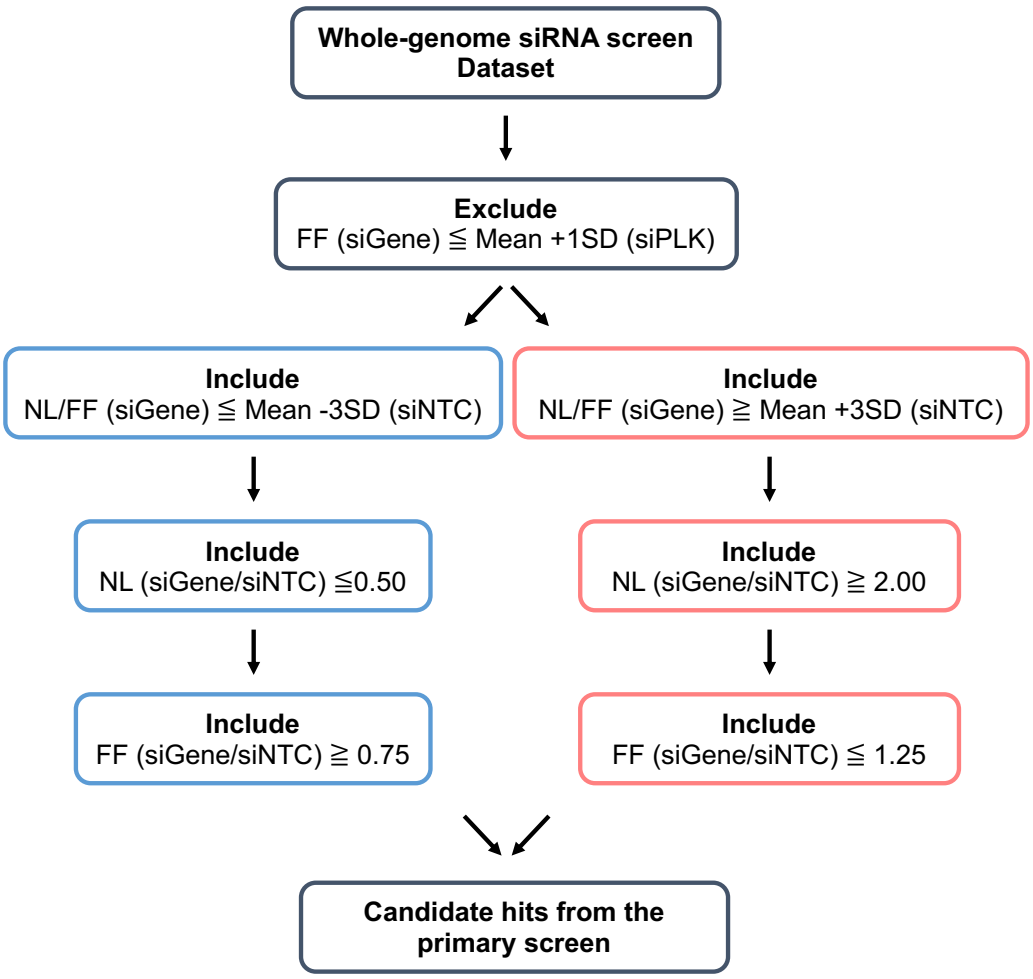

Figure 4-4. Original algorithm used for screen data analysis.

The following algorithm previously applied for data analysis and used to filter 2,175 genes as candidate hits from the C9RAN primary screen for the validation library.

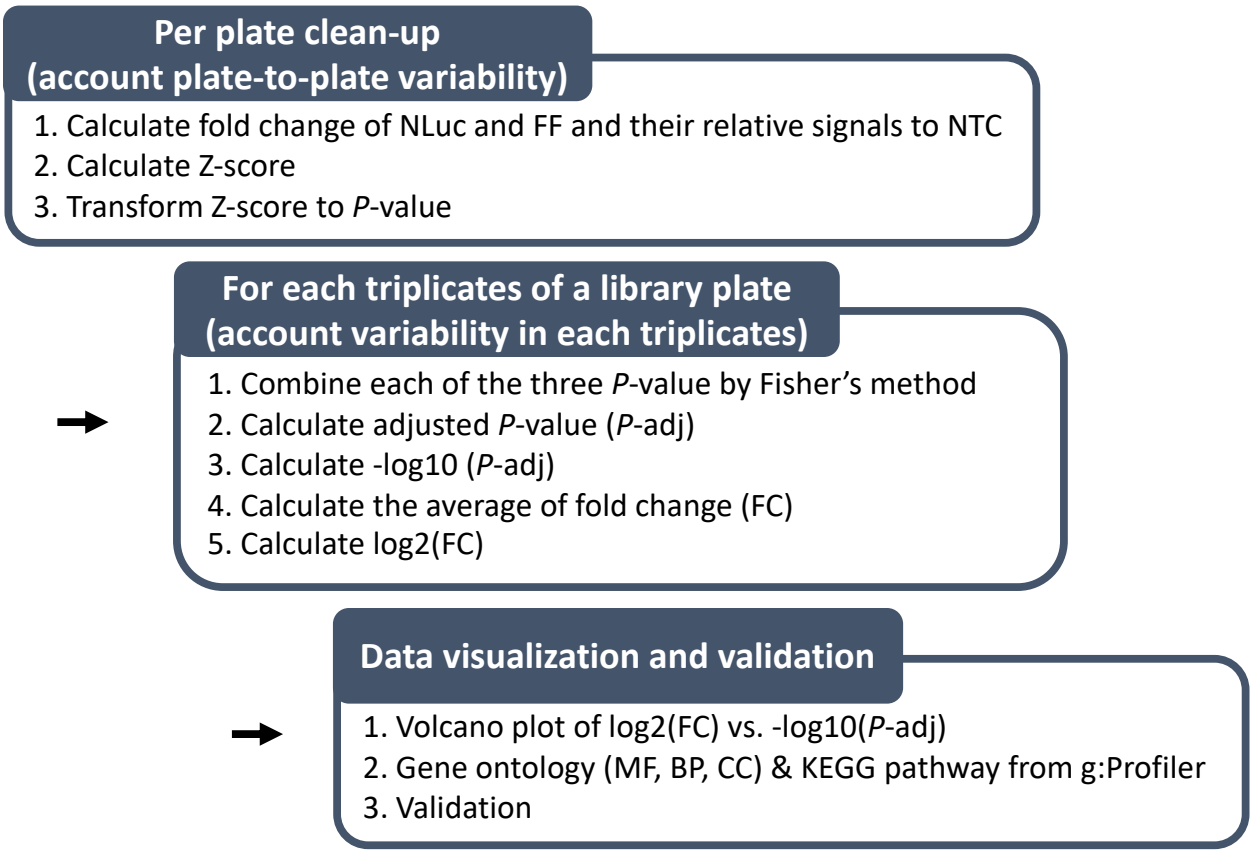

Figure 4-5. Updated algorithm for data analysis

Because of concerns related ot plate-to-plate and experimental variability, we designed a different method for analyzing the data from the primary screens. This method also uses statistical significance as an alternative strategy to advance specific hits for further investigation.

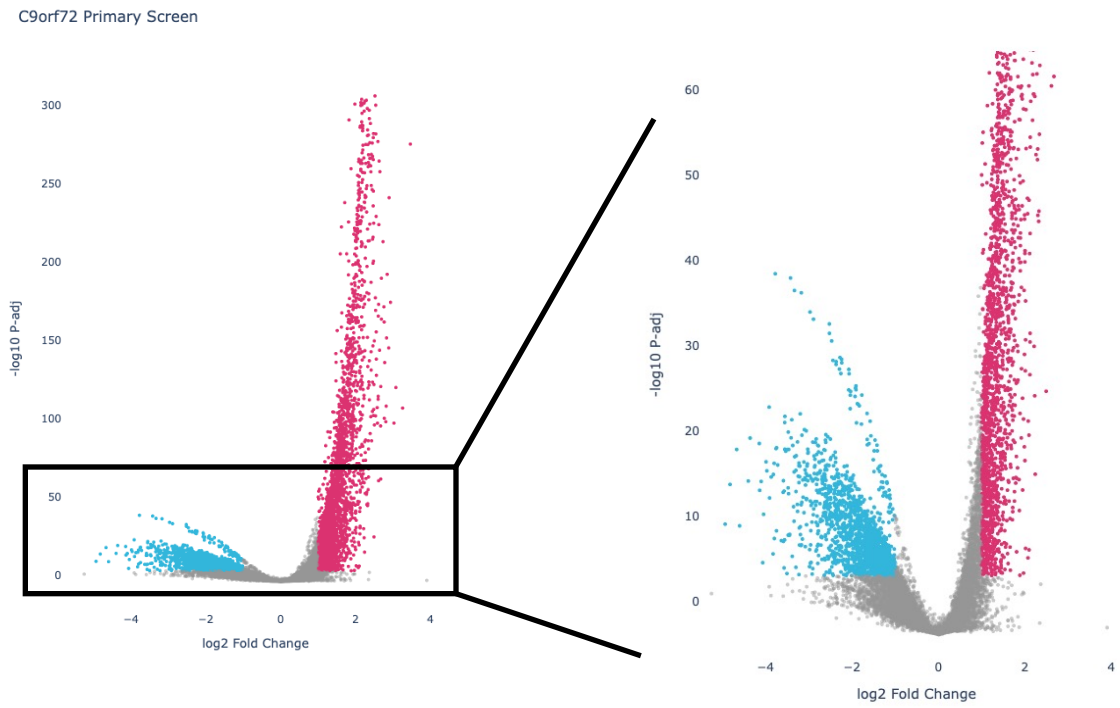

Figure 4-6. C9RAN primary screen

Volcano plots of C9RAN primary screen data. The cutoffs of colored hits are log2(Fold Change) greater than 1 or less than -1, and -log10(P-adj) of greater than 3. The right panel is an expanded view of the left panel. N = 16,851; Z'-factor = 0.663.

A

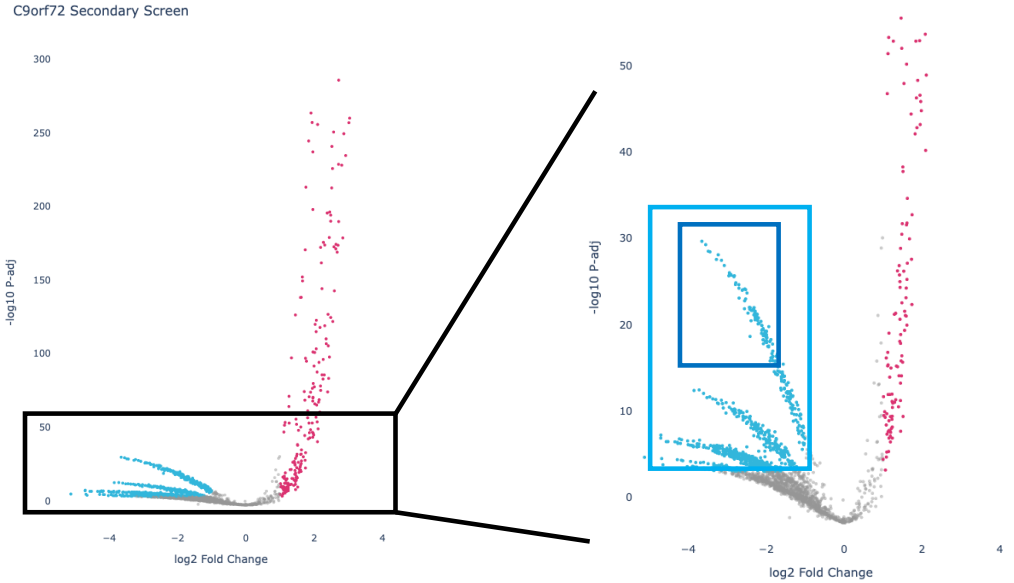
C9orf72 Secondary Screen
-log10 P-adj
log2 Fold Change

B

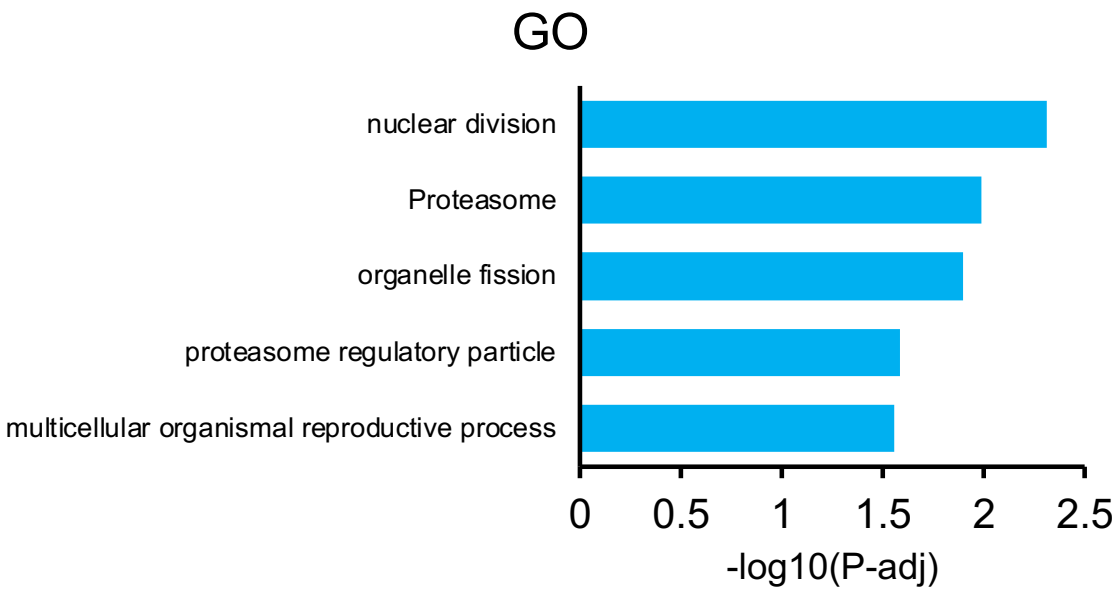
GO
nuclear division
Proteasome
organelle fission
proteasome regulatory particle
multicellular organismal reproductive process
0
0.5
1
1.5
2
2.5
-log10(P-adj)

C

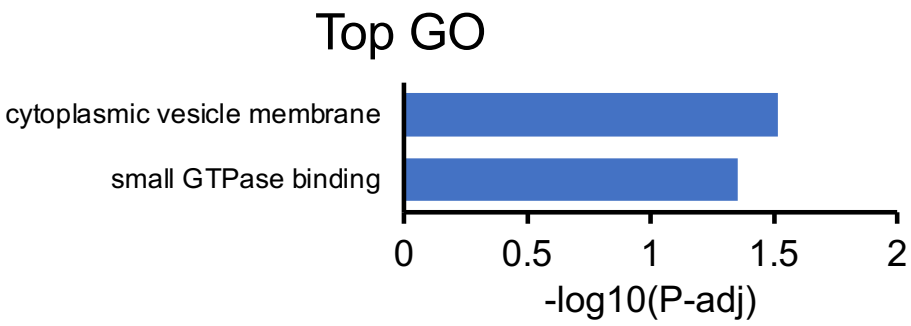
Top GO
cytoplasmic vesicle membrane
small GTPase binding
0
0.5
1
1.5
2
-log10(P-adj)

Figure 4-7. C9RAN translation validation screen and gene ontology analysis of C9RAN suppressors (i.e. gene loss leads to a selective decrease in C9RAN)

(A) Volcano plot of C9RAN validation screen. The cutoffs of colored hits are log2(Fold Change) is greater than 1 or less than -1, and -log10(P-adj) is greater than 3. The right panel is an expanded view of the left panel. N = 2,175; Z'-factor = 0.605. **(B)** Gene ontology analysis of all C9RAN suppressors from the validation screen (light blue frame from **(A)**). **(C)** Gene ontology analysis of top 100 hits as C9RAN suppressors from the validation screen (dark blue frame from **(A)**).

A

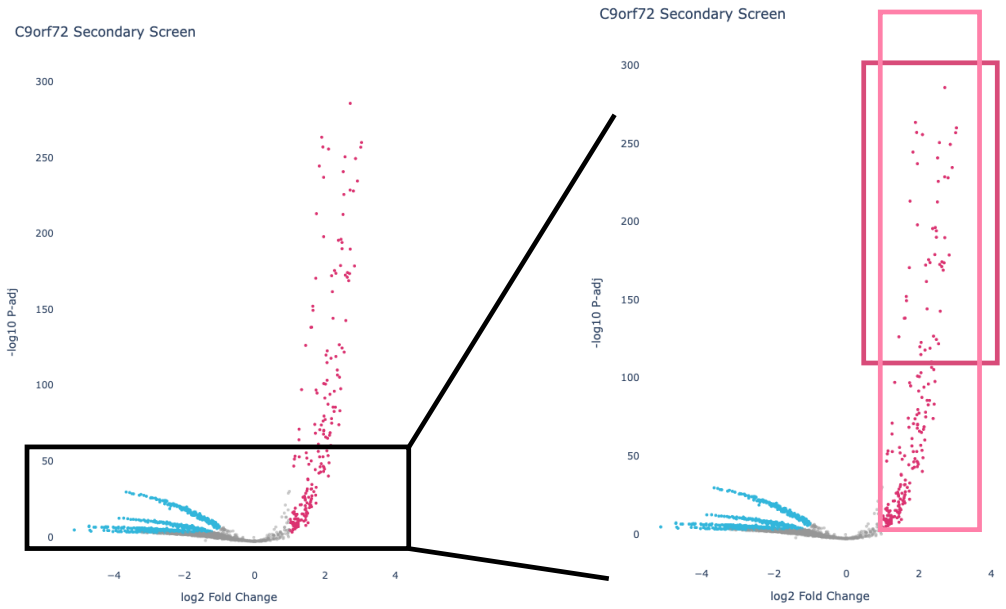
C9orf72 Secondary Screen
-log10 P-adj
log2 Fold Change
C9orf72 Secondary Screen
-log10 P-adj
log2 Fold Change

B

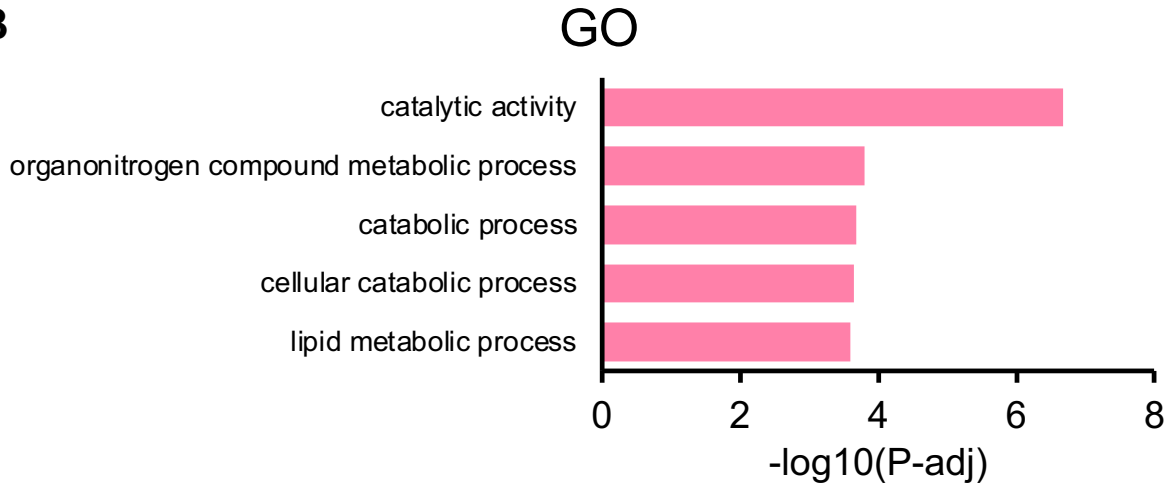
GO
catalytic activity
organonitrogen compound metabolic process
catabolic process
cellular catabolic process
lipid metabolic process
0
2
4
6
8
-log10(P-adj)

C

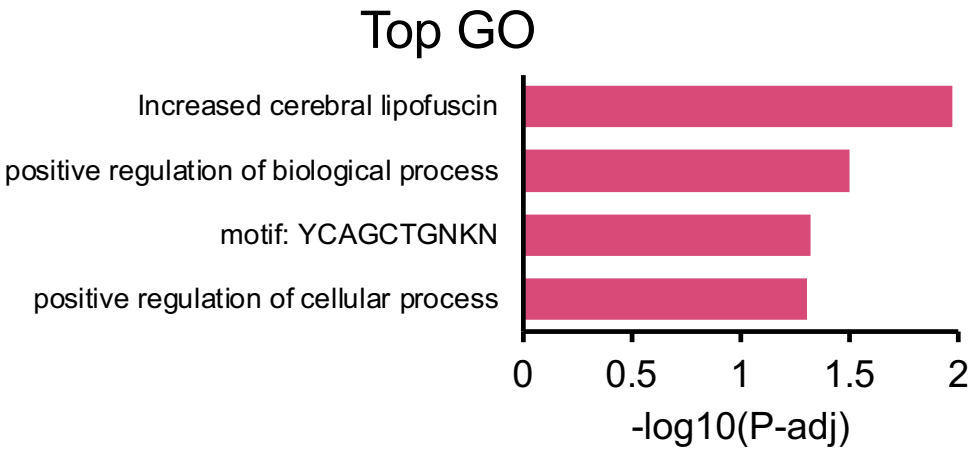
Top GO
Increased cerebral lipofuscin
positive regulation of biological process
motif: YCAGCTGNKN
positive regulation of cellular process
0
0.5
1
1.5
2
-log10(P-adj)

Figure 4-8. C9RAN validation screen and gene ontology analysis of C9RAN enhancers

(A) The volcano plot of the C9RAN validation screen. The cutoffs of colored hits are log2(Fold Change) is greater than 1 or less than -1, and -log10(P-adj) is greater than 3. The right panel is an expanded view of the left panel. **(B)** Gene ontology analysis of all C9RAN enhancers from the validation screen (light pink frame from **(A)**). **(C)** Gene ontology analysis of top 50 hits as C9RAN enhancers from the validation screen (dark pink frame from **(A)**).

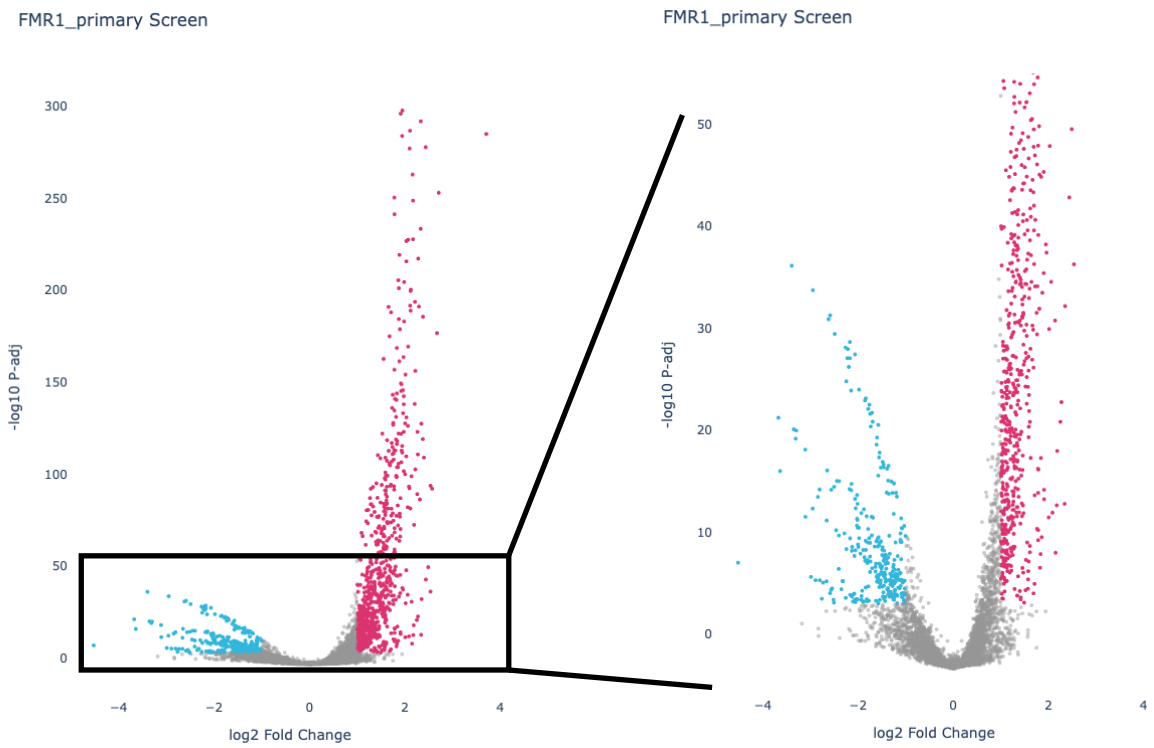

Figure 4-9. FMR1RAN translation modifier primary screen

The volcano plot of FMR1RAN primary screen. The cutoffs of colored hits are log2(Fold Change) is greater than 1 or less than -1, and -log10(P-adj) is greater than 3. The right panel is an expanded view of the left panel. N = 5,892; Z'-factor = 0.630.

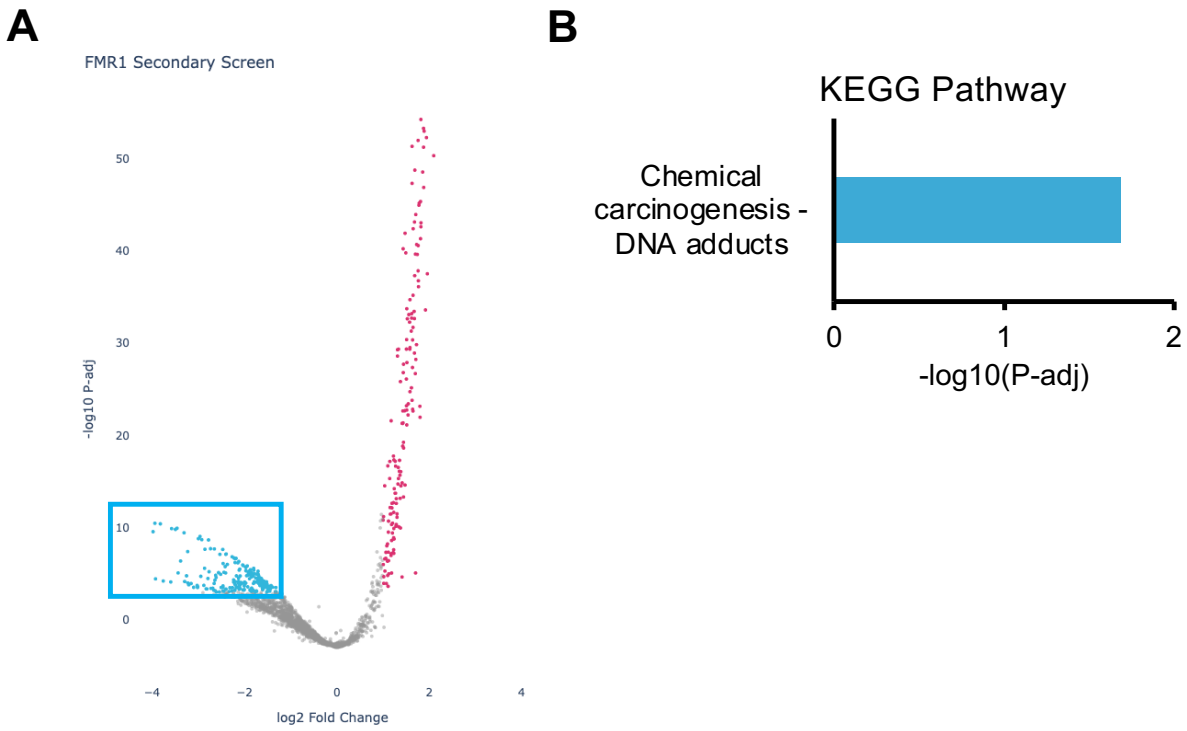

Figure 4-10. FMR1RAN validated screen and gene ontology analysis of FMR1RAN suppressors

(A) The volcano plot of the FMR1RAN validation screen. The cutoffs of colored hits are log2(Fold Change) is greater than 1 or less than -1, and -log10(P-adj) is greater than 3. N = 2,175; Z'-factor = 0.550. **(B)** Gene ontology analysis of all FMR1RAN suppressors from the validation screen (light blue frame from **(A)**).

A

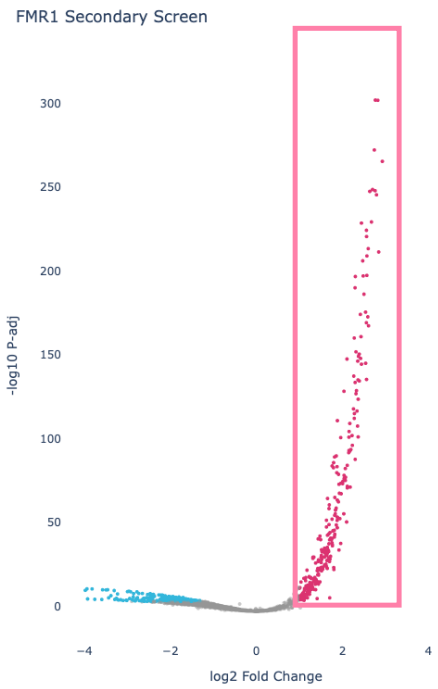
FMR1 Secondary Screen
300
250
200
150
100
50
0
-log10 P-adj
−4
−2
0
2
4
log2 Fold Change

B

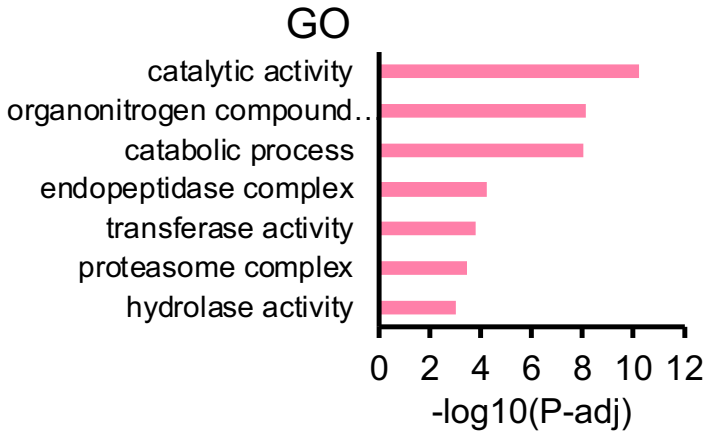
GO
catalytic activity
organonitrogen compound..
catabolic process
endopeptidase complex
transferase activity
proteasome complex
hydrolase activity
0 2 4 6 8 10 12
-log10(P-adj)

C

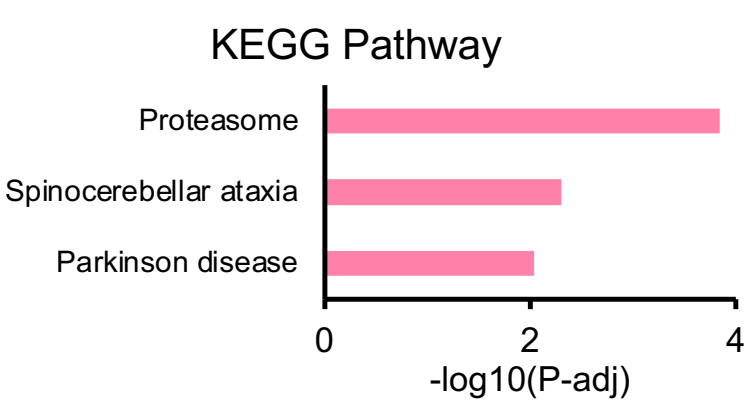
KEGG Pathway
Proteasome
Spinocerebellar ataxia
Parkinson disease
0
2
4
-log10(P-adj)

Figure 4-11. FMR1RAN validation screen; gene ontology and KEGG pathway analysis of FMR1 enhancers (i.e. siRNA knockdown leads to more FMR1 RAN)

(A) Volcano plot of the FMR1RAN validation screen. The cutoffs of colored hits are log2(Fold Change) is greater than 1 or less than -1, and -log10(P-adj) is greater than 3. **(B)** Gene ontology analysis of all FMR1RAN enhancers from the validation screen (pink frame from **(A)**). **(C)** KEGG pathway analysis of all FMR1RAN enhancers from the validation screen (pink frame from **(A)**).

A

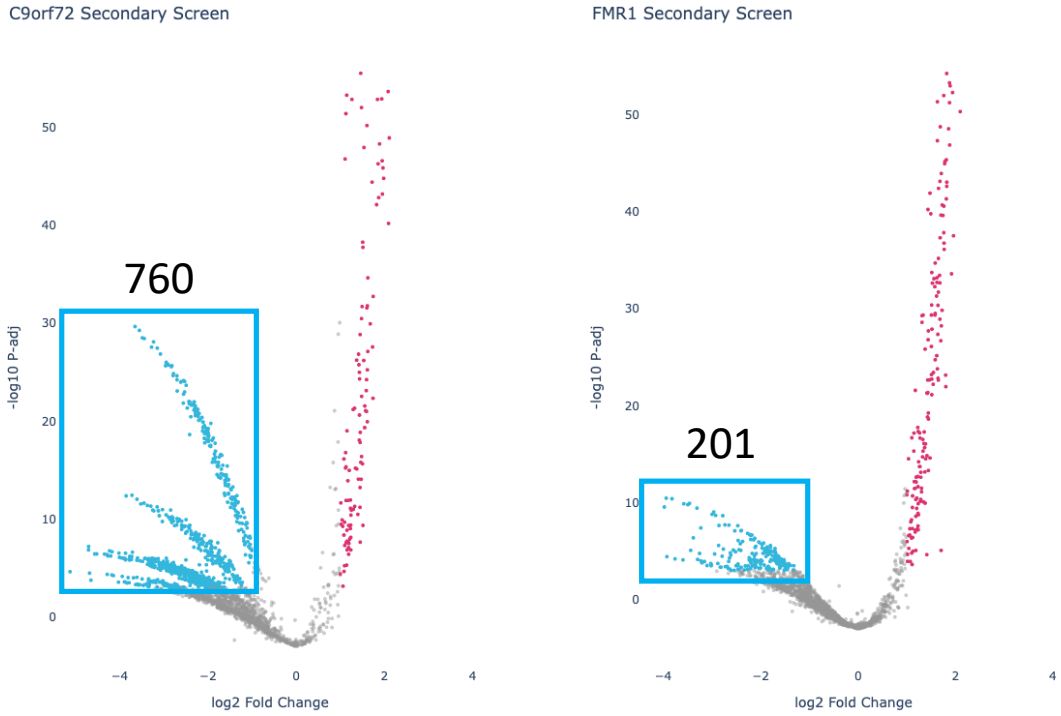

B

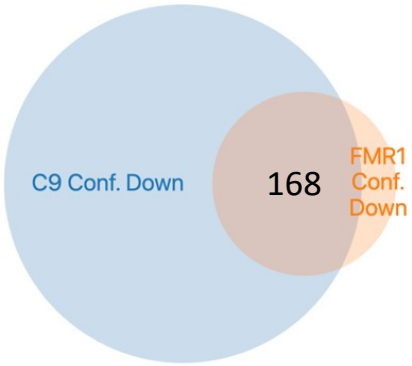

PABP
DNAJB13
NUP50
RARS
HYPK
HSPH1

MID1
HNRNPM

C

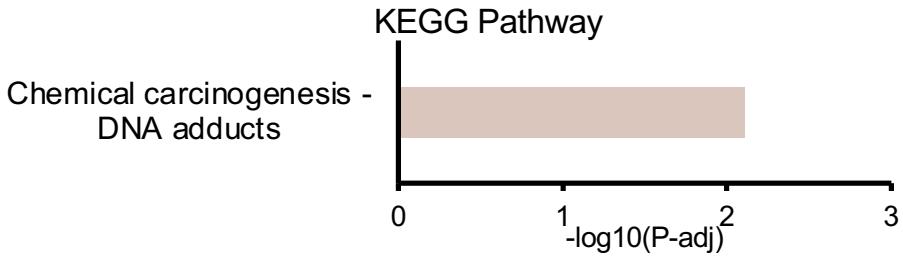

Figure 4-12. Shared suppressors from C9RAN and FMR1RAN validation screen

(A) Volcano plot of the C9RAN and FMR1RAN validation screen. Hits colored in blue and in the blue square are subject to Venn diagram analysis. **(B)**Venn diagrams and some exciting hits. **(C)** KEGG pathway analysis of the hits from the intersection.

A

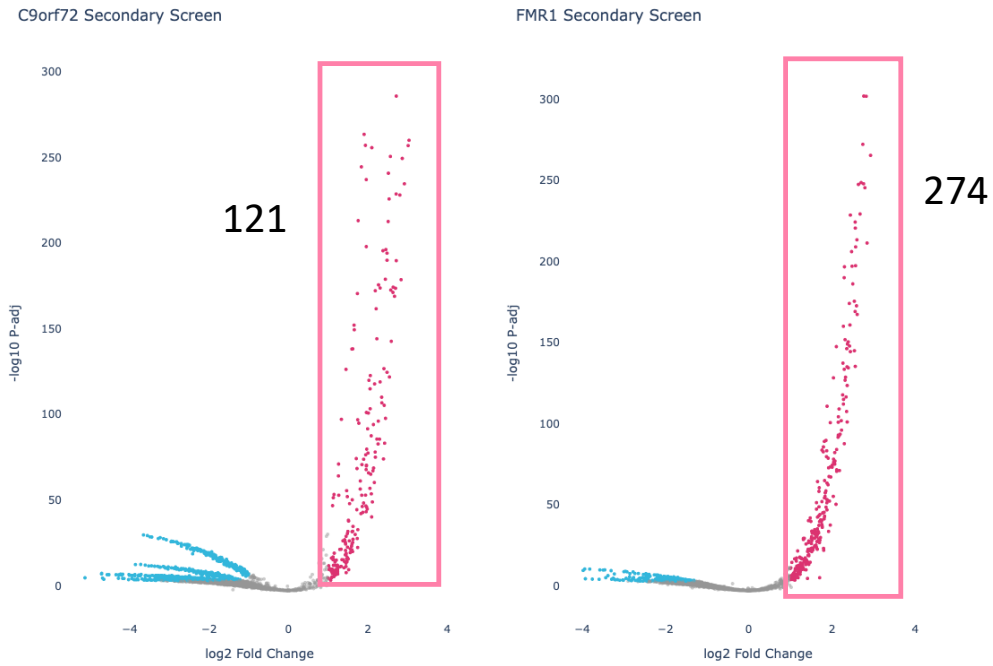

B

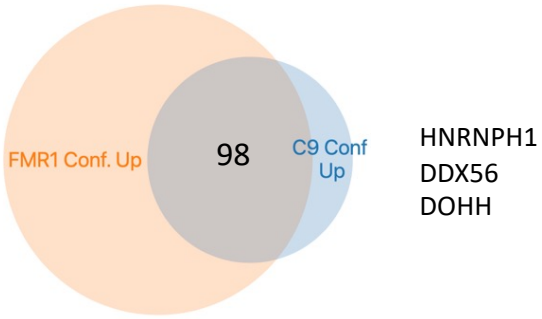

HNRNPH1
DDX56
DOHH

C

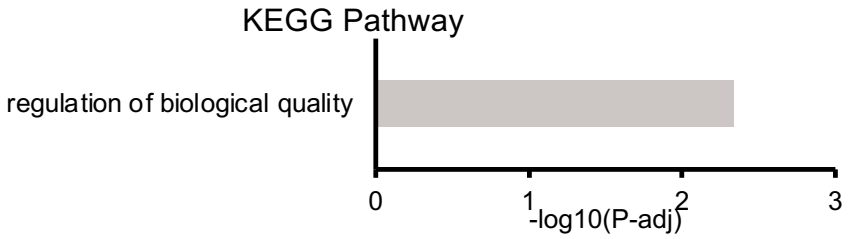

Figure 4-13. Shared enhancers from C9RAN and FMR1RAN validation screen

(A) Volcano plot of the C9RAN and FMR1RAN validation screen. Hits colored in pink and in the pink square are subject to Venn diagram analysis. **(B)**Venn diagrams and some exciting hits. **(C)** KEGG pathway analysis of the hits from the intersection.

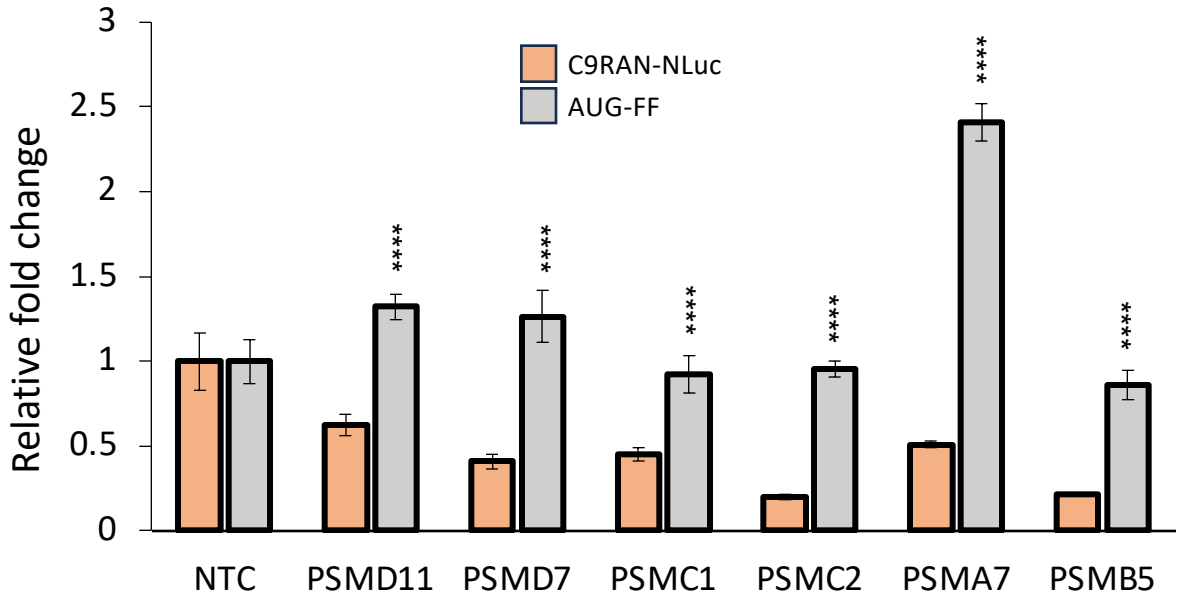

Figure 4-14. Effect of proteasome subunit knockdown on C9RAN translation from validation screen

Relative luciferase signals of PSMD11, PSMD7, PSMC1, PSMC2, PSMA7, and PSMB5 to NTC control. Graph show mean with error bars ± SD, N=3 from the screen. Asterisks above each bar are comparisons of expression between NTC and each gene knockdown of the NLuc signal. ****$P \leq 0.0001$, represent unpaired t-tests with Welch's correction for multiple comparison.

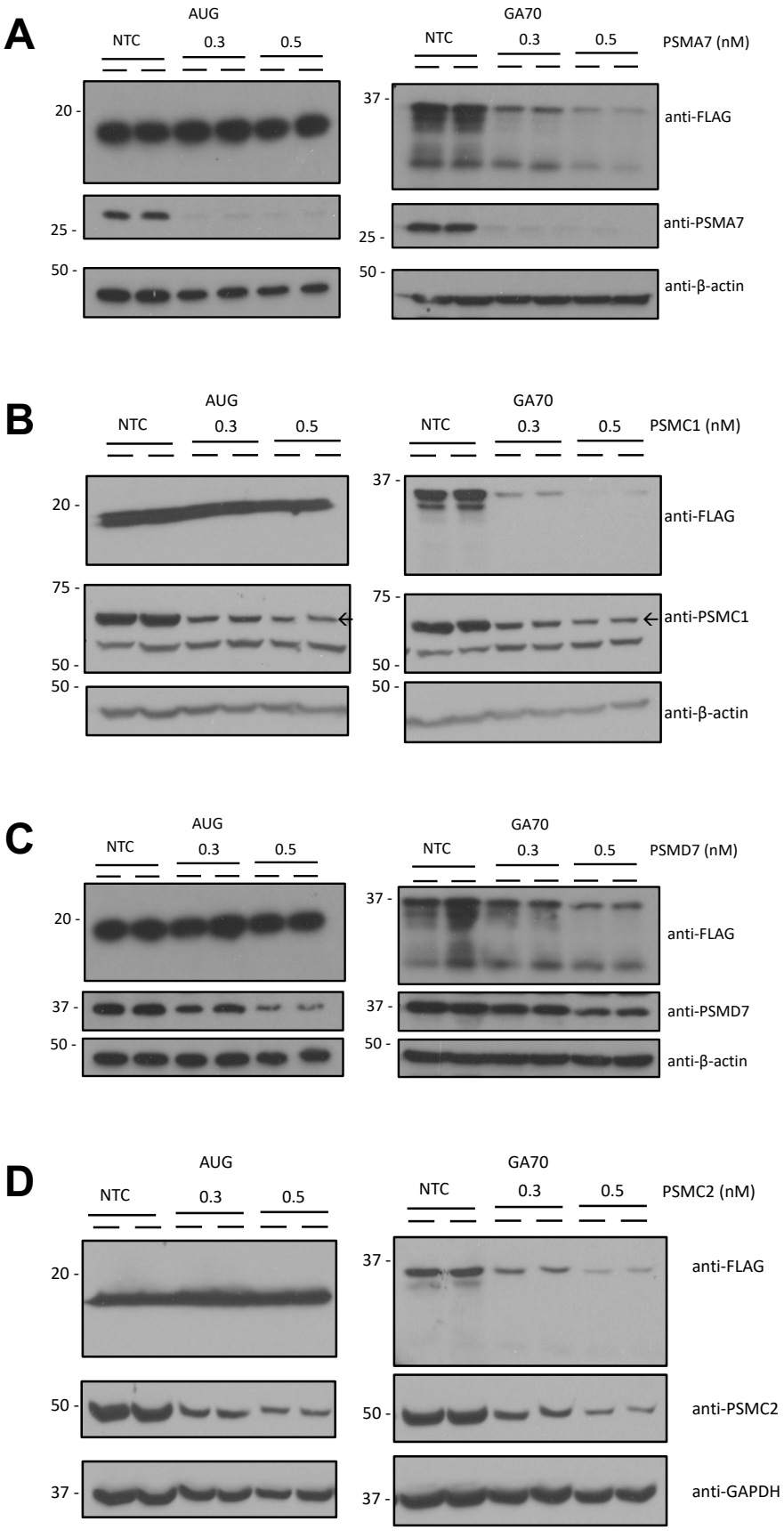
A
AUG
GA70
NTC
0.3
0.5
PSMA7 (nM)
20 -
37 -
anti-FLAG
25 -
anti-PSMA7
50 -
anti-β-actin
B
AUG
GA70
NTC
0.3
0.5
PSMC1 (nM)
20 -
37 -
anti-FLAG
75 -
anti-PSMC1
50 -
anti-β-actin
C
AUG
GA70
NTC
0.3
0.5
PSMD7 (nM)
20 -
37 -
anti-FLAG
anti-PSMD7
50 -
anti-β-actin
D
AUG
GA70
NTC
0.3
0.5
PSMC2 (nM)
20 -
37 -
anti-FLAG
50 -
anti-PSMC2
anti-GAPDH

Figure 4-15. Validation of proteasome subunits knockdown effects on C9RAN with immunoblotting of reporters an different siRNAs

Validation of **(A)** PSMA7 **(B)** PSMC1 **(C)** PSMD7 **(D)** PSMC2 knockdown effects with 0.3 and 0.5 nM of a second set of siRNAs in GA70-NLuc-3xFLAG and AUG-NLuc-3xFLAG. Each lane represents an independent biological replicates, N=2.

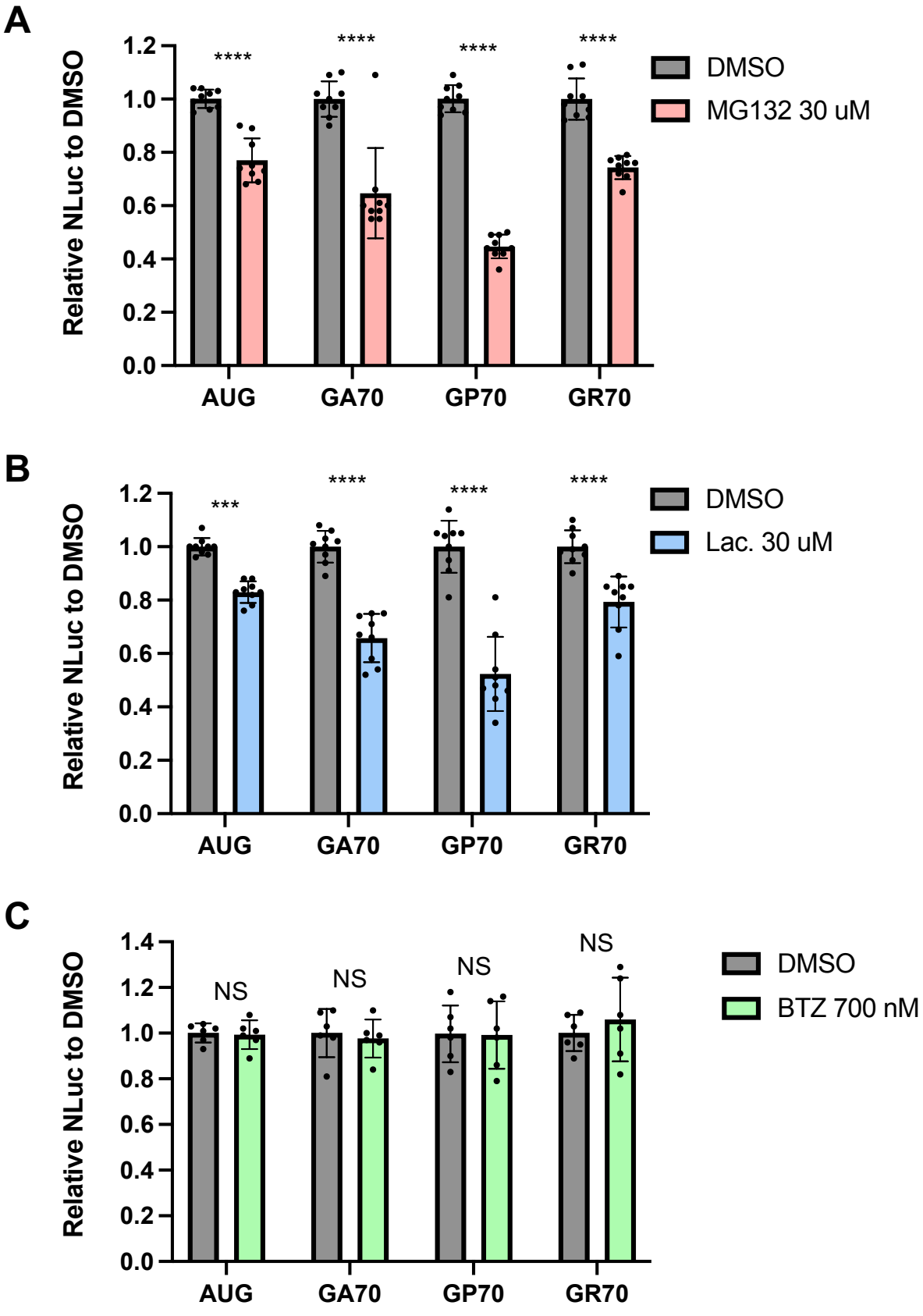
A
Relative NLuc to DMSO
1.2
1.0
0.8
0.6
0.4
0.2
0.0
****
****
****
****
AUG
GA70
GP70
GR70
DMSO
MG132 30 uM
B
Relative NLuc to DMSO
1.2
1.0
0.8
0.6
0.4
0.2
0.0
***
****
****
****
AUG
GA70
GP70
GR70
DMSO
Lac. 30 uM
C
Relative NLuc to DMSO
1.4
1.2
1.0
0.8
0.6
0.4
0.2
0.0
NS
NS
NS
NS
AUG
GA70
GP70
GR70
DMSO
BTZ 700 nM

Figure 4-16. Effect of proteasome inhibitors C9RAN translation in GA, GP, ad GR frames in RRL system.

RRL in vitro translation system expressing GA, GP, and GR T7 synthesized reporter RNAs after treating the lysate with proteasome inhibitors including **(A)** 30μM MG132 **(B)** 30μM lactacystin (Lac.) **(C)** 700 μM Bortezomib. All graphs show mean with error bars ± SD. Each N is shown as a dot (n=9/group). Asterisks above each bar are comparisons of expression between vehicle and proteasome inhibitor treatment. NS = not significant; ***P ≤ 0.001; ****P ≤ 0.0001, as determined with two-way ANOVA with Sidak's multiple comparison test.

A

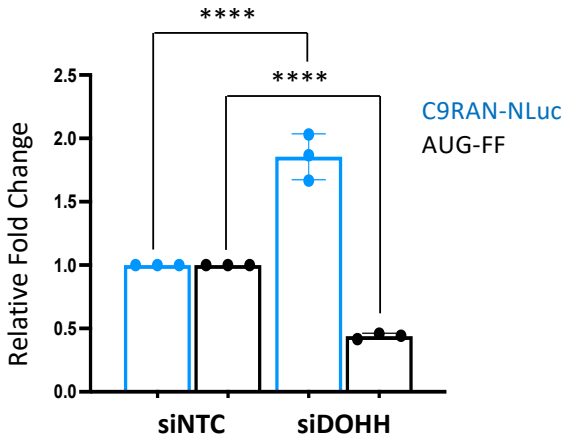
****
****
2.5
2.0
1.5
1.0
0.5
0.0
Relative Fold Change
C9RAN-NLuc
AUG-FF
siNTC
siDOHH

B

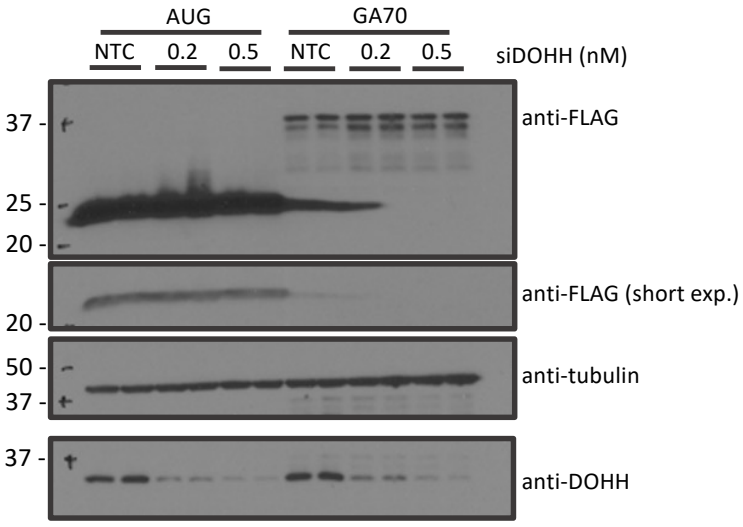
AUG
GA70
NTC
0.2
0.5
NTC
0.2
0.5
siDOHH (nM)
37 -
25 -
20 -
anti-FLAG
20 -
anti-FLAG (short exp.)
50 -
37 -
anti-tubulin
37 -
anti-DOHH

C

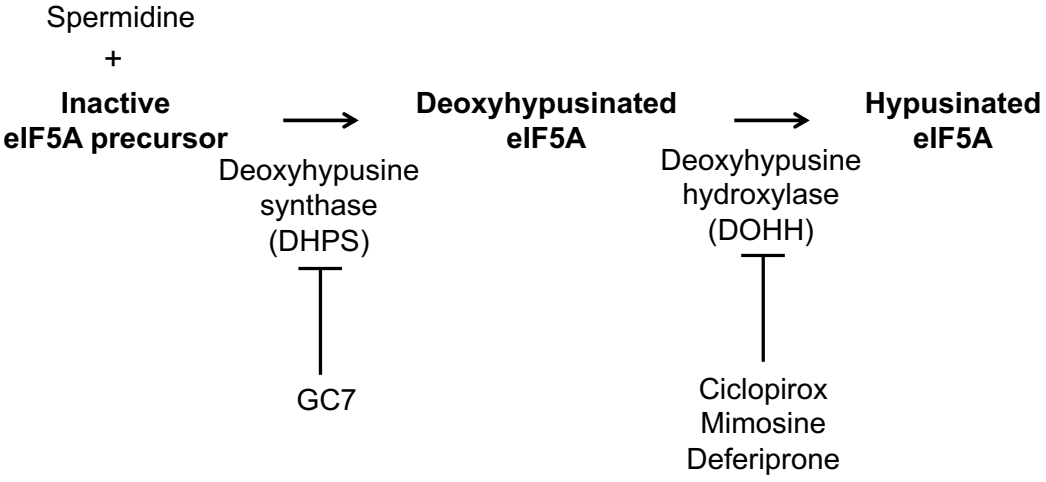
Spermidine
+
Inactive
eIF5A precursor
Deoxyhypusine
synthase
(DHPS)
GC7
Deoxyhypusinated
eIF5A
Deoxyhypusine
hydroxylase
(DOHH)
Ciclopirox
Mimosine
Deferiprone
Hypusinated
eIF5A

Figure 4-17. DOHH knockdown enhances C9 RAN translation.

(A) Relative luciferase signals of DOHH to NTC control from the C9RAN validation screen. Graph show mean with error bars ± SD, N=3 from the screen. Asterisks above each bar are comparisons of expression between NTC and each gene knockdown of the NLuc and FF signal. ****$P \leq 0.0001$, represent unpaired t-tests with Welch's correction for multiple comparison. **(B)** Validation of the effect of DOHH on C9RAN with a second set of siRNA at 0.2 and 0.5 nM and using immunoblotting as an alternative readout. **(C)** Post-translational modification pathway underlying hypusination of eIF5A.

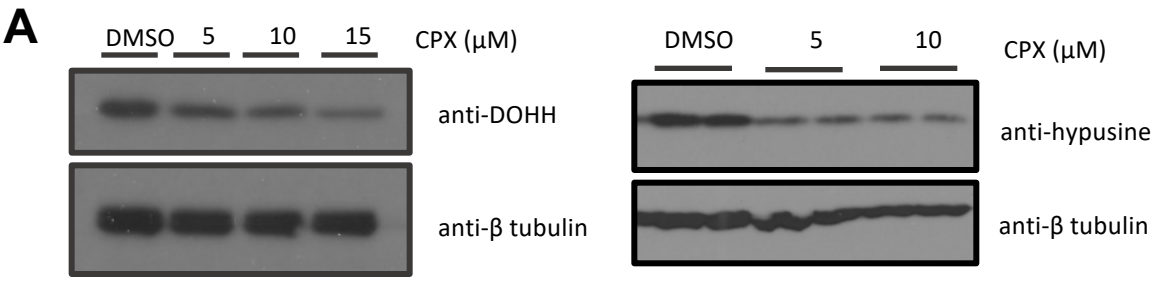
A
DMSO
5
10
15
CPX (μM)
anti-DOHH
anti-β tubulin
DMSO
5
10
CPX (μM)
anti-hypusine
anti-β tubulin

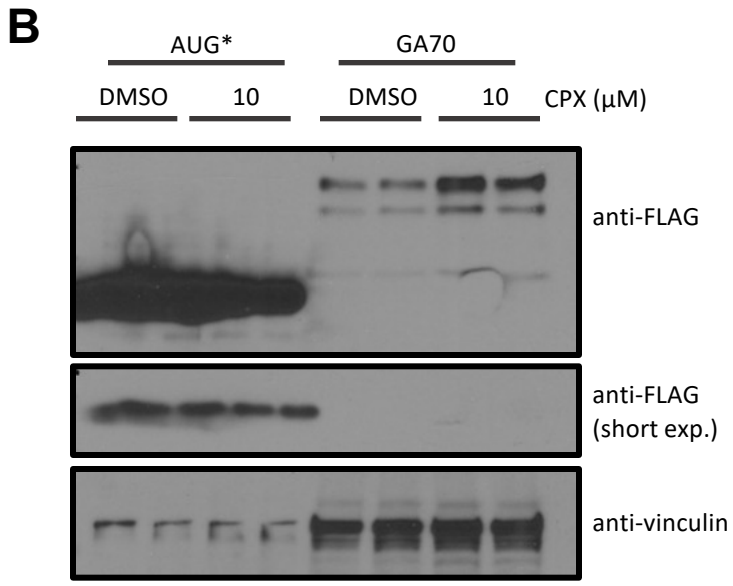
B
AUG*
GA70
DMSO
10
DMSO
10
CPX (μM)
anti-FLAG
anti-FLAG
(short exp.)
anti-vinculin

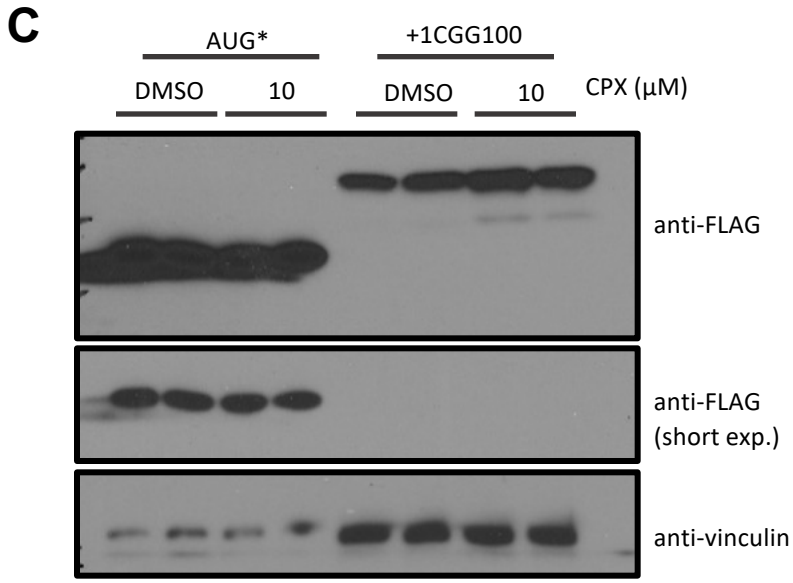
C
AUG*
+1CGG100
DMSO
10
DMSO
10
CPX (μM)
anti-FLAG
anti-FLAG
(short exp.)
anti-vinculin

Figure 4-18. DOHH inhibitor treatment selectively enhances C9RAN and FMR1RAN translation in HEK293 Cells.

(A) Ciclopirox (CPX) is an inhibitor of DOHH. in HEK293 were treated with 5, 10, and 15 μM of CPX for 48 hr to test for the efficiency of suppressing the level of DOHH and hypusine. **(B)** HEK293 cells expressing either AUG-NLuc-FLAG or GA70-NLuc-FLAG were treated with 10 μM of CPX for 48 hr. **(C)** HEK293 cells expressing either AUG-NLuc-FLAG or +1CGG100-NLuc-FLAG were treated with 10 μM of CPX for 48 hr. We applied anti-Vinculin here as loading control.

4.8. References

Aravind L, Ponting CP. 1998. Homologues of 26S proteasome subunits are regulators of transcription and translation. *Protein Science* **7**:1250–1254. doi:10.1002/pro.5560070521

Barba-Aliaga M, Alepuz P. 2022. Role of eIF5A in Mitochondrial Function. *Int J Mol Sci*. doi:10.3390/ijms23031284

Baugh JM, Pilipenko E V. 2004. 20S proteasome differentially alters translation of different mRNAs via the cleavage of eIF4F and eIF3. *Mol Cell* **16**:575–586. doi:10.1016/j.molcel.2004.10.017

Bence NF, Sampat RM, Kopito RR. 2001. Impairment of the ubiquitin-proteasome system by protein aggregation. *Science (1979)* **292**:1552–1555. doi:10.1126/science.292.5521.1552

Cheng W, Wang S, Mestre AA, Fu C, Makarem A, Xian F, Hayes LR, Lopez-Gonzalez R, Drenner K, Jiang J, Cleveland DW, Sun S. 2018. C9ORF72 GGGGCC repeat-associated non-AUG translation is upregulated by stress through eIF2α phosphorylation. *Nat Commun*. doi:10.1038/s41467-017-02495-z

Ciechanover A, Orian A, Schwartz AL. 2000. Ubiquitin-mediated proteolysis: Biological regulation via destruction. *BioEssays* **22**:442–451. doi:10.1002/(SICI)1521-1878(200005)22:5<442::AID-BIES6>3.0.CO;2-Q

DeJesus-Hernandez M, Mackenzie IR, Boeve BF, Boxer AL, Baker M, Rutherford NJ, Nicholson AM, Finch NCA, Flynn H, Adamson J, Kouri N, Wojtas A, Sengdy P, Hsiung GYR, Karydas A, Seeley WW, Josephs KA, Coppola G, Geschwind DH, Wszolek ZK, Feldman H, Knopman DS, Petersen RC, Miller BL, Dickson DW,

Boylan KB, Graff-Radford NR, Rademakers R. 2011. Expanded GGGGCC Hexanucleotide Repeat in Noncoding Region of C9ORF72 Causes Chromosome 9p-Linked FTD and ALS. *Neuron*. doi:10.1016/j.neuron.2011.09.011

Faundes V, Jennings MD, Crilly S, Legraie S, Withers SE, Cuvertino S, Davies SJ, Douglas AGL, Fry AE, Harrison V, Amiel J, Lehalle D, Newman WG, Newkirk P, Ranells J, Splitt M, Cross LA, Saunders CJ, Sullivan BR, Granadillo JL, Gordon CT, Kasher PR, Pavitt GD, Banka S. 2021. Impaired eIF5A function causes a Mendelian disorder that is partially rescued in model systems by spermidine. *Nat Commun* **12**. doi:10.1038/s41467-021-21053-2

Fujino Y, Mori K, Nagai Y. 2023. Repeat-associated non-AUG translation in neuromuscular diseases: mechanisms and therapeutic insights. *The Journal of Biochemistry*. doi:10.1093/jb/mvad012

Gijselinck I, Van Langenhove T, van der Zee J, Sleegers K, Philtjens S, Kleinberger G, Janssens J, Bettens K, Van Cauwenberghe C, Pereson S, Engelborghs S, Sieben A, De Jonghe P, Vandenberghe R, Santens P, De Bleecker J, Maes G, Bäumer V, Dillen L, Joris G, Cuijt I, Corsmit E, Elinck E, Van Dongen J, Vermeulen S, Van den Broeck M, Vaerenberg C, Mattheijssens M, Peeters K, Robberecht W, Cras P, Martin J-J, De Deyn PP, Cruts M, Van Broeckhoven C. 2012. A C9orf72 promoter repeat expansion in a Flanders-Belgian cohort with disorders of the frontotemporal lobar degeneration-amyotrophic lateral sclerosis spectrum: a gene identification study. *Lancet Neurol* **11**:54–65. doi:10.1016/S1474-4422(11)70261-7

Gillette TG, Gonzalez F, Delahodde A, Johnston SA, Kodadek T. 2004. Physical and functional association of RNA polymerase II and the proteasome. *Proc Natl Acad Sci U S A* **101**:5904–5909. doi:10.1073/pnas.0305411101

Green KM, Glineburg MR, Kearse MG, Flores BN, Linsalata AE, Fedak SJ, Goldstrohm AC, Barmada SJ, Todd PK. 2017. RAN translation at C9orf72-associated repeat expansions is selectively enhanced by the integrated stress response. *Nat Commun* **8**. doi:10.1038/s41467-017-02200-0

Guo Q, Lehmer C, Martínez-Sánchez A, Rudack T, Beck F, Hartmann H, Pérez-Berlanga M, Frottin F, Hipp MS, Hartl FU, Edbauer D, Baumeister W, Fernández-Busnadiego R. 2018. In Situ Structure of Neuronal C9orf72 Poly-GA Aggregates Reveals Proteasome Recruitment. *Cell* **172**:696-705.e12. doi:10.1016/j.cell.2017.12.030

Gutierrez E, Shin BS, Woolstenhulme CJ, Kim JR, Saini P, Buskirk AR, Dever TE. 2013. eif5A promotes translation of polyproline motifs. *Mol Cell* **51**. doi:10.1016/j.molcel.2013.04.021

Henderson A, Hershey JW. 2011. Eukaryotic translation initiation factor (eIF) 5A stimulates protein synthesis in Saccharomyces cerevisiae. *Proc Natl Acad Sci U S A* **108**. doi:10.1073/pnas.1008150108

Joazeiro CAP. 2019. Mechanisms and functions of ribosome-associated protein quality control. *Nat Rev Mol Cell Biol*. doi:10.1038/s41580-019-0118-2

Kearse MG, Green KM, Krans A, Rodriguez CM, Linsalata AE, Goldstrohm AC, Todd PK. 2016. CGG Repeat-Associated Non-AUG Translation Utilizes a Cap-

Dependent Scanning Mechanism of Initiation to Produce Toxic Proteins. *Mol Cell*. doi:10.1016/j.molcel.2016.02.034

Kemper WM, Berry KW, Merrick WC. 1976. Purification and properties of rabbit reticulocyte protein synthesis initiation factors M2Bα and M2Bβ. *Journal of Biological Chemistry* **251**. doi:10.1016/s0021-9258(17)33095-8

Kong HE, Lim J, Linsalata A, Kang Y, Malik I, Allen EG, Cao Y, Shubeck L, Johnston R, Huang Y, Gu Y, Guo X, Zwick ME, Qin Z, Wingo TS, Juncos J, Nelson DL, Epstein MP, Cutler DJ, Todd PK, Sherman SL, Warren ST, Jin P. 2022. Identification of PSMB5 as a genetic modifier of fragile X–associated tremor/ataxia syndrome. *Proc Natl Acad Sci U S A* **119**. doi:10.1073/pnas.2118124119

Kramer NJ, Haney MS, Morgens DW, Jovičić A, Couthouis J, Li A, Ousey J, Ma R, Bieri G, Tsui CK, Shi Y, Hertz NT, Tessier-Lavigne M, Ichida JK, Bassik MC, Gitler AD. 2018. CRISPR-Cas9 screens in human cells and primary neurons identify modifiers of C9ORF72 dipeptide-repeat-protein toxicity. *Nat Genet* **50**. doi:10.1038/s41588-018-0070-7

Kulak NA, Pichler G, Paron I, Nagaraj N, Mann M. 2014. Minimal, encapsulated proteomic-sample processing applied to copy-number estimation in eukaryotic cells. *Nat Methods* **11**. doi:10.1038/nmeth.2834

Landau G, Bercovich Z, Park MH, Kahana C. 2010. The role of polyamines in supporting growth of mammalian cells is mediated through their requirement for translation initiation and elongation. *Journal of Biological Chemistry* **285**. doi:10.1074/jbc.M110.106419

Liang YT, Piao C, Beuschel CB, Toppe D, Kollipara L, Bogdanow B, Maglione M, Lützkendorf J, See JCK, Huang S, Conrad TOF, Kintscher U, Madeo F, Liu F, Sickmann A, Sigrist SJ. 2021. eIF5A hypusination, boosted by dietary spermidine, protects from premature brain aging and mitochondrial dysfunction. *Cell Rep* **35**. doi:10.1016/j.celrep.2021.108941

Lomen-Hoerth C, Anderson T, Miller B. 2002. The overlap of amyotrophic lateral sclerosis and frontotemporal dementia. *Neurology* **59**:1077–1079. doi:10.1212/WNL.59.7.1077

Lomen-Hoerth C, Murphy J, Langmore S, Kramer JH, Olney RK, Miller B. 2003. Are amyotrophic lateral sclerosis patients cognitively normal? *Neurology* **60**:1094–1097. doi:10.1212/01.WNL.0000055861.95202.8D

Luukkainen L, Bloigu R, Moilanen V, Remes AM. 2015. Epidemiology of Frontotemporal Lobar Degeneration in Northern Finland. *Dement Geriatr Cogn Dis Extra* **5**:435–441. doi:10.1159/000440858

Majounie E, Renton AE, Mok K, Dopper EGP, Waite A, Rollinson S, Chiò A, Restagno G, Nicolaou N, Simon-Sanchez J, van Swieten JC, Abramzon Y, Johnson JO, Sendtner M, Pamphlett R, Orrell RW, Mead S, Sidle KC, Houlden H, Rohrer JD, Morrison KE, Pall H, Talbot K, Ansorge O, Hernandez DG, Arepalli S, Sabatelli M, Mora G, Corbo M, Giannini F, Calvo A, Englund E, Borghero G, Floris GL, Remes AM, Laaksovirta H, McCluskey L, Trojanowski JQ, Van Deerlin VM, Schellenberg GD, Nalls MA, Drory VE, Lu CS, Yeh TH, Ishiura H, Takahashi Y, Tsuji S, Le Ber I, Brice A, Drepper C, Williams N, Kirby J, Shaw P, Hardy J, Tienari PJ, Heutink P, Morris HR, Pickering-Brown S, Traynor BJ, Adamson G, Bayer AJ,

Beck J, Callister JB, Blake DJ, Blumen SC, Collinge J, Dunckley T, Ealing J, East S, Elman L, Gerhard A, Guerreiro RJ, Gwinn K, Halliwell N, Hamdalla HH, Hewitt C, Ince P, Jablonka S, James C, Kent L, Knock JC, Lynch T, Mahoney C, Mann D, Neal J, Norris D, O'Dowd S, Richardson A, Rossor M, Rothstein J, Scholz SW, Snowden J, Stephan DA, Toulson G, Turner MR, Warren JD, Young K, Weng YH, Kuo HC, Lai SC, Huang CL, Camuzat A, Entraingues L, Guillot-Noël, Verpillat P, Clerget-Darpoux F, Corcia P, Couratier P, Didic M, Dubois B, Duyckaerts C, Guedj E, Golfier V, Habert MO, Hannequin D, Lacomblez L, Meininger V, Salachas F, Levy R, Michel BF, Pasquier F, Puel M, Thomas-Anterion C, Sellal F, Vercelletto M, Moglia C, Cammarosano S, Canosa A, Gallo S, Brunetti M, Ossola I, Marinou K, Papetti L, Pisano F, Pinter GL, Conte A, Luigetti M, Zollino M, Lattante S, Marangi G, la Bella V, Spataro R, Colletti T, Battistini S, Ricci C, Caponnetto C, Mancardi G, Mandich P, Salvi F, Bartolomei I, Mandrioli J, Sola P, Lunetta C, Penco S, Monsurrò MR, Tedeschi G, Conforti FL, Gambardella A, Quattrone A, Volanti P, Cannas A, Piras V, Marrosu F, Marrosu MG, Murru MR, Pugliatti M, Parish LD, Sotgiu A, Solinas G, Ulgheri L, Ticca A, Simone I, Logroscino G. 2012. Frequency of the C9orf72 hexanucleotide repeat expansion in patients with amyotrophic lateral sclerosis and frontotemporal dementia: A cross-sectional study. *Lancet Neurol* **11**. doi:10.1016/S1474-4422(12)70043-1

Malik I, Kelley CP, Wang ET, Todd PK. 2021. Molecular mechanisms underlying nucleotide repeat expansion disorders. *Nat Rev Mol Cell Biol* **22**:589–607. doi:10.1038/s41580-021-00382-6

May S, Hornburg D, Schludi MH, Arzberger T, Rentzsch K, Schwenk BM, Grässer FA, Mori K, Kremmer E, Banzhaf-Strathmann J, Mann M, Meissner F, Edbauer D. 2014. C9orf72 FTLD/ALS-associated Gly-Ala dipeptide repeat proteins cause neuronal toxicity and Unc119 sequestration. *Acta Neuropathol* **128**:485–503. doi:10.1007/s00401-014-1329-4

Melnikov S, Mailliot J, Shin BS, Rigger L, Yusupova G, Micura R, Dever TE, Yusupov M. 2016. Crystal Structure of Hypusine-Containing Translation Factor eIF5A Bound to a Rotated Eukaryotic Ribosome. *J Mol Biol* **428**. doi:10.1016/j.jmb.2016.05.011

Miller-Fleming L, Olin-Sandoval V, Campbell K, Ralser M. 2015. Remaining Mysteries of Molecular Biology: The Role of Polyamines in the Cell. *J Mol Biol*. doi:10.1016/j.jmb.2015.06.020

Neary D, Snowden JS, Gustafson L, Passant U, Stuss D, Black S, Freedman M, Kertesz A, Robert PH, Albert M, Boone K, Miller BL, Cummings J, Benson DF. 1998. Frontotemporal lobar degeneration: A consensus on clinical diagnostic criteria. *Neurology* **51**:1546–1554. doi:10.1212/WNL.51.6.1546

Neumann M, Sampathu DM, Kwong LK, Truax AC, Micsenyi MC, Chou TT, Bruce J, Schuck T, Grossman M, Clark CM, McCluskey LF, Miller BL, Masliah E, Mackenzie IR, Feldman H, Feiden W, Kretzschmar HA, Trojanowski JQ, Lee VM-Y. 2006. Ubiquitinated TDP-43 in Frontotemporal Lobar Degeneration and Amyotrophic Lateral Sclerosis. *Science (1979)* **314**:130–133. doi:10.1126/science.1134108

Oh SY, He F, Krans A, Frazer M, Taylor JP, Paulson HL, Todd PK. 2015. RAN translation at CGG repeats induces ubiquitin proteasome system impairment in models of fragile X-associated tremor ataxia syndrome. *Hum Mol Genet* **24**:4317–4326. doi:10.1093/hmg/ddv165

Onyike CU, Diehl-Schmid J. 2013. The epidemiology of frontotemporal dementia. *International Review of Psychiatry* **25**:130–137. doi:10.3109/09540261.2013.776523

Park MH, Kar RK, Banka S, Ziegler A, Chung WK. 2022. Post-translational formation of hypusine in eIF5A: implications in human neurodevelopment. *Amino Acids*. doi:10.1007/s00726-021-03023-6

Pelechano V, Alepuz P. 2017. EIF5A facilitates translation termination globally and promotes the elongation of many non polyproline-specific tripeptide sequences. *Nucleic Acids Res* **45**. doi:10.1093/nar/gkx479

Petrucelli L, Dawson TM. 2004. Mechanism of neurodegenerative disease: Role of the ubiquitin proteasome system. *Ann Med* **36**:315–320. doi:10.1080/07853890410031948

Puleston DJ, Buck MD, Klein Geltink RI, Kyle RL, Caputa G, O'Sullivan D, Cameron AM, Castoldi A, Musa Y, Kabat AM, Zhang Y, Flachsmann LJ, Field CS, Patterson AE, Scherer S, Alfei F, Baixauli F, Austin SK, Kelly B, Matsushita M, Curtis JD, Grzes KM, Villa M, Corrado M, Sanin DE, Qiu J, Pällman N, Paz K, Maccari ME, Blazar BR, Mittler G, Buescher JM, Zehn D, Rospert S, Pearce EJ, Balabanov S, Pearce EL. 2019. Polyamines and eIF5A Hypusination Modulate

Mitochondrial Respiration and Macrophage Activation. *Cell Metab* **30**. doi:10.1016/j.cmet.2019.05.003

Renton AE, Majounie E, Waite A, Simón-Sánchez J, Rollinson S, Gibbs JR, Schymick JC, Laaksovirta H, van Swieten JC, Myllykangas L, Kalimo H, Paetau A, Abramzon Y, Remes AM, Kaganovich A, Scholz SW, Duckworth J, Ding J, Harmer DW, Hernandez DG, Johnson JO, Mok K, Ryten M, Trabzuni D, Guerreiro RJ, Orrell RW, Neal J, Murray A, Pearson J, Jansen IE, Sondervan D, Seelaar H, Blake D, Young K, Halliwell N, Callister JB, Toulson G, Richardson A, Gerhard A, Snowden J, Mann D, Neary D, Nalls MA, Peuralinna T, Jansson L, Isoviita V-M, Kaivorinne A-L, Hölttä-Vuori M, Ikonen E, Sulkava R, Benatar M, Wuu J, Chiò A, Restagno G, Borghero G, Sabatelli M, Heckerman D, Rogaeva E, Zinman L, Rothstein JD, Sendtner M, Drepper C, Eichler EE, Alkan C, Abdullaev Z, Pack SD, Dutra A, Pak E, Hardy J, Singleton A, Williams NM, Heutink P, Pickering-Brown S, Morris HR, Tienari PJ, Traynor BJ. 2011. A Hexanucleotide Repeat Expansion in C9ORF72 Is the Cause of Chromosome 9p21-Linked ALS-FTD. *Neuron* **72**:257–268. doi:10.1016/J.NEURON.2011.09.010

Ringholz GM, Appel SH, Bradshaw M, Cooke NA, Mosnik DM, Schulz PE. 2005. Prevalence and patterns of cognitive impairment in sporadic ALS. *Neurology* **65**:586–590. doi:10.1212/01.wnl.0000172911.39167.b6

Rodriguez CM, Todd PK. 2019. New pathologic mechanisms in nucleotide repeat expansion disorders. *Neurobiol Dis*. doi:10.1016/j.nbd.2019.104515

Saini P, Eyler DE, Green R, Dever TE. 2009. Hypusine-containing protein eIF5A promotes translation elongation. *Nature* **459**. doi:10.1038/nature08034

Schmidt C, Becker T, Heuer A, Braunger K, Shanmuganathan V, Pech M, Berninghausen O, Wilson DN, Beckmann R. 2015. Structure of the hypusinylated eukaryotic translation factor eIF-5A bound to the ribosome. *Nucleic Acids Res* **44**. doi:10.1093/nar/gkv1517

Schnier J, Schwelberger HG, Smit-McBride Z, Kang HA, Hershey JW. 1991. Translation initiation factor 5A and its hypusine modification are essential for cell viability in the yeast Saccharomyces cerevisiae. *Mol Cell Biol* **11**. doi:10.1128/mcb.11.6.3105

Schreier MH, Erni B, Staehelin T. 1977. Initiation of mammalian protein synthesis. I. Purification and characterization of seven initiation factors. *J Mol Biol* **116**. doi:10.1016/0022-2836(77)90268-6

Schuller AP, Wu CCC, Dever TE, Buskirk AR, Green R. 2017. eIF5A Functions Globally in Translation Elongation and Termination. *Mol Cell* **66**. doi:10.1016/j.molcel.2017.03.003

Sha Z, Brill LM, Cabrera R, Kleifeld O, Scheliga JS, Glickman MH, Chang EC, Wolf DA. 2009. The eIF3 Interactome Reveals the Translasome, a Supercomplex Linking Protein Synthesis and Degradation Machineries. *Mol Cell*. doi:10.1016/j.molcel.2009.09.026

Tank EM, Figueroa-Romero C, Hinder LM, Bedi K, Archbold HC, Li X, Weskamp K, Safren N, Paez-Colasante X, Pacut C, Thumma S, Paulsen MT, Guo K, Hur J, Ljungman M, Feldman EL, Barmada SJ. 2018. Abnormal RNA stability in amyotrophic lateral sclerosis. *Nat Commun* **9**. doi:10.1038/s41467-018-05049-z

Tauc M, Cougnon M, Carcy R, Melis N, Hauet T, Pellerin L, Blondeau N, Pisani DF. 2021. The eukaryotic initiation factor 5A (eIF5A1), the molecule, mechanisms and recent insights into the pathophysiological roles. *Cell Biosci*. doi:10.1186/s13578-021-00733-y

Tesina P, Ebine S, Buschauer R, Thoms M, Matsuo Y, Inada T, Beckmann R. 2023. Molecular basis of eIF5A-dependent CAT tailing in eukaryotic ribosome-associated quality control. *Mol Cell* **83**. doi:10.1016/j.molcel.2023.01.020

Tiburcio AF, Altabella T, Bitrián M, Alcázar R. 2014. The roles of polyamines during the lifespan of plants: From development to stress. *Planta*. doi:10.1007/s00425-014-2055-9

von der Haar T. 2008. A quantitative estimation of the global translational activity in logarithmically growing yeast cells. *BMC Syst Biol* **2**. doi:10.1186/1752-0509-2-87

Wątor E, Wilk P, Biela A, Rawski M, Zak KM, Steinchen W, Bange G, Glatt S, Grudnik P. 2023. Cryo-EM structure of human eIF5A-DHS complex reveals the molecular basis of hypusination-associated neurodegenerative disorders. *Nat Commun* **14**. doi:10.1038/s41467-023-37305-2

Yamakawa M, Ito D, Honda T, Kubo K, Noda M, Nakajima K, Suzuki N. 2015. Characterization of the dipeptide repeat protein in the molecular pathogenesis of c9FTD/ALS. *Hum Mol Genet* **24**:1630–1645. doi:10.1093/hmg/ddu576

Zhang Y-J, Jansen-West K, Xu Y-F, Gendron TF, Bieniek KF, Lin W-L, Sasaguri H, Caulfield T, Hubbard J, Daughrity L, Chew J, Belzil V V., Prudencio M, Stankowski JN, Castanedes-Casey M, Whitelaw E, Ash PEA, DeTure M,

Rademakers R, Boylan KB, Dickson DW, Petrucelli L. 2014. Aggregation-prone c9FTD/ALS poly(GA) RAN-translated proteins cause neurotoxicity by inducing ER stress. *Acta Neuropathol* **128**:505–524. doi:10.1007/s00401-014-1336-5

Zhao YG, Liu N, Miao G, Chen Y, Zhao H, Zhang H. 2018. The ER Contact Proteins VAPA/B Interact with Multiple Autophagy Proteins to Modulate Autophagosome Biogenesis. *Current Biology* **28**:1234-1245.e4. doi:10.1016/j.cub.2018.03.002

Zu T, Gibbens B, Doty NS, Gomes-Pereira M, Huguet A, Stone MD, Margolis J, Peterson M, Markowski TW, Ingram MAC, Nan Z, Forster C, Low WC, Schoser B, Somia N V., Clark HB, Schmechel S, Bitterman PB, Gourdon G, Swanson MS, Moseley M, Ranum LPW. 2011. Non-ATG-initiated translation directed by microsatellite expansions. *Proceedings of the National Academy of Sciences* **108**:260–265. doi:10.1073/pnas.1013343108

Zu T, Liu Y, Banez-Coronel M, Reid T, Pletnikova O, Lewis J, Miller TM, Harms MB, Falchook AE, Subramony SH, Ostrow LW, Rothstein JD, Troncoso JC, Ranum LPW. 2013. RAN proteins and RNA foci from antisense transcripts in C9ORF72 ALS and frontotemporal dementia. *Proceedings of the National Academy of Sciences* **110**:E4968–E4977. doi:10.1073/pnas.1315438110

Chapter 5: Discussion and Future Directions

5.1. Conclusion

Toxic products generated by repeat-associated non-AUG (RAN) translation contribute to pathogeneses in at least 10 different nucleotides repeat expansion diseases (Fujino et al., 2023; Malik et al., 2021; Rodriguez and Todd, 2019; Zu et al., 2011). However, the mechanisms by which RAN translation occurs are still unclear, and there is still no effective treatment for these nucleotide repeat expansion diseases. This thesis aims to better understand RAN translation and identify selective RAN translation modifiers, with a long-term goal of shedding light on novel potential therapeutic targets.

The two diseases that I focused on in this thesis are a G4C2 repeat expansion in the intronic region of *C9orf72* that causes amyotrophic lateral sclerosis (ALS) and frontotemporal dementia (FTD) (C9ALS/FTD) and a CGG repeats expansion in the 5'UTR of FMR1 that causes Fragile X-associated tremor/ataxia syndrome (FXTAS). They both support RAN translation as a mechanism that generates toxicity in disease models and patients (Todd et al., 2013; Zu et al., 2013). To identify RAN translation modifiers, I used model systems that express G4C2 or CGG repeats in mammalian cells, *Drosophila*, and patient-derived iPSC iNeurons to study selective modifiers. I applied three general strategies to identify these modifiers: a single gene approach based on the structure of the repeat RNA, a candidate-pathway based approach based on my hypothesis and the

literature, and an unbiased whole genome-based screen approach to expand the scope of potential RAN modifiers outside of expected targets.

C9ALS/FTD and FXTAS harbor a GC-rich regions within the transcripts that form stable RNA secondary structures (Fratta et al., 2012; Haeusler et al., 2014; Reddy et al., 2013; Wang et al., 2019). As GC-rich regions undergo RAN translation to generate toxic RAN products, the process by which translation elongation happens within these GC-rich regions is important. I suggest that RNA structures formed within these GC-rich regions actively impede RAN translation elongation, making this process less efficient. The first question I asked was if the RNA structures exist and whether they affect RAN translation. To do this, I investigated whether altering expression of a g-quadruplex helicase, DHX36, might impact RAN translation. I hypothesized that g-quadruplex structures formed by the repeat might be more stable if I depleted DHX36, and that this would result in reduced RAN translational efficiency. The key finding of this study is that when I depleted the function of DHX36 in both G4C2 and CGG repeats, there was a decrease in RAN products. In C9RAN, defective DHX36 decreases RAN product in a length-dependent manner, regardless of the reading frame of the G4C2 repeats. This suggests that g-quadruplexes exist in G4C2 and CGG repeats in cells and that DHX36 acts normally to destabilize these structures. This suggests further that both protein factors and small molecule which modify the dynamics of repeat folding might serve as selecitve modifiers of RAN translation and as such good platforms for future therapeutic development.

This finding from DHX36 raised a larger question of what and how RNA structures impact the scanning of the ribosomes during translation elongation. Moreover, from a broader view, what happens if ribosomes slow down or stall during translation elongation?

Previous studies reveal mRNA and protein quality control surveillance pathways when ribosomes stall or collide(Inada, 2020; Joazeiro, 2019). These are the quality control pathways that recycle stalled ribosomes, degrade aberrant mRNA, target falsely made peptide chains for proteasome degradation, and, most importantly, ensure protein fidelity in organisms. I wondered if the RNA secondary structures from GC-rich repeats might trigger these pathways and if altering expression of proteins within these pathways might impact RAN translation.

Therefore, I performed a candidate-based screen by knocking down expression of key factors from the mRNA and protein quality control pathway. I found that depletion especially from the ribosome-associated quality control (RQC) pathway, including NEMF, LTN1, and ANKZF1, significantly increased the abundance of RAN products. This result suggests that the RQC pathway is involved in RAN translation. In addition, as previous studies showed that stalling of ribosomes is one of the events that trigger these pathways, I wonder if stalling of ribosomes happens in those GC-rich repeats and if I can detect any partially made products from stalled ribosomes. With an N-terminal tagging system, I detected smaller products generated from both G4C2 and CGG repeats; furthermore, when I depleted the functions of RQC factors, I also saw increases in the smaller products. These results suggest that G4C2 and CGG repeat cause stalling of ribosomes that generate partial and full-length products. Later, the RQC pathway is involved downstream of this stalling event, and RAN products increase their abundance in the absence of RQC.

Finally, I performed an unbiased genome-wide siRNA screen in a high-throughput format to the primary screen for G4C2 repeats and a subset screen for CGG repeats. I

surprisingly identified a group of proteasome subunits as selective C9RAN suppressors. The results show knockdown of PSMC1, PSMC2, PSMD11, PSMD7, PSMB5, and PSMA7 proteasome subunits decrease the abundance of C9RAN product. I also identified DOHH, from the last step of the eukaryotic eIF5A hypusination pathway, as an enhancer of C9RAN and FMR1RAN. When I deplete the function of DOHH by siRNA or with a pharmacological inhibitor of DOHH, Ciclopirox (CPX), there is an increase in both C9RAN and FMR1RAN products. These findings suggest that proteasomal activity and matured, hypusinated eIF5A may play roles in either the RAN translation process, in RQC, or in turnover of RAN translated proteins.

In my thesis, I found that RNA helicases, RQC factors, general proteasome components, and enzymes which hypusinate eIF5A all act as selective modifiers of RAN translation. I therefore have been trying to discern how all of these factors could inter-relate. Recently, a study showed that eIF5A is involved in the RQC complex, which binds with LTN1 during the CAT-tailing process during the RQC pathway (Tesina et al., 2023). From our results, the depletion of RQC factors and DOHH show an increase in RAN products, but I need further investigation to know if there is an epistatic effect of these factors on the RQC pathway. Previous studies found that variants of NEMF and mutation of LTN1 linked to neurodegenerative disease patients and mouse models (Chu et al., 2009; Martin et al., 2020). It is not clear whether there is a RQC deficiency in GC-rich nucleotide repeat expansion diseases. As our results show increases in abundance from both partially made and full-length RAN products in the absence of RQC, I am curious about how RQC is affecting accumulation of fully translated products. I hypothesize that other processes may be acting in concert with or in competition with the RQC pathway

when ribosome stalling occurs. These alternative processes may include specialized helicases, ribosomal frameshifting, or other factors that trigger self-resolution of ribosomal stalling events. When RQC is active, it is removing ribosomes from repeat RNAs and potentially triggering RNA degradation and a loss of the template for RAN translation. However, when RQC factors are depleted, these alternative processes become favored. Now, helicases may act to allow stall resolution, or translational frameshifts may become more prominent- or the stalls may simply self-resolve if given sufficient time. However, I do not know the exact relationship between helicases and stalling of GC-rich transcripts, and I do not know if the depletion of DHX36 also affects the production of partially made RAN products or RQC activity. There are still many undiscovered questions related to ribosome stalling within the GC-rich transcripts, RAN translation elongation, and subsequent ribosome stalling events. I eagerly anticipate more studies to reveal the field.

An ideal RAN modifier should fulfill the following criteria:

1) the effect of the modifier is valid across multiple RAN-translated repeat sequences
2) the effect of the modifier is valid across multiple disease model systems
3) the modifier is specific to RAN translation, so it does not affect global translation.
4) the modifier does not cause intrinsic toxicity in model organisms

After a thesis spent trying to identify an ideal RAN modifier, I am disappointed to say that I have not found any that meet all the above criteria. Most translation initiation/elongation factors affect both RAN and AUG-driven translation. Although some show a more significant effect in RAN translation, I cannot exclude other potential effects on global translation. I also found that many modifiers were difficult to validate in different

model organisms- often producing contradictory results. I think this is because some modifier shows a slight but statistically significant impact from a transient transfected cellular model, where effects are often exaggerated compared to more endogenous model systems. I also focued here mainly on modifiers of C9RAN and FMR1RAN from linear mRNAs- however there are more RAN-related repeat sequences and contexts that I could have included. But even with my focus just on just these two RAN-related diseases, I was still limited to patient-derived iPSC lines and imperfect assays to measure all endogenous RAN products.

In the future, more screens from advanced disease models with accurate gene editing, control of protein expression, or capture and identification of proteins by mass spectrometry during the process of RAN translation on repeat RNAs (such as capturing interacting proteins from 60S ribosome subunits during translation or during stall events) migh identify more consistent and selective modifiers. Other than screening, multi-omics analysis from advanced disease models may also identify genes with differential expression between healthy and disease models that might impact these processes in patients. More advanced model systems that mimic endogenous disease states and more advanced assays to measure RAN products will help identify and validate better and more precise RAN modifiers from either a screen or multi-omic analysis.

5.2. References

Chu J, Hong NA, Masuda CA, Jenkins B V., Nelms KA, Goodnow CC, Glynne RJ, Wu H, Masliah E, Joazeiro CAP, Kay SA. 2009. A mouse forward genetics screen identifies LISTERIN as an E3 ubiquitin ligase involved in

neurodegeneration. Proc Natl Acad Sci U S A 106. doi:10.1073/pnas.0812819106

Fratta P, Mizielinska S, Nicoll AJ, Zloh M, Fisher EMC, Parkinson G, Isaacs AM. 2012. C9orf72 hexanucleotide repeat associated with amyotrophic lateral sclerosis and frontotemporal dementia forms RNA G-quadruplexes. Sci Rep. doi:10.1038/srep01016

Fujino Y, Mori K, Nagai Y. 2023. Repeat-associated non-AUG translation in neuromuscular diseases: mechanisms and therapeutic insights. The Journal of Biochemistry. doi:10.1093/jb/mvad012

Haeusler AR, Donnelly CJ, Periz G, Simko EAJ, Shaw PG, Kim M-S, Maragakis NJ, Troncoso JC, Pandey A, Sattler R, Rothstein JD, Wang J. 2014. C9orf72 nucleotide repeat structures initiate molecular cascades of disease. Nature 507:195–200. doi:10.1038/nature13124

Inada T. 2020. Quality controls induced by aberrant translation. Nucleic Acids Res 48. doi:10.1093/NAR/GKZ1201

Joazeiro CAP. 2019. Mechanisms and functions of ribosome-associated protein quality control. Nat Rev Mol Cell Biol. doi:10.1038/s41580-019-0118-2

Malik I, Kelley CP, Wang ET, Todd PK. 2021. Molecular mechanisms underlying nucleotide repeat expansion disorders. Nat Rev Mol Cell Biol 22:589–607. doi:10.1038/s41580-021-00382-6

Martin PB, Kigoshi-Tansho Y, Sher RB, Ravenscroft G, Stauffer JE, Kumar R, Yonashiro R, Müller T, Griffith C, Allen W, Pehlivan D, Haral T, Zenker M, Howting D, Schanze D, Faqeih EA, Almontashiri NAM, Maroofian R, Houlden

H, Mazaheri N, Galehdari H, Douglas G, Posey JE, Ryan M, Lupski JR, Laing NG, Joazeiro CAP, Cox GA. 2020. NEMF mutations that impair ribosome-associated quality control are associated with neuromuscular disease. Nat Commun 11. doi:10.1038/s41467-020-18327-6

Reddy K, Zamiri B, Stanley SYR, Macgregor RB, Pearson CE. 2013. The disease-associated r(GGGGCC)n repeat from the C9orf72 gene forms tract length-dependent uni- and multimolecular RNA G-quadruplex structures. Journal of Biological Chemistry 288. doi:10.1074/jbc.C113.452532

Rodriguez CM, Todd PK. 2019. New pathologic mechanisms in nucleotide repeat expansion disorders. Neurobiol Dis. doi:10.1016/j.nbd.2019.104515

Tesina P, Ebine S, Buschauer R, Thoms M, Matsuo Y, Inada T, Beckmann R. 2023. Molecular basis of eIF5A-dependent CAT tailing in eukaryotic ribosome-associated quality control. Mol Cell 83. doi:10.1016/j.molcel.2023.01.020

Todd PK, Oh SY, Krans A, He F, Sellier C, Frazer M, Renoux AJ, Chen K chun, Scaglione KM, Basrur V, Elenitoba-Johnson K, Vonsattel JP, Louis ED, Sutton MA, Taylor JP, Mills RE, Charlet-Berguerand N, Paulson HL. 2013. CGG repeat-associated translation mediates neurodegeneration in fragile X tremor ataxia syndrome. Neuron. doi:10.1016/j.neuron.2013.03.026

Wang Z, Ursu A, Childs-disney JL, Rice JE, Petrucelli L, Disney MD, Wang Z, Ursu A, Childs-disney JL, Guertler R, Yang W, Bernat V. 2019. The Hairpin Form of r (G 4 C 2) exp in c9ALS / FTD Is Repeat-Associated Non-ATG Translated and a Target for Bioactive Small Molecules Article The Hairpin Form of r (G 4 C 2) exp in c9ALS / FTD Is Repeat-Associated Non-ATG

Translated and a Target for B. Cell Chem Biol 26:179-190.e12. doi:10.1016/j.chembiol.2018.10.018

Zu T, Gibbens B, Doty NS, Gomes-Pereira M, Huguet A, Stone MD, Margolis J, Peterson M, Markowski TW, Ingram MAC, Nan Z, Forster C, Low WC, Schoser B, Somia N V., Clark HB, Schmechel S, Bitterman PB, Gourdon G, Swanson MS, Moseley M, Ranum LPW. 2011. Non-ATG-initiated translation directed by microsatellite expansions. Proceedings of the National Academy of Sciences 108:260–265. doi:10.1073/pnas.1013343108

Zu T, Liu Y, Banez-Coronel M, Reid T, Pletnikova O, Lewis J, Miller TM, Harms MB, Falchook AE, Subramony SH, Ostrow LW, Rothstein JD, Troncoso JC, Ranum LPW. 2013. RAN proteins and RNA foci from antisense transcripts in C9ORF72 ALS and frontotemporal dementia. Proceedings of the National Academy of Sciences 110:E4968–E4977. doi:10.1073/pnas.1315438110